CELLIANT®

Celliant Published Studies: Compilation of Clinical, Preclinical, Technical and Physical Trials

Updated May 2021

SUMMARY OF CLINICAL & PRECLINICAL TRIALS

Clinical Trials

Year	End Point	Title	Institution	Primary Investigators	N	Journal /Publication	Outcome
2019	Grip Strength	Effect of Shirts with 42% Celliant® Fiber on tcPO2 Levels and Grip Strength in Healthy Subjects: A Placebo-Controlled Clinical Trial	Long Beach VA Memorial Hospital	Dr. Ian Gordon, Dr. Mark Vangel and Dr. Michael R Hamblin	24	Journal of Textile Science and Engineering	Improved grip strength of over 12% in the dominant hand after 90 minutes
2014	Tissue Oxygen (TCPO2)	Randomized Controlled Trial Comparing the Effects of Far-Infrared Emitting Ceramic Fabric Shirts and Control Polyester Shirts on Transcutaneous PO2	Long Beach VA Memorial Hospital	Dr. Ian Gordon, James Wason, Dr. Lawrence Lavery, Dr. Michael R Hamblin and MS Thein	153	Journal of Textile Science and Engineering	Average increase in TCPO2 of 8.4% after 90 minutes for 71% of the subjects
2012	Elbow and Wrist Pain	Effect of Celliant® Materials on Pain and Strength in Subjects with Chronic Elbow and Wrist Pain	Long Beach VA Memorial Hospital	Dr. Ian Gordon and Dr. Michael R Hamblin	70	Pending Publication	Improved grip strength
2012	Tissue Oxygen (TCPO2)	The Test Report on the Impacts of Subject Socks with the Application of Celliant® Technical Fibers on Transcutaneous Oxygen Pressure on a Man's Foot	Academy of Chinese Sciences	Dr. Li Shaojing, Wu Chuanhong, Gao Jian, Zhu Li and Wen Liwei	100	N/A	Increase in TCPO2 across all healthy subjects
2012	Tissue Oxygen (TCPO2)	Transcutaneous Partial Pressure of Oxygen (tcPO2) as a Primary Endpoint to Assess the Efficacy of Celliant® as a Vasoactive Material	Long Beach VA Memorial Hospital	Dr. Ian Gordon and Dr. Michael Coyle	51	N/A	An average increase of 7% in TCPO2
2011	Performance & Recovery	Apparel with Far Infrared Radiation for Decreasing an Athlete's Oxygen Consumption During Submaximal Exercise	University of Calgary	Dr. Jay Worobets, Dr. Darren Stefanyshyn and Emma Skolnik	12	Research Journal of Textile and Apparel	Elite/club cyclists VO2 reduced by 1.1%, increasing anaerobic threshold
2010	Sleep (pilot)	Double Blind, Placebo Controlled, Crossover Trial on the Effect of Optically Modified Polyethylene Terephthalate Fiber Mattress Covers on Sleep Disturbances in Patients with Chronic Back Pain	University of CA Irvine	Dr. Marcel Hungs and Dr. Annabel Wang	6	N/A	Nighttime awakenings, sleep quality and sleep efficiency improved
2009	Foot Pain	Effect of Optically Modified Polyethylene Terephthalate Fiber Socks on Chronic Foot Pain	University of CA Irvine	Dr. Ian Gordon and Dr. Robyn York	55	BioMed Central Complementary & Alternative Medicine	Statistically significant reduction of pain and improved comfort for subjects (diabetic/foot neuropathy)
2005	Tissue Oxygen (TCPO2)	Holofiber Study of Thirteen (13) Healthy Subjects	University of Texas A&M	Dr. Graham McClue	13	N/A	An average increase in TCPO2 levels from 10% to 24%
2003	Tissue Oxygen (TCPO2)	Improving Blood Flow with Holofiber in the Hands and Feet of High-Risk Diabetics	Loyola University Chicago	Dr. Lawrence Lavery	20	N/A	An average increase in TCPO2 levels from 12% in the hands and 8% in the feet of diabetic subjects

Preclinical Trial

Year	End Point	Title	Institution	Primary Investigator	Journal /Publication	Outcome
2021	Anti-inflammatory Markers and Improved Motion	Celliant Bedding Moderates Autoimmune and Inflammatory Responses	University of Belgrade	Dr. Jasmina Djuretić, Dr. Mirjana Dimitrijević, Dr. Marija Stojanović, Dr. Jelena Kotur Stevuljević, Dr. Michael R Hamblin, Dr. Ana Micov, Dr. Radica Stepanović-Petrović and Dr. Gordana Leposavić	Scientific Reports	The appearance of the symptoms of collagen type II induced arthritis was postponed, while the disease was milder in infrared radiation exposed rats compared to non-exposed rats. Objective biochemical measurements of cytokines and autoimmunity were improved.

The FDA has determined that Celliant products are medical devices as defined in section 201(h) of the Federal Food, Drug and Cosmetic Act and are general wellness products.

Celliant is designated as a Class 1 Medical Device in Canada, the United Kingdom, the European Union, Australia, New Zealand and Japan. Celliant is cleared to market in Mexico, India, Korea, Russia, China and Taiwan, with more countries and regions to follow.

SUMMARY OF TECHNICAL & PHYSICAL TRIALS

Year	End Point	Title	Institution	Primary Investigators	Journal /Publication	Outcome
2017	Solar IR Emissivity	Infrared Radiative Properties and Thermal Modeling of Ceramic-Embedded Textile Fabrics	Exponent	Dr. David Anderson, John Fessler, Matthew Pooley, Scott Seidel, Dr. Michael R Hamblin, Haskell Beckham and Dr. James F Brennan	Biomedical Optics Express	Emissivity increased by approximately 10x when sunlight is also used to power Celliant technology
2016	IR Emissivity	Engineered Emissivity of Textile Fabrics by the Inclusion of Ceramic Particles	Exponent	Dr. David M. Anderson, Matthew Pooley, Haskell W. Beckham and Dr. James F Brennan	Optics Express	Emissivity increased by .14 MW per CM2 at fabric temperature of 32 Celsius with a 42% Celliant fabric vs. control
2012	Principals of IR	Far Infrared Radiation (FIR): Its Biological Effects and Medical Applications	Harvard/Wellman Center for Photomedicine	Dr. Michael R Hamblin and Dr. Fatma Vatansever	Photonics and Lasers in Medicine	Far Infrared Radiation (FIR) its biological effects and medical applications

Effect of Shirts with 42% Celliant® Fiber on tcPO2 Levels and Grip Strength in Healthy Subjects: A Placebo-controlled Clinical Trial

Dr. Ian Gordon, Dr. Mark Vangel and Dr. Michael R Hamblin

Journal of Textile Science & Engineering

Effect of Shirts with 42% Celliant® Fiber on tcPO$_2$ Levels and Grip Strength in Healthy Subjects: A Placebo-controlled Clinical Trial

Ian L Gordon[1], Seth Casden[2], Mark Vangel[3] and Michael R Hamblin[4,5*]

[1]Veterans Affairs Long Beach Healthcare System 5901 E, 7th Street, Long Beach, California, USA
[2]Hologenix LLC, Santa Monica, CA 90403, USA
[3]Department of Biostatistics, Massachusetts General Hospital, Boston, MA 02114, USA
[4]Wellman Center for Photomedicine, Massachusetts General Hospital, Boston, MA 02114, USA
[5]Department of Dermatology, Harvard Medical School, Boston, MA 02115, USA

Abstract

Celliant™ fabric contains quartz, silicon oxide and titanium oxide particles embedded into polymer fibers. Garments woven with Celliant™ yarns can be activated by body heat (conduction, convection and radiation) and remit the energy as far infrared radiation (FIR) back into the body. Wearing Celliant garments has been shown to increase blood flow and oxygen levels in the skin. In the present study we recruited twenty-four healthy volunteers (18-60 years of age) to wear a placebo shirt for 90 minutes, and after a 15-minute break, to wear a real Celliant shirt for 90 minutes. The mean transcutaneous oxygen (tcPO$_2$) measured over two sites (biceps and abdomen) was significantly increased at 3 time points (30, 60, and 90 minutes) by between 5-8% (P<0.05) in Celliant vs. placebo. The mean grip strength in the dominant hand measured at 90 minutes was 12.44% higher after wearing Celliant vs. after placebo (p=0.0002). There was a small but significant increase in systolic blood pressure (113.71 vs. 109.38; p=0.02) but no statistically significant changes in diastolic or mean blood pressure, heart rate, or skin temperature. These data provide more evidence of the physiological effects of FIR emitting garments and suggest they could be used for athletic training and recovery.

Keywords: Far-infrared emitting fabric; Transcutaneous oxygen; Grip strength; Blood pressure; Clinical trial

Introduction

Far infrared emitting fabrics and garments are becoming increasingly popular both for general health and wellness, and for the treatment of various medical conditions. Far-infrared radiation (FIR) therapy has long been used for the treatment of a wide range of diseases and conditions [1-3], including pain [4-6], wound healing [7], recovery from exercise [8], heart failure [9], and disturbed sleep [10]. The FIR is often delivered by an electrically-powered device such as an infrared heat lamp, an infrared sauna, or a tourmaline and/or jade heating pad.

However, an alternative way to deliver FIR to the body employs clothing, bandages, or patches constructed from fibers embedded with ceramic particles that emit FIR when powered by the body heat of the wearer [3]. These fabrics consist of a variety of different mineral particles incorporated into the polymer fibers, which are then woven into garments or patches. The mechanism of action involves natural heat from the body (radiation, conduction and radiation) being absorbed by the fabric, which then re-emits the energy back into the body in the form of FIR as a broad peak with a wavelength centered about 10 µm according to the Stefan-Boltzmann law.

The effective power density emitted by these fabrics is low (<1 mW/cm^2) compared to that emitted by externally-powered devices (>10 mW/cm^2). Nevertheless, garments, bed sheets, bandages, and patches can be worn for much longer times, many hours or even continuously, allowing a physiologically relevant amount of FIR to be delivered to the body. At a molecular level the mechanism is thought to involve the absorption of the FIR by "nanostructured water" which forms at hydrophobic/hydrophilic interfaces at cellular membranes including the mitochondrial membrane. The stimulation of mitochondria along with the release of nitric oxide, can increase cutaneous blood flow, tissue oxygenation, and produce beneficial effects such as reducing pain, inflammation, and stimulating wound healing and muscle recovery.

We previously showed [11] that the wearing of a Celliant shirt for 90 minutes could significantly increase the mean tcPO$_2$ by 6.7% compared to a placebo shirt (p <0.0003) and also produce a small but significant increase in the arterial oxygen saturation (p=0.0002). Moreover these effects were independent of the sequence in which the two shirts were worn, thus eliminating a possible source of bias.

The present study was designed to confirm the previous findings of increased tcPO$_2$ after wearing a Celliant shirt, and also to test the novel hypothesis that these physiological changes could result in improvement in an indicator of real-life muscular performance, namely the grip strength of the dominant hand.

Material and Methods

Celliant™ technology is a patented process for adding micron sized optically active quartz, silicon oxide and titanium oxide particles to polyethylene terephalate (PET) fibers. The resulting Celliant™ yarns are woven into golf-shirts containing either 42% Celliant (active) or zero Celliant (placebo). The two shirts are shown in Figure 1.
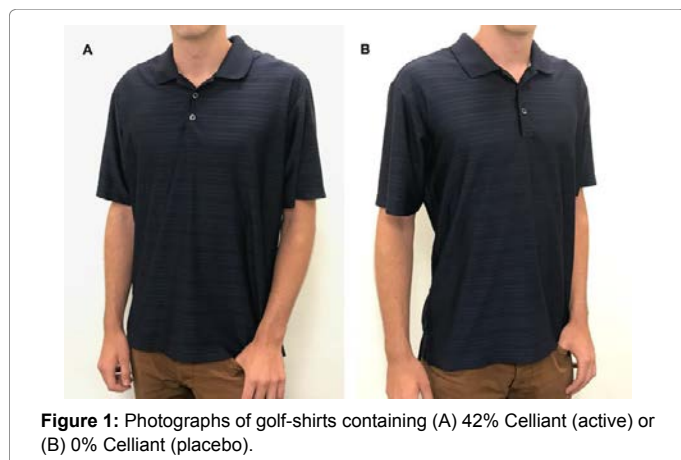
Transcutaneous oxygen measurements were recorded using Radiometer TCM 30 Module supplied by Radiometer America, Inc. (Brea, CA), and modified Clarke Electrodes supplied by Radiometer America, Inc. Data was acquired using Perisoft Version 2.10 supplied

Figure 1: Photographs of golf-shirts containing (A) 42% Celliant (active) or (B) 0% Celliant (placebo).

by Perimed America, Inc. (North Royalton, OH). The grip strength was tested using the dominant hand using the Baseline Hydraulic Hand Dynamometer manufactured by Fabrication Enterprises Inc. (White Plains, NY).

Clinical trial

Twenty-four healthy subjects (males and females between the ages of 18-60 years) were recruited under a protocol approved by the IRB via an on-line advertisement for subjects that paid $25. The trial was registered at clinicaltrials.gov NCT02798640 (https://clinicaltrials.gov/ct2/show/NCT02798640). The protocol was in accordance with the Declaration of Helsinki and verbal informed consent was obtained. Exclusion criteria included cardiovascular disease, smoking, pregnancy, recreational drug use within 6 months, or consumption of alcohol within 48 hours or caffeine within 3 hours of testing. The demographics of the subjects are given in Table 1.

Procedures

The subjects underwent preparation as follows. The hair was shaved from the test sites (biceps of the dominant hand and center of abdominal wall); the skin surface was then abraded with a fine abrasive material; the stratum corneum was then removed by the use of light-weight adhesive tape; and finally, the probe site was wiped with an alcohol preparation swab.

Subjects were then situated in a seated position on a comfortable chair. The room temperature was maintained at a constant temperature over the duration of the study. Blood pressure, heart rate and body temperature were recorded at three intervals: before the test was administered, after the 90 minute placebo garment period and finally after the 90 minute Celliant™ garment period.

The transcutaneous oxygen electrodes were heated to 45°C and allowed to equilibrate on the skin for 10 minutes (until stable values were achieved). The resultant tcPO$_2$ values were measured in mmHg.

Two self-adhesive fixation rings were affixed (biceps of dominant arm and abdomen) and the probes attached thereto. A buffer (KCl) solution was added (3 drops to each fixation ring). Each probe was calibrated to an assumed atmospheric pressure of 159 mmHg, 20.9% of the standard atmospheric pressure of 760 mmHg. Each subject therefore had the same baseline atmospheric pressure, thus compensating for any pressure changes due to weather variations during the periods of testing.

Total subjects	24
Males	17
Females	8
Age (years)	30.05 + 10.56
Weight (lbs)	167.2 ± 42.9
Body mass index (BMI)	25.7 ± 5.5

Table 1: Demographics of subjects (mean ± SD).

Measurements of tcPO$_2$ were taken every two minutes during the 90-minute placebo and 90-minute active study periods. Blood pressure, heart rate and body temperature were recorded before and after each period. The entire study involved an acclimatization period (5 minutes) with vital sign measurement, placebo probe equilibration (10 minutes), placebo shirt period (90 minutes), break (15 minutes), active probe equilibration (10 minutes), active-shirt period (90 minutes). During the break (after the placebo period) subjects were encouraged to walk about, relieve themselves if necessary, and consume water and/or a small snack. After the break, the electrodes were reattached and equilibrated; subjects donned the second shirt and resumed quietly sitting.

The grip strength of the dominant hand was measured as follows. For each test of grip strength, the subject was seated with shoulder adducted and neutrally rotated, elbow flexed at 90°, forearm in neutral position, and wrist between 0° and 30° dorsiflexion and between 0° and 15° ulnar deviation.

During the preliminary acclimatization process, the subject was asked to squeeze the dynamometer initially at less than full strength simply to experience holding and using the device. The first measurement was taken after the 90-minute period of wearing the placebo garment. This served as the baseline or control measurement. The second measurement was taken following the 90-minute period after the Celliant™ garment was worn.

Statistics

Grip strength was compared using a paired t-test. Time trends in tcPO$_2$ were estimated using mixed-model regression with subject as a random effect. Data were smoothed as necessary using cubic regression splines. The data were analyzed using R [12].

Results and Discussion

There was a small but significant increase in systolic blood pressure (113.71 vs. 109.38; p=0.02), but no statistically significant changes in diastolic or mean blood pressure, heart rate, or skin temperature as shown in Table 2. The mean transcutaneous oxygen (tcPO$_2$) measured over two sites (biceps and abdomen) was significantly increased at 3 time points (30, 60, and 90 minutes) by between 6-10% (p <0.05) in Celliant vs. placebo as shown in Table 3. When the two different sites (biceps and abdomen) were compared, it could be seen that the increase in the tcPO$_2$ measured at the biceps site was higher than that measured for the abdomen site and the corresponding p values were lower. This is probably because the biceps site was covered by the shirt while the abdomen was not.

The mean grip strength in the dominant hand measured at 90 minutes was 95.92 ± 26.36 after wearing the placebo shirt, and 105.20 ± 23.82 after wearing the Celliant shirt. This represents an increase of 12.44% (p=0.0002). There was an increase in grip strength for 19 subjects, no measurable difference in strength for four subjects, and a decrease for one subject as shown in Figure 2. For seven subjects with TCPO$_2$ measurements at one-minute intervals, and also for a second

	Placebo	Celliant	P value
Systolic BP mmHg	109.38 ± 15.74	113.71 ± 14.0	0.0198
Diastolic BP mmHg	70.96 ± 9.05	71.38 ± 10.58	0.7177
Mean BP mmHg	83.76 ± 10.64	85.49 ± 11.39	0.1207
Pulse Rate	65.67 ± 10.17	66.08 ± 10.85	0.8127
Skin Temperature °F	92.63 ± 1.95	92.75 ± 2.21	0.6893

Table 2: Physiological variables (mean ± SD).

	Placebo	Celliant	% increase	P value
Mean 30 min	75.4 ± 19.37	79.63 ± 14.0	5.61	0.0417
Mean 60 min	74.81 ± 19.52	79.52 ± 19.53	6.29	0.0196
Mean 90 min	76.08 ± 20.05	81.62 ± 20.27	7.28	0.0029

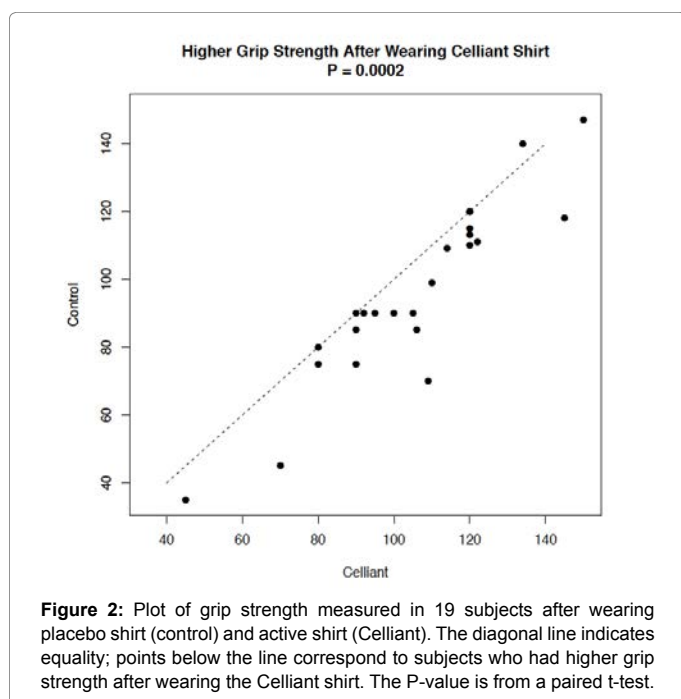**Table 3:** Mean $tcPO_2$ data recorded at the biceps and abdominal sites (mean ± SD).

Figure 2: Plot of grip strength measured in 19 subjects after wearing placebo shirt (control) and active shirt (Celliant). The diagonal line indicates equality; points below the line correspond to subjects who had higher grip strength after wearing the Celliant shirt. The P-value is from a paired t-test.

Figure 3: Average $tcPO_2$ as functions of time for seven subjects with measurements at one-minute intervals (broken lines), and for eight subjects with measurements at two-minute intervals (solid lines), from a single probe location, for Celliant (red) and Placebo (blue) shirts. The values were first smoothed using cubic regression splines with four degrees of freedom and equally spaced knots, then averaged over subjects.
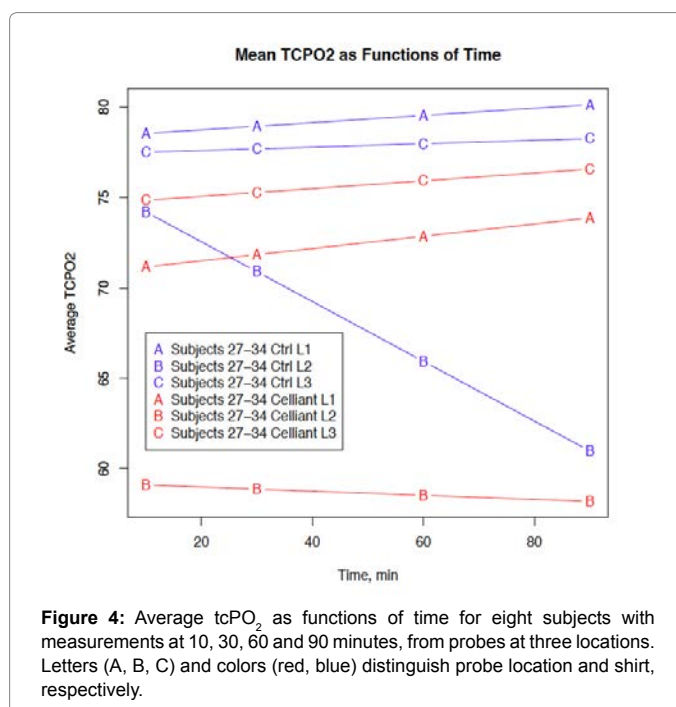
Figure 4: Average $tcPO_2$ as functions of time for eight subjects with measurements at 10, 30, 60 and 90 minutes, from probes at three locations. Letters (A, B, C) and colors (red, blue) distinguish probe location and shirt, respectively.

group of eight subjects with measurements at two-minute intervals, the average values as functions of time are lower for Celliant shirts as shown in Figure 3. For eight subjects with $TCPO_2$ measurements from four time points at each of three probe locations, the average values for the Celliant shirts are lower than the corresponding values for the Placebo shirt, for each location and measurement time as shown in Figure 4.

This study confirmed the previously reported increase in $tcPO_2$ produced by wearing a Celliant shirt for 90 minutes [11]. However it also produced a somewhat surprising and impressive finding, namely that the grip strength in the dominant hand was significantly increased by wearing the Celliant shirt compared to the placebo shirt. There was a small increase in systolic blood pressure, but this is probably too small to represent any significant health hazard.

A previous study at Exponent Consulting compared the emissivity of PET fabric with or without Celliant particles using sophisticated optical spectroscopic techniques. The intensity of infrared emission between 7.5 to 14 μm was 2.1% higher when fabric containing 1.22% w/w Celliant, was compared to fabric without ceramic particles [12]. This finding was consistent with the finding that the absorption co-efficient of Celliant fibers in the infrared spectrum was higher than the absorption co-efficient of pure PET fibers. In other words, the PET fibers were semi-transparent to infrared radiation, while the Celliant particles were opaque. A follow-up study from the same group [13] examined in more detail the influence of Celliant particles on the infrared reflectance of the PET fabric, and measured the transmission, and absorption. The findings confirmed that the addition of ceramic particles to PET fabric led to increased incidence of infrared radiation

upon the skin at wavelengths longer than 4 μm, with a maximum effect at approximately 9.4 μm. The effect was attributed to increased absorption of infrared radiation at shorter wavelengths and reemission at longer wavelengths.

The emission of FIR from ceramic particle-embedded fibers can interact with molecular and cellular structures by increasing the vibrational energy stored in chemical bonds, particularly in water clusters in cell membranes and cellular organelles. Pertubation of the vibrational energy of water clusters could affect the tertiary conformation of protein molecules tightly associated with this "nanostructured" water [14,15]. Low intensity FIR lamps and topically applied (non-powered) FIR-emitting ceramic materials have been shown to induce cellular changes *in vitro,* and produce physiologic changes in both preclinical animal models and clinical studies. In none of these studies were the effects shown to be associated with significant changes in temperature, consistent with the low power from both FIR lamps and non-powered ceramics in thermal equilibrium with skin (on the order of 0.1-1 mW/cm^2) [3].

Ting-Kai Leung and colleagues in Taiwan have studied the effect of FIR-emitting ceramic powders in a range of non-clinical biological studies. In one report [16], they cultured murine myoblast cells (C_2C_{12}) with bags of ceramic powder placed under the culture plates and found that FIR irradiation improved cell viability and prevented lactate dehydrogenase release when hydrogen peroxide was added, and also increased the intracellular levels of nitric oxide and calmodulin. They also employed electro-stimulation of amphibian skeletal muscle, and found that FIR emitting ceramics delayed the onset of fatigue, induced by muscle contraction. They went on to show [13] that ceramic-emitted FIR (cFIR) could increase the generation of intracellular nitric oxide in breast cancer cells and inhibit growth of murine melanoma cells. Similarly, they found [14] that cFIR increased calmodulin and nitric oxide production in RAW 264.7 macrophages. cFIR also increased the viability of murine macrophages with different concentrations of H_2O_2. In the same study, it was also shown that cFlR blocked ROS-mediated cytotoxicity (shown by measurements of cytochrome c and the ratio of NADP+/NADPH). The Leung group went on to study [15] a rabbit model of rheumatoid arthritis in which rabbits received intra-articular injections of lipopolysaccharide (LPS) to induce inflammation that mimics rheumatoid arthritis. FDG-PET scans were used to monitor the inflammation 16 hours and 7 days after the LPS injection. Rabbits were treated with cFIR in a cage surrounded by paper sheets impregnated with a thin layer of the ceramic powder, while the control group were surrounded by the same sheets without the material. Comparison of the final and initial uptakes of FDG in the LPS-injected left knee-joints of the rabbits indicated decreases in the cFlR exposed group compared to the control group indicating that FIR reduced inflammation.

With regard to clinical studies, FIR-emitting ceramics and fabrics have been employed both as ceramic discs held next to the body, and as garments or patches manufactured from FIR emitting ceramic material and subsequently applied to the human body.

For instance, a blanket containing discs was reported to improve quality of sleep [2]. 542 users of far-infrared emitting disks embedded in bedclothes revealed that the majority of the users reported a subjective improvement in their health, by completing a questionnaire. These improvements included the disappearance or reduction of feeling cold, stiffness of muscles in the shoulders, loins and legs, and improved sleep.

Gloves constructed from FIR emitting fabrics have been reported to treat arthritis of the hands and Raynaud's syndrome [16]. This was a randomised placebo controlled study in 60 patients who suffered from Raynard's syndrome, and reported significant improvements in subjective measures of pain and discomfort and in objective measures of temperature, grip and dexterity. Another study looked at pain reduction in fibromyalgia using a bioceramic shirt [17]. The study recruited 39 female patients (20 active and 19 placebo) who wore the shirts 8 hours/day for 60 days. The women in the active group showed a significant reduction in pain in the VAS (p<0.001), fewer tender points (p<0.001), improvement in the algometer score (p<0.001), and a significant reduction in FM symptoms and daily tablet intake (p<0.001). No significant changes in the placebo group were found.

A study employed socks made from PET fibers incorporating Celliant particles, designed to treat chronic foot pain resulting from diabetic neuropathy or other foot disorders [18]. A double-blind, randomized trial recruited 55 subjects (38 men, 17 women, average age 59.7 ± 11.9 years), 26 with diabetic neuropathy and 29 with other pain etiologies. Subjects were provided 3 pairs of socks (Celliant or placebo) in a closed container, and asked to wear them exclusively for the next two weeks. One and two weeks after the end of the period they filled out the same panel of questions. Greater reduction in pain was reported by Celliant subjects for 8 of the 9 pain questions employed, with a significant (p=0.043) difference between controls and Celliant for McGill question III. In neuropathic subjects, Celliant caused greater pain reduction in 6 of the 9 questions, but not significantly. In non-neuropathic subjects 8 of 9 questions showed greater pain reduction with the Celliant socks.

The increase in tcPO$_2$ observed in the present study is likely to be a consequence of increased oxygen availability in the tissue receiving FIR, possibly through a vasodilatory effect in the dermal circulation or, alternatively, effects on oxygen binding to hemoglobin. The increase in grip strength after only 90 minutes of wearing the shirt, is probably also due to increased oxygen availability and improved blood flow to the muscles of the dominant hand. Although our understanding of the mechanisms responsible for the effect of ceramic polyester composites on human physiology is still incomplete, our data confirm that it is a real scientific phenomenon. Even without completely understanding the effect, it may be possible to design ceramic polyester composite garments that can improve strength and performance in athletic training, and improve muscle recovery after exercise. The recent decision by the US FDA that Celliant garments will be regulated as medical devices and as general wellness products (http://www.medicaldevices-business-review.com/news/fda-determines-celliant-products-meet-criteria-as-medical-devices-260717-5882229) encourages clinical testing in multiple disease indications.

Conclusion

The data from this study suggests that wearing Celliant® fabric shirts for only 90 minutes can increase tissue oxygenation in the skin, and increase grip strength in the dominant hand.

Competing interests

Authors' contributions

ILG participated in the conception and design of the study, carried out subject recruitment and data collection, took part in the statistical analysis, and helped draft the manuscript. SC participated in the conception and design of the study, provided materials and funding, and helped draft the manuscript. MV carried out the majority of the statistical analysis and helped draft the manuscript. MRH wrote the manuscript and critically reviewed the data. All authors read and approved the final manuscript.

References

1. Tsai SR, Hamblin MR (2017) Biological effects and medical applications of infrared radiation. J Photochem Photobiol B 170: 197-207.

2. Inoue S, Kabaya M (1989) Biological activities caused by far-infrared radiation. Int J Biometeorol 33: 145-50.

3. Vatansever F, Hamblin MR (2012) Far infrared radiation (FIR): its biological effects and medical applications. Photonics Lasers Med 4: 255-266.

4. Lai CH (2014) Effects of far-infrared irradiation on myofascial neck pain: a randomized, double-blind, placebo-controlled pilot study. J Altern Complement Med 20: 123-129.

5. Lai YT (2017) Far-infrared ray patches relieve pain and improve skin sensitivity in myofascial pain syndrome: A double-blind randomized controlled study. Complement Ther Med 35: 127-132.

6. Lee CH (2011) A multicenter, randomized, double-blind, placebo-controlled trial evaluating the efficacy and safety of a far infrared-emitting sericite belt in patients with primary dysmenorrhea. Complement Ther Med 19: 187-93.

7. Toyokawa H (2003) Promotive effects of far-infrared ray on full-thickness skin wound healing in rats. Exp Biol Med 228: 724-729.

8. Irineu L, Cesar CCA, Fabio YN, Solange de PR, Ronaldo K, et al. (2016) Effects of far infrared rays emitting clothing on recovery after an intense plyometric exercise bout applied to elite soccer players: a randomized double-blind placebo-controlled trial. Biol Sport 33: 277-283.

9. Marcelo VL, Marcelo EO, Kelly NV, Airton S, Juliano NC, et al. (2014) Thermal vasodilation using a portable infrared thermal blanket in decompensated heart failure. Int Heart J 55: 433-439.

10. Honda K, Inoue S (1988) Sleep-enhancing effects of far-infrared radiation in rats. Int J Biometeoro 32: 92-94.

11. Washington K, Wason J, Thein MS, Lavery LA, Hamblin MR, et al. (2018) Randomized controlled trial comparing the effects of Far-Infrared emitting ceramic fabric shirts and control polyester shirts on transcutaneous PO₂. J Text Sci Eng 8.

12. R_Core_Team, R: A language and environment for statistical computing. R Foundation for Statistical Computing, Vienna, Austria.

13. Ting-Kai L, Chin-Feng C, Ping-Shan L, Chih-Hui Y, Chia-Yen H, et al. (2012) Inhibitory effects of Far Infrared irradiation generated by ceramic material on murine melanoma cell growth. Int J Photoenergy 646-845.

14. Ting-Kai L,Yung-Sheng L, Chi-Ming L, Yen-CC, Huey-FS (2011) Direct and indirect effects of ceramic far Infrared radiation on the hydrogen peroxide scavenging capacity and on murine macrophages under oxidative stress. J Med Biol Eng 31: 345-351.

15. Leung TK (2012) Bone and joint protection ability of ceramic material with biological effects. Chin J Physiol 55: 47-54.

16. Ko GD, Berbrayer D (2002) Effect of ceramic-impregnated "thermoflow" gloves on patients with Raynaud's syndrome: randomized, placebo-controlled study. Altern Med Rev 7: 328-35.

17. Santos ECMA, Garcia Pinillos F, Latorre Roman PA (2017) Reduction in pain after use of bioceramic undershirt for patients with Fibromyalgia. Altern Ther Health Med 23: 18-22.

18. York RM, Gordon IL (2009) Effect of optically modified polyethylene terephthalate fiber socks on chronic foot pain. BMC Complement Altern Med 9: 10.

Randomized Controlled Trial Comparing the Effects of Far-Infrared Emitting Ceramic Fabric Shirts and Control Polyester Shirts on Transcutaneous PO2

Dr. Ian Gordon, James Wason, Dr. Lawrence Lavery, Dr. Michael R Hamblin and MS Thein

Journal of Textile Science & Engineering

Research Article   **Open Access**

Randomized Controlled Trial Comparing the Effects of Far-Infrared Emitting Ceramic Fabric Shirts and Control Polyester Shirts on Transcutaneous PO$_2$

Washington K[1], Wason J[2], Thein MS[3], Lavery LA[4], Hamblin MR[5]* and Gordon IL[6]

[1]Hologenix LLC, 1112 Montana Avenue, Santa Monica, California, USA
[2]Maelor Group 7 Village Woods Dr. Amherst, Massachusetts, USA
[3]Veterans Affairs Long Beach Healthcare System 5901 E. 7th Street, Long Beach California, USA
[4]University of Texas Southwestern 1801 Inwood Road Dallas, Texas, USA
[5]Wellman Centre for Photo-medicine, Massachusetts General Hospital, Harvard Medical School, Boston, Massachusetts 02114, USA
[6]Veterans Affairs Long Beach Healthcare System 5901 E. 7th Street, Long Beach California, USA

Abstract

Our aim was to confirm earlier studies showing tcPO$_2$ to be higher under clothing made with polyethylene terephalate (PET) fabric containing ceramic particles (CEL) compared to standard PET fabric. In previous studies PET garments were donned first to avoid possible persistent effects from ceramic particles. This study randomized donning sequence to avoid bias.

Methods: Subjects were randomized to don either PET shirts first (PETF n=73) or CEL first (CELF n=80), switching garments after 90 minutes. Skin temperature (ST), arterial oxygen saturation (O$_2$sat), and tcPO$_2$ were measured every 30 minutes.

Results: Baseline ST and O$_2$ sat were nearly identical in the two groups. Baseline tcPO$_2$ was modestly higher in the CELF group than with PETF: 66.4 ± 18.9 vs. 63.9 ± 18.8 mmHg (n.s.). Independent of donning sequence, tcPO$_2$ measurements 90 minutes after wearing CEL were 6.7% higher than after 90 minutes wearing PET (p<0.0003). Sequence analysis found tcPO$_2$ in PETF subjects to gradually rise before and after switching garments, but tcPO$_2$ fell immediately after switching garments in CELF subjects. PETF baseline O$_2$sat of 98.1 ± 1.3 increased insignificantly after 90 minutes, and then increased further to 98.6 ± 0.8 after wearing CEL ninety minutes (p=0.0001). CELF baseline O$_2$sat of 97.9 ± 1.7 increased to 98.5 ± 1.1 90 minutes after donning CEL (p=0.0002) and fell to 98.3 ± 1.0 ninety minutes after switching to PET (p=0.0033).

Conclusions: The ability of ceramic-embedded fabric to induce higher tcPO2 measurements is not due to sequence bias.

Keywords: FIR-emitting garments; Randomized controlled trial; Ceramic-embedded fabric; Ceramic-embedded clothing; Far-infrared radiation; Tissue oxygenation; Transcutaneous PO$_2$; Donning sequence

Background

Far-infrared radiation (FIR) therapy has been used for the treatment of a variety of diseases and conditions [1-3], including pain [4-6], wound healing [7], recovery from exercise [8], heart failure [9], and disturbed sleep [10]. Often the FIR is delivered from an electrically-powered device such as an infrared heat lamp, an infrared sauna or a tourmaline/jade heating pad. However, there is an alternative way to deliver FIR to the body, which is by the wearing of clothing constructed from ceramic particle-embedded fibers that emit FIR when powered by the wearer's own body heat [3]. Celliant® (CEL, Hologenix LLC, Santa Monica, CA) yarn for clothing is constructed from standard polyester (polyethylene terephthalate --PET) extruded molten from a two-barrel machine with a proprietary mixture of ceramic particles added to produce a bicompatible fiber, with the center-load containing approximately 1 micron diameter particles [11]. CEL has been designed to capture heat from the body and re-emit radiant far-infrared energy to induce health benefits, and is thought to improve sleep and speed recovery from exercise. In one randomized clinical trial CEL socks were found to decrease chronic foot pain [12]. Three previous unpublished studies examined the effects of CEL garments on transcutaneous partial pressure of oxygen (tcPO$_2$) using Clark electrodes placed on the skin underneath either control PET garments or active CEL garments (http://www.pureenergysleep.ca/clinical-studies/). Lavery in 2003 studied 20 subjects with diabetes and

peripheral vascular disease wearing socks and gloves made from PET or CEL while resting quietly. With PET socks, foot tcPO$_2$ levels fell on average 2.6% from baseline over 60 minutes, compared to an increase of 4.7% after 60 minutes wearing CEL socks. Hand tcPO$_2$ increased 15.4% while wearing PET gloves for 60 minutes, compared to a significantly greater increase (30.8%) wearing CEL. A study in 13 normal subjects (McClue and Lavery, 2005, unpublished) compared tcPO$_2$ values of the hands and feet after wearing either PET or CEL garments. One hour of wearing CEL gloves induced mean tcPO$_2$ values in the hand to be 25.0% higher than those found with PET. Foot tcPO$_2$ was 10.2% higher under CEL socks than under PET socks; both hand and foot differences were significant.

Gordon in 2009 measured tcPO$_2$ in 24 healthy volunteers wearing

either PET or CEL shirts. After one hour the tcPO$_2$ was 7.1% higher under CEL shirts compared to PET shirts (p<0.05). No significant differences in mean blood pressure, heart rate, or temperature were found comparing measurements obtained while wearing CEL or PET. Due to a possible concern that the effects of CEL might persist after switching from active CEL garments to PET control garments, in these studies the PET garments were always worn first, before switching to CEL garments. This protocol could induce bias if, for example, tcPO$_2$ steadily rises in resting subjects independent of fabric type. The current study compared measurements of skin temperature (ST), arterial oxygen saturation (O$_2$sat) and tcPO$_2$ obtained while subjects wore PET shirts or CEL shirts. In one group PET shirts were worn first and in the second CEL garments were worn first, with the order sequence being randomized. Our goal was to confirm earlier findings without risk of bias from influences of the sequence of wearing.

Methods

Between October 2013 and January 2014, healthy volunteers aged 18 to 60 were recruited for an IRB approved protocol via on-line advertisement for subjects that paid $25. The trial was registered at clinicaltrials.gov NCT02798640 (https://clinicaltrials.gov/ct2/show/NCT02798640). The protocol was in accordance with the Declaration of Helsinki and informed consent was obtained. Exclusion criteria included cardiovascular disease, smoking, recreational drug use within 6 months, pregnancy, or consumption of alcohol within 48 hours or caffeine within 4 hours of enrolment. The garments employed were short sleeved shirts. PET and CEL garments were constructed at the same mill using either standard PET fiber or CEL fiber containing 1.25 % (mass ratio) proprietary ceramic particles. CEL and PET shirts were of identical fabrication and dernier differing only in color: PET was white and CEL was a light grey color (Figure 1).

Subjects were blinded to shirt composition and donning sequence. Assignment to either donning CEL shirts first (CELF) or control PET shirts first (PETF) was based 1:1 on a random allocation table. Studies were performed at the same constant temperature (24.0 ± 0.88°C), in a constant humidity (37.1 ± 5.0%) room with overhead fluorescent lighting. Prior to donning the first shirt, if necessary the anterior right shoulder skin was shaved, followed by gentle application of a fine abrasive and cleaning with tape and isopropyl alcohol. A probe with an electrolyte fluid ring, Clark electrode and a heating element set to heat the skin to 44°C was applied attached to a Periflux System 5000 monitor (Perimed, Kings Park, New York) with continuous monitoring software (Perisoft v2.55) as previously described [12]. Left forearm volar skin temperature (ST) was determined with an infrared thermometer. Fingertip pulse oximeter probes (CMS50DL, Crucial Medical Systems, and Atlanta, Georgia) monitored arterial oxygen saturation (O$_2$sat). After preparation, subjects donned the first shirt, and sat quietly.

Figure 1: Appearance of CEL and PET shirts.

Subjects were allowed to read or play video games but not sleep or converse.

Recordings of ST, O$_2$sat, and tcPO$_2$ began to be collected once tcPO$_2$ measurements were deemed stable, which generally required 10 to 15 minutes. The tcPO$_2$ signal representing mean ± s.d. was sampled at 32 Hz over 5 minutes. If s.d. was > 2 mmHg, the data was rejected as unstable. Cases in which the electrode membrane had to be replaced during measurements were also rejected. In 23 subjects data was excluded for one of these two problems, but all 23 returned on a later day to successfully repeat the entire protocol. No other data was excluded and all enrolled subjects completed the protocol.

Once the initial tcPO$_2$ signal stabilized, baseline measurements were obtained followed by recordings 30, 60, and 90 minutes after baseline (A30, A60. A90). After the A90 measurement, subjects were encouraged to walk about, relieve themselves if necessary, and consume water and/or a small snack. The break interval was approximately 15 minutes. After the break, subjects donned the second shirt and resumed quiet sitting. A second set of measurements was obtained 30, 60, and 90 minutes after tcPO$_2$ stabilized (B30, B60 and B90). Sample size was based on measurement of the variance in tcPO$_2$ in 45 subjects with power analysis indicating that a minimum of 147 subjects would be required to achieve a 95% confidence level and power of 80%. Statistical analyses were performed only after all data had been acquired with subgroup analysis based only on gender and donning sequence.

Results

Table 1 shows the demographics of the study population. The subjects were 54.3% male; 62.5% of the CELF sequence and 45.2% of the ConF sequence subjects were male (p=0.047, chi square test with Yates' correction). The age, height, weight, and BMI distribution were similar in the CELF and ConF subjects with no significant differences. Overall 52% of the subjects were Caucasian, 22% African-American, 16% Hispanic, 8% Asian, and 1% other – the ethnic distributions were comparable in the active and control sequences (53, 18, 20, 9, and 1% versus 52, 26, 20, 9, and 1%) (Table 1).

As shown in Table 2 is the baseline physiologic parameters. Mean baseline skin temperatures were nearly identical in the CELF and PETF groups 33.1 ± 0.9°C for CELF and 33.2 ± 1.1°C for PETF, as were baseline tcPO$_2$ and O$_2$sat. There were gender differences in baseline physiologic parameters: men had higher ST, lower O$_2$sat, and lower tcPO$_2$ then women. Mean baseline tcPO$_2$ was 2.5 mmHg higher in the CELF group compared to the PETF group, (66.4 ± 18.9 versus 63.9 ± 18.8 mmHg) but not significantly (p=0.424 unpaired t test) (Table 2).

Table 3 shows ST and O$_2$sat measurements. The mean baseline ST for all subjects was 33.1 ± 1.0˚C, significantly higher (p<0.0001, paired t test) than mean 32.7± 1.1°C ST for all combined B90 measurements (the last measurements in each groups (data not shown). The difference between baseline and final B90 ST was significant in the CELF group (p<0.0001, paired t test) but not in the PETF group.

In contrast to the fall in ST observed from beginning to end of

Subject	% Male	Age (years)	Heights (inches)	Weights (ibs)	BMI
All (n=153)	54.3	38.3 ± 12.3	67.4 ± 3.9	167.2 ± 42.9	25.7 ± 5.5
CELF (n=180)	62.5[a]	37.9 ± 12.1	67.5 ± 3.8	171.3 ± 43.5	26.2 ± 5.7
PETF (n=73)	45.2[a]	38.7 ± 12.6	67.2 ± 4.0	162.8 ± 40.3	25.0 ± 5.2

[a]p=0.047, chi-square.

Table 1: Subject demographics.

Subject	tcPO$_2$ (mmHg)	ST (°C)	%O$_2$Sat
All (n=153)	64.9 ± 18.5	33.1 ± 1.0	98.0 ± 1.3
Male (n=83)	60.2 ± 18.5[a]	33.3 ± 0.9[d]	97.6 ± 1.7[f]
Female (n=70)	70.3 ± 17.2[a]	32.9 ± 1.2[d]	98.5 ± 1.1[f]
CELF (n=80)	66.4 ± 18.9	33.1 ± 0.9	98.0 ± 1.0
CELF Male (n=50)	62.9 ± 18.1[b]	33.3 ± 0.8[e]	97.6 ± 1.9[g]
CELF Female (n=30)	70.7 ± 18.1[b]	32.6 ± 1.0[e]	98.5 ± 0.9[g]
PETF (n=73)	63.9 ± 18.8	33.2 ± 1.1	98.1 ± 1.3
PETF Male (n=33)	56.2 ± 18.6[c]	33.3 ± 1.1	97.5 ± 1.3[h]
PETF Female (n=40)	70.0 ± 16.7[c]	33.3 ± 1.1	98.5 ± 1.3[h]

[a]p=0.0008 [b]p=0.059 [c]p=0.003 [d]p=0.01 [e]p=0.0009 [f]p<0.001 [g]p=0.023 [h]p=0.003

Table 2: Baseline physiologic parameters.

	ST (°C)		
	Baseline	**CEL 90 minutes**	**PET 90 minutes**
All	33.1 ± 1.0	32.8 ± 1.0	32.6 ± 1.0
CELF	33.1 ± 1.0[a]	32.8 ± 1.0	32.4 ± 1.0a
PETF	33.2 ± 1.1[b]	32.9 ± 1.1b	32.8 ± 1.0
	%O$_2$ Sat		
	Baseline	**CEL 90 minutes**	**PET 90 minutes**
All	98.0 ± 1.3	98.5 ± 0.8[c]	98.2 ± 1.0[c]
CELF	97.9 ± 1.7[e]	98.5 ± 1.1 [e,f]	98.3 ± 1.0[f]
PETF	98.1 ± 1.3[d]	98.6 ± 0.8[d]	98.2 ± 1.2

[a]p<0.0001, paired t test [b]p=0.064, paired t test [c]p<0.0001 paired t test [d]p=0.0001, paired t test [e]p=0.0002, paired t test [f]p=0.003, paired t test

Table 3: Effects of Garments on ST and O₂Sat.

Figure 2: Combined tcPO₂ measurements for PET and CEL garments independent of donning sequence.

Figure 3: TcPO₂ measurements based on gender.

testing, O₂sat increased from beginning to end. Combining all subjects, the mean baseline O₂sat was 98.0 ± 1.3 compared to a mean value of 98.4 ± 0.9 for all B90 measurements (data not shown, p<0.0001, paired t test). Mean O₂sat for all subjects after wearing CEL 90 minutes was significantly higher than O₂sat for all subjects wearing PET 90 minutes (98.5 ± 0.8 vs. 98.2 ± 1.0, p<0.0001, paired t test). In PETF subjects, mean O₂sat was 98.1 ± 1.3 at baseline and increased insignificantly (p=0.30 paired t test) to 98.2 ± 1.2 after ninety minutes, and then increased further to 98.6 ± 0.8 after wearing CEL shirts for ninety minutes (p=0.0001, paired t test). In the CELF group, however, mean baseline O₂sat of 97.9±1.7 increased significantly to 98.5 ± 1.1 (p=0.0002, paired t test) after wearing CEL 90 minutes, then fell to 98.3 ± 1.0 after wearing PET 90 minutes (p=0.0033, paired t test) (Table 3).

Figure 2 shows tcPO₂ for all the subjects combined, independent of donning sequence. Plotted are mean tcPO₂ 30, 60, and 90 minutes after donning each garment-the baseline value is the mean for all subjects. At each interval tcPO₂ is significantly higher for CEL compared to controls (p ≤ 0.0003, paired t tests). At 30 minutes, the difference between CEL and PET tcPO₂ levels was 3.42 ± 11.29 mmHg (5.5%); at 60 minutes 4.30 ± 10.16 mmHg (6.4%); and at 90 minutes 4.44 ± 9.51 mmHg (6.7%). Each point represents the combined mean ± s.e.m tcPO₂ for all subjects at the specified time interval after establishment of stable tcPO₂ measurements after donning PET or CEL shirts (Figure 2).

Figure 3 shows the same analysis performed comparing female and male subjects' responses to PET and CEL-the same pattern was observed, but the differences in tcPO₂ levels based on garment worn were more pronounced in women. Each point represents mean values ± s.e.m combining data from one gender at the specified time interval after establishment of stable tcPO₂ measurements (Figure 3).

Figure 4 shows the results of separating tcPO₂ measurements based on donning sequence. The CELF and PETF baseline values are different. Mean tcPO₂ is plotted in the temporal sequence with
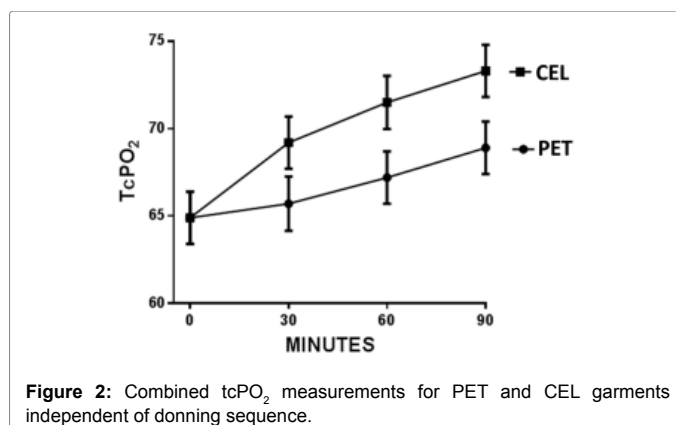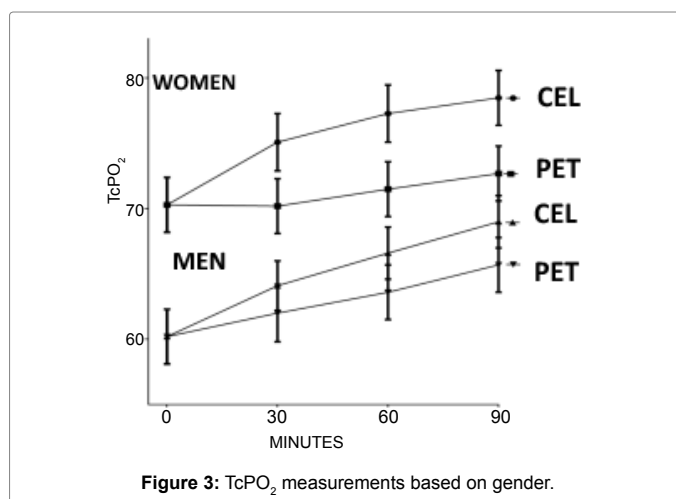
which it was measured. The PETF plot shows 30, 60, and 90 minute measurements obtained under PET shirts followed by 30, 60, and 90 minute measurements under CEL shirts. The plot for CELF subjects has the temporal sequence reversed: measurements obtained under CEL shirts are plotted before PET measurements. In the PETF group tcPO₂ rose from baseline through A90 and continued to increase after switching garments. In contrast, tcPO₂ levels in the CELF group increased through the A90 measurement but then fell after switching to PET. When the differences between tcPO₂ measurements at each time interval are separately compared within sequence groups, i.e., 30 minute tcPO₂ values for PET versus CEL in the CELF group, without inclusion of data from the PETF group and vice versa, two separate trends emerge. In the PETF group, differences between tcPO₂ levels under PET vs. CEL are highly significant (p<0.0001) for each 30-minute interval by paired t testing. In contrast, in the CELF group, differences in tcPO₂ between CEL and PET garments at 30 and 60 minutes are not significant, but approach significance at 90 minutes (p=0.051). Data from male and female subjects were combined and depicted in the sequence with which they were obtained (Figure 4).

When the same sequence analysis was applied to each gender, the same patterns were seen: tcPO₂ levels fell in both CELF male and female subjects after switching from CEL to PET shirts, but continued to increase in both male and female PETF subjects after switching from PET to CEL (data not shown).
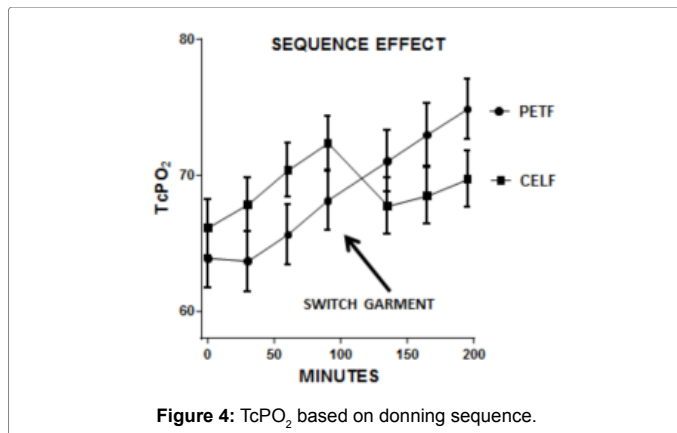
Figure 4: TcPO₂ based on donning sequence.

Discussion

This study measured changes in tcPO₂ at 30 minute intervals up to 90 minutes using Clark electrodes placed under either PET and CEL shirts which differed only by the presence or absence of ceramic particles in otherwise identical PET fibers. Subjects were randomized to wear either PET or CEL garments first. In general, tcPO₂ levels tended to increase while wearing either garment from baseline to end of the complete protocol. When tcPO₂ measurements were combined without reference to the sequence with which garments were worn, measurements under CEL garments were 5.5% higher at 30 minutes and 6.7% higher at 90 minutes (p<0.05). A different pattern of tcPO₂ measurements emerges, however, when tcPO₂ is plotted based on donning sequence (Figure 4). In subjects who wore CEL first, tcPO₂ fell immediately after switching to control PET garments, but the opposite result was seen in subjects who donned PET first--tcPO₂ continued to rise after switching to CEL. The sequence data support the conclusion that wearing CEL is associated with greater increases in tcPO₂ than PET, independent of donning sequence. Interestingly, the differences in tcPO2 measured at each interval between garments (e.g., mean A60 and mean B60 values) within the PETF group were significant, but not in the CELF group. This finding, in conjunction with the sequence pattern suggests that CEL effects might persist long enough to influence measurements taken after switching to PET. The 9.7% difference in mean tcPO2 levels between PET and CEL in the PETF group at 90 minutes (68.2 mmHg versus 74.9 mmHg) is comparable to results of the previous studies which employed that sequence.

CELF subjects had a mean baseline tcPO₂ that was 2.5 mmHg higher than mean for PETF baseline, but this alone should not skew this analysis as most comparisons are based on paired measurements of the same individual, as, for example, the results shown in Figure 2. As baseline measurements were obtained after subjects donned the first garment, the higher baseline in CELF subjects conceivably resulted from ceramic particles influencing tcPO₂ during the interval required to achieve stable measurements.

Another factor, the greater proportion of males to females in the CELF group versus PETF (62.5% vs. 45.2%) could have skewed the data analysis to show more of effects by CEL than is indeed the case, but as the men had lower baseline tcPO₂ levels, and showed a moderately lower response to CEL than women, this seems unlikely.

If ST or core temperatures were higher under CEL than PET, then differences in tcPO₂ might be due to heat induced vasodilation of the dermal microcirculation. Our study did not directly measure either core

temperature or ST directly under the shirts, but the ST measurements from the subject's uncovered forearm make this explanation seem unlikely-ST generally fell throughout the protocol while tcPO₂ generally rose. If temperature were the dominant factor influencing tcPO₂, the later should have fallen in parallel with ST. Further, tcPO₂ measurements entail heating skin to 44 °C, which should minimize the impact of variations in core or surface temperatures.

O₂sat measurements differed when data from both sequence groups were combined. Ninety minutes after wearing CEL, mean O₂sat was 98.5% for all subjects, significantly higher than the mean O₂sat of 98.2% measured 90 minutes after donning PET. The pattern of change in O₂sat with time in each group paralleled that observed with tcPO₂. In PETF subjects, baseline O₂sat rose slightly after 90 minutes of wearing PET, and then rose significantly more after 90 minutes wearing CEL With CELF subjects, baseline O₂sat increased significantly over 90 minutes while wearing CEL, and after switching garments decreased significantly over 90 minutes while wearing PET. The modest similarity in the kinetic patterns observed with O₂sat and tcPO₂ measurements suggests they might be the result of the same ceramic particle influence. This raises the question of what is the underlying mechanism for the tcPO₂ changes observed. Ceramic particles absorb heat (whether that be radiant, converted or conducted) emitted from the body, and then re-emit the thermal energy as IR (with a peak at 9.4 μm) back into the body. Re-emission occurs near the same wavelength as absorption, but may be at slightly a longer wavelength due to differences in temperature between the body and the fabric. This is not an energy neutral phenomenon, as the ceramics decrease the loss of infrared energy away from the body, those otherwise escapes through normal clothing.

The likely net result is increased absorption of FIR energy into the skin and underlying tissues. A recent study by scientists at Exponent Consulting compared the emissivity of PET fabric with or without CEL particles using sophisticated optical spectroscopic techniques. The intensity of infrared emission between 7.5 to 14 μm was 2.1% greater with fabric containing CEL particles (1.22% by weight) compared to fabric without ceramic particles [13]. This finding is consistent with the finding that the absorption co-efficient of the ceramic particles in the infrared spectrum was higher than the absorption co-efficient of pure PET fibers. In other words, the PET fibers are semi-transparent to infrared radiation, while the CEL particles are opaque. A follow-up study from the same group examined in more detail the influence of the ceramic particles on the infrared reflectance of the PET fabric, and measured the transmission, and absorption [14]. This analysis modeled the effects of the particles on infrared radiation incident upon the skin, as a function of wavelength, skin temperature, and ambient temperature, proportion of ceramic particles, air velocity, and influence of sunlight. The findings confirmed that the addition of ceramic particles to PET fabric leads to increased incidence of infrared radiation upon the skin at wavelengths longer than 4 μm, with a maximum effect at approximately 9.4 μm. The effect was attributed to increased absorption of infrared radiation at shorter wavelengths and reemission at longer wavelengths.

Increased emission of infrared from PET fibers with ceramic particles has the potential to interact with molecular and cellular structures by increasing the vibrational energy stored in chemical bonds, particularly in water clusters in cell membranes and cellular organelles. Perturbation of the vibrational energy of water clusters could affect the tertiary conformation of protein molecules tightly associated with this "nanostructured" water [15,16]. Low intensity far infrared (FIR-wavelength >14 um) lamps and topically applied (non-powered) FIR-emitting ceramic materials have been shown to induce cellular

changes in vitro, and produce physiologic changes in both preclinical animal models and clinical studies. In none of these studies were the effects associated with significant changes in temperature, consistent with the low power associated with both far infrared lamps and non-powered ceramics in thermal equilibrium with skin (on the order of 0.1-1 mW/cm^2 [3]. In vitro studies have found infrared radiation to inhibit cellular proliferation and be associated with increased reactive oxygen species; decreased production of intracellular nitric oxide and heat shock protein; inhibition of prostaglandin E2 synthesis; inhibition of kinase dependent nuclear signalling; and decreased production of inflammatory mediators and cell adhesion molecules [4,5,17-19].

Preclinical studies of infrared effects have shown inhibition of prostaglandin mediated inflammation in a rabbit arthritis model and delayed onset of muscle contraction induced fatigue [20]. Particular relevant to our findings are two reports in rats, one showing that infrared increased skin blood flow [21] and the other showed that infrared accelerated wound healing [7].

Three clinical studies have reported that blood flow was increased by infrared exposure from powered IR sources or non-powered ceramics [2,22,23] and one clinical study found alleviation of the symptoms of Raynaud's syndrome with ceramic impregnated gloves [24]. Other clinical studies with topically applied ceramic materials have demonstrated changes in body measurements (fat loss) [25,26], reduced dysmenorrhea [27], and improved lactation [28].

The increase in tcPO2 observed in this study likely is a consequence of increased oxygen availability in infrared illuminated tissue, possibly through a vasodilatory effect on the dermal circulation or, alternatively, effects on oxygen binding to hemoglobin. Although our understanding of the mechanism responsible for the effect of ceramic polyester composites on tcPO2 still incomplete, our data confirm that it is a real scientific phenomenon. Even without completely understanding the effect, it may be possible to design ceramic polyester composite garments or dressings that could improve wound healing, which is both sensitive to tissue perfusion and a critical problem for patients with diabetes. The recent decision by the US FDA that CEL garments will be regulated as medical devices and as general wellness products (http://www.medicaldevices-business-review.com/news/fda-determines-celliant-products-meet-criteria-as-medical-devices-260717-5882229) encourages clinical testing in multiple disease indications.

Conclusion

The present study has added to the body of evidence that suggest that FIR-emitting garments can exert real measurable physiological effects, and deserve further study for medical indications. Especially the potential for ceramic-embedded fabrics to improve skin and wound perfusion has particular relevance to diabetes and warrants further study.

Ethics Approval and Consent to Participate

Between October 2013 and January 2014, healthy volunteers aged 18 to 60 were recruited for an IRB approved protocol via on-line advertisement for subjects that were paid $25. The trial was registered at clinicaltrials.gov NCT02798640 (https://clinicaltrials.gov/ct2/show/NCT02798640). The protocol was in accordance with the Declaration of Helsinki and informed consent was obtained.

Consent to Publish

Not applicable, no identifying data

Availability of Data and Materials

The datasets generated and/or analyzed during the current study are not publicly available but are available from the corresponding authors on reasonable request.

Competing Interests

Funding

References

1. Tsai SR, Hamblin MR (2017) Biological effects and medical applications of infrared radiation. J Photochem Photobiol B 170: 197-207.

2. Inoue S, Kabaya M (1989) Biological activities caused by far-infrared radiation. Int J Biometeorol 33: 145-150.

3. Vatansever F, Hamblin MR (2012) Far infrared radiation (FIR): its biological effects and medical applications. Photonics Lasers Med 4: 255-266.

4. Lai CH, Leung TK, Peng CW, Chang KH, Lai MJ, et al. (2014) Effects of far-infrared irradiation on myofascial neck pain: a randomized, double-blind, placebo-controlled pilot study. J Altern Complement Med 20: 123-129.

5. Lai YT, Chan HL, Lin SH, Lin CC, Li SY, et al. (2017) Far-infrared ray patches relieve pain and improve skin sensitivity in myofascial pain syndrome: A double-blind randomized controlled study. Complement Ther Med 35: 127-132.

6. Lee CH, Roh JW, Lim CY, Hong JH, Lee JK, Min EG. (2011) A multicenter, randomized, double-blind, placebo-controlled trial evaluating the efficacy and safety of a far infrared-emitting sericite belt in patients with primary dysmenorrhea. Complement Ther Med 19: 187-193.

7. Toyokawa H, Matsui Y, Uhara J, Tsuchiya H, Teshima S, et al. (2003) Promotive effects of far-infrared ray on full-thickness skin wound healing in rats. Exp Biol Med (Maywood) 228: 724-729.

8. Loturco I, Abad CCC, Nakamura FY, Ramos SP, Kobal R, et al. (2016) Effects of far infrared rays emitting clothing on recovery after an intense plyometric exercise bout applied to elite soccer players: a randomized double-blind placebo-controlled trial. Biol Sport 33: 277-283.

9. Lima MV, Ochiai ME, Vieira KN, Scipioni A, Cardoso JN, et al. (2014) Thermal vasodilation using a portable infrared thermal blanket in decompensated heart failure. Int Heart J 55: 433-439.

10. Honda K, Inoue S (1988) Sleep-enhancing effects of far-infrared radiation in rats. Int J Biometeorol 32: 92-94.

11. Schnurer JH, Klein RM, Horinek DD (2004) Polymeric fiber composition and method U.P.U. B2, Editor.USA.

12. York RM, Gordon IL (2009) Effect of optically modified polyethylene terephthalate fiber socks on chronic foot pain. BMC Complement Altern Med 9: 10.

13. Pooley MA, et al. (2016) Engineered emissivity of textile fabrics by the inclusion of ceramic particles. Opt Express 24: 10556-10564.

14. Anderson, D.M., et al. (2017) Infrared radiative properties and thermal modeling of ceramic-embedded textile fabrics. Biomed Opt Express 8: 1698- 1711.

15. Pollack GH (2015) Water, Energy and Life: Fresh Views from the Water's Edge. Int J Des Nat Ecodyn 5: 27-29.

16. Martseniuk LS (2001) The Properties of Water Nanostructures in Nanosystems, in Nanoplasmonics, Nano-Optics, Nanocomposites, and Surface Studies O. Fesenko and L. Yatsenko, Editors. 2014, Springer: New York, P: 133-148.

17. Leung TK, Chen CH, Tsai SY, Hsiao G, Lee CM (2012) Effects of far infrared rays irradiated from ceramic material (BIOCERAMIC) on psychological stress-conditioned elevated heart rate, blood pressure, and oxidative stress-suppressed cardiac contractility. Chin J Physiol 55: 323-330.

18. Leung TK, Kuo CH, Lee CM, Kan NW, Hou CW (2013) Physiological effects of bioceramic material: harvard step, resting metabolic rate and treadmill running assessments. Chin J Physiol 56: 334-340.

19. Leung TK, Lee CM, Tsai SY, Chen YC, Chao JS (2011) A Pilot Study of Ceramic Powder Far-Infrared Ray Irradiation (cFIR) on Physiology: Observation of Cell Cultures and Amphibian Skeletal Muscle. Chin J Physiol 54: 247-54.

20. Leung TK, Chen CH, Lai CH, Lee CM, Chen CC, et al. (2012) Bone and joint protection ability of ceramic material with biological effects. Chin J Physiol 55: 47-54.

21. Yu SY, Chiu JH, Yang SD, Hsu YC, Lui WY, et al. (2006) Biological effect of far-infrared therapy on increasing skin microcirculation in rats. Photodermatol Photoimmunol Photomed 22: 78-86.

22. Lin CC, Liu XM, Peyton K, Wang H, Yang WC, et al. (2008) Far infrared therapy inhibits vascular endothelial inflammation via the induction of heme oxygenase-1. Arterioscler Thromb Vasc Biol 28: 739-45.

23. Yoo BH, Park CM, Oh TJ, Han SH, Kang HH, et al. (2002) Investigation of jewelry powders radiating far-infrared rays and the biological effects on human skin. J Cosmet Sci 53: 175-184.

24. Ko GD, Berbrayer D (2002) Effect of ceramic-impregnated "thermoflow" gloves on patients with Raynaud's syndrome: randomized, placebo-controlled study. Altern Med Rev 7: 328-335.

25. Conrado LA, Munin E (2011) Reduction in body measurements after use of a garment made with synthetic fibers embedded with ceramic nanoparticles. J Cosmet Dermatol 10: 30-35.

26. Conrado LA, Munin E (2013) Reductions in body measurements promoted by a garment containing ceramic nanoparticles: a 4-month follow-up study. J Cosmet Dermatol 12: 18-24.

27. Ke YM, Ou MC, Ho CK, Lin YS, Liu HY, et al. (2012) Effects of somatothermal far-infrared ray on primary dysmenorrhea: a pilot study. Evid Based Complement Alternat Med 2012: 240314.

28. Ogita S, Imanaka M, Matsuo S, Takebayashi T, Nakai Y, et al. (1990) Effects of far-infrared radiation on lactation. Ann Physiol Anthropol 9: 83-91.

The Test Report on the Impacts of Subject Socks with the Application of Celliant® Technical Fibers on Transcutaneous Oxygen Pressure on a Man's Foot

Dr. Li Shaojing, Wu Chuanhong, Gao Jian, Zhu Li and Wen Liwei

应用 Celliant®技术纤维的受试袜对人体足部经皮氧分压影响试验报告

The Test Report on the Impacts of Subject Socks with the Application of Celliant® Technical Fibers on Transcutaneous Oxygen Pressure on a Man's Foot

研究机构（盖章）：中国中医科学院中药研究所

Research Institution (Seal): Institute of Chinese Material Medical China Academy of Chinese Medical Sciences

研究机构地址：北京东直门内南小街 16 号

Address of the Research Institution: No. 16 Nanxiaojie, Dongzhimennei Ave, Beijing

主要研究者姓名（签字）：李韶菁

Main Researcher (Signature): LI Shaojing

主要研究者电话：010-64032656

Telephone Number of the Main Researcher: 010-64032656

研究参加者姓名：吴传鸿、高健、朱丽、文丽梅

Names of Other Researchers: Wu Chuanhong, Gao Jian, Zhu Li, and Wen Liwei

试验起止日期：2012 年 11 月 13 号-2012 年 11 月 24 号

Starting and Finishing Date of the Test: November 13th, 2012--November 24th, 2012

原始资料保存地点：中国中医科学院中药研究所

The Site of the Original Materials: Institute of Chinese Material Medical China Academy of Chinese Medical Sciences

一． 实验目的

1. The Purpose of the Test

通过对青岛新永国际贸易有限公司提供的应用 Celliant®技术纤维生产的袜子穿着前后对人体足背处局部经皮氧分压影响进行随机、双盲、对照的临床研究，对其改善人体局部微循环作用进行初步研究。

To do the preliminary study of the effects of socks that use Celliant® technical fibers provided by Qingdao ReY.S International Co., Ltd. on local transcutaneous Oxygen Pressure on human the foot dorsum through the clinical research before and after the wearing of the socks in a randomized, double-blind, and controlled way and on improving human body's local microcirculation.

二． 实验材料

2. Materials of the Test

应用 Celliant®技术纤维的袜子（简称，受试袜），对照袜（市售普通，无保健功能袜），医用胶带等。

Socks with the application of Celliant® technical fibers (for short: subjects socks), control socks (regular socks sold in the market with no health care function), medical tapes, etc.

三． 实验仪器和设备

3. Instruments and Equipment of the Test

单通道经皮氧分压／二氧化碳分压测定仪（PF5040 TcpO$_2$/pCO$_2$），帕瑞医学科技（北京）有限公司，型号：PeriFlux 5000.

Single-channel transcutaneous oxygen/ carbon dioxide partial pressure tester, (PF5040 TcpO$_2$/pCO$_2$), Perimed China LTD., Model: PeriFlux 5000.

四． 检测原理

4. Principle of the Detection

经皮氧分压/二氧化碳分压（TcpO$_2$/pCO$_2$)）测定仪原理：本技术采用克拉克电极，通过预设电热调节器，将温度保持在 37-45 。在 45 时，毛细血管血流动脉化。皮肤加热后，毛细血管扩张，氧离曲线右移，并允许氧气从皮肤扩散进入接触液。加热可以溶解死亡的上皮脂质层，改善气体透过皮肤的弥散性。已通过皮肤的氧气溶解在解除液中，然后降低到可测量的气流量。该气流量等于皮肤溢出的氧量，因此，测量接触液中的氧分压，相当于电极应用于皮肤 10-15 分钟后皮下组织中的氧分压。
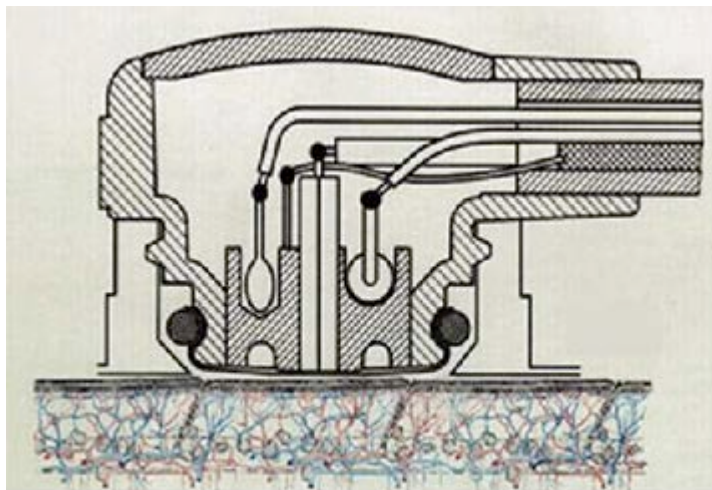
图1.经皮氧分压检测原理图

The principle of the transcutaneous oxygen/carbon dioxide partial pressure（TcpO$_2$/pCO$_2$)）tester: Through the preinstalled electric regulator, this technology uses Clark electrode to control the temperature at the 37 to 45 . At 45 , the blood flow of the capillary is arterialized. When the skin temperature rises, capillary expands and the oxygen dissociation curve moves towards the right side and the spread of oxygen from the skin into the contact liquid begins. Heating can dissolve the dead skins of epithelial lipid layer, and improve the dispersing of gas into skin. The passed oxygen dissolves into the contact liquid and then decreases the amount of measurable gas. The amount of the decreased gas equals the amount of oxygen that passes through the skin. Therefore, to test the oxygen partial pressure in contact liquid is to measure the oxygen partial pressure in subcutaneous tissue after using the Clark electrode to heat skin for ten to fifteen minutes.

测量传感器中加热部件将对传感器下的皮肤进行加热，从而使组织中毛细血管的血流量增加，其中运输的 O$_2$/pCO$_2$ 将透过皮肤表面被传感器接收。具体示意见图1。

The heating parts in the measuring sensors will heat the skin under the sensors,

which will increase the blood flow in capillary in the tissue and the passed O_2/pCO_2 through the skin will be absorbed by the sensors. Details are shown in Figure one.

五． 实验方法

5. Methods of the Test

（一）实验原则

(1) The testing principles

在参加本研究前，研究者将询问受试者的病史、健康状况等，如有需要，需进行体检和相关的实验室检查（如血常规、尿常规和血生化检查等），以确定受试者是否适合参加本研究。所有健康状态调查表和原始化验单将由检测机构保存。

Before the test, the researchers will ask participants about their medical history, heath conditions and so on. And if necessary, they are asked to do medical check-ups and other tests related to the research (such as blood routine, urine routine and blood biochemical inspection, etc.) to find out whether the participants are fit to participate in this research. All the investigation forms on health conditions and the original test reports will be kept by the research institution.

若受试者通过了相关的筛选，将在受试实验当天分别先后穿着对照袜和受试袜各一次，每次不超过 60 分钟，同时监测右侧足背处局部经皮氧分压的变化。

After the whole screening procedures, the participants will wear control socks and subjects socks once successively on the test day. The time for each is no more than 60 minutes and meanwhile the changes of local transcutaneous oxygen partial pressure at the right side of foot dorsum will be monitored.

1. 受试者入选标准

1. The criteria for qualified participants

男女各 50 人；

Fifty men and fifty women

年龄在 18-25 岁；

Ages are between eighteen and twenty-five

体重指数（BMI）在 19-24 之间，BMI＝体重（kg）/身高（m²）；

Body Mass Index (BMI) is between nineteen and twenty-four. BMI = weight

(kg)/ height (m^2)

无心、肝、肾、消化道、神经系统、精神异常及代谢异常等病史；

No medical history of heart, liver, kidney, alimentary canal, nerve system, mental disorder, and metabolic disorder, etc.

无药物或其他物质过敏史；

No drug or other substance allergy history

体格检查示血压、心率、呼吸状况正常；

Normal blood pressure, heart rate and breathing condition shown by the physical examinations.

受试前一年内实验室检查：血常规、尿常规、肝肾功能基本正常（肌酐、尿素氮不超过正常上限，ALT、AST 在正常上限 1.5 倍以内）；

The tests in the year before the research include: blood test and urine test. And the liver and kidney function is basically normal (creatinine and urea nitrogen does not exceed the normal limit and ALT and AST are within 1.5 times more than the normal limit).

无不良习惯及嗜好，试验前两周及试验期间未服用其他药物及含有酒精和咖啡因的饮料；

No bad habits or hobbies. And two weeks before the test and during the test, there is no taking of any drugs or drinks that contain alcohol or caffeine;

自愿参加试验并签署知情同意书。

Voluntarily participate in the test and sign the informed consent form.

2. 受试者排除标准

2. **The criteria for unqualified participants**

主要脏器有器质性病变（如肝、肾、心血管疾病，代谢异常，神经系统疾病及其它慢性疾病）；

The main organs have organic diseases (such as liver, kidney, cardiovascular disease, metabolic disorder, nerve system disease, and other chronic disease);

常出现头痛、头晕者；

Regular headache or dizziness

收缩压＞130mmHg 和/或舒张压＞90mmHg 者；

Systolic pressure＞130mmHg and/or diastolic pressure＞90mmHg;

有任何物质或皮肤过敏史者；

Persons allergic to substances or have skin allergies;

有出血性疾病或明显的出血体质者；

Hemorrhagic disease or bleeding disorders;

药物滥用者；

Drug abuse;

嗜烟、酒者；

Smoking or drinking alcohol;

半年内有严重疾病史；

Serious disease history within half a year;

近三个月内参加过献血者；

Donating blood within the last three months;

近三个月内参加过其他药物临床试验者；

Participating in clinical tests of other drugs within three months;

三天前至试验期间服用过其他任何药物者；

Persons who take any other drugs three days before and during the test;

HBV、HCV 抗原阳性者；

Positive to antigen of HBV and HCV;

HIV 抗体阳性者；

Positive to antibody of HIV;

（二）具体实验过程

(2) Detailed Procedure of the Test

符合筛选标准的受试者知情同意书后在签订完，休息 15-20min 待状态稳定后，进行体温、血压及心率的测量，并记录。

After the qualified participants have signed the consent form, they will rest for a period of 15 to 20 minutes until they are calm. Their temperature, blood pressure and heart rate will be tested and the test results will be recorded.

双盲情况下，受试者先后穿着对照袜和受试袜，进行右侧足背部局部经皮氧分压的监测各 45 分钟，两双袜子之间的实验检测间隔 15 分钟。对照袜监测结束后进行体温、血压及心率的再次检测，并记录。

On the double-blind test, the participants will wear control socks and subjects socks successively. The monitoring time for the local transcutaneous oxygen partial pressure at the right side of the foot dorsum is 45 minutes for each. The time between the monitoring of two kinds of socks should be 15 minutes. After the monitoring of control socks, the temperature, blood pressure, and heart rate of participants should be measured and recorded.

对照袜及受试袜监测完毕后，受试者休息 15 分钟后，进行最后一次体温、血压及心率的检测，并记录。

After the ending of the monitoring of the control socks and subjects socks, participants will rest 15 minutes and then their temperature, blood pressure and heart rate will be measured and recorded again.

（三）数据处理方法

(3) Data processing methods

受试者分别穿着对照袜或受试袜后，进行足背处同一部位局部经皮氧分压动态监测，监测时间均为 45 分钟，两种袜子均选取稳定状态下的数据平均值（图 2）作为数据分析用局部经皮氧分压值（单位 mmHg），采用单因素方差分析对数据进行统计分析。

To monitor the dynamics of local transcutaneous oxygen partial pressure at the same spot of foot dorsum when the participants wear control socks and subjects socks respectively for 45 minutes, then the average of data under the stable state of both kinds of socks (Figure 2) will be used. Local transcutaneous oxygen partial pressure value (unit mmHg) will be used for analysis and data will be analyzed by using single factor variance analysis.
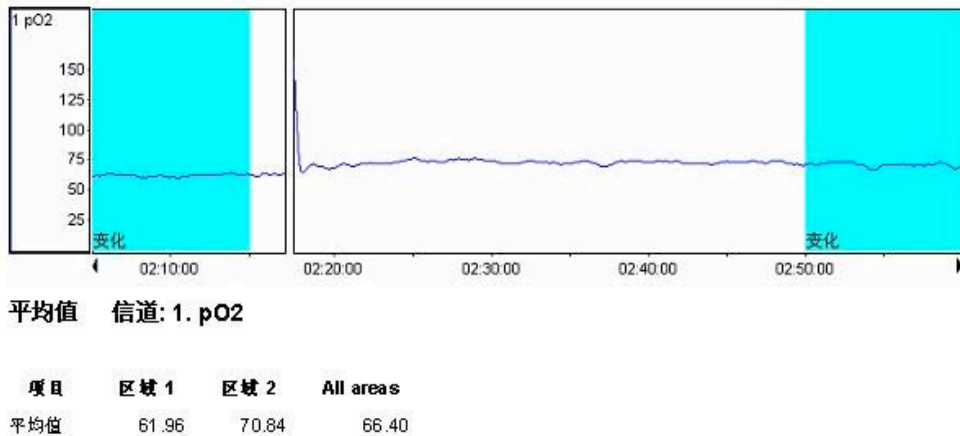
图 2 局部经皮氧分压动态数据采集示意图

Figure 2 The collecting of dynamic data of local transcutaneous oxygen partial pressure

区域 1 为对照袜稳态区域（图中时间点在前的有颜色标示区域），显示数值为此区域经皮氧分压动态数值的均值；区域 2 为受试袜稳态区域（图中时间点在后的另一段有颜色标示区域），显示数值为此区域经皮氧分压动态数值的均值。

Area one is the stable section of the control socks test (In the figure, the time before the stable section is marked with color.). The shown figure is the average of the dynamic values of local transcutaneous oxygen partial pressure of this area. Area two is the stable section of subjects socks test (In the figure, the time after the stable section is marked with color).The shown figure is the average of the dynamic values of local transcutaneous oxygen partial pressure of this area.

六． 实验结果

6. The Result of the Test

（一）受试袜及其对照袜对人体足背处局部经皮氧分压的影响

(1) The impacts of subjects socks and control socks on local transcutaneous oxygen partial pressure at foot dorsum

受试者穿着受试袜后，监测 45 分钟，足背处局部经皮氧分压为 (73.28±14.93)mmHg；受试者穿着对照袜后，监测 45 分钟，足背处局部经皮氧分压为（62.60±15.69）mmHg（表 1）。方差齐性检验知：两种袜子对人体足背处局部经皮氧分压的方差齐性（表 2）。进一步方差分析结果显示，受试袜与对照袜

相比，受试袜对人体足背处局部经皮氧分压的影响具有极显著差异（P＜0.01，表 3），可见受试袜与对照袜相比，在监测时间窗内，可更好的提高人体足背处经皮氧分压。

The participants wear subjects socks and then researchers monitor the local transcutaneous oxygen partial pressure at foot dorsum for 45 minutes. The result is (73.28±14.93)mmHg. The participants wear control socks and then researchers monitor the local transcutaneous oxygen partial pressure at foot dorsum for 45 minutes. The result is （62.60±15.69）mmHg (Table 1). Homogeneity of variance of local transcutaneous oxygen partial pressure at foot dorsum of two kinds of socks is shown (Table 2). Further variance analysis shows that compared with control socks, subjects socks' impacts on local transcutaneous oxygen partial pressure at foot dorsum has significant difference ($P < 0.01$, Table 3). This demonstrates that compared with control socks, subjects socks within the monitoring period, can better improve the local transcutaneous oxygen partial pressure at foot dorsum.

表 1.两种袜子对人体足背处局部经皮氧分压的数据描述

Table 1 The data of the local transcutaneous oxygen partial pressure at foot dorsum of two kinds of socks

组别	N	均值	标准差	标准误	均值的 95%置信区间	
					下限	上限
对照袜	100	62.60	15.69	1.57	59.49	65.72
受试袜	100	73.28	14.93	1.49	70.32	76.24
总数	200	67.94	16.19	1.14	65.68	70.20

Groups	N	Average value	Standard deviation	Standard Error	95% confidence interval of the mean	
					lower limit	Upper limit
Control socks	100	62.60	15.69	1.57	59.49	65.72
Subjects socks	100	73.28	14.93	1.49	70.32	76.24
total	200	67.94	16.19	1.14	65.68	70.20

表 2 两种袜子对人体足背处局部经皮氧分压的方差齐性检验

Table 2 Homogeneity of variance of local transcutaneous oxygen partial pressure at foot dorsum of two kinds of socks

Levene 统计量	df1	df2	显著性
0.454	1	198	0.501

Levene statistics	df1	df2	Significance
0.454	1	198	0.501

表 3 两种袜子对人体足背处局部经皮氧分压的单因素方差分析

Table 3 Single factor variance analysis of local transcutaneous oxygen partial pressure at foot dorsum of two kinds of socks

	平方和	df	均方	F	显著性
组间	5697.568	1	5697.568	24.284	0.000
组内	46455.626	198	234.624		
总数	52153.194	199			

	Sum of squares	df	Mean square	F	Significance
Among groups	5697.568	1	5697.568	24.284	0.000
Within groups	46455.626	198	234.624		
Total	52153.194	199			

（二）受试袜对于人体足背处局部经皮氧分压的影响是否存在性别差异的分析

(2) Whether there is gender difference of subjects socks' local transcutaneous oxygen partial pressure at foot dorsum

1.受试袜及对照袜对男性足背处局部经皮氧分压的影响

1. The impacts of two kinds of socks' local transcutaneous oxygen partial pressure at men's foot dorsum

表 4 数据显示，男性受试者穿着受试袜后，监测 45 分钟，足背处局部经皮

氧分压为 (72.06±15.73)mmHg；受试者穿着对照袜后，监测 45 分钟，足背处局部经皮氧分压为（61.65±16.65）mmHg。方差齐性检验知：两种袜子对男性足背处局部经皮氧分压的方差齐性（表 5）。进一步方差分析结果显示，受试袜与对照袜相比，其对于男性足背处局部经皮氧分压的影响具有极显著差异（P＜0.01，表6），可见受试袜与对照袜相比，可更好的提高男性足背处经皮氧分压。

Statistics in Table 4 shows that after the male participants wear subjects socks and then researchers monitor the local transcutaneous oxygen partial pressure at foot dorsum for 45 minutes, the result is(72.06±15.73)mmHg. After the male participants wear control socks and then researchers monitor the local transcutaneous oxygen partial pressure at foot dorsum for 45 minutes, the result is (61.65±16.65)mmHg. Homogeneity of variance of local transcutaneous oxygen partial pressure at men's foot dorsum of two kinds of socks is shown (Table 5). Further variance analysis shows that compared with control socks, the subjects socks' impacts on local transcutaneous oxygen partial pressure at men's foot dorsum has significant difference ($P＜0.01$, Table 6). It demonstrates that compared with control socks, subjects socks can better improve the local transcutaneous oxygen partial pressure at the men's foot dorsum.

表 4 两种袜子对男性足背处局部经皮氧分压影响的数据描述

Table 4 Statistics of the impacts of two kinds of socks' local transcutaneous oxygen partial pressure at men's foot dorsum

组别	N	均值	标准差	标准误	均值的 95% 置信区间	
					下限	上限
对照袜	50	61.65	16.65	2.35	56.92	66.38
受试袜	50	72.06	15.73	2.22	67.59	76.53
总数	100	66.85	16.94	1.69	63.49	70.22

Groups	N	Average value	Standard deviation	Standard Error	95% confidence interval of the mean

				lower limit	Upper limit
Control socks	50	61.65	16.65	2.35	56.92	66.38
Subjects socks	50	72.06	15.73	2.22	67.59	76.53
total	100	66.85	16.94	1.69	63.49	70.22

表 5 两种袜子对男性足背处局部经皮氧分压影响的方差齐性检验

Table 5 The homogeneity of variance test of the impacts of two kinds of socks' local transcutaneous oxygen partial pressure at men's foot dorsum

Levene 统计量	df1	df2	显著性
0.102	1	98	0.750

Levene statistics	df1	df2	**Significance**
0.102	1	98	0.750

表 6 两种袜子对男性足背处局部经皮氧分压的单因素方差分析

Table 6 single factor variance analysis of local transcutaneous oxygen partial pressure at men's foot dorsum of two kinds of socks

	平方和	df	**Mean square**	F	显著性
组间	2708.578	1	2708.578	10.326	0.002
组内	25705.992	98	262.306		
总数	28414.570	99			

	Sum of squares	df	Mean square	F	Significance
Among groups	2708.578	1	2708.578	10.326	0.002
Within groups	25705.992	98	262.306		

Total	28414.570	99	

3. 受试袜及对照袜对女性足背处局部经皮氧分压的影响

3. The impacts of two kinds of socks' local transcutaneous oxygen partial pressure at women's foot dorsum

表 7 数据显示，女性受试者穿着受试袜后，监测 45 分钟，足背处局部经皮氧分压为 (74.50±14.17)mmHg；受试者穿着对照袜后，监测 45 分钟，足背处局部经皮氧分压为（63.56±14.79）mmHg。方差齐性检验知：两种袜子对女性足背处局部经皮氧分压的方差齐性（表 8）。进一步方差分析结果显示，受试袜与对照袜相比，其对于女性足背处局部经皮氧分压的影响具有极显著差异（$P < 0.01$，表 9），可见受试袜与对照袜相比，也可更好的提高女性足背处经皮氧分压。

Statistics in Table 7 shows that after the female participants wear subjects socks and then researchers monitor the local transcutaneous oxygen partial pressure at foot dorsum for 45 minutes, the result is(74.50±14.17)mmHg. After the female participants wear control socks and then researchers monitor the local transcutaneous oxygen partial pressure at foot dorsum for 45 minutes, the result is (63.56±14.79)mmHg. Homogeneity of variance of local transcutaneous oxygen partial pressure at women's foot dorsum of two kinds of socks is shown (Table 8). Further variance analysis shows that compared with control socks, subjects socks' impacts on local transcutaneous oxygen partial pressure at women's foot dorsum has significant difference ($P < 0.01$, Table 9). It demonstrates that compared with control socks, subjects socks can better improve the local transcutaneous oxygen partial pressure at women's foot dorsum.

表 7 两种袜子对女性足背处局部经皮氧分压影响的数据描述

Table 7 Statistics of the impacts of two kinds of socks' local transcutaneous oxygen partial pressure at women's foot dorsum

组别	N	均值	标准差	标准误	均值的 95% 置信区间

					下限	上限
对照袜	50	63.56	14.79	2.09	59.36	67.76
受试袜	50	74.50	14.14	2.00	70.48	78.52
总数	100	69.03	15.41	1.54	65.97	72.09

Groups	N	Average value	Standard deviation	Standard Error	95% confidence interval of the mean	
					lower limit	Upper limit
Among groups	50	63.56	14.79	2.09	59.36	67.76
Within groups	50	74.50	14.14	2.00	70.48	78.52
Total	100	69.03	15.41	1.54	65.97	72.09

表 8 两种袜子对女性足背处局部经皮氧分压影响的方差齐性检验

Table 5 The homogeneity of variance test of the impacts of two kinds of socks' local transcutaneous oxygen partial pressure at women's foot dorsum

Levene 统计量	df1	df2	显著性
0.102	1	98	0.750

Levene statistics	df1	df2	Significance
0.102	1	98	0.750

表 9 两种袜子对女性足背处局部经皮氧分压的单因素方差分析

Table 6 Single factor variance analysis of local transcutaneous oxygen partial pressure at women's foot dorsum of two kinds of socks

	平方和	df	均方	F	显著性
组间	2992.528	1	2992.528	14.299	0.000

	Sum of squares	df	Mean square		
组内	20509.696	98	209.283		
总数	23502.223	99			

	Sum of squares	df	Mean square	F	Significance
Among groups	2992.528	1	2992.528	14.299	0.000
Within groups	20509.696	98	209.283		
Total	23502.223	99			

4. 两种袜子对男性及女性足背处局部经皮氧分压的影响

4. The impacts of two kinds of socks' local transcutaneous oxygen partial pressure at men's and women's foot dorsum

图 3 显示，虽然受试袜与对照袜相比，不论对于男性及女性，足背处局部经皮氧分压存在数值上的差异，但是男性和女性的数据统计并无显著性差异。提示受试袜对于人体的足背处局部经皮氧分压的影响，并无性别之间的差别。结果如图 4，受试袜对于男性及女性均可显著性提高其足背处局部经皮氧分压，但无性别差异。

Statistics in Figure 3 shows that although compared with control socks, there is difference of subjects socks' impacts on local transcutaneous oxygen partial pressure at men's or women's foot dorsum, however the difference between the impacts on men's and women's are not significant. It shows that there is no gender difference in the impacts of subjects socks' local transcutaneous oxygen partial pressure at men's or women's foot dorsum. As shown in Figure 4, subjects socks can significantly improve local transcutaneous oxygen partial pressure at both men's and women's foot dorsum, and there is no gender difference.
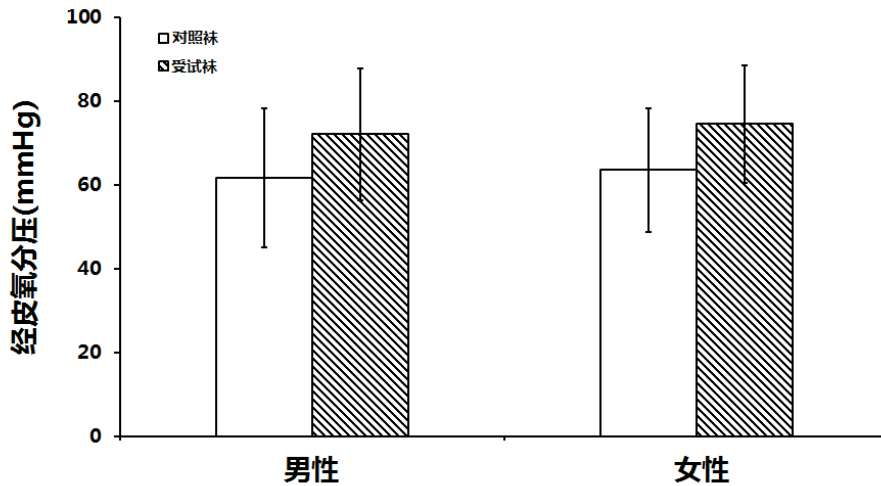
图 3 两种袜子对男性及女性足背处局部经皮氧分压差异性比较（n=50）

Figure 3 The comparison of difference between two kinds of socks' local transcutaneous oxygen partial pressure at men's and women's foot dorsum （n=50）
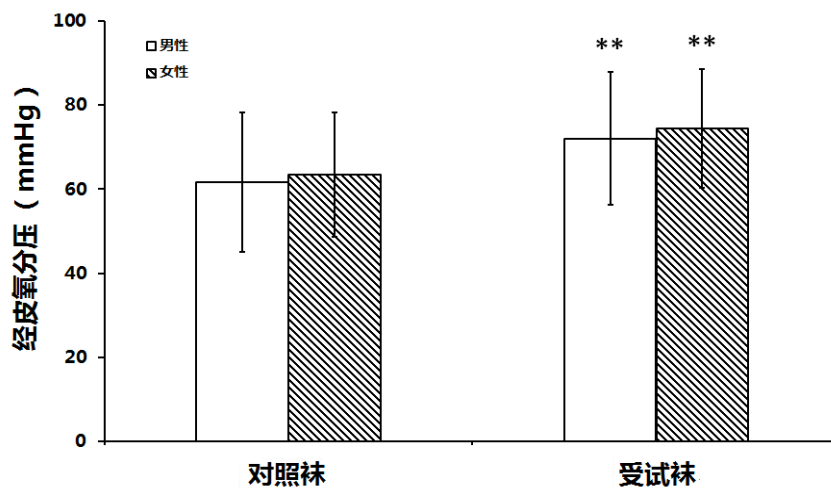
图 4 两种袜子对男性及女性足背处局部经皮氧分压的影响（n=50）

Figure 4 The impact of two kinds of socks' local transcutaneous oxygen partial pressure at men's and women's foot dorsum（n=50）

七． 讨论：

7. Discussion

经皮氧分压（$TcpO_2$）检测是一项能够反映毛细血管营养血流的技术。从 19

世纪 70 年代以来已经成为非侵袭性微循环血流的经典评价方法之一[1]，其能很好反映出下肢血管尤其踝以下皮肤微循环状态，进而反映周围动脉灌注情况，是一种操作简单，无创性的微血管病变检测的重要手段[2]。已有文献报道，相关的保健品如外用剂，涂抹剂，穿着材料等可通过微循环的改善作用来进行相关的保健评价[3]，而经皮氧分压可较好地反映局部微循环状态。本研究采用帕瑞医学 PeriFlux 5000 型单通道经皮氧分压／二氧化碳分压测定仪（PF5040 TcpO₂/pCO₂）对**青岛新永国际贸易有限公司**提供的应用 celliant®技术纤维的功能性受试袜穿着前后人体足部经皮氧分压进行检测，对其改善人体局部微循环作用进行初步探讨。

The measuring of transcutaneous oxygen partial pressure （TcpO₂） is a technology to reflect capillary's blood flow. Since the1870s, it has become one of classic methods to evaluate noninvasive blood microcirculation. It can well reflect the microcirculation state of lower limb blood vessel especially that of the skin beneath the ankle, which further reflects the peripheral artery perfusion situation. It is an important method that is easy to operate and has no invasive diagnosis at detecting capillaries. And there are documents which show that relative health-care products like topical agent, daub agent, dress materials and others can fulfill their function by improving micro circulation and transcutaneous oxygen partial pressure can relatively well reflect the local microcirculation state. This research uses a single-channel transcutaneous oxygen/carbon dioxide partial pressure tester, (PF5040 TcpO₂/pCO₂), model of PeriFlux 5000, generated by Perimed China Ltd to test the impacts on local transcutaneous oxygen partial pressure at the foot dorsum of subjects socks that adopts Celliant® technical fibers provided by **Qingdao ReY.S International Co.** before and after wearing them. The purpose of the preliminary research of Celliant® socks' is to improve the human body's local microcirculation.

微循环是指微动脉和微静脉之间的血液循环，是细胞供氧和排除废物的唯一通道[4]，是循环系统中最基本的结构和功能单位。人体单纯靠心脏的收缩力量不能将血液直接灌注到人体各器官的组织细胞，必需靠微循环部分的毛细血管不与心脏跳动同步的自律运动将血液进行第二次调节及第二次灌注，所以在医学上

把微循环比喻为人体的第二心脏[5]。

Microcirculation refers to the blood circulation between the arterioles and micro vein. It is the only channel[4] through which cells provide oxygen and eliminates waste and is the basic structural and functional unit in the microcirculation system. Only by cardiac contraction, the human body can't directly pour blood into cells of all organs of the body. It has to rely on the asynchronous (with the heart beat) self- discipline movement of capillaries of microcirculation part to adjust or pour the blood into organs for the second time. Therefore, in the medicine field, microcirculation is compared to the second heart[5] of the human body.

随着运动负荷加大的过程，微循环流速变缓，代谢产物（乳酸、尿素氮、肌酸、破碎细胞残片等）滞留，渗透压上升[6]，局部水肿（如大强度训练导致的小腿围度增加、肢端水肿）。由于微循环与人体各个部位的不可分割性，在不同的器官中微循环以其最小单元保持着与各器官的一致性。当疲劳程度进一步增加时，微循环代谢的迟滞使代谢产物不能及时从体内排除，电解质发生紊乱[7]，滞留组织的毒素会影响到中枢器官心、脑、肺、肾以及运动神经系统，使之出现灵敏度下降、反应迟滞、体能下降等疲劳现象。人体在微循环功能状态失常的情况下进行运动，会加速机体运动性疲劳的形成，微循环结构遭到破坏，容易导致微循环状态失常，运动性疲劳形成运动损伤[8]。微循环本身运行不受心脏能量控制，不受心率影响，但它随时可以作用于人体的健康状态，轻则影响局部组织和器官健康，如缺氧引起的肢端紫绀。当内环境持续高温，渗透压升高，毛细血管通透性增高可以促进渗出，发生在心包会压迫心脏，喉头水肿会导致窒息，严重微循环障碍甚至可以发生休克、昏迷甚至死亡。

With the increase of exercise load, the velocity of microcirculation slows, metabolites (lactic acid, urea nitrogen, creatine, segments of cells and others) accumulate, osmotic pressure rises[6], and local edema appears (such as increase of crus's girth, and acra edema brought by intensive training). Because of the integrity of microcirculation and the organs of the body, microcirculation maintains its uniformity with organs in the form of its smallest units. When the degree of tiredness further increases, the slowing of microcirculation can't eliminate metabolic wastes out of the body in a timely manner, electrolyte disorder occurs[7], and the accumulated toxin will

negatively affect the central organs, heart, brain, lung, kidney and motor nerve system, which leads to decreased sensitivity, lagged response, declined physical strength and tiredness, etc. If the human body exercises under the situation of microcirculation's abnormal state, it will accelerate the body's tiredness, damage the microcirculation structure, easily cause the abnormal microcirculation state, and lead to exercise injuries[8]. Although microcirculation itself is under no influence of the heart's energy and heart rate, it can affect the body's heath anytime. To a lower degree of damage, it affects the health of local tissue and organs, like acra cyanosis due to the lack of oxygen. When the inner temperature remains high, osmotic pressure rises. And the increase of capillary's permeability can facilitate the seepage. If it occurs at the pericardial area, it will press the heart and laryngeal edema will lead to suffocation. And the serious microcirculation malfunction will even lead to shock, coma and even death.

通过随机、双盲、对照的临床实验研究表明，应用celliant®技术纤维的功能性受试袜与对照袜相比，可显著性提高安静状态下人体足背处局部经皮氧分压，并且无男女性别的差异。这提示此受试袜可能促进人体足背处局部的微循环，进而对人体产生保健作用。与此同时，大量文献报道，微循环的改善有助于促进正常人体组织营养物质的供应和代谢产物的交换，有助于提高体能，恢复疲劳，强健身体[9]。这也提示应用celliant®技术纤维的功能性受试袜有可能促进人体疲劳的恢复，但这一结论还需要进一步的实验加以验证。

After the research done in a randomized, double-blind, and controlled way, it shows that compared with control socks, subjects socks adopting Celliant® technical fibers can significantly improve local transcutaneous oxygen partial pressure at the foot dorsum in a stable state, and there is no gender difference. This shows that this kind of subjects socks may improve the local microcirculation at the foot dorsum and thus fulfill their health care function for the human bodies. Meanwhile, much literature shows that the improvement of microcirculation is helpful to promote the nutrient supply and the exchange of metabolic products of normal human bodies, improve physical strength, alleviate tiredness, and strengthen the body. And this also implies that functional subjects socks adopting Celliant® technical fibers may be helpful for

the recovery of the body from tiredness. However, this waits for further testing.

参考文献：

[1]董雪红，胡仁明.微循环功能的检测方法及其在糖尿病中的应用[J].国际内科学杂志. 2009, 36(4): 196-210.

[1]Dong Xuehong, and Hu Renming, Evaluation of the microcirculation and its clinical applications in diabetes mellitus[J], International Journal of Internal Medicine.2009, 36(4): 196-210

[2]王芳，李素梅.经皮氧分压测定在糖尿病足病中的临床应用[J]. 临床医学与护理研究.2010, 9(3):18-19.

[2]Wang, Fang and Li Sumei, Clinical Use of Transcutaneous Oxygen Pressure Measurement in Diabetic Foot[J].Clinical Medicine and Nursing Research. 2010, 9(3): 18-19

[3]刘育英.微循环检测对保健纺织品作用的评价[C].第三届功能性纺织品及纳米技术应用研讨会论文集.北京 2003: 97-99.

[3]Liu Yuying, The evaluation of microcirculation detection on the function of health-care textiles[C]. The Paper Collection of the 3rd Conference on the Application of Functional Textiles and Nanometer Technology. Beijing 2003: 97-99

[4]Mader SS. Human anatomy and physiology[M]. Wm. C. Brown publishers 1991: 216-219.

[5]Nase GP. Modulation of sympathetic constriction by the arteriolar endothelium does not involve the cyclooxygenase pathway[J]. Int J microcirc.1997, 17:41.

[6]Tortora CJ. Principles of anatomy and physiology [M].7th ed.Harper Collins college publishers. 1993: 624-628.

[7] Arthur C. Overview of the circulation, and medical physics of pressure, flow, and resistance. In guyeon AC: Textbook of medical physiology[M].8th ed. Saunders Philadelphia. 1991:150-155.

[8]梁静群，梁敬军.人体肢端微循环改善对于体能恢复作用研究[J].军事体育进修

学院学报. 2011, 30 (2): 116-119.

[8]Liang Jingqun, and Ling Jingjun, The research of the impact of improving the acra's microcirculation on physical recovery[J]. Junshi Tiyu Jinxiu Xueyuan Xuebao, 2011, 30(2): 116-119

[9]赵克森，朱佐江，黄绪亮. 微元生化纤维（天年素纤维）——一种改善微循环的新途径[C].中国国际保健博览会第四届中国国际保健节论文集, 2004:69-72.

[9]Zhao Kesen, Zhu Zuojiang and Huang Xuliang, Infinitesimal biochemical fiber (Natural fiber) - a new way to improve microcirculation[C]. The Paper Collection of the 4th China Health Care Fair China International Healthcare Expo. 2004:69-72

附表 1：受试者穿着两种袜子足背处局部经皮氧分压数值。

Attached table 1 Statistics of two kinds of socks' local transcutaneous oxygen partial pressure at the foot dorsum

受试者	经皮氧分压（mmHg）	
	对照袜	保健袜
男 1	61.96	70.84
男 2	61.96	70.84
男 3	82.23	89.80
男 4	55.46	66.41
男 5	55.46	66.41
男 6	55.96	71.48
男 7	94.45	102.16
男 8	74.98	81.90
男 9	51.79	54.14
男 10	60.37	68.16
男 11	75.35	91.23
男 12	74.44	77.67
男 13	68.31	79.83
男 14	61.76	75.00
男 15	87.04	88.88
男 16	20.34	28.99
男 17	45.03	52.10
男 18	72.89	77.49
男 19	54.23	88.50
男 20	43.71	51.69
男 21	89.86	92.15

男 22	30.57	39.95
男 23	86.13	90.31
男 24	62.78	68.46
男 25	34.12	48.75
男 26	78.21	110.67
男 27	74.11	82.15
男 28	79.04	86.45
男 29	62.69	72.92
男 30	49.96	57.42
男 31	77.03	89.04
男 32	62.91	66.63
男 33	61.07	73.94
男 34	71.51	82.96
男 35	62.23	73.47
男 36	66.90	76.41
男 37	36.24	66.17
男 38	56.20	72.76
男 39	66.70	75.96
男 40	31.07	53.22
男 41	56.11	63.21
男 42	23.05	46.08
男 43	58.44	59.21
男 44	57.07	64.88
男 45	67.74	82.70
男 46	71.04	71.74
男 47	71.61	77.97
男 48	63.72	74.54
男 49	72.05	75.73
男 50	44.60	53.55
女 1	51.23	66.74
女 2	23.59	43.67
女 3	77.67	104.09
女 4	43.08	62.73
女 5	59.09	59.27
女 6	52.43	58.85
女 7	77.62	87.22
女 8	40.36	47.54
女 9	81.28	83.22
女 10	83.12	107.13
女 11	50.08	90.62
女 12	58.35	69.55
女 13	60.92	61.14
女 14	60.92	61.14
女 15	74.61	79.80

女 16	74.61	79.80
女 17	77.91	81.54
女 18	79.52	82.02
女 19	68.65	72.30
女 20	58.95	72.52
女 21	56.21	67.17
女 22	56.21	67.17
女 23	50.82	65.69
女 24	74.12	83.87
女 25	64.98	73.80
女 26	58.97	64.33
女 27	75.91	81.59
女 28	71.37	80.17
女 29	42.46	76.76
女 30	76.51	84.36
女 31	93.71	97.99
女 32	61.40	68.83
女 33	93.71	97.99
女 34	67.06	73.86
女 35	51.67	73.30
女 36	48.70	64.07
女 37	56.80	68.06
女 38	35.17	35.29
女 39	58.64	71.97
女 40	65.18	75.25
女 41	72.52	83.62
女 42	68.65	96.98
女 43	54.46	62.03
女 44	70.10	81.39
女 45	79.25	84.27
女 46	62.34	66.95
女 47	38.99	72.88
女 48	75.37	79.19
女 49	62.78	71.71
女 50	79.85	83.51

Participants	transcutaneous oxygen partial pressure（mmHg）	
	control socks	subjects socks/ health -care socks
Male 1	61.96	70.84
Male 2	61.96	70.84
Male 3	82.23	89.80

Male 4	55.46	66.41
Male 5	55.46	66.41
Male 6	55.96	71.48
Male 7	94.45	102.16
Male 8	74.98	81.90
Male 9	51.79	54.14
Male 10	60.37	68.16
Male 11	75.35	91.23
Male 12	74.44	77.67
Male 13	68.31	79.83
Male 14	61.76	75.00
Male 15	87.04	88.88
Male 16	20.34	28.99
Male 17	45.03	52.10
Male 18	72.89	77.49
Male 19	54.23	88.50
Male 20	43.71	51.69
Male 21	89.86	92.15
Male 22	30.57	39.95
Male 23	86.13	90.31
Male 24	62.78	68.46
Male 25	34.12	48.75
Male 26	78.21	110.67
male 27	74.11	82.15
Male 28	79.04	86.45
Male 29	62.69	72.92
Male 30	49.96	57.42
Male 31	77.03	89.04
Male 32	62.91	66.63
Male 33	61.07	73.94
Male 34	71.51	82.96
Male 35	62.23	73.47
Male 36	66.90	76.41
Male 37	36.24	66.17
Male 38	56.20	72.76
Male 39	66.70	75.96
Male 40	31.07	53.22
Male 41	56.11	63.21
Male 42	23.05	46.08
Male 43	58.44	59.21
Male 44	57.07	64.88
Male 45	67.74	82.70
Male 46	71.04	71.74
Male 47	71.61	77.97

Male 48	63.72	74.54
Male 49	72.05	75.73
Male 50	44.60	53.55
Female 1	51.23	66.74
Female 2	23.59	43.67
Female 3	77.67	104.09
Female 4	43.08	62.73
Female 5	59.09	59.27
Female 6	52.43	58.85
Female 7	77.62	87.22
Female 8	40.36	47.54
Female 9	81.28	83.22
Female 10	83.12	107.13
Female 11	50.08	90.62
Female 12	58.35	69.55
Female 13	60.92	61.14
Female 14	60.92	61.14
Female 15	74.61	79.80
Female 16	74.61	79.80
Female 17	77.91	81.54
Female 18	79.52	82.02
Female 19	68.65	72.30
Female 20	58.95	72.52
Female 21	56.21	67.17
Female 22	56.21	67.17
Female 23	50.82	65.69
Female 24	74.12	83.87
Female 25	64.98	73.80
Female 26	58.97	64.33
Female 27	75.91	81.59
Female 28	71.37	80.17
Female 29	42.46	76.76
Female 30	76.51	84.36
Female 31	93.71	97.99
Female 32	61.40	68.83
Female 33	93.71	97.99
Female 34	67.06	73.86
Female 35	51.67	73.30
Female 36	48.70	64.07
Female 37	56.80	68.06
Female 38	35.17	35.29
Female 39	58.64	71.97
Female 40	65.18	75.25
Female 41	72.52	83.62

Female 42	68.65	96.98
Female 43	54.46	62.03
Female 44	70.10	81.39
Female 45	79.25	84.27
Female 46	62.34	66.95
Female 47	38.99	72.88
Female 48	75.37	79.19
Female 49	62.78	71.71
Female 50	79.85	83.51

Transcutaneous Partial Pressure of Oxygen (tcPO2) as a Primary Endpoint to Assess the Efficacy of Celliant® as a Vasoactive Material

Dr. Ian Gordon and Dr. Michael Coyle

Transcutaneous Partial Pressure of Oxygen (tcPO$_2$) as a Primary Endpoint to Assess the Efficacy of Celliant® as a Vasoactive Material

INTRODUCTION

Celliant® technology is a patented process for adding micron sized optically active quartz, silicon oxide and titanium oxide particles to polymer fibers. The resulting Celliant® yarns have unique effects on the electromagnetic energy environment of the skin in the visible and near infrared portion of the spectrum leading to increased blood flow and oxygen levels in the tissue.

This report is a summary of data collected under the auspices of Ian Gordon, M.D., Ph.D., Associate Clinical Professor of Surgery at the University of California- Irvine Medical School. Fifty-one (51) healthy men and women were enrolled in the study. This study was a within subjects trial, which is noted for its ability to control for individual differences among subjects. Since each subject is assessed under each level of the independent variable or condition, the subjects serve as their own control, with the result that one of the largest sources of between treatment differences, inter-subject variation, is controlled (Keppel, 1991; Lindquist, 1953).

In the medical sciences, statistical significance levels are stated, *a. priori*, to know whether or not the treatment was efficacious relative to the control or baseline. A stringent statistical significance level (alpha = 0.05) is typically chosen so that if the study were to be reproduced, one would get the exact same results 95 times out of 100. Therefore, a p-value of _less_ than 0.05 is perfunctory to meet this requirement. This represents a reasonable and realistic value for research in the medical and biological sciences (Cohen, 1965, 1977) and suggests that the likelihood is decent that a treatment effect will be detected, assuming a modest effect size (Chase & Tucker, 1976).

OBJECTIVES

The objective of this pilot study was to test the null hypothesis that a novel, optically active garment made with Celliant® (CL) material would not influence mean $tcPO_2$ over a 90-min period differently than when compared to a baseline (BL) period of the same duration (90-min).

PRIMARY ENDPOINT

The primary endpoint in this study was transcutaneous partial pressure of oxygen (tcPO2), measured in units of mmHg, which was used to assess treatment efficacy. This endpoint has been

used in numerous clinical trials and is a well-accepted clinical measure for tissue perfusion and oxygenation (Burgess, Matsen, Wyss, & Simmons, 1982; Dooley, Schirmer, Slade, & Folden, 1996; Franzeck, Talke, Bernstein, Golbranson, & Fronek, 1982; Hanna et al., 1997; Jaszczak, 1988; Le Devehat & Khodabandehlou, 1990; Le Devehat, Khodabandehlou, & Vimeux, 2001; Matsen, Bach, Wyss, & Simmons, 1980; Matsen et al., 1980; Matsi, Manninen, Suhonen, Pirinen, & Soimakallio, 1993; Shoemaker & Vidyasagar, 1981; White et al., 1982) with well established norms for intra-subject variability (Coleman, Dowd, & Bentley, 1986; Wagener & Hendricker, 1987)

MATERIALS AND METHODS

Subjects

Fifty-one (51) heathy men and women enrolled in the study (37 men; age 33.4 yrs (SD 9.3) and 14 women; age 37.2 yrs (SD 7.7). Subjects known to be active smokers (Fewings, Rand, Scroop, & Whelan, 1966; Mayhan & Patel, 1997) or engaged in recreational drug use for the six months prior to the start of the study were excluded. Patients were postprandial two (2) hours and refrained from alcohol ingestion (Altura & Altura, 1982; Fewings, Hanna, Walsh, & Whelan, 1966) within forty-eight (48) hours and caffeine ingestion (Umemura et al., 2006) within four (4) hours prior to testing.

Methods

Skin Preparation. Preparation of the subject was standardized to the following: the hair was shaved from the bicep of dominant arm; the dermis was then abraded with a fine abrasive material; the stratum corneum was then removed by the use of light weight adhesive tape; and finally, the probe site was wiped with an alcohol preparation swab.

Measurement of transcutaneous oxygen (tcPO$_2$). Subjects were seated in a comfortable chair. Room temperature was maintained at a constant temperature over the duration of the study. Baseline measurements (BL) of tcPO$_2$ were recorded for ninety (90) minutes at the bicep. During this time, the subject wore a standard shirt. After the baseline period, subjects donned a Celliant® shirt and subsequent measurements of tcPO$_2$ were recorded at the bicep for ninety (90) minutes. Transcutaneous partial pressure of oxygen (tcPO$_2$) data points were taken at t=10-min,

30-min and 90-min during BL and with CL. All measurements of transcutaneous oxygen tension were recorded using a PeriFlux System 5000 (Perimed, Inc., Kings Park, NY, USA) and modified Clarke Electrodes (Radiometer America, Inc., Ohio, USA). Data were sampled using Perisoft Version 2.10 (Perimed America, Inc., North Royalton, Ohio, USA).

All subjects received the same treatment in the same order: Baseline (BL) followed by Celliant® (CL). Transcutaneous oxygen tension ($tcPO_2$) does not vary significantly over time, therefore, establishing a baseline prior to measuring a treatment effect was warranted.

STATISTICAL ANALYSES

Continuous variables are summarized with standard descriptive statistics including means, standard deviations (SD) and 95% confidence intervals (95% CI). Inferential analyses were conducted using two-way repeated measures analyses of variance (ANOVA). All data were analyzed using SPSS (IBM, 2011). Statistical significance for this study was set at alpha = 0.05. Thus, a p-value < 0.05 was necessary to be considered statistically significant.

An analysis of the entire data set identified four (4) missing data points (three (3) data points from the Celliant® condition and one (1) data point from the Baseline condition). This resulted in a data set equal to 98.7% of the total expected data.

Multiple analyses were executed to evaluate the data. At the highest level, to evaluate whether or not the primary efficacy variable was sensitive enough to detect a difference between the Baseline and the Celliant® conditions, a one-way ANOVA was employed to test the means. The Celliant® treatment was statistically greater than the Baseline after ninety (90-min) (CL = 81.5 mmHg (SD 14.5), 95% CI [79.1, 83.7]; BL = 76.6 mmHg (SD 14.1), 95% CI [74.3, 78.9], $F(1, 294) = 8.602$, p. = 0.004. This represented a mean percent change from Baseline of seven percent (7%).

Figure 1 demonstrates the mean treatment difference between Celliant® and Baseline, as defined by the primary efficacy variable, $tcPO_2$, over the ninety (90) minute measurement period.

Figure 1. Difference in Treatments as Measured by tcPO2

Error Bars: 95% CI

* p. = 0.004
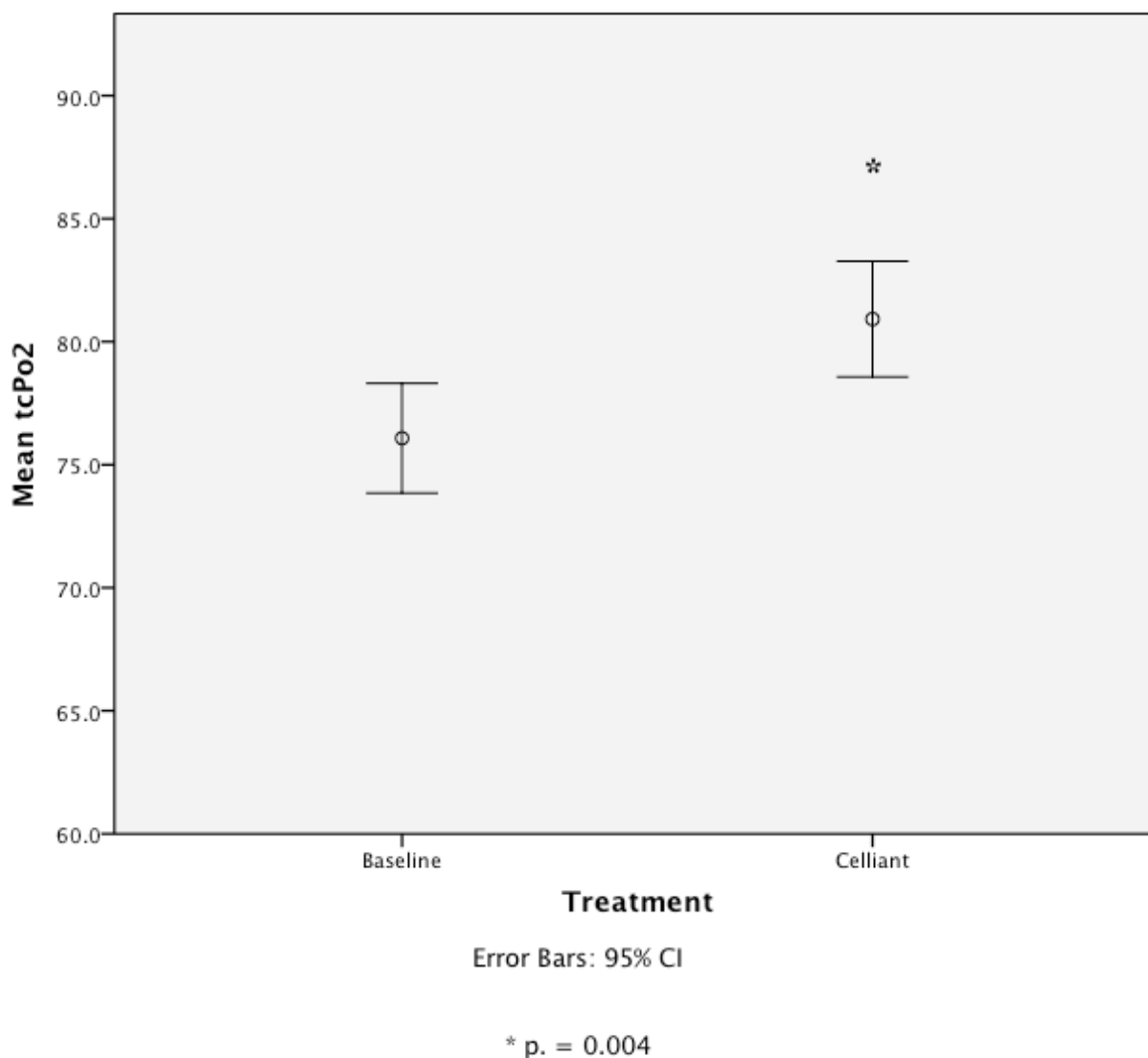
A two-way Repeated Measures ANOVA was employed to evaluate the influence of treatment at the different time points. The interaction between Condition (BL & CL) and Time was not significant (($F_{(1, 45)}$ = 0.012, p. = 0.914). However, there was a significant within subject contrast for Time ($F_{(1, 45)}$ = 7.423), p. = 0.009). Pairwise comparisons were conducted using dependent sample t-tests to evaluate the differences between the means to identify statistical differences between specific time points. At all time points, the Celliant® condition was statistically greater than the Baseline as assessed by two-tailed, paired t-tests and corresponded to

a mean change from the Baseline condition of seven percent (7%). See Table 1 for a summary of these data.

Table 1. Summary of Two-tailed Paired *t*-tests vs. Time

Time	Mean CL tcPO2 mmHg	Mean BL tcPO2 mmHg	*t* statistic	d.f.	P-value
10-min	80.3	76.1	-2.60	50	0.012
30-min	80.7	75.9	-3.14	50	0.003
90-min	83.8	78.6	-3.22	46	0.002

To be certain that mean tcPO$_2$ did not significantly increase over time during the Baseline, as well as to show that the Baseline did not influence the Celliant® condition, a two-tailed paired *t*-test was executed in the Baseline condition between t=10-min (76.2 mmHg (SD 14.2)) and t=90-min (77.8 mmHg (SD 14.1), *t*(49) = -1.18, p. = 0.242. Figure 2 shows the difference in treatment means graphically.

Figure 2. Mean tcPO2 by Condition Over Time

Error Bars: 95% CI
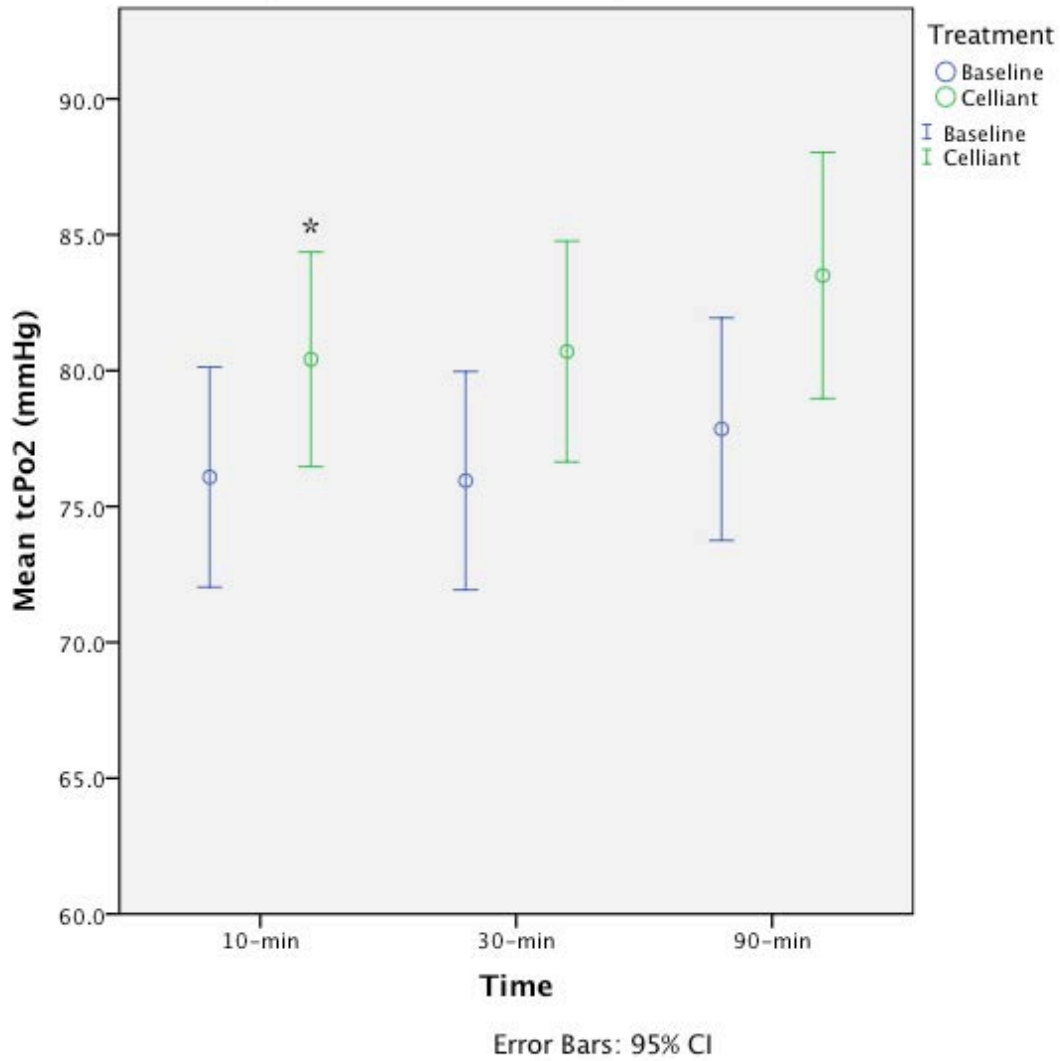
* At all time points, Celliant was statistically greater than Baseline. See Table 1 for p values.

A boxplot of the treatment means (Figure 3) is helpful to identify skewed data. The median is the line in the middle of the box; the upper edge of the box is the 75th percentile and the lower edge is the 25th percentile. The ends of the vertical bars or "whiskers" indicate the minimum and maximum data values. A datum outside the whiskers is an outlier, in this case there were none (McGill, Tukey, & Larsen, 1978). This graphic suggests that these data show good symmetry and are not skewed.

Figure 3. Distribution of tcPO2 values Between Baseline & Celliant
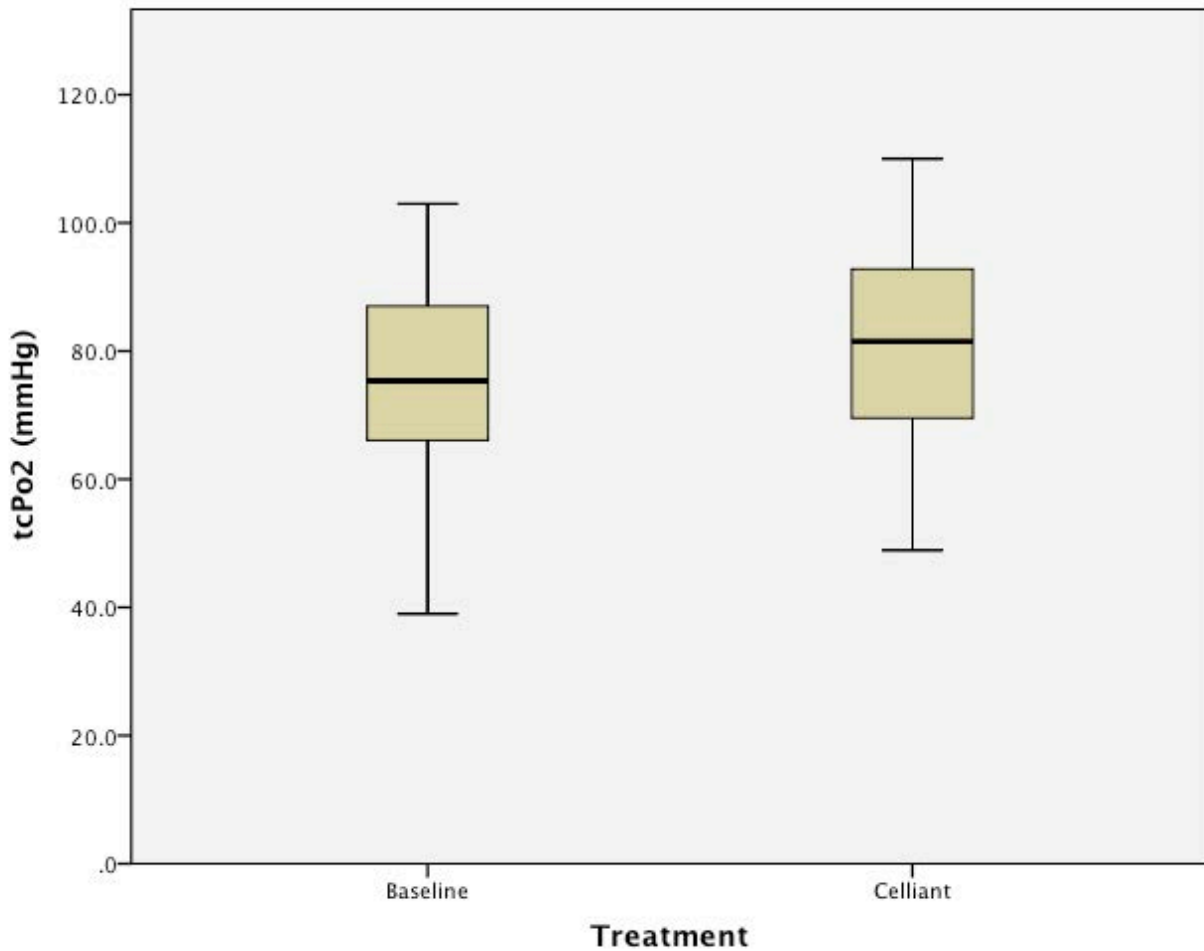
SUMMARY

Fifty-one subjects underwent separate ninety (90) minute testing periods where transcutaneous partial pressure of oxygen (tcPO$_2$), a well-accepted clinical measurement for tissue perfusion and oxygenation, was used as the primary endpoint. First, a Baseline was established. Then, a shirt made with Celliant® material was worn during a subsequent session. All measurements were taken at the bicep.

Transcutaneous oxygen tension proved to be a sensitive measure of efficacy, which resulted in the rejection of the null hypothesis. Thus, mean tcPO$_2$ values for the Celliant® garment were statistically greater than the Baseline at all time points (t= 10-min, 30-min & 90-min), as well as showed an over all treatment effect when mean tcPO$_2$ values were condensed across time. In all cases, the observed mean increases in tcPO$_2$ represented a seven percent (7%) increase in tissue oxygenation in the Celliant® condition when compared to Baseline.

REFERENCES

Altura, B.M., & Altura, B.T. (1982). Microvascular and vascular smooth muscle actions of ethanol, acetaldehyde, and acetate. *Fed Proc, 41*(8), 2447-2451.

Burgess, E.M., Matsen, F.A., 3rd, Wyss, C.R., & Simmons, C.W. (1982). Segmental transcutaneous measurements of PO2 in patients requiring below-the-knee amputation for peripheral vascular insufficiency. *J Bone Joint Surg Am, 64*(3), 378-382.

Chase, L.J., & Tucker, R.K. (1976). Statistical power: Derivation, development, and data-analytic implications. *The Physiological Record, 26*, 473-486.

Coleman, L.S., Dowd, G.S., & Bentley, G. (1986). Reproducibility of tcPO2 measurements in normal volunteers. *Clinical Physics and Physiological Measurement, 7*(3), 259-263.

Dooley, J., Schirmer, J., Slade, B., & Folden, B. (1996). Use of transcutaneous pressure of oxygen in the evaluation of edematous wounds. *Undersea & Hyperbaric Medicine, 23*(3), 167-174.

Fewings, J.D., Hanna, M.J., Walsh, J.A., & Whelan, R.F. (1966). The effects of ethyl alcohol on the blood vessels of the hand and forearm in man. *Br J Pharmacol Chemother, 27*(1), 93-106.

Fewings, J.D., Rand, M.J., Scroop, G.C., & Whelan, R.F. (1966). The action of nicotine on the blood vessels of the hand and forearm in man. *Br J Pharmacol Chemother, 26*(3), 567-579.

Franzeck, U.K., Talke, P., Bernstein, E.F., Golbranson, F.L., & Fronek, A. (1982). Transcutaneous PO2 measurements in health and peripheral arterial occlusive disease. *Surgery, 91*(2), 156-163.

Hanna, G.P., Fujise, K., Kjellgren, O., Feld, S., Fife, C., Schroth, G., et al. (1997). Infrapopliteal transcatheter interventions for limb salvage in diabetic patients: importance of aggressive interventional approach and role of transcutaneous oximetry. *Journal of the American College of Cardiology, 30*(3), 664-669.

IBM. (2011). SPSS 19 for Mac OS X User's Guide. Chicago, IL: IBM, Inc.

Jaszczak, P. (1988). Blood flow rate, temperature, oxygen tension and consumption in the skin of adults measured by a heated microcathode oxygen electrode. *Danish Medical Bulletin, 35*(4), 322-334.

Keppel, G. (1991). Using sample size to control power *Design and Analysis: A Researcher's Handbook* (3rd ed., pp. 76-92). Upper Saddle River: Prentice Hall.

Le Devehat, C., & Khodabandehlou, T. (1990). Transcutaneous oxygen pressure and hemorheology in diabetes mellitus. *International Angiology, 9*(4), 259-262.

Le Devehat, C., Khodabandehlou, T., & Vimeux, M. (2001). Impaired hemorheological properties in diabetic patients with lower limb arterial ischaemia. *Clinical Hemorheology and Microcirculation, 25*(2), 43-48.

Lindquist, E.F. (1953). *Design and analysis of experiments in psychology and education*. Boston: Houghton Mifflin.

Matsen, F.A., 3rd, Bach, A.W., Wyss, C.R., & Simmons, C.W. (1980). Transcutaneous PO2: a potential monitor the status of replanted limb parts. *Plastic and Reconstructive Surgery, 65*(6), 732-737.

Matsen, F.A., 3rd, Wyss, C.R., Pedegana, L.R., Krugmire, R.B., Jr., Simmons, C.W., King, R.V., et al. (1980). Transcutaneous oxygen tension measurement in peripheral vascular disease. *Surgery, Gynecology & Obstetrics, 150*(4), 525-528.

Matsi, P.J., Manninen, H.I., Suhonen, M.T., Pirinen, A.E., & Soimakallio, S. (1993). Chronic critical lower-limb ischemia: prospective trial of angioplasty with 1-36 months follow-up. *Radiology, 188*(2), 381-387.

Mayhan, W.G., & Patel, K.P. (1997). Effect of nicotine on endothelium-dependent arteriolar dilatation in vivo. *Am J Physiol, 272*(5 Pt 2), H2337-2342.

McGill, R., Tukey, J.W., & Larsen, W.A. (1978). Variations of box plots. *The American Statistician, 32*(1), 12-16.

Shoemaker, W.C., & Vidyasagar, D. (1981). Physiological and clinical significance of PtcO2 and PtcCO2 measurements. *Critical Care Medicine, 9*(10), 689-690.

Umemura, T., Ueda, K., Nishioka, K., Hidaka, T., Takemoto, H., Nakamura, S., et al. (2006). Effects of acute administration of caffeine on vascular function. *Am J Cardiol, 98*(11), 1538-1541.

Wagener, J.S., & Hendricker, C. (1987). Intra-subject variability of noninvasive oxygen measurements. *Chest, 92*(6), 1047-1049.

White, R.A., Nolan, L., Harley, D., Long, J., Klein, S., Tremper, K., et al. (1982). Noninvasive evaluation of peripheral vascular disease using transcutaneous oxygen tension. *American Journal of Surgery, 144*(1), 68-75.

Apparel with Far Infrared Radiation for Decreasing an Athlete's Oxygen Consumption During Submaximal Exercise

Dr. Jay Worobets, Dr. Darren Stefanyshyn and Emma Skolnik

Apparel with Far Infrared Radiation for Decreasing an Athlete's Oxygen Consumption during Submaximal Exercise

Jay T. Worobets*, Emma R. Skolnik and Darren J. Stefanyshyn

Human Performance Lab, Faculty of Kinesiology, University of Calgary, Canada

ABSTRACT

Far infrared radiation (FIR) has been shown to have physiological effects when used as a treatment modality for certain medical conditions. Athletic apparel are currently commercially available that are constructed with fabrics that purportedly emit FIR. If apparel with this technology are capable of inducing positive physiological effects, then there may be important implications when worn by an athlete during exercise. The purpose of this study is to examine whether FIR apparel has an effect on oxygen consumption during exercise at submaximal intensities. Twelve male cyclists have completed submaximal incremental cycling tests. Each subject is tested on 4 separate days, twice while wearing a full body Control garment, and twice while wearing a similar garment made out of FIR fabric. Throughout each cycling test, the volume of oxygen uptake is monitored by using a breathing mask and metabolic analysis cart. At lower cycling intensities, the subjects consume statistically significantly less oxygen when wearing the FIR apparel compared to the Control garment, despite performing the same amount of mechanical work. Additional research is required to determine the implication of this effect for a training or competing athlete; however, the results indicate that this apparel technology does elicit a physiological effect.

Keywords: Athletic Apparel, Far Infrared Radiation, Oxygen Consumption, Performance

1. Introduction

Far infrared radiation (FIR) is a subdivision of the electromagnetic radiation spectrum that has been investigated for biological effects (Vatansever & Hamblin, 2012). The FIR band comprises the longest wavelengths ($\lambda = 3 - 100 \ \mu$m) of the infrared radiation band. FIR transfers energy purely in the form of heat, which can be perceived by the thermoregulators in human skin as radiant heat (Plaghki et al., 2010).

Laboratory studies have shown that FIR emitting heat lamps can induce positive effects. Yu et al. (2006) found that FIR increases skin blood flow in rats. Toyokawa et al. (2003) reported that FIR significantly quickens skin wound healing in rats. Akasaki et al. (2006) showed that FIR could induce angiogenesis in mice with hindlimb ischemia. The findings of Ishibashi et al. (2008) suggest that FIR may suppress the proliferation of some human cancer cell lines.

FIR is not limited to powered devices: ceramic materials can emit FIR depending on their temperature (Liang et al. 2008; Wang et al. 2010). The nanoparticles of such ceramic materials can be incorporated into fibers and then woven into fabrics and manufactured into wearable apparel; theoretically, body heat would cause the ceramics to emit FIR. Such apparel have been linked to positive physiological effects; FIR gloves were reported to help treat arthritis of the hands and Raynaud's syndrome (Ko & Berbrayer, 2002), FIR belts were found to reduce body measurements (Conrado & Munin, 2011) and menstrual pain (Lee et al., 2011), and FIR socks were shown to have a beneficial impact on chronic foot pain (York & Gordon, 2009).

If FIR apparel is capable of inducing positive physiological effects, then there may be important implications if applied to sport. As an athlete could wear FIR apparel at any time, this type of apparel could possibly help an athlete warm up before exercise, enhance performance during competition, and/or facilitate recovery post exercise. The purpose of this study is to examine

---
* Corresponding author. Tel.: 1 (403) 220 2704
   E-mail address: worobets@ucalgary.ca (Jay Worobets)

whether FIR apparel has an effect on oxygen consumption during submaximal exercise.

2. Methods

Twelve male aerobically fit recreational cyclists are recruited for this study. The height, mass, body mass index (BMI), and age of each subject are shown in Table 1. Informed written consent was obtained from all subjects prior to data collection in accordance with the Conjoint Health Research Ethics Board at the University of Calgary.

Table 1. Characteristics of the test subjects.

Subject	Height [m]	Mass [kg]	BMI [kg/m^2]	Age [yrs]
1	1.85	92.9	27.1	29
2	1.75	73.8	24.1	24
3	1.88	76.2	21.6	21
4	1.73	69.5	23.2	26
5	1.82	83.8	25.3	28
6	1.74	78.2	25.8	30
7	1.76	72.0	23.2	32
8	1.75	69.1	22.6	34
9	1.75	75.8	24.8	23
10	1.86	80.3	23.2	23
11	1.84	87.9	26.0	22
12	1.81	83.8	25.6	22

Two full body, non-compression apparel conditions were tested; one with FIR properties (termed FIR) and one without (termed Control). The fabrics for both apparel conditions were obtained from Hologenix LLC. The Control apparel was built by using 180 grams/m^2 fabric woven from polyethylene terephthalate (PET) and spandex fibers. The FIR apparel was built by using 180 grams/m^2 fabric woven 70% with PET fibers embedded with 1.25% by weight FIR that emitted ceramic nanoparticles (silicon dioxide, alumina oxide, and titanium dioxide), and 30% with standard PET and spandex fibers. The apparel consisted of pants with an elastic waistband and a long sleeved shirt (Figure 1). Both conditions were visually identical, except for a code written on a label on the inside of the clothing. Four sets of the apparel were built in a range of sizes (small, medium, large, and extra-large) in order to ensure that each subject had an appropriate fit. The apparel were machine washed after each use by using a warm water cycle and mild commercially available laundry detergent.

In general, the data collection sessions comprised a subject who cycled on a cycle ergometer at a constant cadence while the workload was increased every two minutes. During this exercise test, oxygen consumption data were continuously collected by using a TrueMax 2400 metabolic cart (ParvoMedics, Salt Lake City, USA), and blood samples were drawn from a fingertip every two minutes to measure blood lactate concentration with a Lactate Pro analyzer (Arkray Inc., Kyoto, Japan). Each subject completed four test sessions (two per apparel test condition), with each session being at least 48 hours apart. The subjects were instructed to refrain from any behavior outside of their normal physical activity, diet, and sleeping patterns during their entire testing period.

Fig. 1. Photograph of the test apparel.

Immediately prior to each data collection session, the metabolic cart, lactate probe, and cycle ergometer resistance were calibrated. As soon as the subject arrived, height and mass were measured and the subject was given the test apparel and asked to go change (the apparel test order was randomized for each subject). The exercise physiologist who was running the data collection sessions determined the starting cycle ergometer workload (100, 125, or 150 W) of each subject, depending on the size and fitness level of the athlete: this was determined during the first session of each subject and applied to all sessions.

The subjects warmed up for the test by cycling for 5 minutes at a workload 25 W below their defined starting workload at a self-selected 'easy' and 'natural' cadence. After the warm up, a resting

blood lactate measurement was taken to ensure that the value was less than 2 mmol/L. At this time, a breathing mask (including head gear and nose clip) was put on the subject, and connected to the metabolic cart.

To begin the test, the subject started pedaling at their starting workload at a maintainable cadence between 80-90 rpm (the ergometer displayed cadence in real time for feedback to the subject and exercise physiologist for monitoring purposes); whatever cadence the subject naturally adopted at the very beginning of their first session was set as their cadence for the rest of the test and all following test sessions. At the two minute mark, the first blood lactate sample was taken, and the cycle ergometer workload was increased by 25 W. Every two minutes, blood was again sampled and workload increased another 25 W. During the first collection session of each subject, as soon as the blood lactate reading was greater than 6 mmol/L, the workload that the subject was currently cycling at was defined as their final workload, after which the test session was ended.

The first test session therefore established the initial and final workloads (and so also trial duration) that the subject would begin and end at in all four test sessions (Table 2). As such, each subject performed the same amount of mechanical work in each of their four test sessions; increasing in relative intensity from a blood lactate concentration less than 2 mmol/L to greater than 6 mmol/L.

Table 2. Test protocol details for each subject.

Subject #	Initial Workload [W]	Final Workload [W]	Trial Duration [min]
1	125	300	16
2	125	300	16
3	150	325	16
4	125	300	16
5	125	375	22
6	100	250	14
7	125	275	14
8	125	350	20
9	100	250	14
10	125	350	20
11	100	275	16
12	100	325	20

For each test session, the blood lactate data were plotted against time, and a curve was best fit to

the data. The equation for this best fit curve was used to calculate the time at which the blood lactate concentration of the subject reached 2, 4, and 6 mmol/L. These time points therefore define three relative intensity intervals: < 2 mmol/L, 2 - 4 mmol/L, and 4 - 6 mmol/L. The oxygen consumption data were integrated over these intervals to determine the volume of oxygen consumed by the subject when cycling within each relative intensity (the data in Figure 2 in the Results section illustrate this analysis procedure).

For each subject, the data from the two test sessions were averaged for each apparel condition. The data were checked for normality by using Shapiro-Wilk tests, and then paired t-tests or Wilcoxon signed-rank tests were used to identify statistically significant differences between apparel conditions at the $\alpha = 0.05$ level.

3.   Results

The graph in Figure 2 shows the raw oxygen consumption and blood lactate concentration data for the first trial of Subject 1. The graph also illustrates how the blood data points are used to define a best fit curve, the function of which identifies the times when the subject reached blood lactate concentrations of 2, 4, and 6 mmol/L. These time markers establish the intervals over which the oxygen consumption data are integrated.
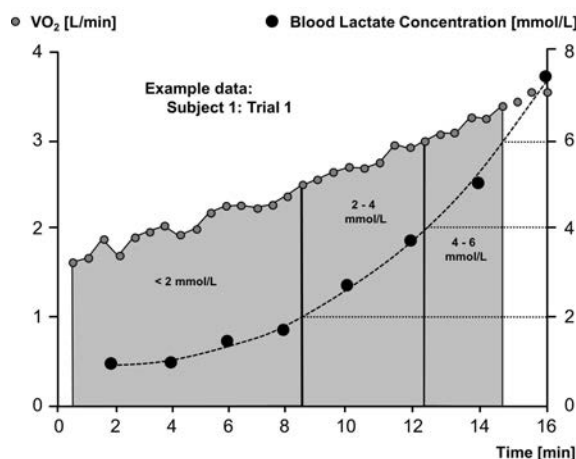
Fig. 2. Raw data from the first trial of Subject 1. Three relative intensity intervals are defined: <2, 2 - 4, and 4 - 6 mmol/L. Total oxygen consumed during each of these 3 intervals is calculated and compared between conditions.

On average, the subjects were in the < 2 mmol/L interval for 432 s, during which they consumed

15.40 L of oxygen with a day to day standard deviation of 0.32 L. The subjects were in the 2 - 4 mmol/L interval for 255 s, during which they consumed 11.81 L of oxygen with a day to day standard deviation of 0.25 L. The subjects were in the 4 - 6 mmol/L interval for 158 s, during which they consumed 8.92 L of oxygen with a day to day standard deviation of 0.20 L. There is no statistically significant difference in interval time between the two apparel conditions for any of the three intensity levels.

The mean oxygen consumption values for each apparel condition are shown for each interval in Table 3. In the < 2 mmol/L interval, the subjects consume statistically significantly less oxygen in the FIR condition than the Control condition; 1.1% less oxygen on average. In the 2 - 4 mmol/L interval, the subjects consume statistically significantly less oxygen in the FIR condition than the Control condition; 0.9% less oxygen on average. There is no statistically significant difference between conditions in the 4 - 6 mmol/L interval.

Table 3. Oxygen consumption results for each intensity level. The mean values are the average of all 12 subjects.

< 2 mmol/L	Control	FIR
Mean O_2 Consumed	15.48 L	15.31 L
p-value	0.014	
% Difference	1.1%	
2 - 4 mmol/L	Control	FIR
Mean O_2 Consumed	11.87 L	11.76 L
p-value	0.048	
% Difference	0.9%	
4 - 6 mmol/L	Control	FIR
Mean O_2 Consumed	8.94 L	8.90 L
p-value	0.511	
% Difference	---	

The individual responses of the subjects to the FIR apparel are not statistically significantly correlated with their mass, height, or BMI.

4. Discussion

The purpose of this study is to examine whether athletic apparel that emit FIR has a measurable physiological effect on athletes during submaximal exercise. Prior research has shown that apparel that emit FIR can have an effect on certain medical conditions (Vatansever & Hamblin, 2012), but it has not been shown if the effects of this apparel technology extend to an exercising athlete.

The results of this study show that apparel that emit FIR can have an effect on an athlete during exercise. When the subjects were cycling at lower intensities (blood lactate concentrations of < 2 mmol/L and 2 - 4 mmol/L) they consumed statistically significantly less oxygen when wearing the FIR apparel compared to when they were wearing the Control apparel (Table 3). On average, this difference in oxygen consumption is 1.1% for the < 2 mmol/L interval, and 0.9% for the 2 - 4 mmol/L interval. There was no difference in oxygen consumption for the 4 - 6 mmol/L interval; it appears that the benefit provided by the FIR apparel is greatest at lower exercise intensities and diminishes as intensity increases.

These results show that the FIR emitting apparel does have an effect on oxygen consumption. However, it is unknown if the oxygen consumption benefit occurs at a high enough intensity to provide a cyclist with a competitive advantage during an endurance race. Theoretically, the race pace of an endurance cyclist would be slightly below their anaerobic threshold, near a blood lactate concentration of 4 mmol/L (Heck et al., 1985; Kindermann et al., 1979; Sjodin & Jacobs, 1981; Skinner & McLellan, 1980). In this study, the subjects consume less oxygen in the FIR apparel when cycling at intensities less than 4 mmol/L, but there is no effect when cycling above 4 mmol/L. Therefore, it is unclear from these results whether the FIR apparel would provide a benefit when cycling at an endurance race pace. A future experiment that examines oxygen consumption while subjects cycle at their endurance race pace would be required to determine if there is a benefit to wearing the FIR apparel.

The mechanism by which the FIR apparel decreases oxygen consumption is unknown and is not elucidated in this experiment. It has been hypothesized that FIR may stimulate the release of nitric oxide and cause vasodilation (Vatansever & Hamblin, 2012), which could increase blood circulation and the ability of the body to deliver oxygen to the working muscles. However, verification of whether this is in fact what occurred is beyond the scope of the present experiment. To the knowledge of the authors, there are no studies to date that have conclusively demonstrated the mechanism by which FIR elicits

positive physiological effects.

5. Conclusion

Apparel that emit FIR have been previously shown to elicit physiological effects in humans (Conrado & Munin, 2011; Ko & Berbrayer, 2002; Lee et al. 2011; York & Gordon, 2009). The results of this study show that this apparel technology can also have a physiological effect on athletes during exercise. When cycling at lower relative intensities (< 4 mmol/L), the subjects consume approximately 1.0% less oxygen when wearing FIR emitting apparel. This effect diminishes with increasing cycling intensity; therefore, further study is required to determine if this effect is relevant for a competing endurance cyclist.

Acknowledgements

REFERENCES

[1] Akasaki Y., Miyata M., Eto H., Shirasawa T., Hamada N., Ikeda Y., Biro S., Otsuji Y. & Tei C. 2006, 'Repeated thermal therapy up-regulates endothelial nitric oxide synthase and augments angiogenesis in a mouse model of hindlimb ischemia', *Circulation Journal,* vol. 70, no. 4, pp. 463-470.

[2] Conrado L.A. & Munin E. 2011, 'Reduction in body measurements after use of a garment made with synthetic fibers embedded with ceramic nanoparticles', *Journal of Cosmetic Dermatology*, vol. 10, no. 1, pp. 30-35.

[3] Heck H., Mader A., Hess G., Mucke S., Muller R. & Hollman W. 1985, 'Justification of the 4 mmol/L lactate threshold', *International Journal of Sports Medicine*, vol. 6, pp. 117-130.

[4] Ishibashi J., Yamashita K., Ishikawa T., Hosokawa H., Sumida K. & Nagayama M., Kitamura S. 2008, 'The effects inhibiting the proliferation of cancer cells by far-infrared radiation (FIR) are controlled by the basal expression level of heat shock protein (HSP) 70A', *Medical Oncology*, vol. 25, no. 2, pp. 229-237.

[5] Kindermann W., Simon G. & Keul J. 1979, 'The significance of the aerobic-anaerobic transition for the determination of work load intensities during endurance training', *European Journal of Applied Physiology,* vol. 42, pp. 25-34.

[6] Ko G.D. & Berbrayer D. 2002, 'Effect of ceramic-impregnated "thermoflow" gloves on patients with Raynaud's syndrome: randomized, placebo-controlled study', *Alternative Medicine Review*, vol. 7, no. 4, pp. 328-335.

[7] Lee C.H., Roh J.W., Lim C.Y., Hong J.H., Lee J.K. & Min E.G. 2011, 'A multicenter, randomized, double-blind, placebo-controlled trial evaluating the efficacy and safety of a far infrared-emitting sericite belt in patients with primary dysmenorrhea', *Complementary Therapies in Medicine,* vol. 19, no. 4, pp. 187-193.

[8] Liang J., Zhu D., Meng J., Wang L., Li F., Lui Z., Ding Y., Liu L. & Liang G. 2008, 'Performance and application of far infrared rays emitted from rare earth mineral composite materials', *Journal of Nanoscience & Nanotechnology*, vol. 8, no. 3, pp. 1203-1210 .

[9] Plaghki, L., Decruynaere, C., Van Dooren P. & Le Bars, D. 2010, 'The fine tuning of pain thresholds: a sophisticated double alarm system', *PLoS One,* vol. 5, no. 4, e10269.

[10] Sjodin, B. & Jacobs, I. 1981, 'Onset of blood lactate accumulation and marathon running performance', *International Journal of Sports Medicine,* vol. 2, pp. 23-26.

[11] Skinner, J.S. & McLellan, T.M. 1980, 'The transition from aerobic to anaerobic metabolism', *Research Quarterly in Exercise & Sport,* vol. 51, pp. 234-248.

[12] Toyokawa, H., Matsui, Y., Uhara, J., Tsuchiya, H., Teshima, S., Nakanishi, H., Kwon, A.H., Azuma, Y., Nagaoka, T., Ogawa, T. & Kamiyama, Y. 2003, 'Promotive effects of far-infrared ray on full-thickness skin wound healing in rats', *Experimental Biology & Medicine*, vol. 228, no. 6, pp. 724-729.

[13] Vatansever, F. & Hamblin, M.R. 2012, 'Far infrared radiation (FIR): Its biological effects and medical applications', *Photonics & Lasers in Medicine,* vol. 1, no. 4, pp. 255-266.

[14] Wang, F., Liang, J., Tang, Q., Li, L. & Han L. 2010, 'Preparation and far infrared emission properties of natural sepiolite nanofibers', *Journal of Nanoscience & Nanotechnology*,

vol. 10, no. 3, pp. 2017-2022.

[15] York, R.M. & Gordon, I.L. 2009, 'Effect of optically modified polyethylene terephthalate fiber socks on chronic foot pain', *BMC Complementary and Alternative Medicine,* vol. 9, no. 10.

[16] Yu, S.Y., Chiu, J.H., Yang, S.D., Hsu, Y.C., Lui, W.Y., Wu & C.W. 2006, 'Biological effect of far-infrared therapy on increasing skin microcirculation in rats', *Photodermatology Photoimmunology & Photomedicine,* vol. 22, no. 2, pp. 78-86.

Double Blind, Placebo Controlled, Crossover Trial on the Effect of Optically Modified Polyethylene Terephthalate Fiber Mattress Covers on Sleep Disturbances in Patients with Chronic Back Pain

Dr. Marcel Hungs and Dr. Annabel Wang

Center for Sleep Medicine
Department of Neurology
101 The City Drive S
Building 22C, Rte. 23
Orange, CA 92868
Tel: (714) 456-5105
Fax: (714) 456-7822

02/15/10

Seth Casden, CEO
Hologenix, LLC
1112 Montana Ave., Suite 13
Santa Monica, CA 90403

RE: Final results of the trial:
        Double blind, placebo controlled, crossover pilot trial on the effect of Optically Modified Polyethylene
        Terephthalate Fiber mattress covers on sleep disturbances in patients with chronic back pain.
        ClinicalTrials.gov Identifier: NCT00969540

Dear Mr. Casden:

The trial "Double blind, placebo controlled, crossover pilot trial on the effect of Optically Modified Polyethylene
Terephthalate Fiber mattress covers on sleep disturbances in patients with chronic back pain" is now completed
with all six enrolled subjects trial parameters analyzed.

The double blind, placebo controlled, crossover pilot trial evaluated the effect of Optically Modified
Polyethylene Terephthalate Fiber mattress covers on sleep disturbances in patients with chronic back pain.

We assessed sleep quality in six patients with lower back pain as measured by Clinical Global Impression
(CGI), sleep variables measured with actigraphy and exploratory objectives including the Pittsburgh Sleep
Quality Index, visual analogue scale for pain, Clinical Global Impression of Sleep and Clinical Global
Impression of Pain.

The total duration of the study for a participant was approximately 49 days, including 14 days of screening prior
to treatment and 28 days of treatment interrupted by a wash-out phase of seven days. Subjects who met the initial
screening criteria underwent actigraphy monitoring for a period of 14 days to record a baseline sleep pattern.
Subjects were then offered, in this crossover double blind designed trial, either the active or the placebo garment
mattress cover. 14 day actigraphy with use of the provided study material was performed followed by the
crossover offering of the alternate garment for the next 14 days.

Here are some key findings:
- The median time spent awake at night after falling asleep was reduced by 18.3 minutes.
- Individuals spent 42 minutes less time sleeping, suggesting less need to sleep on Celliant (perhaps
  consolidating and improving sleep on the active garment).
- The median sleep efficiency improved by 2.6 %.
- Three out of six participants reported a subjective improvement of their sleep with the use of the active
  garment mattress cover as measured in the Clinical Global Impression scale.
- Two participants also reported that nocturnal back pain was better with the use of the active garment as
  measured in the Clinical Global Impression scale for pain.

Below is the summarized tabulated data for the six subjects who have completed the trial.

Average changes	Subject	Wake after sleep onset (min)	Total Sleep (min)	Number of nocturnal Awakenings	Sleep Efficiency (%)	Sleep Latency (min)
	1	-22.18	-14.53	-3.64	3.76	1.84
	2	7.71	-27.49	-1.81	-2.06	15.62
	3	-9.62	-89.61	5.63	-2.39	5.19
	4	-18.54	-13.77	-1.15	2.53	-10.92
	5	-46.01	-52.90	1.11	2.63	-15.50
	6	-1.27	-1.08	-0.50	-0.56	-0.40
	Average	**-14.98**	**-33.23**	**-0.06**	**0.65**	**-0.70**

Median values changes	Subject	Wake after sleep onset (min)	Total Sleep (min)	Number of nocturnal Awakenings	Sleep Efficiency (%)	Sleep Latency (min)
	1	-17.50	-4.50	-6.50	4.00	0.50
	2	-17.50	-26.00	-3.00	2.69	10.50
	3	-34.00	-138.00	5.00	3.93	0.00
	4	-21.00	-33.00	-2.00	2.27	-7.00
	5	-18.00	-59.00	-2.00	2.38	0.00
	6	-2.00	4.00	-1.00	0.29	0.00
	Average	**-18.33**	**-42.75**	**-1.58**	**2.59**	**0.67**

These results show tendencies toward the use of Celliant mattress covers in order to improve sleep but not lower back pain. The only participant without subjective or objective improvements had significant, acute chronic back pain at the time of enrollment. As the study is expanded, subjects with acute and severe back pain will not be admitted.

Other studies have shown that randomized, single-blinded, parallel-group studies evaluating structurally different mattresses, that bedding system differences can influence chronic low back pain and sleep (Bergholdt K et al 2008, Jacobson BH et al 2008, Jacobson BH et al 2002, Monsein M et al, 2000). A recent study showed improvements in mild back pain, sleep quality, and perceived stress in 59 patients after introduction of new bedding systems (Jacobson BH et al 2009).

Using the Wilcoxon Rank Sum Test, it is possible that with 12 additional subjects tested, more clear trends indicating the benefit of Celliant may emerge. Also, mild lower back pain is more likely to respond to Celliant then severe pain syndromes. Dr. Annabel Wang of the UCI Neurology Department will be continuing the project.

Regards,

Marcel Hungs, M.D., Ph.D.
Assistant Professor of Clinical Neurology

Effect of Optically Modified Polyethylene Terephthalate Fiber Socks on Chronic Foot Pain

Dr. Ian Gordon and Dr. Robyn York

Effect of optically modified polyethylene terephthalate fiber socks on chronic foot pain

Robyn M B York (robyn.burgess@va.gov)

Ian L Gordon (ilgordon@uci.edu)

Effect of optically modified polyethylene terephthalate fiber socks on chronic foot pain

Robyn M B York and Ian L Gordon

Division of Vascular Surgery, Department of Surgery, University of California Irvine

Medical Center, Orange CA, USA

Correspondence: Ian L. Gordon

UCI Medical Center

101 The City Dr.

Orange, CA 92868

USA

FAX (714) 456-8919

Email addresses:

RMBY: Robyn.Burgess@va.gov

ILG: ilgordon@uci.edu

Abstract

Background

Increasing experimental and clinical evidence suggests that illumination of the skin with relatively low intensity light may lead to therapeutic results such as reduced pain or improved wound healing. The goal of this study was to evaluate prospectively whether socks made from polyethylene terephthalate (PET) incorporating optically active particles (Celliant™) ameliorates chronic foot pain resulting from diabetic neuropathy or other disorders. Such optically modified fiber is thought to modify the illumination of the skin in the visible and infrared portions of the spectrum, and consequently reduce pain.

Methods

A double-blind, randomized trial with 55 subjects (38 men, 17 women) enrolled (average age 59.7 ± 11.9 years), 26 with diabetic neuropathy and 29 with other pain etiologies. Subjects twice completed the Visual Analogue Scale (VAS), Brief Pain Inventory (BPI), McGill Pain Questionnaire (MPQ), and SF-36 a week apart (W_{1+2}) before receiving either control or Celliant™ socks. The same questionnaires were answered again one and two weeks (W_{3+4}) later. The questionnaires provided nine scores for analyzing pain reduction: one VAS score, two BPI scores, five MPQ scores, and the bodily pain score on the SF-36. Mean W_{1+2} and W_{3+4} scores were compared to measure pain reduction.

Results

More pain reduction was reported by Celliant™ subjects for 8 of the 9 pain questions employed, with a significant ($p = 0.043$) difference between controls and Celliant™ for McGill question III. In neuropathic subjects, Celliant™ caused more pain

reduction in 6 of the 9 questions, but not significantly. In non-neuropathic subjects 8 of 9 questions showed more pain reduction with the Celliant™ socks.

Conclusions

Socks with optically modified PET (Celliant™) appear to have a beneficial impact on chronic foot pain. The mechanism could be related to the effects seen with illumination of tissues with visible and infrared light.

Trial Registration: ClinicalTrials.gov NCT00458497

Background

Celliant™ is a polymer fabric constructed from polyethylene terephthalate (PET) yarn containing optically active particles – a proprietary mixture of natural and inorganic materials – which scatter and reflect visible and near infrared light. Garments constructed with such optically modified fibers are thought to influence transmission and reflectance of electromagnetic energy into underlying tissue and skin. Numerous anecdotal reports from patients with a variety of chronic pain syndromes indicate that wearing Celliant™ garments for even a few days leads to dramatic improvement or complete resolution in subjective pain. We report here the results of a prospective, blinded study designed to substantiate the ability of Celliant™ socks to ameliorate chronic pain resulting from diabetic neuropathy and other disorders of the foot.

Methods

This study was conducted at the Veterans Administration Medical Center Long Beach and approved by the local ethics board. All subjects reviewed an Informed Consent document and gave consent prior to enrolment. Fifty-five subjects (38 men, 17 women, age 59.7 ± 11.9) were enrolled, 26 with diabetic neuropathy and 29 with

other causes of foot pain. Inclusion criteria included age $\geq$21, foot pain for at least six months, and a score of $\geq$ 3 on question III of the McGill Short Form Pain Questionnaire (MPQ) at screening. Subjects with diabetic neuropathy (DPN) had a minimum of 2/6 anesthetic points by Semmes-Weinstein filament testing on one foot. Subjects without DPN had 0/6 anesthetic points. Exclusion criteria included severe peripheral arterial disease (PAD) (ABI < 0.5), inability to ambulate, chronic ulceration, and severe psychiatric disorders. For subjects without DPN, etiologies included arthritis, erythromelalgia, Parkinson's disease, and PAD (Table 1). The most common foot pain etiology was arthritis.

At screening (week 1) subjects underwent physical examination including monofilament testing and completed a series of four questionnaires (Visual Analogue Scale [1] [VAS], Brief Pain Inventory [2, 3] [BPI], MPQ [4], and SF-36 Quality of Life Inventory [5]). Only the bodily pain score from the SF-36 questionnaire was used to assess pain responses. Subjects completed the same questionnaires a week later (week 2) and were given 3 pairs of socks in a closed container and asked to wear them exclusively for the next two weeks. One (week 3) and two weeks (week 4) later they filled out the same panel of questions. Controls received socks made from standard 1.2 denier PET fabric, while the Celliant™ group received otherwise identical socks except PET containing Celliant™ particles was used to fashion the bottom (plantar) half of the garments. Both study personnel and subjects were blinded to the treatment assigned.

As the MPQ has 5 components (Ia, Ib, Ia+b, II, III) and the BPI 2 components (Pain Severity, Pain Interference), a total of 9 questions assessing pain were analyzed to

measure subjects' responses. Mean scores for individual questions were calculated for the first two (W_{1+2}) and final two visits (W_{3+4}). Differences between W_{1+2} and W_{3+4} scores reflected changes in perceived pain resulting from wearing socks. Non-parametric two tailed t-test analysis (Mann-Whitney) was used to compare changes in scores [(mean W_{1+2}) – (mean W_{3+4})] for individual questions reported by control and Celliant™ subjects. Analyses were performed on all 55 subjects as well as DPN and non-DPN subgroups.

Results

Control and Celliant™ subjects had comparable age and gender distributions upon entry into the study (Table 2). Except for the BPI questions in the non-DPN subjects, there were no significant ($p < 0.05$) differences in the mean scores for individual questions at screening.

Both control and Celliant™ subjects reported decreased subjective pain after wearing socks for every question based on comparing W_{1+2} scores to W_{3+4} scores (see Figures). The differences between W_{1+2} and W_{3+4} scores were significant ($p < 0.05$, Mann Whitney) in 6 of 9 questions for Celliant™ subjects and in 4 of 9 questions for controls. Improvement in pain scores before and after treatment is characteristic of a strong placebo effect generally seen in pain studies. For most questions, however, more improvement was reported by the entire Celliant™ group compared to the entire control group based on the magnitude of differences in [$W_{1+2} - W_{3+4}$] scores.

Questions Ia and Ib of the MPQ rate the intensity of various aspects of pain: Question Ia rates 11 sensory aspects of pain such as throbbing or cramping as absent, mild,

moderate, or severe. Question Ib similarly rates four affective dimensions (e.g., fearful). Question II is a simple scale where the intensity of present pain is marked on a line. Question III rates overall pain on a 0 (absent) to 5 (excruciating) scale. For control and Celliant™ groups, little difference between the improvements in mean scores for questions Ia, Ib, and Ia+b were found. The Celliant™ group demonstrated an improvement in pain for questions Ia (0.34 vs. 0.20, p = 0.634) and Ia+b (0.52 vs. 0.50, p = 0.829). For question Ib controls, however, showed a modestly greater reduction in pain compared to the Celliant™ subjects (0.17 vs. 0.10, p = 0.405). In question III (Figure 1), pain reduction for Celliant™ subjects was significantly greater (0.50 versus 0.00) than for controls (p = 0.043). For subjects with DPN, Celliant™ subjects reported more pain reduction in question Ia (0.22 vs. 0.19, p = 0.978), whereas controls reported more reduction in pain for questions Ib (0.06 vs. -0.01, p = 0.566), and Ia+b (0.45 vs. 0.21, p = 0.587). In question II, 19% more improvement was seen with Celliant™ in DPN subjects (p=0.703). For question III, DPN subjects wearing Celliant™ socks showed a reduction of pain of 0.50 versus 0.00 in controls (p = 0.148). The Celliant™ group displayed minor improvements in pain scores for questions Ia (0.44 vs. 0.22, p = 0.571) and Ia+b (0.79 vs. 0.55, p = 0.896) in non-DPN subjects. Controls demonstrated more improvement for question Ib (0.28 vs. 0.20, p = 0.615) in this group. For question II in the non-DPN subjects, a nearly two-fold difference in pain reduction was seen with Celliant™ socks compared to controls (1.20 vs. 0.65, p = 0.371). For question III in non-DPN subjects, more reduction in pain was reported with Celliant™ (0.50 versus 0.00, p = 0.154).

Two scores are derived from the BPI. The severity score rates pain over the previous 7 days, past 24 hours, and present between 0 (absent) and 10 (worst possible). The

interference score measures interference with activities such as walking and working from 0 (none) to 10 (complete). Celliant™ subjects reported 30% more reduction in severity compared to controls (p = 0.077, Figure 2). For interference, the Celliant™ group reported 18% more reduction than controls (p = 1.000). Celliant™ subjects with DPN reported a reduction in pain severity of 0.75 compared to 0.50 in the controls (p = 0.211) (Figure 2). For interference, controls demonstrated a greater reduction compared with the Celliant™ group (0.35 vs. 0.03 respectively), but this was not significant (p = 0.644). In non-DPN subjects a 40% greater reduction in severity was observed in Celliant™ subjects (p=0.230). Non-DPN Celliant™ subjects reported 34% more reduction in interference compared with controls (p = 0.760).

The Visual Analog Scale (VAS) rated foot pain from 0 (none) to 10 (worst possible) during the previous week. The entire Celliant™ group reported 45% greater reduction in pain compared to controls (p = 0.127; Figure 3). Changes between W_{1+2} and W_{3+4} VAS pain scores did not vary significantly between Celliant™ and control DPN subjects (0.10 compared to 0.00, p = 0.849) (Figure 3). In the non-DPN group, Celliant™ subjects exhibited 54% more reduction in pain compared to controls (p = 0.060).

The SF-36 questionnaire has 10 categories measuring health and wellness. The bodily pain score measures a subject's attitude towards pain. Higher scores reflect less pain and lower scores more. Reduced pain correlates with negative [$W_{1+2} - W_{3+4}$] results. Figure 4 shows the Celliant™ group had 62% more improvement compared to controls (p = 0.058). In DPN subjects, there was 99% greater improvement in the pain score with Celliant™ compared to controls (p = 0.109). For

non-DPN subjects, pain improvement with Celliant™ was 29% greater compared to controls (p = 0.275).

Discussion

This is the first trial assessing the impact of optically modified PET garments on pain. The pain questionnaires employed have been validated in previous studies [1-7], and were modified only by asking subjects to consider foot pain in their replies (except for the SF-36). Although a placebo effect was observed for most questions (controls reported improvement in 7 out of 9, 3 significantly), more reduction in pain was reported by subjects wearing Celliant™. The response to MPQ question III, in particular, showed significantly greater reduction in pain for Celliant® compared to controls. In the DPN subgroup, two questions failed to show greater improvement with Celliant™ compared to placebo: MPQ questions Ib and Ia+b. These questions employ multiple complex scales and are designed more to measure sensory and affective aspects of pain rather than intensity. For all subjects, only question Ib on the MPQ did not display results favouring the Celliant™ group. Similarly, the BPI pain interference question does not address pain intensity and in the DPN subgroup, more improvement was found in the control group (p > 0.566). Table 3 shows the aggregate result for all pain questions.

Overall the data reported show more improvement in pain reported by subjects wearing the Celliant® socks compared to the controls. The lack of statistical significance for the differences in results with most of the questions may be due to the relatively low number of subjects in this pilot study as well as a lack of homogeneity in the subjects.

In our study each questionnaire was administered twice before and after dispensing the study garments with the results averaged, in the hopes of increasing the precision of the pain assessments. This might skew the data if the therapeutic effect of the Celliant™ socks changes with time – either increasing or decreasing. In future studies employing larger number of subjects this methodological problem should be avoided by administering each set of pain questionnaires only once.

In general, non-DPN subjects showed more sensitivity to the beneficial effect of Celliant™ than subjects with DPN. Assuming the effect of Celliant™ on tissue is relatively localized, one might expect less of an effect to be seen in neuropathy, as only a portion of the diseased neuron fibers are in close proximity to the plantar aspect of the socks, and thus likely subject to the effect of the modified fabric.

This raises the question of what mechanism could account for the apparent beneficial impact of optically modified fiber garments. Two unpublished studies, one in healthy subjects and one in diabetics, demonstrated significant increases in transcutaneous oxygen tensions in the skin of the hands and feet when Celliant™ garments were worn compared to placebo garments (Lavery LA, 2003; McClue GM and Lavery LA, 2003). The increased oxygen tensions were observed by 10 minutes and persisted during repeated measurements over 60 minutes. The increase in healthy subjects ranged from 10 to 24%; diabetic subjects showed an average increase of 10%. It is conceivable that some interaction of the Celliant™ particles with light increases reflection or transmission of light in the visible or near infrared portion of the spectrum into the skin, leading to vasodilation of the microcirculation and enhanced

perfusion of tissue, which plausibly could ameliorate some causes of chronic pain. Alternatively, the enhanced illumination of the skin and underlying tissues could influence the biologic activity of endogenous chromophores (cytochromes, flavins, and poryphyrins) involved in energy metabolism in a manner leading to anti-inflammatory or anti-nocioceptive effects.

A large body of evidence suggests that short periods of illuminating skin, tissue, and cells with visible or infrared light has positive effects on pain, injury recovery, and wound healing. A number of studies have looked at joint pain such as temporomandibular joint pain [8], finding that near infrared light (810 nm) appears to reduce pain compared to sham illumination regimens. A meta-analysis of 20 trials employing laser therapy for chronic joint disorders found that when sufficiently intense light was employed, such therapy had a direct anti-inflammatory effect on the joint capsule [9]. A study of the effects of infrared (950 nm) on sural nerve conduction showed significant impact of illumination on nerve conduction velocity and negative peak latency compared to sham illumination [10]. Several studies on diabetic neuropathy showed a favourable impact of intermittent illumination with infrared at 890 nm on sensation and pain [11, 12]. Low level illumination of joints affected by osteoarthritis by infrared diodes emitting at 890 nm has also been reported as effective for alleviating pain, and the effect has been postulated to be related to stimulation of constitutive nitric oxide synthetase [13]. Low intensity laser therapy at 810-820 nm combined with exercise regimens has been shown to benefit patients with chronic back pain and Achilles tendonopathy [14, 15]. Several studies using animal models of wound healing or cell cultures have examined the effects of short exposures to red (e.g., 632nm, 670 nm) or infrared light (e.g., 830 nm), finding wound healing to

be significantly accelerated or increased expression of genes and proteins associated with proliferation [16-21].

Previous studies generally entailed short illumination periods of a few minutes at intensities of 1 to 20 Joules/cm which are much higher than the presumptive low intensity optical effects of Celliant™ garments. Our subjects were wearing socks under ambient light conditions and often shoes. Past demonstrations of interactions between tissues and external light, nonetheless, support the possibility that Celliant™'s effect is due to prolonged exposure of underlying structures to an altered electromagnetic environment. Given the putative anti-inflammatory effects of infrared light, the ability of longer wavelengths to penetrate more deeply, and the likelihood that Celliant™ particles significantly reflect and scatter infrared light, plausibly the Celliant™ effect is mediated by perturbations in the infrared portion of the spectrum. Conceivably, but we think unlikely, the Celliant™ effect may be due to higher skin temperatures resulting from more efficient reflection of infrared energy, but this requires further investigation. We are now planning further studies employing thermography and hyperspectral imaging of skin blood flow to further characterize the effects of wearing Celliant™ garments.

Conclusions

The data from this pilot study suggests that wearing Celliant™ fabric socks may reduce the pain associated with chronic foot disorders. Future studies in larger numbers of subjects looking at other chronic pain conditions such as carpal tunnel syndrome and knee arthropathies are warranted as well as attempts to elucidate the

mechanism by examining the influence of the modified garments on tissue perfusion, temperature, oxygen levels, and inflammation.

Competing interests

Authors' contributions

RY participated in the design of the study, carried out subject recruitment and data collection, took part in the statistical analysis, and helped draft the manuscript. IG conceived of the study, took part in its design and coordination, led the statistical analysis, and helped draft the manuscript. All authors read and approved the final manuscript.

Acknowledgements

References

1. Cleeland CS, Ryan KM. **Pain assessment: global use of the Brief Pain Inventory**. *Ann Acad Med Singap* 1994, **23**:129-138.

2. Farrar JT, Young JP Jr, LaMoreaux L, Werth JL, Poole RM. **Clinical importance of changes in chronic pain intensity measured on an 11-point numerical pain rating scale.** *Pain* 2001, **94**:149-158.

3. Gilron I, Bailey JM, Tu D, Holden RR, Weaver DF, Houlden RL. **Morphine, gabapentin, or their combination for neuropathic pain**. *N Engl J Med* 2005, **352**:1324-1334.

4. Melzack R. **The short-form McGill Pain Questionnaire**. *Pain* 1987, **30**:191-197.

5. Tan G, Jesen M. **Validation of the Brief Pain Inventory for chronic nonmalignant pain.** *J Pain* 2004, **5**:133-137.

6. Ware JE, Snow KK, Kosisnki M, Gandek B. *SF-36 health survey manual and interpretation guide.* Boston, The Health Institute, New England Medical Center 1993.

7. Wernicke JF, Pritchett YL, D'Souza DN, Waninger A, Tran P, Iyengar S, Raskin J. **A randomized controlled trial of duloxetine in diabetic peripheral neuropathic pain.** *Neurology* 2006, **67**:1411-1420.

8. Fikackova H, Dostalova T, Vosicka R, Peterova V, Navratil L, Lesak J. **Arthralgia of the temporomandibular joint and low-level laser therapy.** *Photomed Laser Surg* 2006, **24**:522-527.

9. Bjordal JM, Couppe C, Chow RT, Tuner J, Ljunggren EA. **A systematic review of low level laser therapy with location-specific doses for pain from chronic joint disorders.** *Aust J Physiother* 2003, **49**:107-116.

10. Vinck E, Coorevits P, Cagnie B, De Muynck M, Vanderstraeten G, Cambier D. **Evidence of changes in sural nerve conduction mediated by light emitting diode irradiation**. *Lasers Med Sci* 2005, **20**:35-40.

11. Leonard DR, Farooqi MH, Myers S. **Restoration of sensation, reduced pain, and improved balance in subjects with diabetic peripheral neuropathy: a double-blind, randomized, placebo-controlled study with monochromatic near-infrared treatment.** *Diabetes Care* 2004, **27**:168-172.

12. Harkless LB, DeLellis S, Carnegie DH, Burke TJ. **Improved foot sensitivity and pain reduction in patients with peripheral neuropathy after treatment with monochromatic infrared photo energy – MIRE.** *J Diabetes Complications* 2006, **20**:81-87.

13. Hancock CM, Riegger-Krugh, C. **Modulation of pain in osteoarthritis: The role of nitric oxide.** *Clin J Pain* 2008, **24**(4):353-365.

14. Djavid GE, Mehrdad R, Ghasemi M, Hasan-Zadeh H, Sotoodeh-Manesh A, Pouryaghoub G. **In chronic low back pain, low level laser therapy combined with exercise is more beneficial than exercise alone in the long term: a randomized trial.** *Aust J Physiother* 2007, **52**:155-160.

15. Stergioulas A, Stergioula M, Aarskog R, Lopes-Martins RAB, Bjordal JM. **Effects of low-level laser therapy and eccentric exercises in the treatment of recreational athletes with chronic Achilles tendonopathy.** *Am J Sports Med* 2008, **36**(5):881-887.

16. Enwemeka CS, Parker JC, Dowdy DS, Harkness LE, Woodruff LD. **The efficacy of low-power lasers in tissue repair and pain control: a meta-analysis study**. *Photomed Laser Surg* 2004, **22**:323-329.

17. Erdle BJ, Brouxhon S, Kaplan M, Vanbuskirk J, Pentland AP. **Effect of continuous-wave (670-nm) red light on wound healing**. *Dermatol Surg* 2008, **34**:320-325.

18. Mendez TMTV, Pinheiro ALB, Pacheco MTT, Nascimento PM, Ramalho LMP. **Dose and wavelength of laser light have influence on the repair of cutaneous wounds**. *J Clin Laser Med Surg* 2004, **22**:19-25.

19. Rabelo SB, Villaverde AB, Nicolau RA, Castillo Salgado MA, Melo MDS, Pacheco MTT. **Comparison between wound healing in induced diabetic and nondiabetic rats after low-level laser therapy.** *Photomed Laser Surg* 2006, **24**:474-479.

20. Schramm JM, Warner D, Hardesty RA, Oberg KC. **A unique combination of infrared and microwave radiation accelerates wound healing**. *Plast Reconstr Surg* 2003, **111**:258-266.

21. Hawkins D, Abrahamse H. **Influence of broad-spectrum and infrared light in combination with laser irradiation on the proliferation of wounded skin fibroblasts.** *Photomed Laser Surg* 2007, **25**:159-169.

Figures

Figure 1 - Results of McGill Question III

The difference between mean W_{1+2} and mean W_{3+4} scores is depicted. Solid bars report Celliant™ and stipled bars report control subjects. $*p < 0.05$

Figure 2 – Results of the Brief Pain Inventory – Pain Severity

The difference between mean W_{1+2} and mean W_{3+4} scores is depicted. Solid bars report Celliant™ and stipled bars report control subjects.

Figure 3 – Results of the VAS

The difference between mean W_{1+2} and mean W_{3+4} scores is depicted. Solid bars report Celliant™ and stipled bars report control subjects.

Figure 4 – Results of the SF-36 Bodily Pain

The difference between mean W_{1+2} and mean W_{3+4} scores is depicted. Solid bars report Celliant™ and stipled bars report control subjects.

Tables

Table 1 – Pain etiologies in non-DPN subgroup

Etiology	Celliant™	Control
Arthritis	45%	40%
Edema	7%	0%
Erythromelalgia	0%	7%
Parkinson's Disease	0%	12%
PAD	0%	7%
Plantar Fasciitis	0%	7%
Previous Chemotherapy	7%	0%
Previous Surgery	7%	7%
Other Causes	36%	20%

Table 2 – Subject Characteristics Prior to Treatment

	Demographics		McGill				
All Subjects	**Age**	**% male**	**I-a**	**I-b**	**I-a+b**	**II**	**III**
Celliant™	57.7±11.8	70%	1.2±0.8	0.6±0.7	1.9±1.5	4.7±2.4	2.6±1.0
Control	61.6±11.8	68%	1.3±0.7	1.1±1.0	2.4±1.6	5.4±2.8	3.1±1.1
DPN group							
Celliant™	63.0±7.7	85%	1.2±0.9	0.6±0.7	1.9±1.5	5.1±2.6	2.7±1.1
Control	63.9±11.0	77%	1.4±0.7	1.2±1.1	2.5±1.7	5.2±2.9	2.9±0.9
Non-DPN group							
Celliant™	52.7±13.1	57%	1.2±0.8	0.6±0.8	1.9±1.5	4.4±2.3	2.4±0.9
Control	59.5±12.3	60%	1.3±0.8	1.1±1.0	2.3±1.6	5.6±2.8	3.3±1.2

Brief Pain Inventory

	Pain Severity	**Pain Interference**	**VAS**	**SF-36: Bodily Pain**
All Subjects				
Celliant™	4.2±2.4	5.8±2.4	37.8±8.1	4.2±2.4
Control	5.5±2.6	6.4±1.8	34.6±7.8	5.5±2.6
DPN group				
Celliant™	4.9±2.0	4.7±2.5	5.9±2.4	34.2±7.4
Control	5.1±2.3	5.5±2.9	6.1±1.9	36.1±7.5
Non-DPN group				
Celliant™	3.9±1.9*	3.8±2.3*	5.8±2.5	40.8±7.7
Control	5.3±1.6*	5.6±2.3*	6.6±1.8	33.3±8.1

*denotes significant ($p < 0.05$) differences between Celliant™ and Control subjects.

Table 3 – Results of pain questions

Question	All Subjects	DPN subgroup	Non-DPN subgroup
McGill Ia	+	+	+
McGill Ib	-	-	-
McGill Ia+b	+	-	+
McGill II	+	+	+
McGill III	+**	+	+
BPI Pain Severity	+*	+	+
BPI Pain Interference	+	-	+
VAS	+	+	+*
SF-36 Bodily Pain	+*	+	+

(+) Celliant™ showed greater improvement; (-) Controls showed greater improvement

** p < 0.05, *<0.10
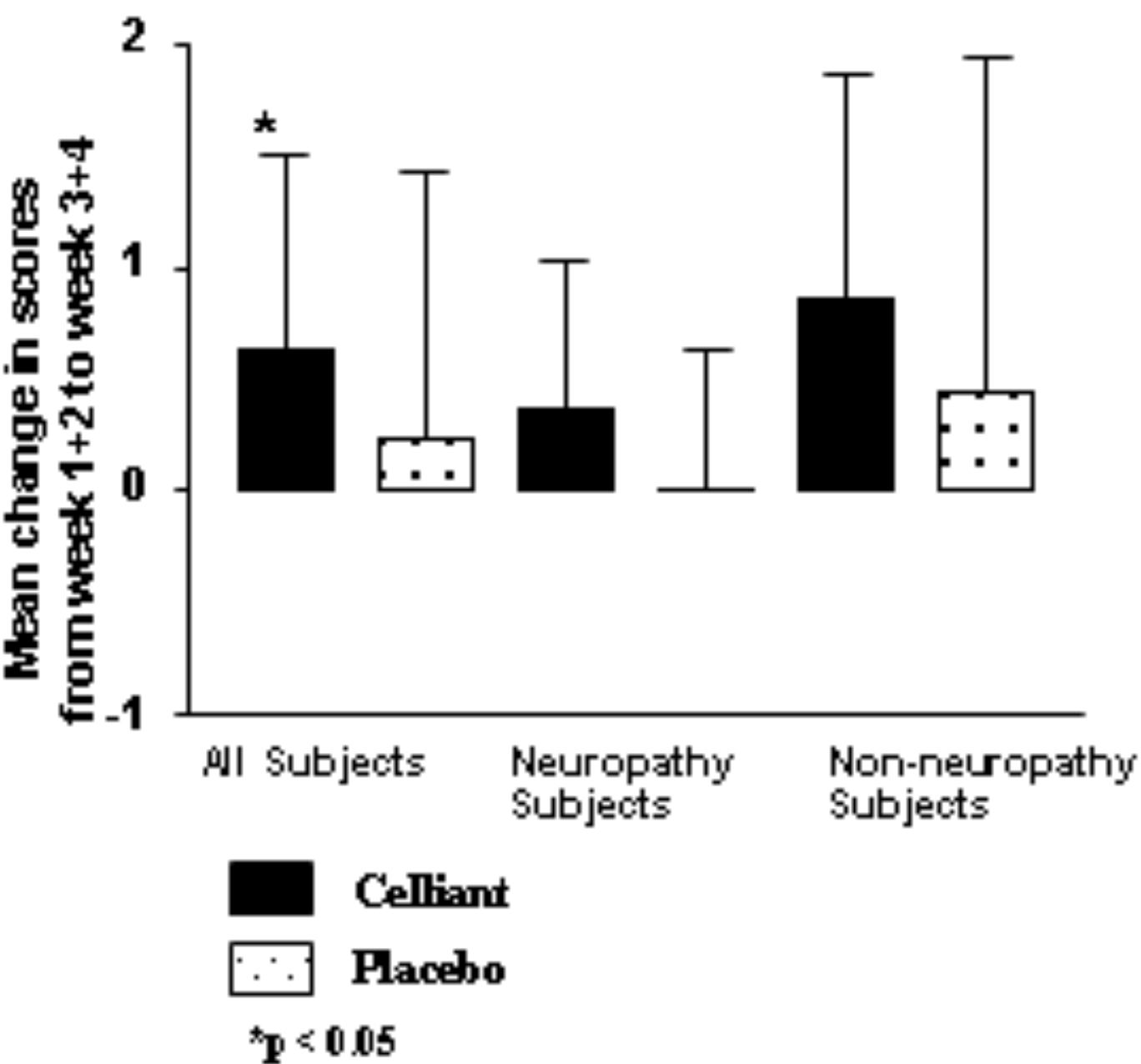
Figure 1

Brief Pain Inventory Pain Severity
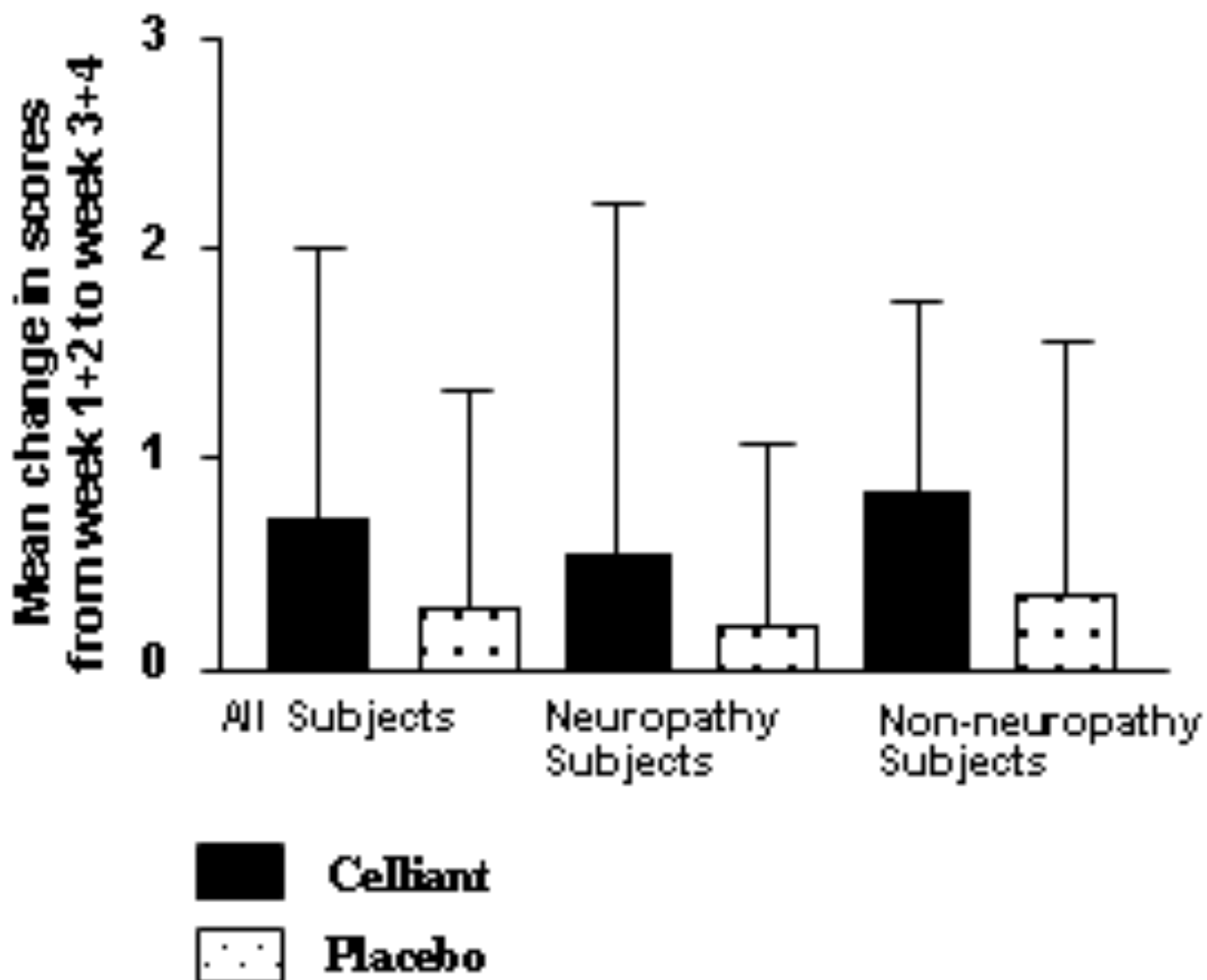
Figure 2
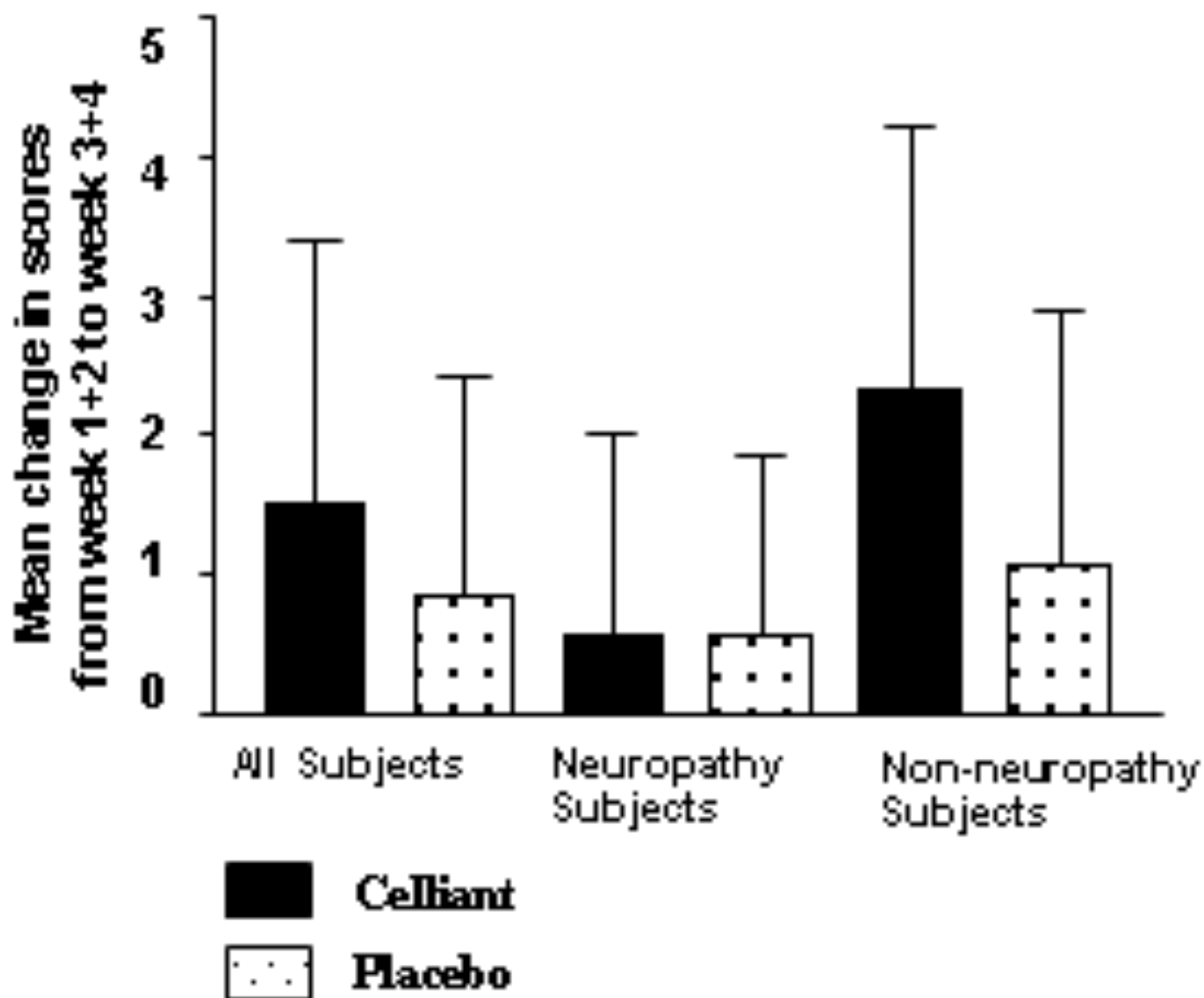
Figure 3

SF-36: Bodily Pain
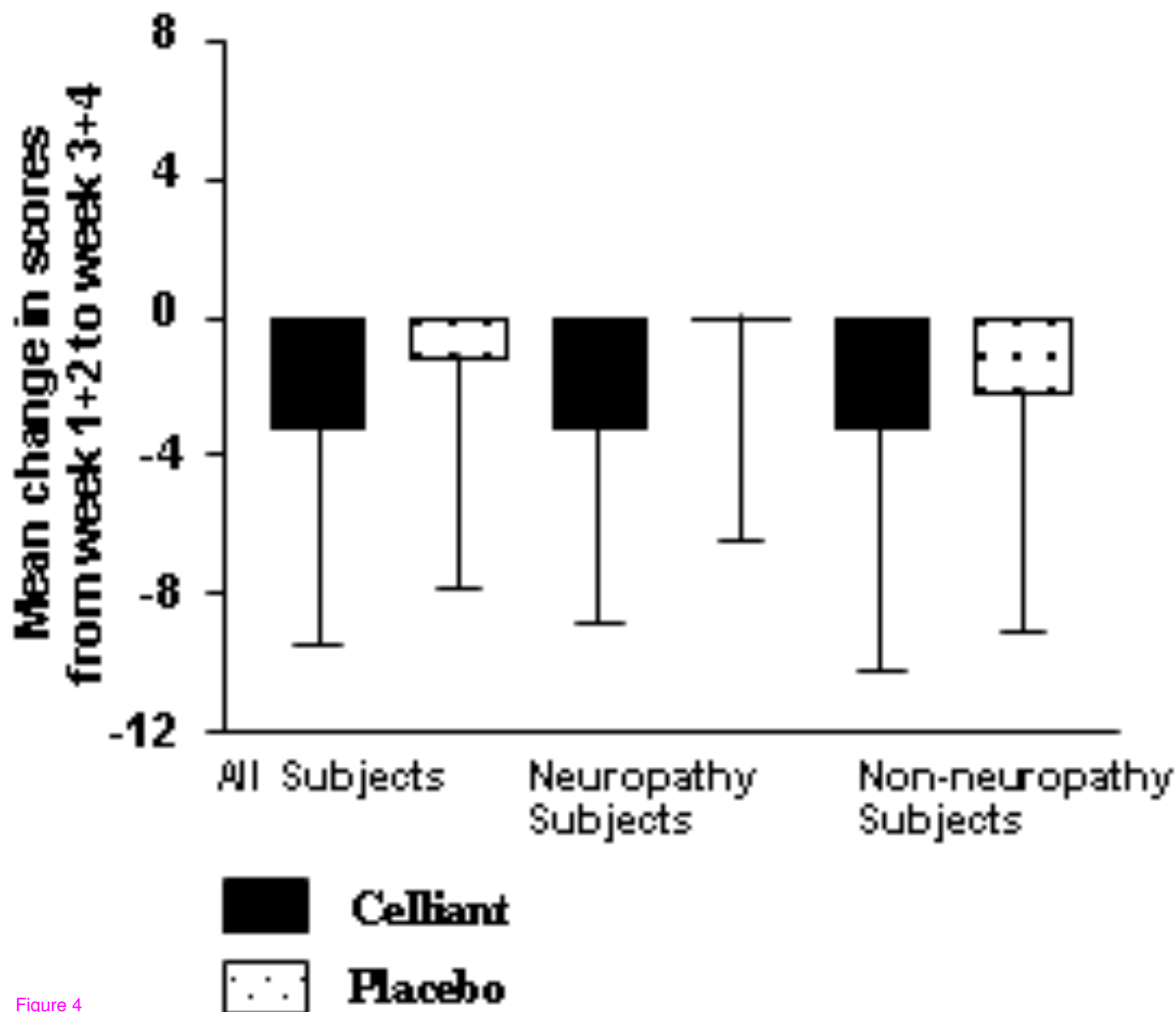
Figure 4

Holofiber Study of Thirteen (13) Healthy Subjects

Dr. Graham McClue

HOLOFIBER STUDY OF THIRTEEN (13) HEALTHY SUBJECTS

OBJECTIVE:

To evaluate changes in peripheral blood flow in the dorsum of the left arm and the Transmetatarsal region of the foot of a healthy group of thirteen (13) persons when a placebo garment and then Holofiber gloves and stockings are worn. It is expected that subjects when wearing the Holofiber garments will have an increase in local tissue perfusion compared to baseline and control garments. The study outcomes are Transcutaneous Oxygen ($TcpO_2$) measurements over the course of one hour each for the placebo and the garment trials, with a ten (10) minute equalization of the probes prior to the start of data acquisition with a 30 minute rest period between studies.

STUDY DESIGN:

This will be an evaluation of changes in peripheral perfusion. Subjects will be selected from a healthy population of males and females between the ages of 18 – 50 and will act as their own controls. I plan to enroll thirteen (13) subjects without a history of diabetes or peripheral vascular disease. Subjects will be evaluated by way of transcutaneous oxygen tension measurement for baseline blood flow status over a period of one (1) hour following a ten (10) minute probe equalization period, during this time the subjects will wear a placebo garment, there will be a 30 minute break between the placebo trial and the product trial.

Subjects will have transcutaneous oxygen measurements recorded using Radiometer TCM 30 Modules supplied by Radiometer America, Inc., Ohio, and modified Clarke Electrodes supplied by Radiometer America, Inc., data will be acquired using Perisoft Version 2.10 supplied by Perimed America, Inc. of North Royalton, Ohio. Each subject will wear stockings and gloves made with and without Holofiber.

Measurements will be recorded prior to wearing the product garments and continuously over a one hour period. I will analyze data at ten (10) minute intervals. Following the 30 minute break, recorded measurements will be taken of both the left arm on the dorsum at a point of mid ulna/radius and left foot at the Transmetatarsal region with study subjects wearing Holofiber versus standard fiber gloves and stockings, the latter being used as the placebo for the purposes of the study. *See Fig. 1 below for study design details*

Step	Duration
Placebo Equalization	10 minutes
Placebo Study	60 minutes
Rest Period	30 minutes
Product Equalization	10 minutes
Product Study	60 minutes
Totals	170 minutes

Fig. 1

8819 Diamond Lake Lane, Houston, Texas – 77083
Telephone: (281) 568-7322
Facsimile: (281) 568-3904
Cell Phone: (832) 287-1758

1

INCLUSION CRITERIA:

1. No known family history of Diabetes or Peripheral Vascular Disease
2. Subjects 18 - 50 years old

EXCLUSION CRITERIA:

1. Patient currently being treated by dialysis, or having serum creatinine greater than or equal to 3.0 mg/dl.

2. Patient known to be an active alcohol or substance abuser for the six months prior to the start of the study.

Subjects will also be excluded if any of the following apply:
1. The use of corticosteriods in a dose equivalent to greater than or equal to 10 mg of prednisone per day.
2. Has ever received immunosuppressive agents.
3. Has ever undergone radiation therapy.
4. Has ever received cytotoxic agents.
5. Subject currently receiving antiviral agents.
6. Subject is a female who is breast feeding, pregnant, or attempting to become pregnant.
7. Patient has other conditions considered by the investigator to be sound reasons for disqualification (e.g., acute illness or exacerbation of chronic illness, lack of motivation, and history of poor compliance).
8. Any history of vascular disease including Arterial or Venous insufficiency.
9. Any history heart disease.

METHOD:

The dynamic non-invasive vascular assessment consisted of transcutaneous oxygen pressure ($TcPO_2$) measurement. I used the Radiometer TCM30 module and data will be acquired using the Perisoft data acquisition software.

The study was non-invasive, and each subject has given verbal consent to the study after an explanation of the methods was explained. Each subject was requested not to smoke or consume liquid containing caffeine at least three (3) hours pre-study.

Preparation of the subject was standardized to the following, the hair was shaved from the test sites, the dermis was then abraded with a fine abrasive material, the stratum corneum was then removed by the use of light weight adhesive tape, and finally the probe site was wiped with an alcohol preparation swab.

8819 Diamond Lake Lane, Houston, Texas – 77083
Telephone: (281) 568-7322
Facsimile: (281) 568-3904
Cell Phone: (832) 287-1758

2

Subjects were then situated in a semi-recumbent position of a Straker gurney, the laboratory was maintained at a constant temperature of 21° C over the duration of the study.

The transcutaneous oxygen electrodes were heated to 45°C and allowed to equilibrate on the skin for ten (10) minutes (until stable values are achieved). The resultant values are measured in mmHg, and is defined as the Partial Pressure or Tension of Oxygen (PpO$_2$). Two self-adhesive fixation rings were affixed and the probes attached thereto. A buffer (KCl) solution was to be used at a rate of three (3) drops in each fixation ring, the probe, a modified Clarke Electrode with heating element and thermsitor was to be utilized. Each module was to be calibrated to an assumed atmospheric pressure of 159 mmHg, this being 20.9% of the standard atmospheric pressure of 760 mmHg, in doing this each patient had the same baseline atmospheric pressure, thus alleviating any pressure changes due to weather variations during the periods of testing. No humidity control was taken into consideration during this study.

I measured transcutaneous oxygen continuously during the one (1) hour placebo evaluation period and recorded seven (7) values for two (2) minutes at each selected marker at random on the dorsum of the foot and hand. During the product trial, I measured continuously and made seven (7) random selections of the 60 minute data collection period at two (2) minute duration each. At the conclusion of each data collection period two (2) comparisons will be made to show the differences recorded between the placebo and the product as outlined in the attached preliminary results.

8819 Diamond Lake Lane, Houston, Texas – 77083
Telephone: (281) 568-7322
Facsimile: (281) 568-3904
Cell Phone: (832) 287-1758

3

PRELIMINARY RESULTS:

SUBJECT 1

Comment: Male, 32 years of age
Non Smoker
Weight: 211 lbs., Height: 5' 7",
BP: 137/85

Percent Change Areas
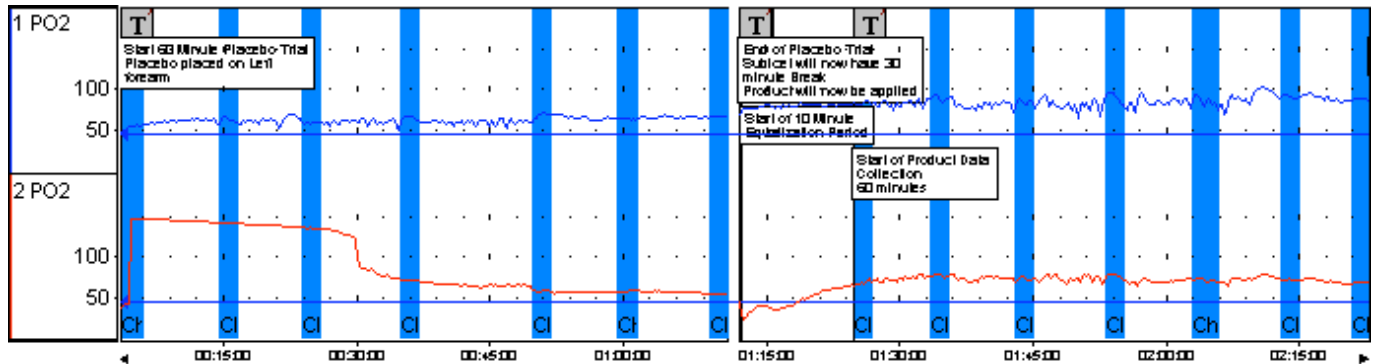
Mean value channel 1 : PO$_2$

Item	Area 1	Area 2	Area 3	Area 4	Area 5	Area 6	Area 7	Area 8	Area 9	Area 10	Area 11	Area 12	Area 13	Area 14	All areas
Mean value	52.51	61.57	58.50	63.73	67.33	62.70	65.46	82.23	88.60	83.64	90.30	85.14	90.22	87.18	74.22

Mean value channel 2 : PO$_2$

Item	Area 1	Area 2	Area 3	Area 4	Area 5	Area 6	Area 7	Area 8	Area 9	Area 10	Area 11	Area 12	Area 13	Area 14	All areas
Mean value	105.72	141.33	135.01	70.47	57.42	57.27	53.69	67.90	76.89	72.41	76.23	70.73	70.85	68.34	80.30

8819 Diamond Lake Lane, Houston, Texas – 77083
Telephone: (281) 568-7322
Facsimile: (281) 568-3904
Cell Phone: (832) 287-1758

4

SUBJECT 2

Comment: Hispanic Male, 23 years of age
Non Smoker.
Weight: 182 lbs., Height: 5' 7"
BP: 132/78
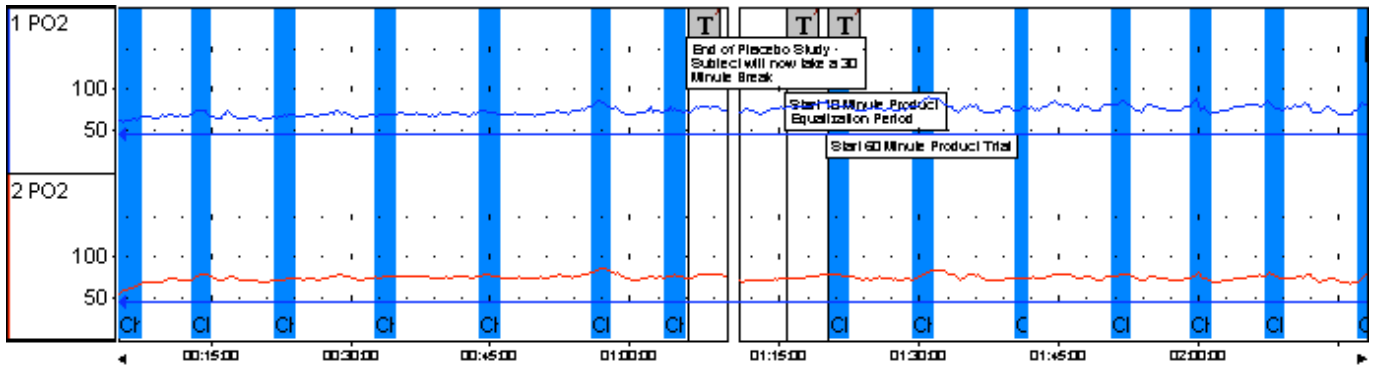
Mean value channel 1 : PO$_2$

Item	Area 1	Area 2	Area 3	Area 4	Area 5	Area 6	Area 7	Area 8	Area 9	Area 10	Area 11	Area 12	Area 13	Area 14	All areas
Mean value	61.46	71.42	66.67	68.44	71.15	81.74	73.58	78.80	84.17	75.46	81.92	78.58	78.44	79.67	75.11

Mean value channel 2 : PO$_2$

Item	Area 1	Area 2	Area 3	Area 4	Area 5	Area 6	Area 7	Area 8	Area 9	Area 10	Area 11	Area 12	Area 13	Area 14	All areas
Mean value	60.47	76.78	71.86	74.80	76.66	83.61	75.54	76.81	77.62	72.96	77.11	75.38	76.29	73.47	74.95

SUBJECT 3

Comment: White Female, 21 years of age
Smoker
Weight: 123 lbs., Height: 5' 8"
BP: 127/76
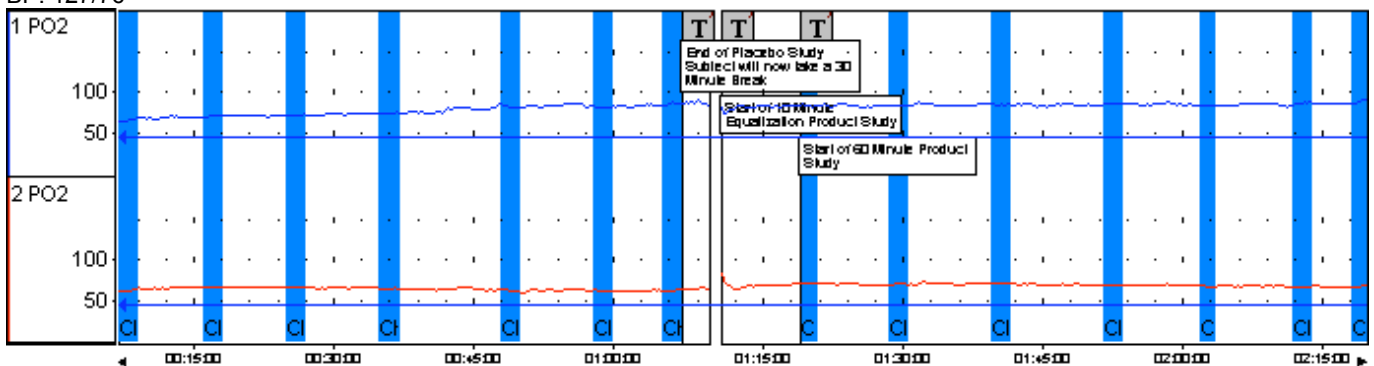
8819 Diamond Lake Lane, Houston, Texas – 77083
Telephone: (281) 568-7322
Facsimile: (281) 568-3904
Cell Phone: (832) 287-1758

5

Mean value channel 1 : PO$_2$

Item	Area 1	Area 2	Area 3	Area 4	Area 5	Area 6	Area 7	Area 8	Area 9	Area 10	Area 11	Area 12	Area 13	Area 14	All areas
Mean value	65.22	69.75	71.26	73.49	81.56	81.23	84.99	82.92	83.26	84.25	84.97	82.66	85.97	87.74	79.95

Mean value channel 2 : PO$_2$

Item	Area 1	Area 2	Area 3	Area 4	Area 5	Area 6	Area 7	Area 8	Area 9	Area 10	Area 11	Area 12	Area 13	Area 14	All areas
Mean value	61.77	66.09	65.54	63.84	62.03	61.54	62.30	70.40	69.58	71.14	68.56	67.01	65.96	66.41	65.87

SUBJECT 4

Comment: Female, 43 years of age
Non Smoker
Weight: 152 lbs., Height: 5' 6"
BP: 118/78

Mean value channel 1 : PO$_2$

Item	Area 1	Area 2	Area 3	Area 4	Area 5	Area 6	Area 7	Area 8	Area 9	Area 10	Area 11	Area 12	Area 13	Area 14	All areas
Mean value	29.07	52.60	54.27	53.21	54.55	62.55	56.05	70.97	71.21	70.35	70.57	69.53	71.97	70.78	61.26

Mean value channel 2 : PO$_2$

Item	Area 1	Area 2	Area 3	Area 4	Area 5	Area 6	Area 7	Area 8	Area 9	Area 10	Area 11	Area 12	Area 13	Area 14	All areas
Mean value	29.12	54.92	52.97	54.03	51.68	55.14	47.01	63.00	61.79	56.86	53.35	51.74	49.19	49.34	52.15

8819 Diamond Lake Lane, Houston, Texas – 77083
Telephone: (281) 568-7322
Facsimile: (281) 568-3904
Cell Phone: (832) 287-1758

6

SUBJECT 5

Comment: White Male, 29 years of age
Non Smoker
Weight: 270 lbs., Height: 5" 10"
BP: 134/76
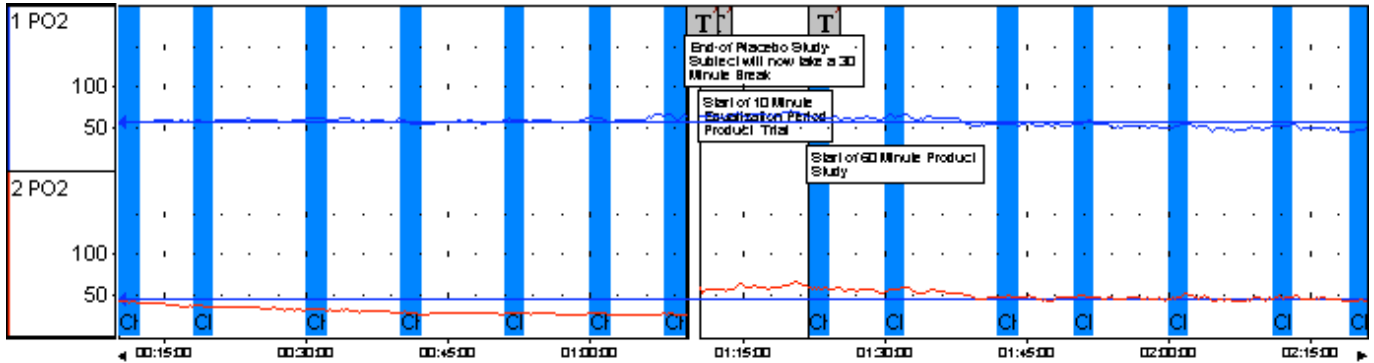
Mean value channel 1 : PO$_2$

Item	Area 1	Area 2	Area 3	Area 4	Area 5	Area 6	Area 7	Area 8	Area 9	Area 10	Area 11	Area 12	Area 13	Area 14	All areas
Mean value	55.80	57.28	60.76	55.87	59.15	60.42	62.79	62.07	63.91	53.51	55.36	51.75	51.31	46.37	56.88

Mean value channel 2 : PO$_2$

Item	Area 1	Area 2	Area 3	Area 4	Area 5	Area 6	Area 7	Area 8	Area 9	Area 10	Area 11	Area 12	Area 13	Area 14	All areas
Mean value	40.57	35.29	31.28	26.77	27.10	26.48	24.87	57.15	56.03	47.23	47.26	46.80	46.22	42.43	39.68

SUBJECT 6

Comment: White Male, 24 years of age
Non Smoker
Weight: 225 lbs., Height: 6' 0"
BP 148/86
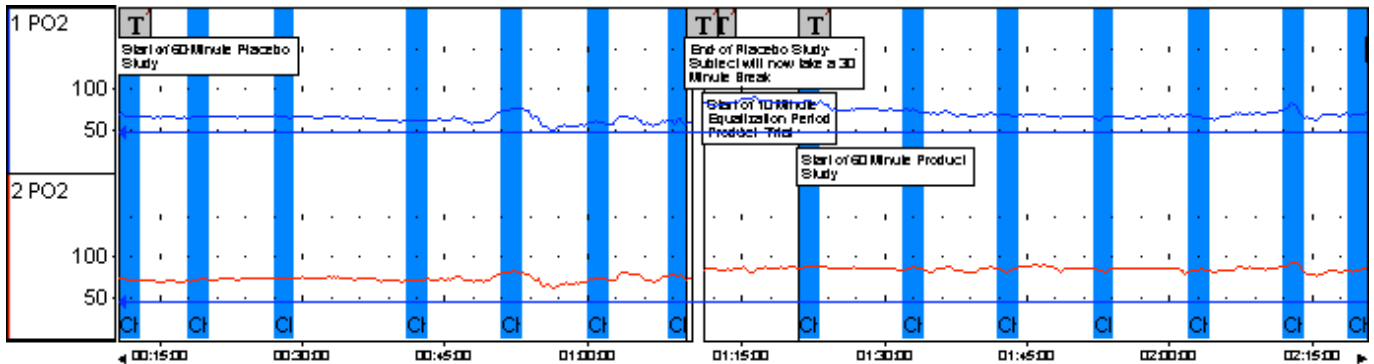
8819 Diamond Lake Lane, Houston, Texas – 77083
Telephone: (281) 568-7322
Facsimile: (281) 568-3904
Cell Phone: (832) 287-1758

7

Mean value channel 1 : PO$_2$

Item	Area 1	Area 2	Area 3	Area 4	Area 5	Area 6	Area 7	Area 8	Area 9	Area 10	Area 11	Area 12	Area 13	Area 14	All areas
Mean value	66.95	65.03	65.37	60.88	74.05	58.72	59.32	66.95	65.03	65.37	60.88	74.05	58.72	59.32	67.77

Mean value channel 2 : PO$_2$

Item	Area 1	Area 2	Area 3	Area 4	Area 5	Area 6	Area 7	Area 8	Area 9	Area 10	Area 11	Area 12	Area 13	Area 14	All areas
Mean value	71.25	71.06	73.43	71.36	80.91	73.02	75.64	87.55	85.67	83.67	83.11	83.53	90.21	83.32	79.55

SUBJECT 7

Comment: White Male, 32 years of age
Non Smoker
Weight: 220 lbs., Height: 5' 7"
BP 122/76
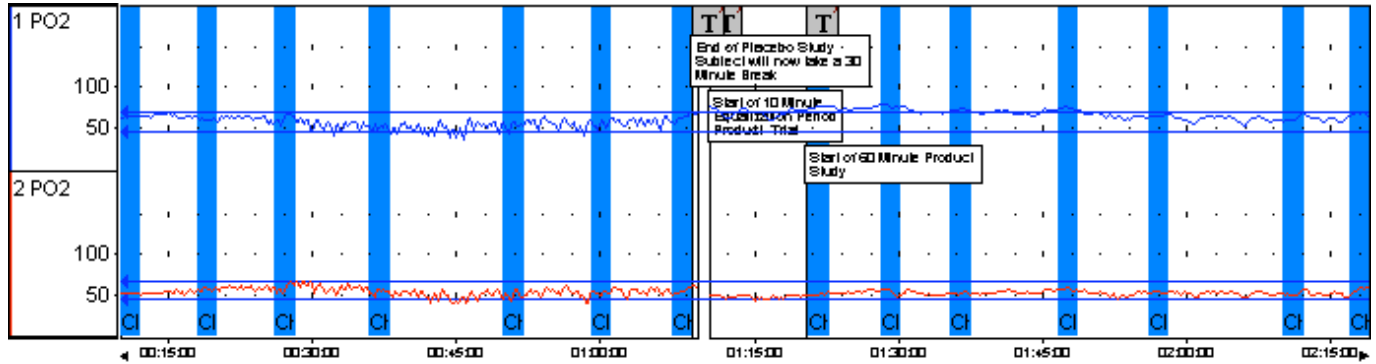
Mean value channel 1 : PO$_2$

Item	Area 1	Area 2	Area 3	Area 4	Area 5	Area 6	Area 7	Area 8	Area 9	Area 10	Area 11	Area 12	Area 13	Area 14	All areas
Mean value	62.73	59.33	60.70	49.25	50.91	52.50	61.59	74.45	75.80	71.58	72.62	63.71	60.16	66.32	62.97

Mean value channel 2 : PO$_2$

Item	Area 1	Area 2	Area 3	Area 4	Area 5	Area 6	Area 7	Area 8	Area 9	Area 10	Area 11	Area 12	Area 13	Area 14	All areas
Mean value	51.17	56.60	57.65	53.15	49.21	51.29	54.27	49.84	53.11	51.36	56.49	52.38	50.32	55.98	53.06

8819 Diamond Lake Lane, Houston, Texas – 77083
Telephone: (281) 568-7322
Facsimile: (281) 568-3904
Cell Phone: (832) 287-1758

8

SUBJECT 8

Comment: White Male, 23 years of age
Smoker
Weight: 177 lbs., Height: 5' 9"
BP
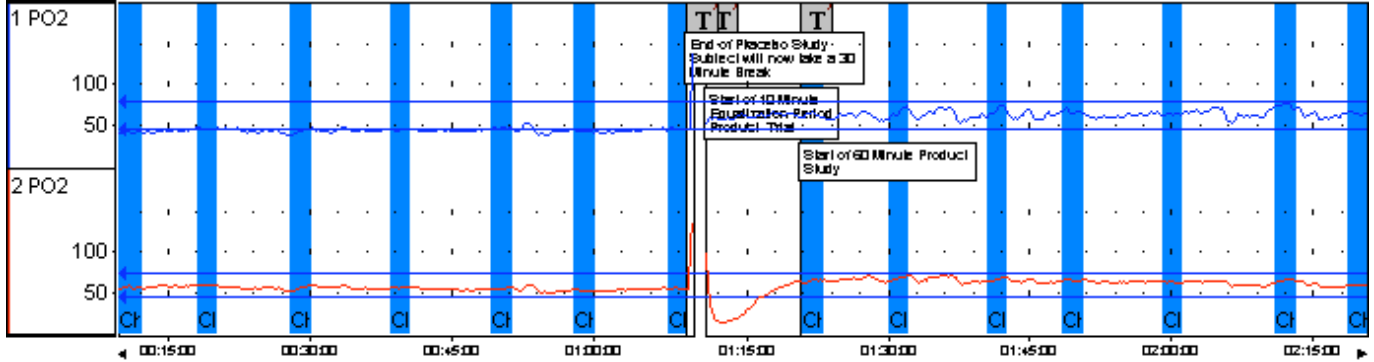
Mean value channel 1 : PO$_2$

Item	Area 1	Area 2	Area 3	Area 4	Area 5	Area 6	Area 7	Area 8	Area 9	Area 10	Area 11	Area 12	Area 13	Area 14	All areas
Mean value	40.21	44.56	41.45	42.86	45.63	41.22	44.78	61.95	64.74	67.84	66.13	62.55	73.45	63.49	54.35

Mean value channel 2 : PO$_2$

Item	Area 1	Area 2	Area 3	Area 4	Area 5	Area 6	Area 7	Area 8	Area 9	Area 10	Area 11	Area 12	Area 13	Area 14	All areas
Mean value	55.57	58.23	54.59	55.08	54.58	51.94	54.28	63.86	66.54	65.61	64.85	62.59	64.64	59.00	59.38

SUBJECT 9

Comment: Hispanic Male, 22 years of age
Non Smoker
Weight: 180 lbs., Height: 5' 7"
BP 128/72
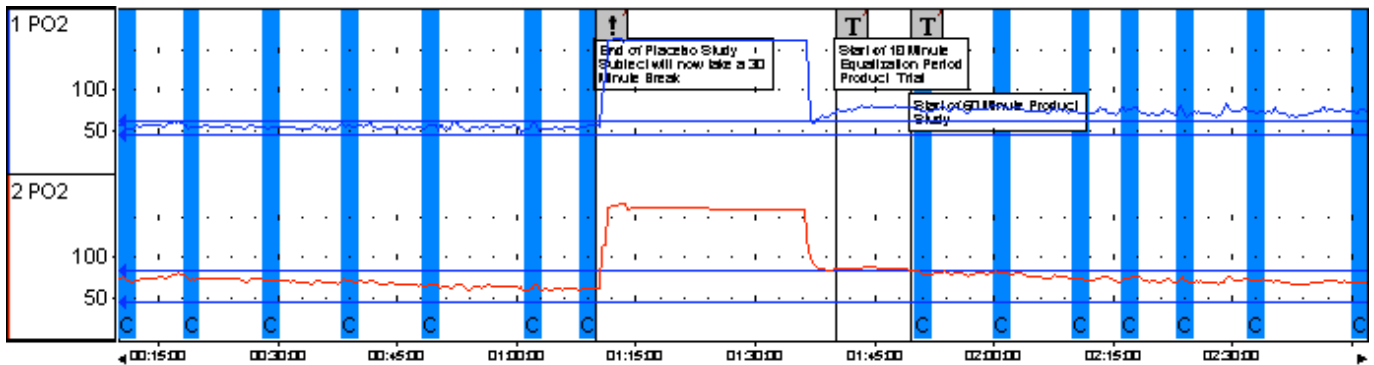
Mean value channel 1 : PO₂

Item	Area 1	Area 2	Area 3	Area 4	Area 5	Area 6	Area 7	Area 8	Area 9	Area 10	Area 11	Area 12	Area 13	Area 14	All areas
Mean value	53.83	54.12	52.73	55.17	54.10	54.12	55.23	73.82	78.59	70.96	76.91	72.29	72.51	73.45	64.13

Mean value channel 2 : PO₂

Item	Area 1	Area 2	Area 3	Area 4	Area 5	Area 6	Area 7	Area 8	Area 9	Area 10	Area 11	Area 12	Area 13	Area 14	All areas
Mean value	71.50	73.64	70.59	69.86	65.00	61.89	60.97	80.17	80.90	72.47	74.01	70.80	70.95	68.63	70.81

SUBJECT 10
Comment: White Male, 45 years of age
Non Smoker
Weight: 157 lbs., Height: 5' 7"
BP 137/82
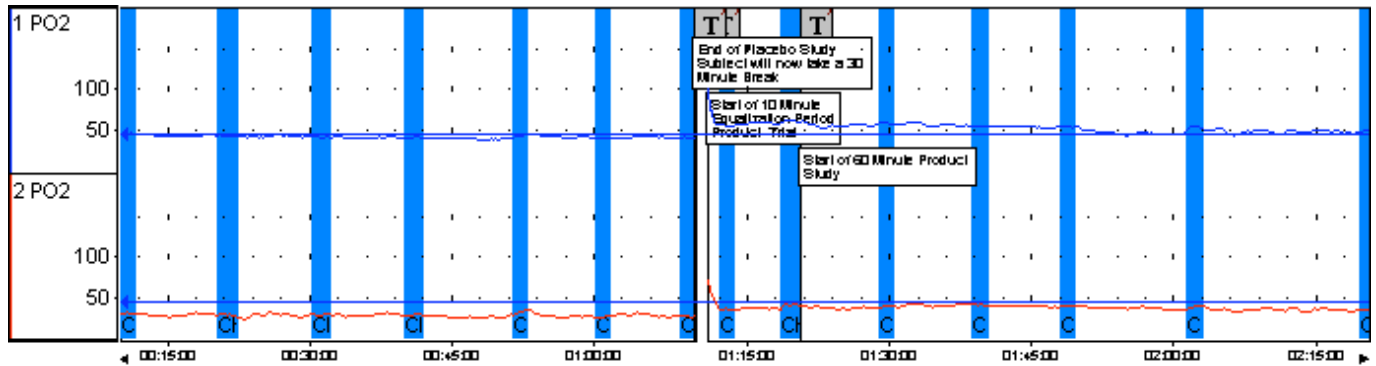
Mean value channel 1 : PO₂

Item	Area 1	Area 2	Area 3	Area 4	Area 5	Area 6	Area 7	Area 8	Area 9	Area 10	Area 11	Area 12	Area 13	Area 14	All areas
Mean value	44.68	42.31	40.45	40.07	41.72	38.89	40.02	55.19	59.96	57.12	52.85	53.47	52.87	48.40	47.71

Mean value channel 2 : PO₂

Item	Area 1	Area 2	Area 3	Area 4	Area 5	Area 6	Area 7	Area 8	Area 9	Area 10	Area 11	Area 12	Area 13	Area 14	All areas
Mean value	29.41	27.81	28.03	27.75	31.32	25.61	25.64	34.21	40.06	38.60	40.44	39.04	37.49	34.06	32.82

8819 Diamond Lake Lane, Houston, Texas – 77083
Telephone: (281) 568-7322
Facsimile: (281) 568-3904
Cell Phone: (832) 287-1758

10

SUBJECT 11

Comment: White Male, 27 years of age
Non Smoker
Weight: 195 lbs., Height: 5' 7"
BP 132/88
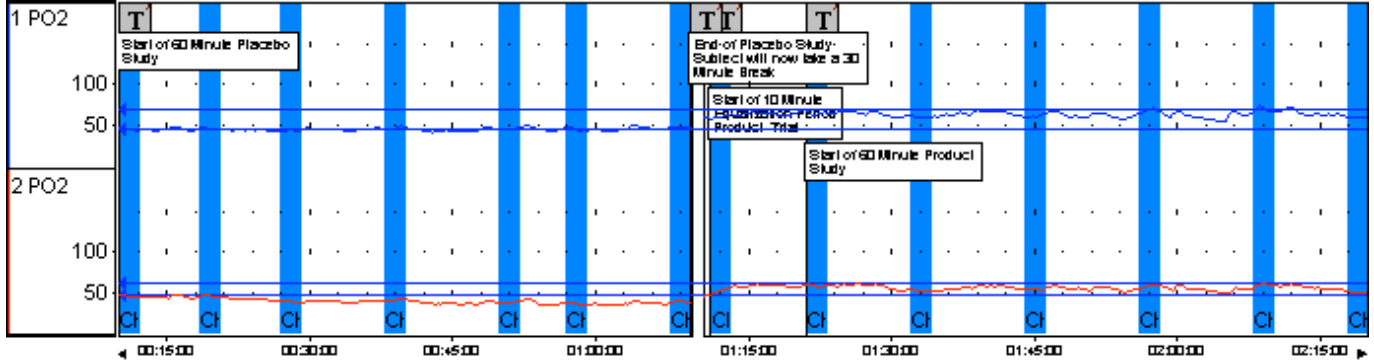
Mean value channel 1 : PO₂

Item	Area 1	Area 2	Area 3	Area 4	Area 5	Area 6	Area 7	Area 8	Area 9	Area 10	Area 11	Area 12	Area 13	Area 14	All areas
Mean value	43.72	44.71	42.37	45.60	44.55	43.88	46.93	59.56	63.30	59.14	60.41	66.90	68.77	57.92	53.41

Mean value channel 2 : PO₂

Item	Area 1	Area 2	Area 3	Area 4	Area 5	Area 6	Area 7	Area 8	Area 9	Area 10	Area 11	Area 12	Area 13	Area 14	All areas
Mean value	44.46	44.84	37.98	40.22	37.50	35.78	37.93	51.87	57.80	52.06	52.80	57.63	58.72	49.27	47.06

SUBJECT 12

Comment: White Female, 44 years of age
Non Smoker
Weight: 130 lbs., Height: 5' 9"
BP 137/78
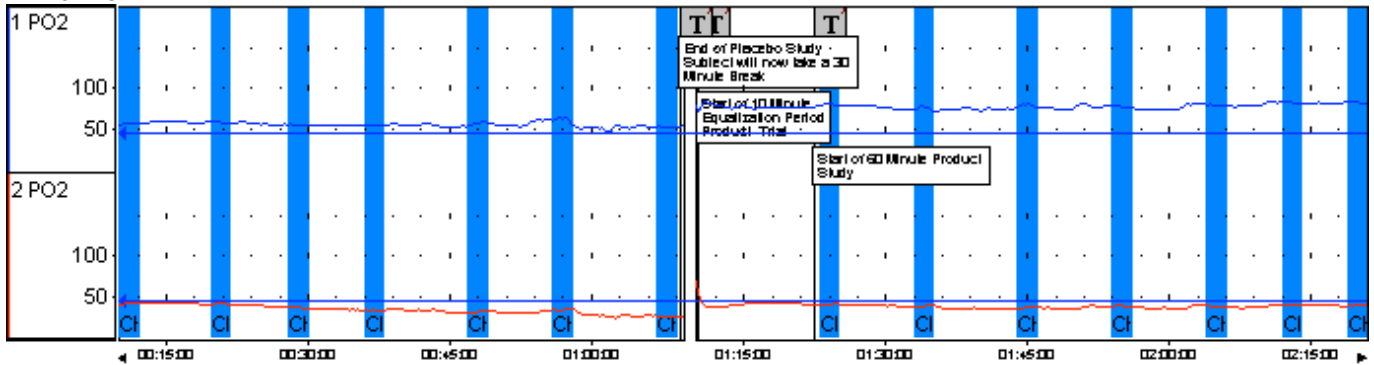
8819 Diamond Lake Lane, Houston, Texas – 77083
Telephone: (281) 568-7322
Facsimile: (281) 568-3904
Cell Phone: (832) 287-1758

11

Mean value channel 1 : PO$_2$

Item	Area 1	Area 2	Area 3	Area 4	Area 5	Area 6	Area 7	Area 8	Area 9	Area 10	Area 11	Area 12	Area 13	Area 14	All areas
Mean value	55.37	57.07	54.35	53.62	56.44	61.37	52.02	79.35	74.93	78.38	76.58	78.16	81.70	81.52	67.20

Mean value channel 2 : PO$_2$

Item	Area 1	Area 2	Area 3	Area 4	Area 5	Area 6	Area 7	Area 8	Area 9	Area 10	Area 11	Area 12	Area 13	Area 14	All areas
Mean value	41.01	40.34	35.60	32.82	30.32	32.98	25.06	39.95	37.33	35.86	37.84	37.25	39.58	38.25	36.02

SUBJECT 13
Comment: White Female, 47 years of age
Non Smoker
Weight: 130 lbs., Height: 5' 5"
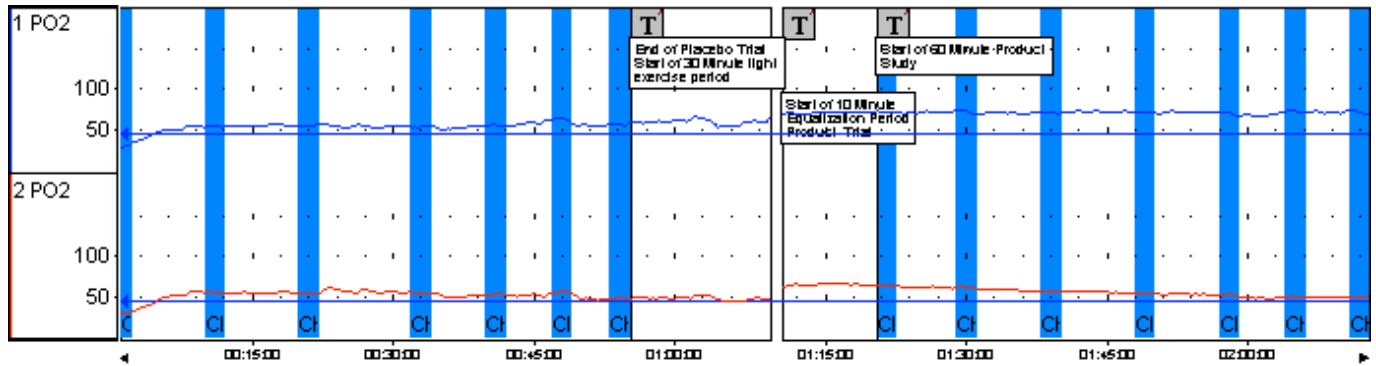BP 118/80
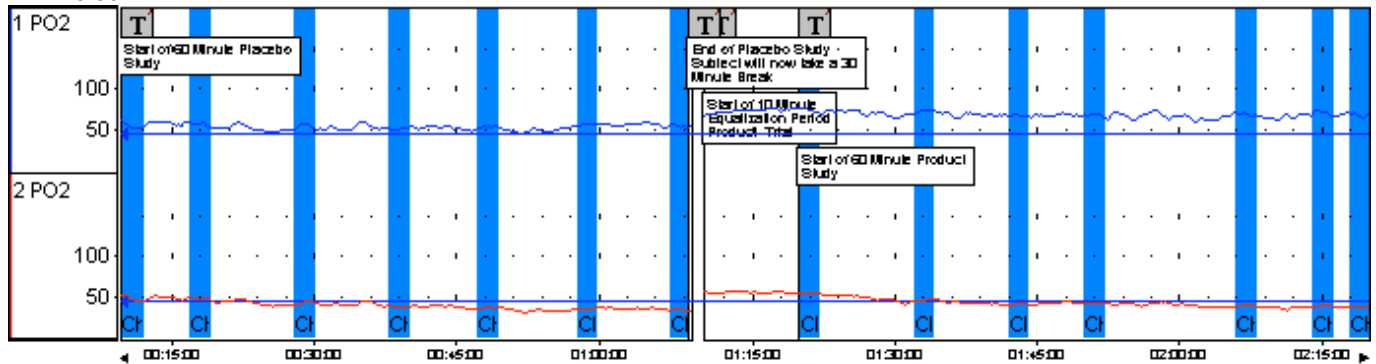
Mean value channel 1 : PO$_2$

Item	Area 1	Area 2	Area 3	Area 4	Area 5	Area 6	Area 7	Area 8	Area 9	Area 10	Area 11	Area 12	Area 13	Area 14	All areas
Mean value	53.61	55.76	54.48	49.76	52.53	55.67	53.79	73.16	71.84	66.51	67.10	68.03	70.36	66.89	61.39

Mean value channel 2 : PO$_2$

Item	Area 1	Area 2	Area 3	Area 4	Area 5	Area 6	Area 7	Area 8	Area 9	Area 10	Area 11	Area 12	Area 13	Area 14	All areas
Mean value	47.43	47.15	42.76	36.98	35.85	34.87	33.37	53.75	44.93	40.19	41.04	38.94	38.43	36.94	40.90

8819 Diamond Lake Lane, Houston, Texas – 77083
Telephone: (281) 568-7322
Facsimile: (281) 568-3904
Cell Phone: (832) 287-1758

12

Subject #	Sex	Age	Area 1	Area 2	Area 3 Placebo (PL)	Area 4	Area 5	Area 6	Area 7	Area Av PL	Area 8	Area 9	Area 10	Area 11 Product (PR)	Area 12	Area 13	Area 14	Area Av PR	% Change PL v PR
1	M	32.75	52.51	61.57	58.50	63.73	67.33	62.70	65.46	**61.69**	82.23	88.60	83.64	90.30	85.14	90.22	87.18	**86.76**	40.65%
1			105.72	141.33	135.01	70.47	57.42	57.27	53.69	**88.70**	67.90	76.89	72.41	76.23	70.73	70.85	68.34	**71.91**	-18.93%
2	M	23.50	61.46	71.42	66.67	68.44	71.15	81.74	73.58	**70.64**	78.80	84.17	75.46	81.92	78.58	78.44	79.67	**79.58**	12.66%
2			60.47	76.78	71.86	74.80	76.66	83.61	75.54	**74.25**	76.81	77.62	72.96	77.11	75.38	76.29	73.47	**75.66**	1.91%
3	F	20.85	65.22	69.75	71.26	73.49	81.56	81.23	84.99	**75.36**	82.92	83.26	84.25	84.97	82.66	85.97	87.74	**84.54**	12.18%
3			61.77	66.09	65.54	63.84	62.03	61.54	62.3	**63.30**	70.4	69.58	71.14	68.56	67.01	65.96	66.41	**68.44**	8.11%
4	F	43.72	29.07	52.6	54.27	53.21	54.55	62.55	56.05	**51.76**	70.97	71.21	70.35	70.57	69.53	71.97	70.78	**70.77**	36.73%
4			29.12	54.92	52.97	54.03	51.68	55.14	47.01	**49.27**	63	61.79	56.86	53.35	51.74	49.19	49.34	**55.04**	11.71%
5	M	29.25	55.8	57.28	60.76	55.87	59.15	60.42	62.79	**58.87**	62.07	63.91	53.51	55.36	51.75	51.31	46.37	**54.90**	-6.74%
5			40.57	35.29	31.28	26.77	27.1	26.48	24.87	**30.34**	57.15	56.03	47.23	47.26	46.8	46.22	42.43	**49.02**	61.57%
6	M	24.37	66.95	65.03	65.37	60.88	74.05	58.72	59.32	**64.33**	66.95	65.03	65.37	60.88	74.05	58.72	59.32	**64.33**	0.00%
6			71.25	71.06	73.43	71.36	80.91	73.02	75.64	**73.81**	87.55	85.67	83.67	83.11	83.53	90.21	83.32	**85.29**	15.56%
7	M	32.65	62.73	59.33	60.7	49.25	50.91	52.5	61.59	**56.72**	74.45	75.8	71.58	72.62	63.71	60.16	66.32	**69.23**	22.07%
7			51.17	56.6	57.65	53.15	49.21	51.29	54.27	**53.33**	49.84	53.11	51.36	56.49	52.38	50.32	55.98	**52.78**	-1.03%
8	M	23.95	40.21	44.56	41.45	42.86	45.63	41.22	44.78	**42.96**	61.95	64.74	67.84	66.13	62.55	73.45	63.49	**65.74**	53.02%
8			55.57	58.23	54.59	55.08	54.58	51.94	54.28	**54.90**	63.86	66.54	65.61	64.85	62.59	64.64	59.00	**63.87**	16.35%
9	M	22.70	53.83	54.12	52.73	55.17	54.1	54.12	55.23	**54.19**	73.82	78.59	70.96	76.91	72.29	72.51	73.45	**74.08**	36.71%
9			71.5	73.64	70.59	69.86	65	61.89	60.97	**67.64**	80.17	80.9	72.47	74.01	70.8	70.95	68.63	**73.99**	9.39%
10	M	44.30	44.68	42.31	40.45	40.07	41.72	38.89	40.02	**41.16**	55.19	59.96	57.12	52.85	53.47	52.87	48.40	**54.27**	31.83%
10			29.41	27.81	28.03	27.75	31.32	25.61	25.64	**27.94**	34.21	40.06	38.60	40.44	39.04	37.49	34.06	**37.70**	34.94%
11	M	27.90	43.72	44.71	42.37	45.6	44.55	43.88	46.93	**44.54**	59.56	63.30	59.14	60.41	66.90	68.77	57.92	**62.29**	39.85%
11			44.46	44.84	37.98	40.22	37.5	35.78	37.93	**39.82**	51.87	57.80	52.06	52.80	57.63	58.72	49.27	**54.31**	36.40%
12	F	44.75	55.37	57.07	54.35	53.62	56.44	61.37	52.02	**55.75**	79.35	74.93	78.38	76.58	78.16	81.70	81.52	**78.66**	41.10%
12			41.01	40.34	35.60	32.82	30.32	32.98	25.06	**34.02**	39.95	37.33	35.86	37.84	37.25	39.58	38.25	**38.01**	11.73%
13	F	46.90	53.61	55.76	54.48	49.76	52.53	55.67	53.79	**53.66**	73.16	71.84	66.51	67.10	68.03	70.36	66.89	**69.13**	28.83%
13			47.43	47.15	42.76	36.98	35.85	34.87	33.37	**39.77**	53.75	44.93	40.19	41.04	38.94	38.43	36.94	**42.03**	5.68%
		32.12																	
			52.70	*56.58*	*55.64*	*54.77*	*57.97*	*58.08*	*58.20*	***56.28***	*70.88*	*72.72*	*69.55*	*70.51*	*69.76*	*70.50*	*68.39*	***70.33***	*24.97%*
			54.57	*61.08*	*58.25*	*52.09*	*50.74*	*50.11*	*48.51*	***53.62***	*61.27*	*62.17*	*58.49*	*59.47*	*57.99*	*58.37*	*55.80*	***59.08***	*10.18%*

Areas 1 -3 = Placebo (PL)

Areas 4 - 10 = Product (PR)

Male 9

Female = 4

CONCLUSIONS:

All the data that these conclusions are drawn from is contained within the information table on page 13 of this document.

Thirteen (13) subjects were chosen at random and tested in accordance with the protocol within the study design, the breakdown of the subjects was:

Female	N = 4
Male	N = 9

With an age range of 20.85 years to 46.75 years (mean 32.12 years).

Data designated in areas 1 – 7 is the Placebo trial and those data within areas 8 – 14 is the Product trial.

In looking at the collective data it will be noted that with the exception of three (3) subjects, Nos: 1, 5, and 7 there was a substantial increase in oxygen perfusion when using the Holofiber product. These increases in the Placebo versus Product vary in range in the mid radial ulna region of the dorsum, designated channel 1, from 0.00% to 53.02% with a mean of 29.97%, these figures exclude the one (1) subject that showed a negative increase in perfusion levels in this region. In channel 2, the Transmetatarsal region of the foot, increases ranged from 1.91 – 61.57% with the mean being 10.18%, these numbers exclude those subjects that showed a diminished perfusion in this region.

In the case of subjects 1, 5, and 7, it will be noted that in the case of subject 1 there was a decrease in the Transmetatarsal region of 18.93% and in subject 5, there was a decrease of 6.74% in the mid radial ulna region of the dorsum, and in subject 7 a decrease of 1.03% was observed in the metatarsal region of the foot. This discrepancy cannot be explained without further medical investigation which is outside the scope of this study.

Increased oxygen profusion has been shown to aid in the increase of energy. Energy produced at the cellular level will accelerate muscle tissue recovery from exercise, which is known to induce lactic acid increases, rebuild strength in muscles damaged by exercise, and also reduce the incidence of cramping, edema, and muscle fatigue post strenuous exercise in athletic conditioning.

In conclusion, it is the opinion of this researcher, based on this study, that Holofiber does, in fact, increase oxygen perfusion levels within by 10% to 24% in a healthy non-compromised population.

_____

Graham M. McClue, Ph.D.   Date

8819 Diamond Lake Lane, Houston, Texas – 77083
Telephone: (281) 568-7322
Facsimile: (281) 568-3904
Cell Phone: (832) 287-1758

14

Improving Blood Flow with Holofiber in the Hands and Feet of High-Risk Diabetics

Dr. Lawrence Lavery

Improving Blood Flow with Holofiber in the Hands and Feet of High-Risk Diabetics

Objective: To evaluate changes in peripheral blood flow in the hands and feet of persons with diabetes when Holofiber gloves and stockings are worn. We expect that patients that wear the Holofiber garments will have an increase in local tissue perfusion compared to baseline and control garments. The study outcomes are transcutaneous oxygen and laser Doppler flowometry measurements over the course of one hour while the study subjects wear Holofiber garments and placebo garments.

Study Design: This will be a double blind evaluation of changes in peripheral perfusion. Subjects will act as their own controls. We plan to enroll 20 subjects with a history of diabetes and vascular impairment. Subjects will be evaluated for baseline blood flow status. They will then have transcutaneous oxygen (Perimed Inc. North Royalton, Ohio, PF5040 transcutaneous module) and laser Doppler flowometry measurements (PF5010Laser Doppler Perfusion module) with stockings and gloves made with and without Holofiber. Measurements will be made prior to wearing the garments and continuously over a one hour period. We will analyze data at ten minute intervals. The tester and subject will be blinded to the study garment. Garments will be randomly selected and tested from a computer generated randomization list. We will take measurements of both the hand and foot with study subjects wearing Holofiber versus standard fiber gloves and stockings.

The diagnosis of diabetes mellitus will be based on World Health Organization criteria.[8] For the purposes of this study, the diagnosis of peripheral vascular disease will be a transcutaneous oxygen measurement > 30mm Hg taken at the transmetatarsal level on the day of enrollment.[5, 9]

Inclusion Criteria:
1. Diagnosis of Diabetes Mellitus by the World Health Organization Criteria
2. Patient 18 -80 years old.

Exclusion Criteria:

1. Patient currently being treated by dialysis, or having serum creatinine greater than or equal to 3.0 mg/dl.
2. Patient known to be an active alcohol or substance abuser for the six months prior to the start of the study.
3. Patient currently receiving systemic corticosteriods in a dose equivalent to greater than or equal to 10 mg of prednisone per day.
4. Patient currently receiving immunosuppressive agents.
5. Patient currently receiving radiation therapy.
6. Patient currently receiving cytotoxic agents.
7. Patient currently receiving antiviral agents.
8. Patient having history of widespread malignant or systemically immunocompromising disease.
9. Patient is a female who is breast feeding, pregnant, or attempting to become pregnant.
10. Patient has other conditions considered by the investigator to be sound reasons for disqualification (e.g., acute illness or exacerbation of chronic illness, lack of motivation, and history of poor compliance).
11. Amputation proximal toLisfranc's(tarsometatarsal) joint or if amputation/surgical debridement has destroyed the venous plexus of the plantar arch.
12. Acute deep venous thrombosis.
13. Active congestive heart failure.
14. Uncontrolled osteomyelitis.
15. Vascular surgery in the past 4 weeks.
16. Patient has a full thickness skin ulcer.

The dynamic non-invasive vascular assessment will consist of transcutaneous oxygen pressure (TcPO$_2$) measurement, and laser Doppler flowmetric measurement. We will use the PeriFlux 5000 System It is a multifunctional system that incorporates four functional units that combine transcutansous oxygen and laser Doppler function units.

The transcutaneous oxygen electrodes are warmed to 44°C and allowed to equilibrate on the skin for 5 minutes (until stable values are achieved). The resultant values are measured in mmHg. [5, 9] The laser Doppler monitor will be used to continuously measure tissue blood perfusion (PF5010 Laser Doppler Perfusion module). The application is non-invasive. Two stick-on probes similar to standard EKG probes are applied to the skin. In the tissue, the laser light is scattered and Doppler shifted by interaction with the moving blood cells according to the well-known Doppler principle. The sampling depth is on the order of 200-500 micrometers. A fraction of the backscattered light is detected by a remotely positioned photo detector.

We will measure transcutaneous oxygen and laser Doppler flowometry measurements continuously during the one hour evaluation period and record values for 60 seconds at ten minute intervals on the dorsum of the foot and hand. In addition, we will measure a two minute interval at the conclusion of each data collection period to compare the change in blood flow parameters in placebo and Holofiber treatment groups.

Results:

We used a paired t-test to compare transcutaneous oxygen (TCOM) and laser Doppler (LD) values on the hand and foot. Treanscutaneous oxygen measures the partial pressure of oxygen at the surface of the skin, and the laser Doppler measures capillary blood flow. As part of the descriptive evaluation of the data we, stratified TCOM and LD into three levels: increase when comparing Holofiber to placebo, no change or a decrease when comparing Holofiber to placebo. If there was less than a 4% change when the placebo vs. Holofiber was used, this was determined to represent "no change". TCOM's in the hand showed 10 subjects with an increase, 4 unchanged and 6 with a decrease when using Holofiber compared to the placebo garment. TCOM's in the foot again showed 10 subjects with an increase when using Holofiber, 4 were unchanged and 6 were decreased.

There was a statistically significant change in transcutaneous oxygen or the oxygen delivery to the skin in the hand and foot when using the paired t-test to compare data collected at time periods 40 and 50 minutes after initiation of testing. The Laser Doppler

studies did not show a difference in blood flow in placebo versus Holofiber in either the hand or the foot. The significant changes observed are very compelling for this type of product. An 8-12% improvement in skin oxygenation could improve marginal circulation enough to improve wound healing or eliminate ischemic pain of the legs.

All 10 Minute Interval Data (Paired)

Paired T-Test and CI: TCOM HAND-Placebo, TCOM HAND-Holofiber

```
Paired T for TCOM HAND-Placebo - TCOM HAND-Holofiber

                 N      Mean     St Dev   SE Mean
TCOM HAND-Pl    120    15.284    7.613     0.695
TCOM HAND-ho    120    17.323   10.505     0.959
Difference      120    -2.039    7.718     0.705

95% CI for mean difference: (-3.434, -0.644)
T-Test of mean difference = 0 (vs not = 0): T-Value = -2.89  P-Value = 0.005
```
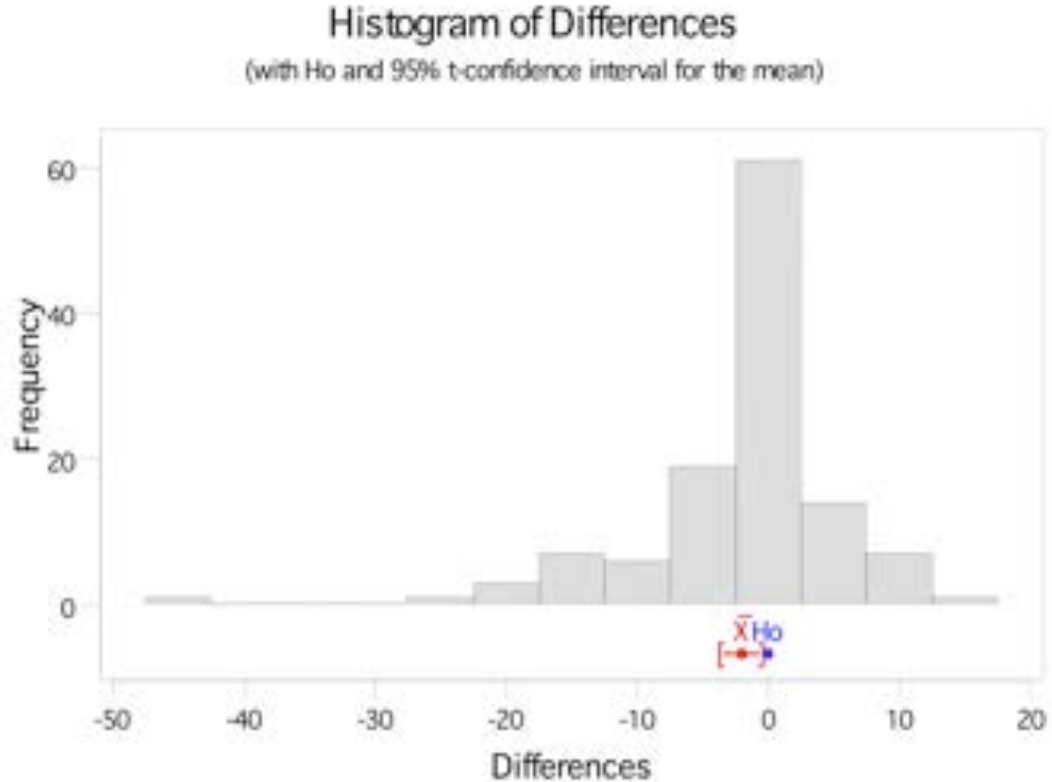

Histogram of Differences
(with Ho and 95% t-confidence interval for the mean)

All 10 Minute Interval Data (Paired)

Paired T-Test and CI: TCOM FOOT-Placebo, TCOM FOOT-Holofiber

```
Paired T for TCOM FOOT-Placebo - TCOM FOOT-Holofiber

                  N       Mean    St Dev   SE Mean
TCOM FOOT-pl     120      52.22    20.39     1.86
TCOM FOOT-ho     120      56.35    20.01     1.83
Difference       120      -4.13    11.25     1.03

95% CI for mean difference: (-6.16, -2.10)
T-Test of mean difference = 0 (vs not = 0): T-Value = -4.02   P-Value = 0.000
```
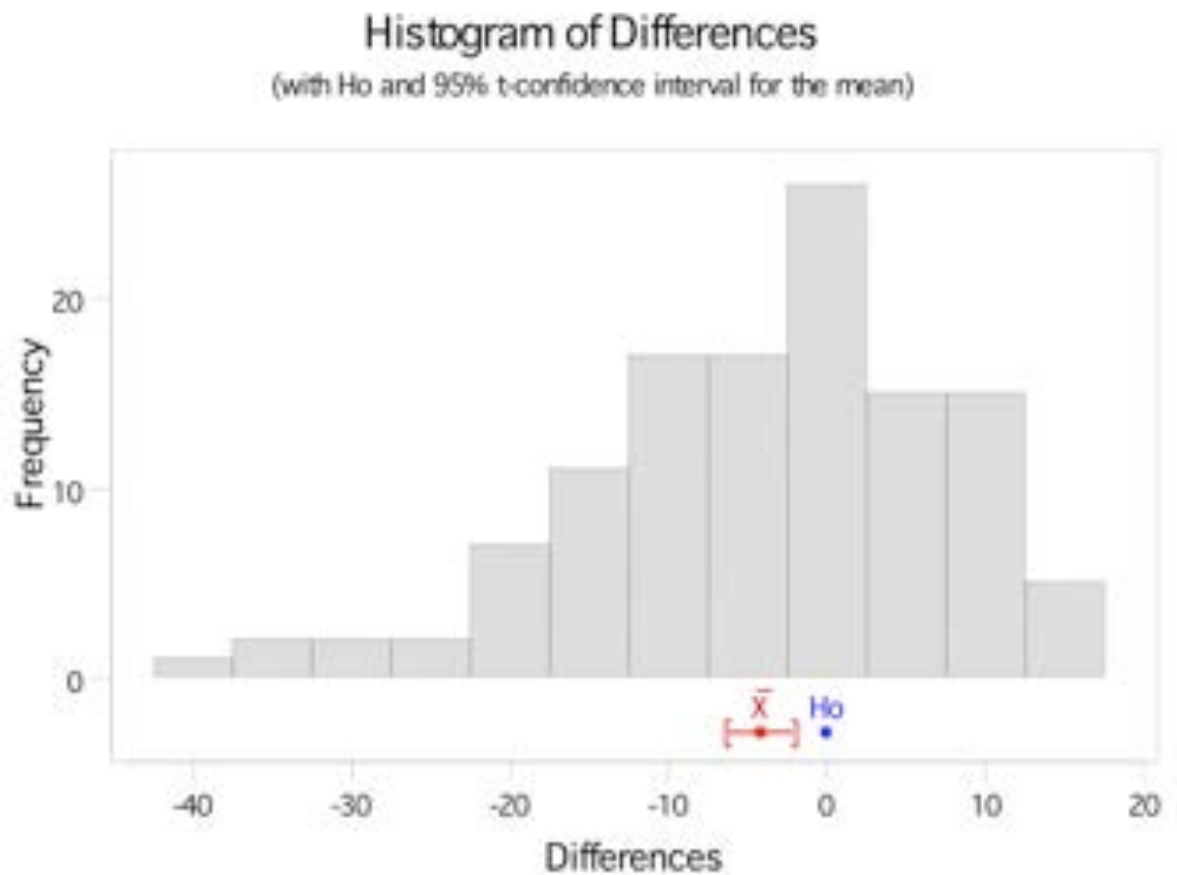
Histogram of Differences
(with Ho and 95% t-confidence interval for the mean)

All 10 Minute Interval Data (Paired)

Paired T-Test and CI: LASER HAND-Placebo, LASER HAND-Holofiber

```
Paired T for LASER HAND-Placebo - LASER HAND-Holofiber

                N      Mean    St Dev   SE Mean
LASER HAND-p   120     35.00    28.84     2.63
LASER HAND-h   120     33.91    25.62     2.34
Difference     120      1.09    15.67     1.43

95% CI for mean difference: (-1.74, 3.92)
T-Test of mean difference = 0 (vs. not = 0): T-Value = 0.76  P-Value = 0.447
```
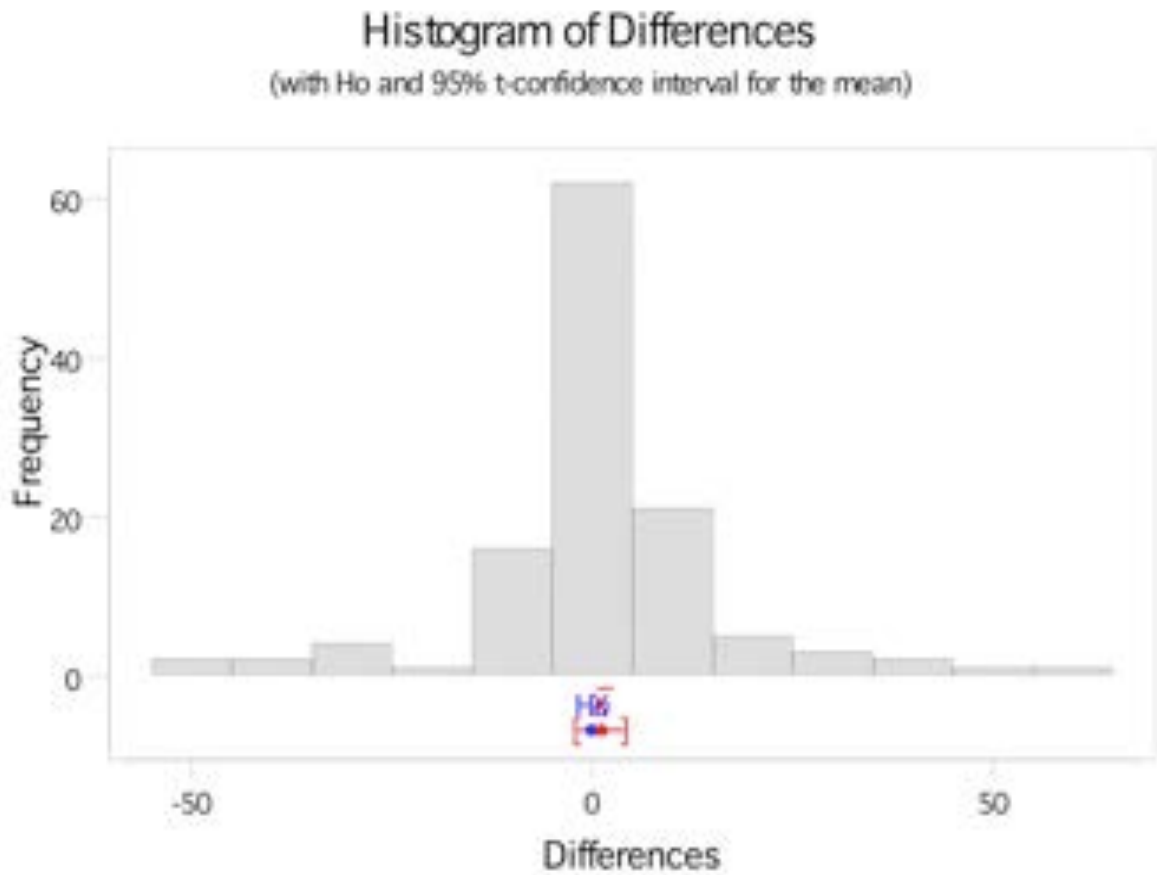

Histogram of Differences
(with Ho and 95% t-confidence interval for the mean)

All 10 Minute Interval Data (Paired)

Paired T-Test and CI: LASER FOOT-Placebo, LASER FOOT-Holofiber

```
Paired T for LASER FOOT-Placebo - LASER FOOT-Holofiber

                 N      Mean     St Dev    SE Mean
LASER FOOT-p    120     49.68     21.12     1.93
LASER FOOT-h    120     49.64     19.55     1.78
Difference      120      0.04     15.79     1.44

95% CI for mean difference: (-2.81, 2.90)
T-Test of mean difference = 0 (vs. not = 0): T-Value = 0.03   P-Value = 0.976
```
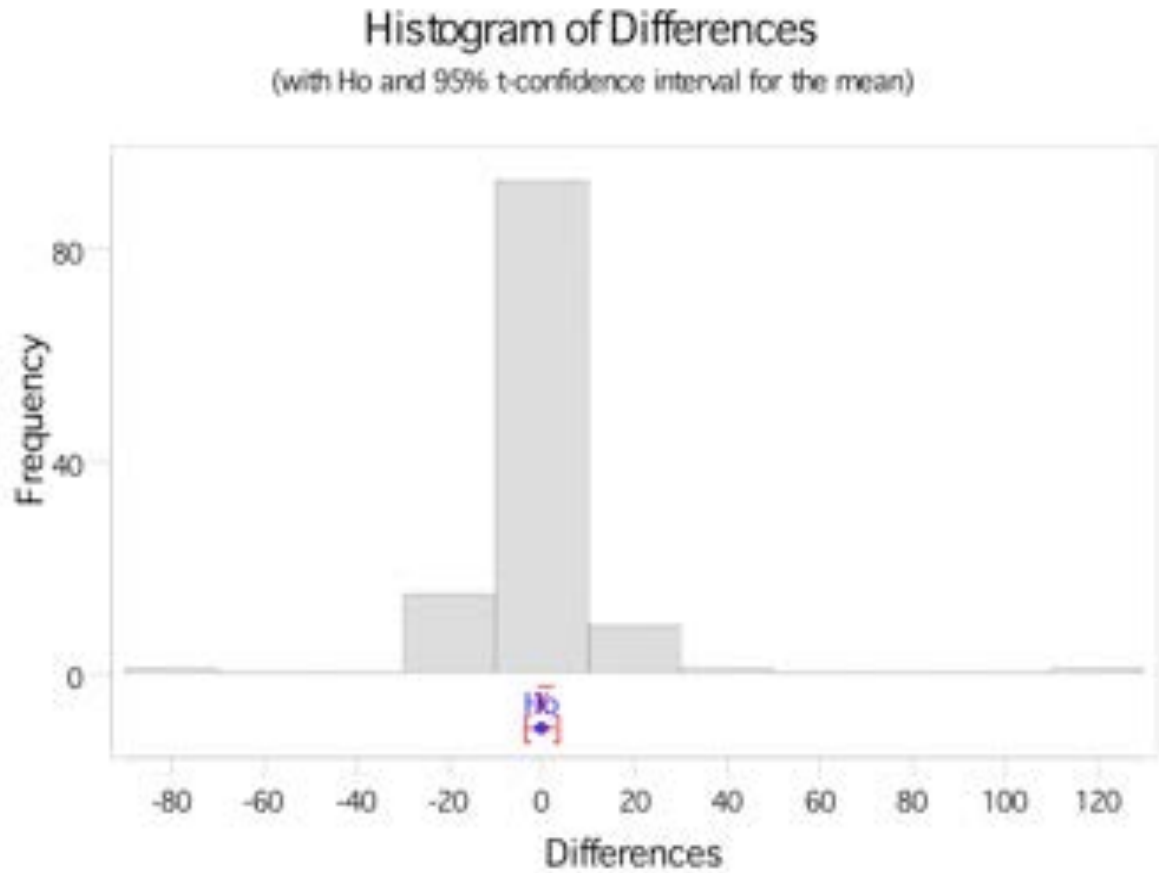

Histogram of Differences
(with Ho and 95% t-confidence interval for the mean)

Last Three Points of 10 Minute Interval Data (Paired)

Paired T-Test and CI: TCOM HAND-Placebo, TCOM HAND-Holofiber

```
Paired T for TCOM HAND-Placebo - TCOM HAND-Holofiber

                 N       Mean      St Dev    SE Mean
TCOM HAND-Pl     60      14.62      7.08       0.91
TCOM HAND-ho     60      17.19      9.75       1.26
Difference       60     -2.572     6.784      0.876

95% CI for mean difference: (-4.325, -0.819)
T-Test of mean difference = 0 (vs. not = 0): T-Value = -2.94   P-Value = 0.005
```


Histogram of Differences
(with Ho and 95% t-confidence interval for the mean)
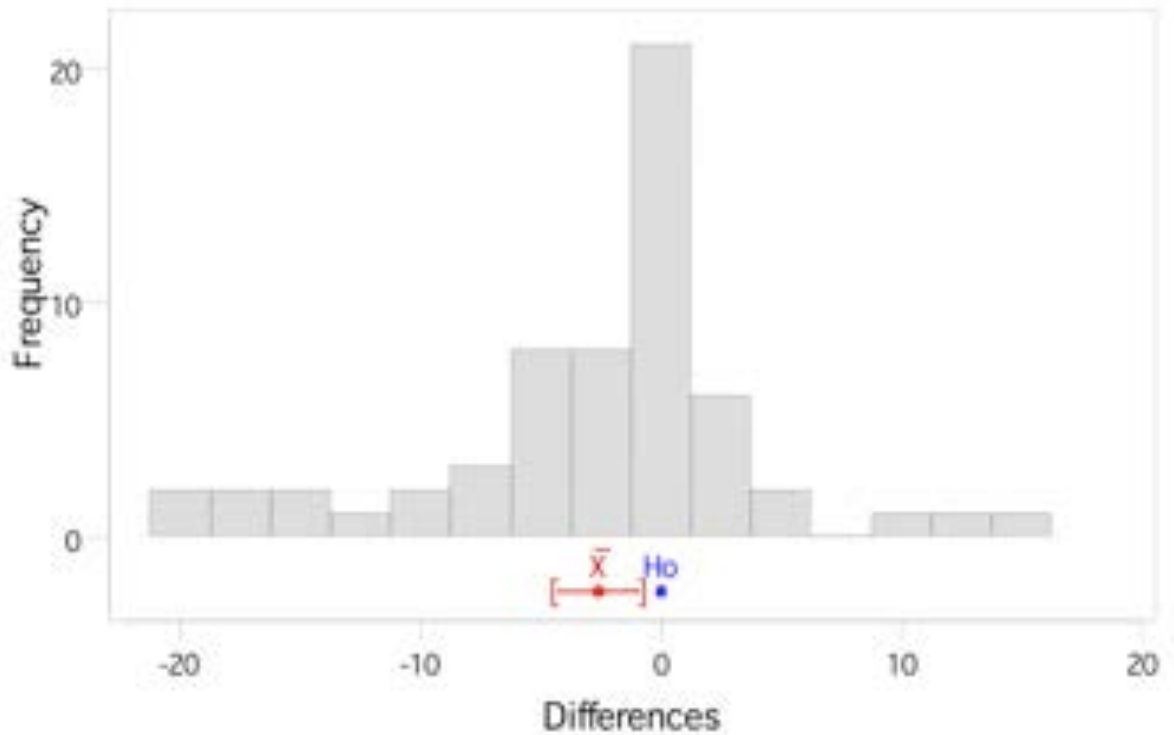
Last Three Points of 10 Minute Interval Data (Paired)

Paired T-Test and CI: TCOM FOOT-Placebo, TCOM FOOT-Holofiber

```
Paired T for TCOM FOOT-Placebo - TCOM FOOT-Holofiber

                   N       Mean     St Dev   St Dev    SE Mean
TCOM FOOT-pl      60      54.19     19.90     2.57
TCOM FOOT-ho      60      58.57     21.29     2.75
Difference        60      -4.38     12.27     1.58

95% CI for mean difference: (-7.55, -1.21)
T-Test of mean difference = 0 (vs. not = 0): T-Value = -2.76   P-Value = 0.008
```


Histogram of Differences
(with Ho and 95% t-confidence interval for the mean)
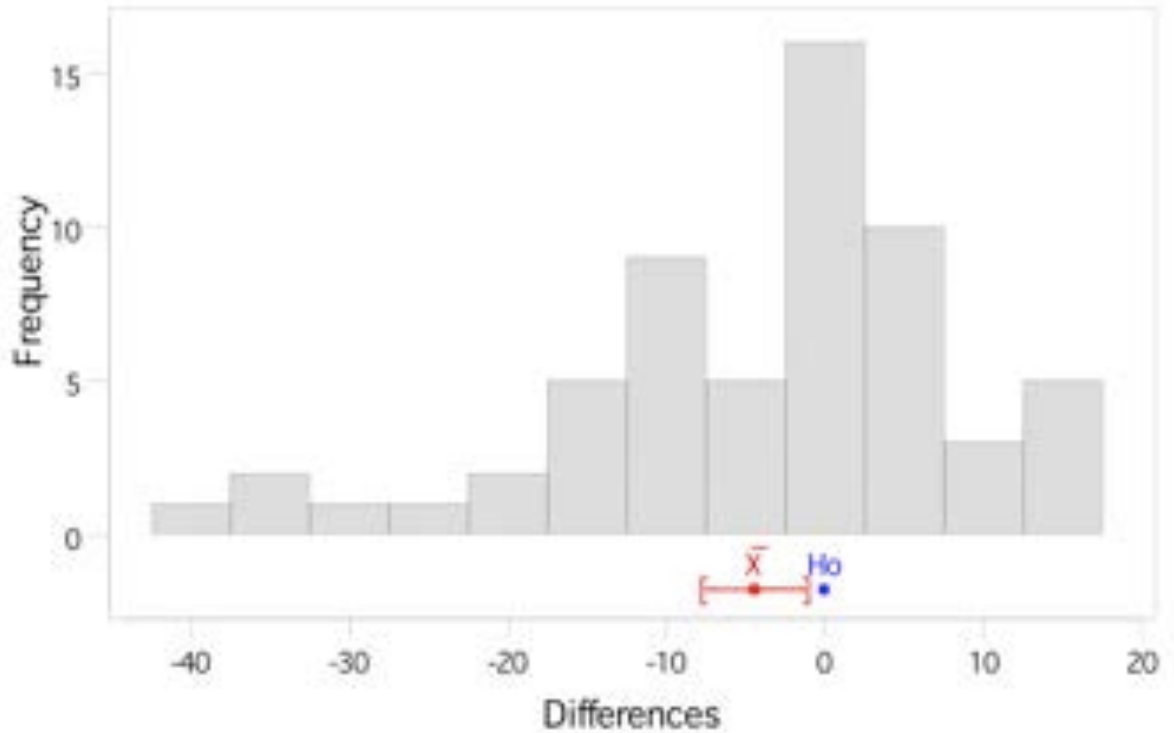
Last Three Points of 10 Minute Interval Data (Paired)

Paired T-Test and CI: LASER HAND-Placebo, LASER HAND-Holofiber

```
Paired T for LASER HAND-Placebo - LASER HAND-Holofiber

                   N       Mean     St Dev    SE Mean
LASER HAND-p      60      33.52     28.32      3.66
LASER HAND-h      60      33.48     25.89      3.34
Difference        60       0.05     15.24      1.97

95% CI for mean difference: (-3.89, 3.98)
T-Test of mean difference = 0 (vs. not = 0): T-Value = 0.02   P-Value = 0.981
```


Paired T-Test and CI: LASER FOOT-Placebo, LASER FOOT-Holofiber

```
Paired T for LASER FOOT-Placebo - LASER FOOT-Holofiber

                   N       Mean     St Dev    SE Mean
LASER FOOT-p      60      49.90     19.48      2.51
LASER FOOT-h      60      51.56     21.49      2.77
Difference        60      -1.65     14.80      1.91

95% CI for mean difference: (-5.48, 2.17)
T-Test of mean difference = 0 (vs. not = 0): T-Value = -0.86   P-Value = 0.391
```

Last Point of 10 Minute Interval Data (Paired)

Paired T-Test and CI: TCOM HAND-Placebo, TCOM HAND-Holofiber

```
Paired T for TCOM HAND-Placebo - TCOM HAND-Holofiber

                N      Mean     St Dev   SE Mean
TCOM HAND-Pl    20     15.15     8.08     1.81
TCOM HAND-ho    20     17.17    10.17     2.28
Difference      20     -2.02     6.60     1.48

95% CI for mean difference: (-5.11, 1.07)
T-Test of mean difference = 0 (vs. not = 0): T-Value = -1.37  P-Value = 0.187
```
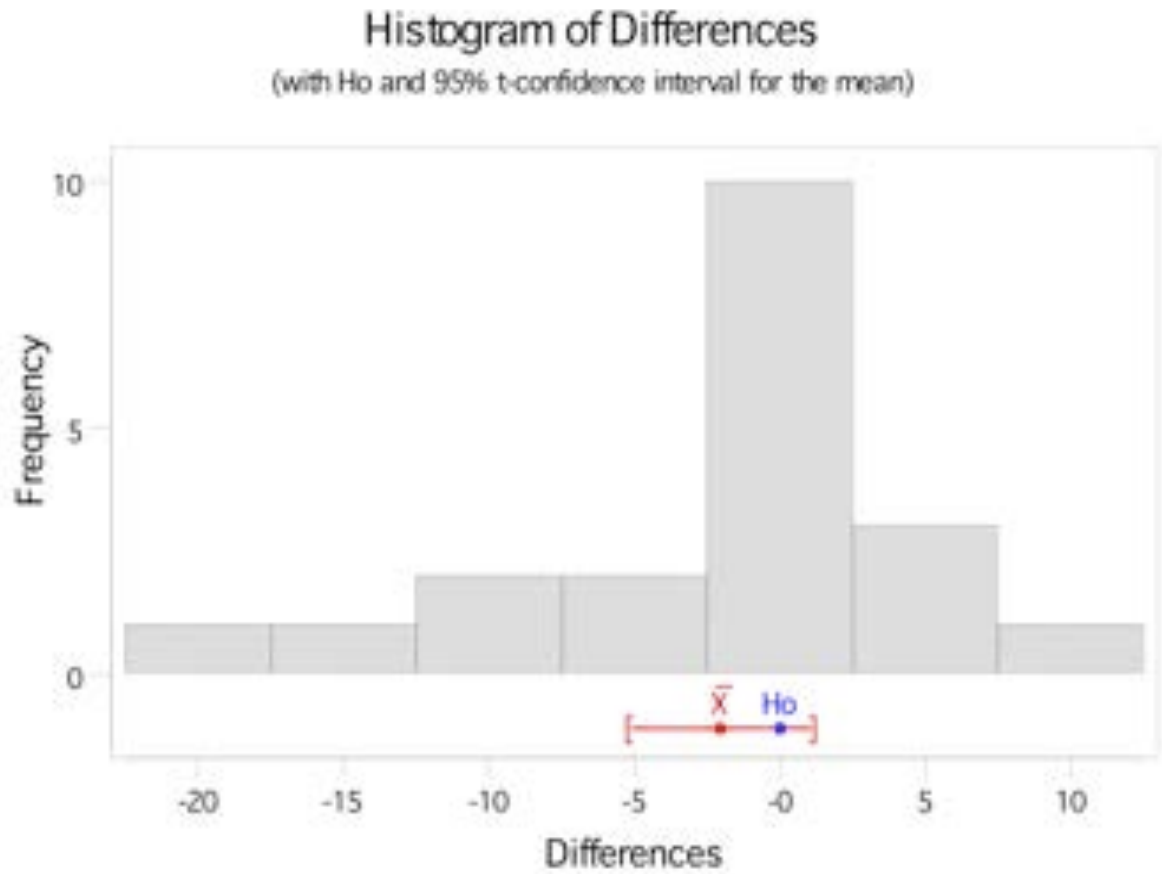

Histogram of Differences
(with Ho and 95% t-confidence interval for the mean)

Last Point of 10 Minute Interval Data (Paired)

Paired T-Test and CI: TCOM FOOT-Placebo, TCOM FOOT-Holofiber

```
Paired T for TCOM FOOT-Placebo - TCOM FOOT-Holofiber

                  N       Mean      S Dev    SE Mean
TCOM FOOT-pl     20      55.42      20.54      4.59
TCOM FOOT-ho     20      59.48      21.65      4.84
Difference       20      -4.05      11.61      2.60

95% CI for mean difference: (-9.49, 1.38)
T-Test of mean difference = 0 (vs. not = 0): T-Value = -1.56  P-Value = 0.135
```

Paired T-Test and CI: LASER HAND-Placebo, LASER HAND-Holofiber

```
Paired T for LASER HAND-Placebo - LASER HAND-Holofiber

                  N       Mean     St Dev    SE Mean
LASER HAND-p     20      33.87      26.02      5.82
LASER HAND-h     20      33.69      27.39      6.13
Difference       20       0.18      15.89      3.55

95% CI for mean difference: (-7.26, 7.62)
T-Test of mean difference = 0 (vs. not = 0): T-Value = 0.05  P-Value = 0.960
```

Paired T-Test and CI: LASER FOOT-Placebo, LASER FOOT-Holofiber

```
Paired T for LASER FOOT-Placebo - LASER FOOT-Holofiber

                  N       Mean     St Dev    SE Mean
LASER FOOT-p     20      52.52      22.57      5.05
LASER FOOT-h     20      54.97      27.41      6.13
Difference       20      -2.45      24.05      5.38

95% CI for mean difference: (-13.70, 8.80)
T-Test of mean difference = 0 (vs. not = 0): T-Value = -0.46  P-Value = 0.654
```

1st Half to 2nd Half of Test

Paired T-Test and CI: 1 Holofiber-TCOM Hand, 2 Holofiber-TCOM Hand

```
Paired T for 1 Holofiber-TCOM Hand - 2 Holofiber-TCOM Hand

                     N      Mean     St Dev    SE Mean
1 Holofiber-TCOM    60     17.45     11.29      1.46
2 Holofiber-TCOM    60     17.19      9.75      1.26
Difference          60     0.256     4.321      0.558

95% CI for mean difference: (-0.860, 1.372)
T-Test of mean difference = 0 (vs. not = 0): T-Value = 0.46   P-Value = 0.648
```


Histogram of Differences
(with Ho and 95% t-confidence interval for the mean)
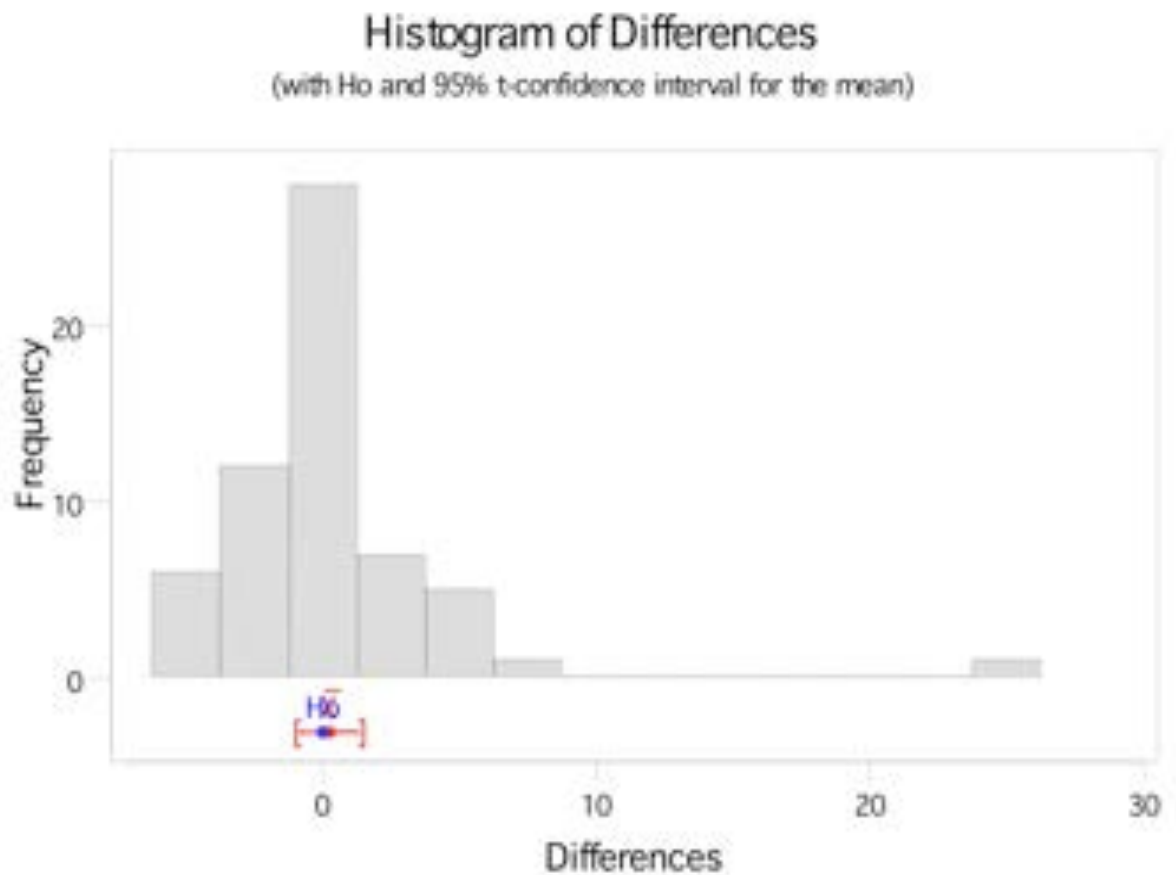
1st Half to 2nd Half of Test

Paired T-Test and CI: 1 Holofiber-TCOM Foot, 2 Holofiber-TCOM Foot

```
Paired T for 1 Holofiber-TCOM Foot - 2 Holofiber-TCOM Foot

                      N       Mean    St Dev   SE Mean
1 Holofiber-TCOM     60      54.14    18.55     2.39
2 Holofiber-TCOM     60      58.57    21.29     2.75
Difference           60      -4.43     9.14     1.18

95% CI for mean difference: (-6.79, -2.07)
T-Test of mean difference = 0 (vs. not = 0): T-Value = -3.76   P-Value = 0.000
```


Histogram of Differences
(with Ho and 95% t-confidence interval for the mean)
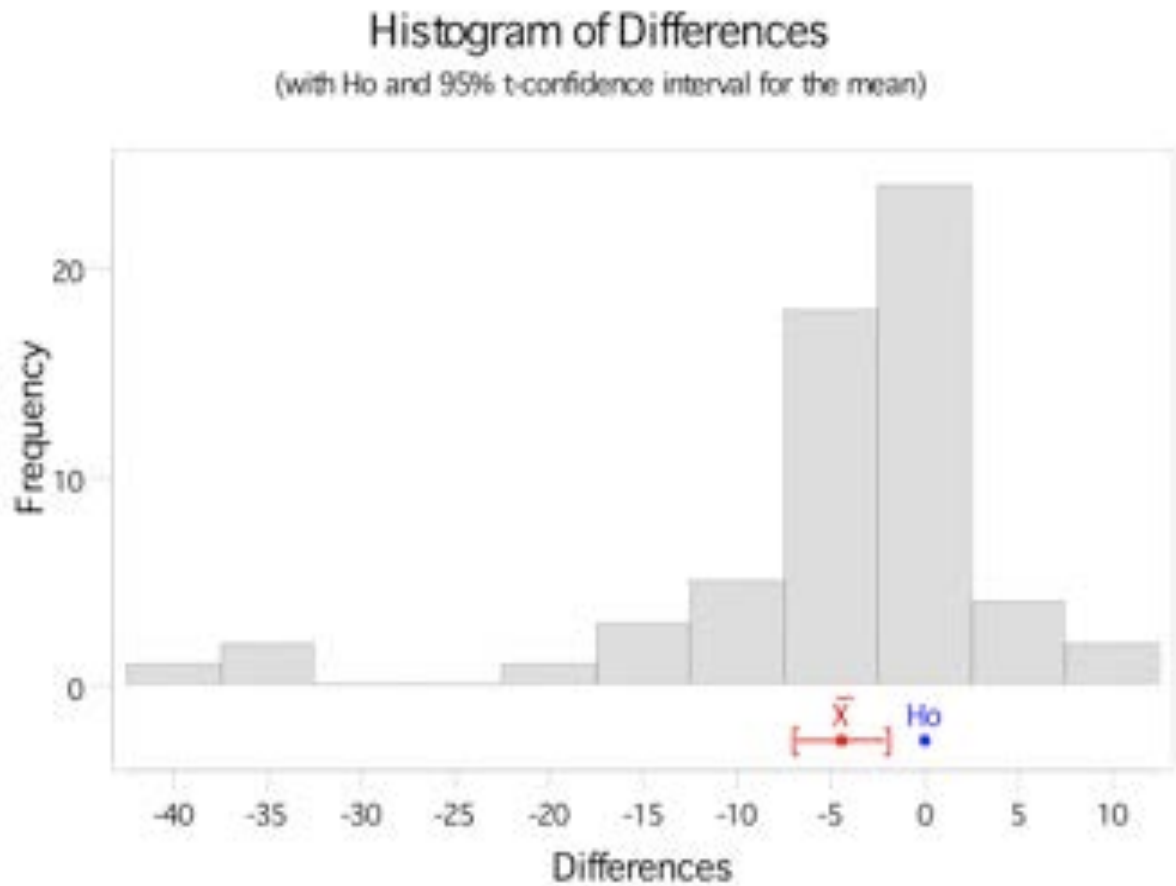
1st Half to 2nd Half of Test

Paired T-Test and CI: 1 Placebo-TCOM Hand, 2 Placebo-TCOM Hand

```
Paired T for 1 Placebo-TCOM Hand - 2 Placebo-TCOM Hand

                 N      Mean     St Dev    SE Mean
1 Placebo -TC    60     15.94     8.12       1.05
2 Placebo -TC    60     14.62     7.08       0.91
Difference       60     1.322     5.102      0.659

95% CI for mean difference: (0.004, 2.640)
T-Test of mean difference = 0 (vs. not = 0): T-Value = 2.01  P-Value = 0.049
```


Histogram of Differences
(with Ho and 95% t-confidence interval for the mean)
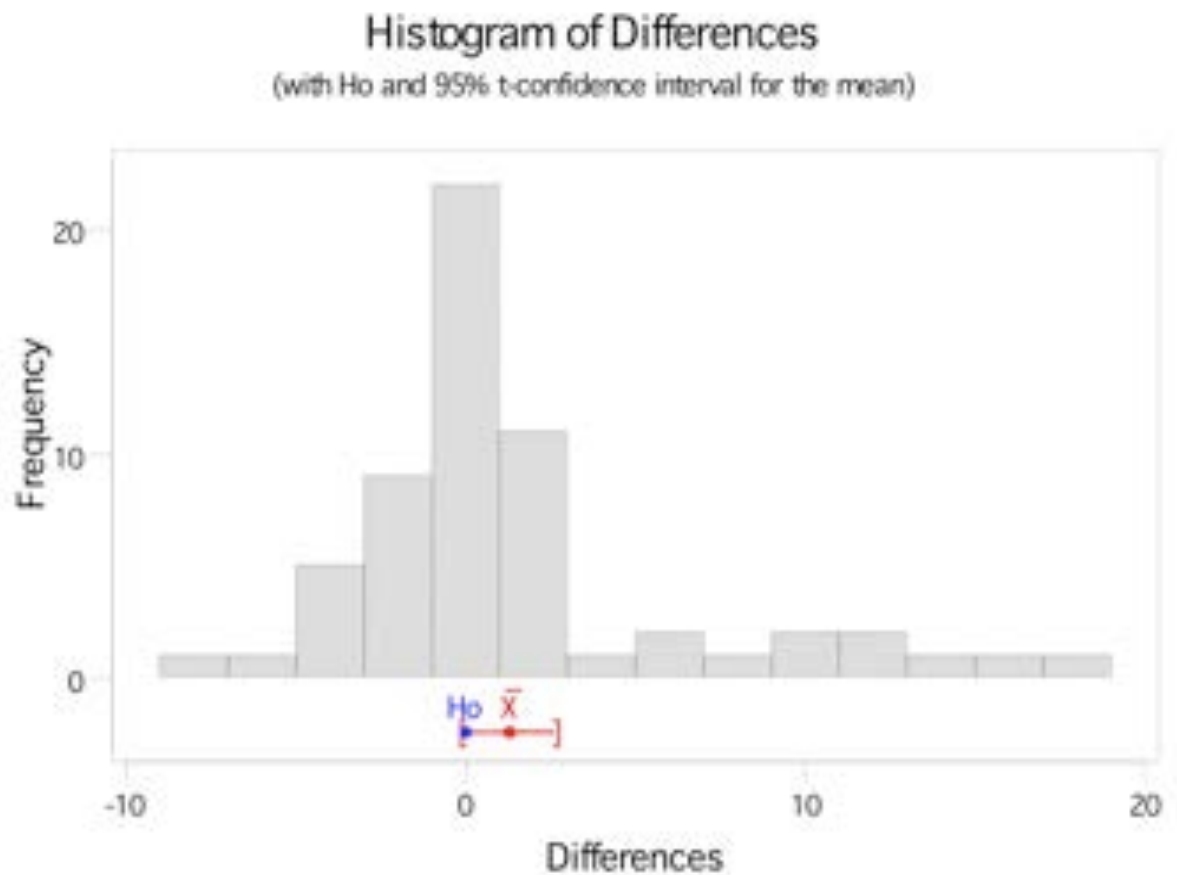
1st Half to 2nd Half of Test

Paired T-Test and CI: 1 Placebo-TCOM Foot, 2 Placebo-TCOM Foot

```
Paired T for 1 Placebo-TCOM Foot - 2 Placebo-TCOM Foot

                 N       Mean     St Dev    SE Mean
1 Placebo-TC     60      50.26    20.85      2.69
2 Placebo-TC     60      54.19    19.90      2.57
Difference       60      -3.930    6.726     0.868

95% CI for mean difference: (-5.668, -2.192)
T-Test of mean difference = 0 (vs. not = 0): T-Value = -4.53   P-Value = 0.000
```


Histogram of Differences
(with Ho and 95% t-confidence interval for the mean)
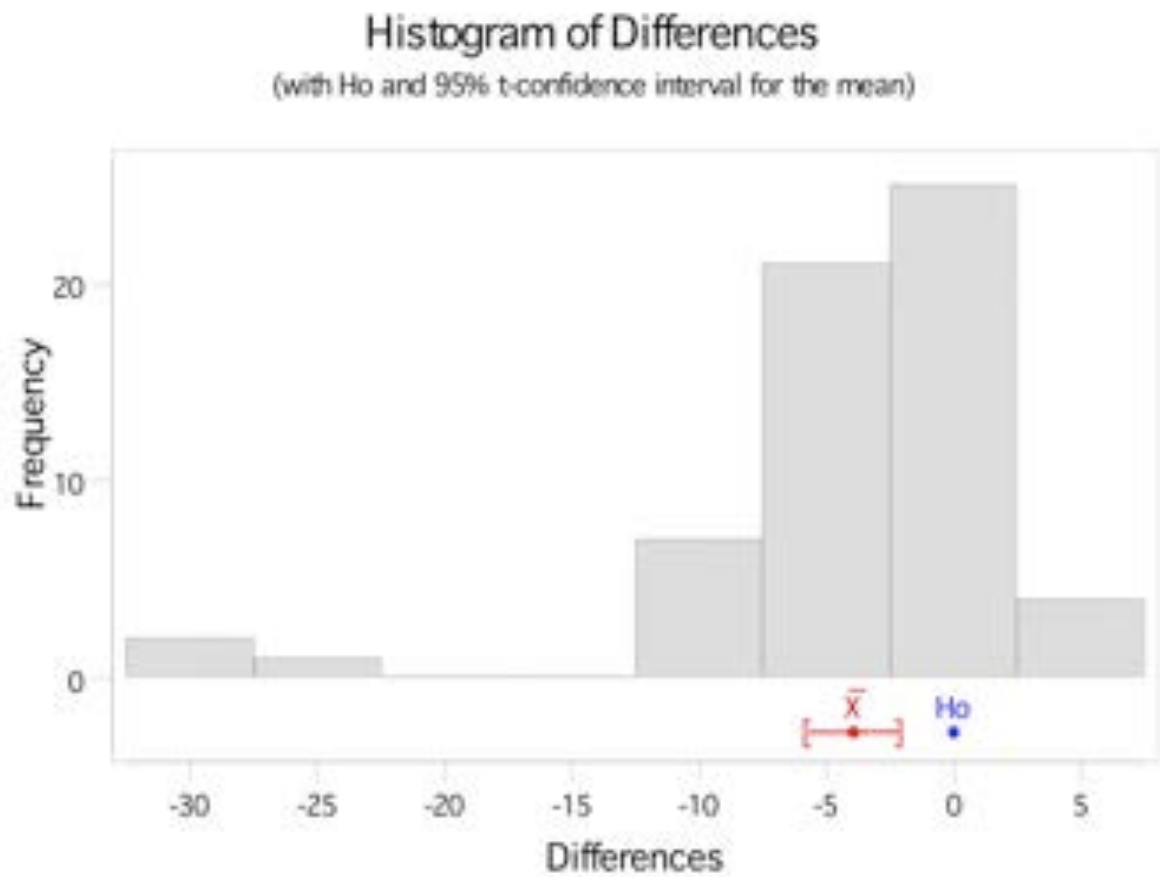
Last Two Points 10 Minute Interval Data (Paired)

Paired T-Test and CI: Placebo-TCOM Hand, Holofiber-TCOM Hand

```
Paired T for Placebo-TCOM Hand - Holofiber-TCOM Hand

                    N      Mean    St Dev   SE Mean
Placebo-TCOM        40     14.68    7.32     1.16
Holofiber-TCOM Ha   40     17.49    9.91     1.57
Difference          40     -2.82    6.67     1.05

95% CI for mean difference: (-4.95, -0.68)
T-Test of mean difference = 0 (vs. not = 0): T-Value = -2.67   P-Value = 0.011
```

Histogram of Differences
(with Ho and 95% t-confidence interval for the mean)
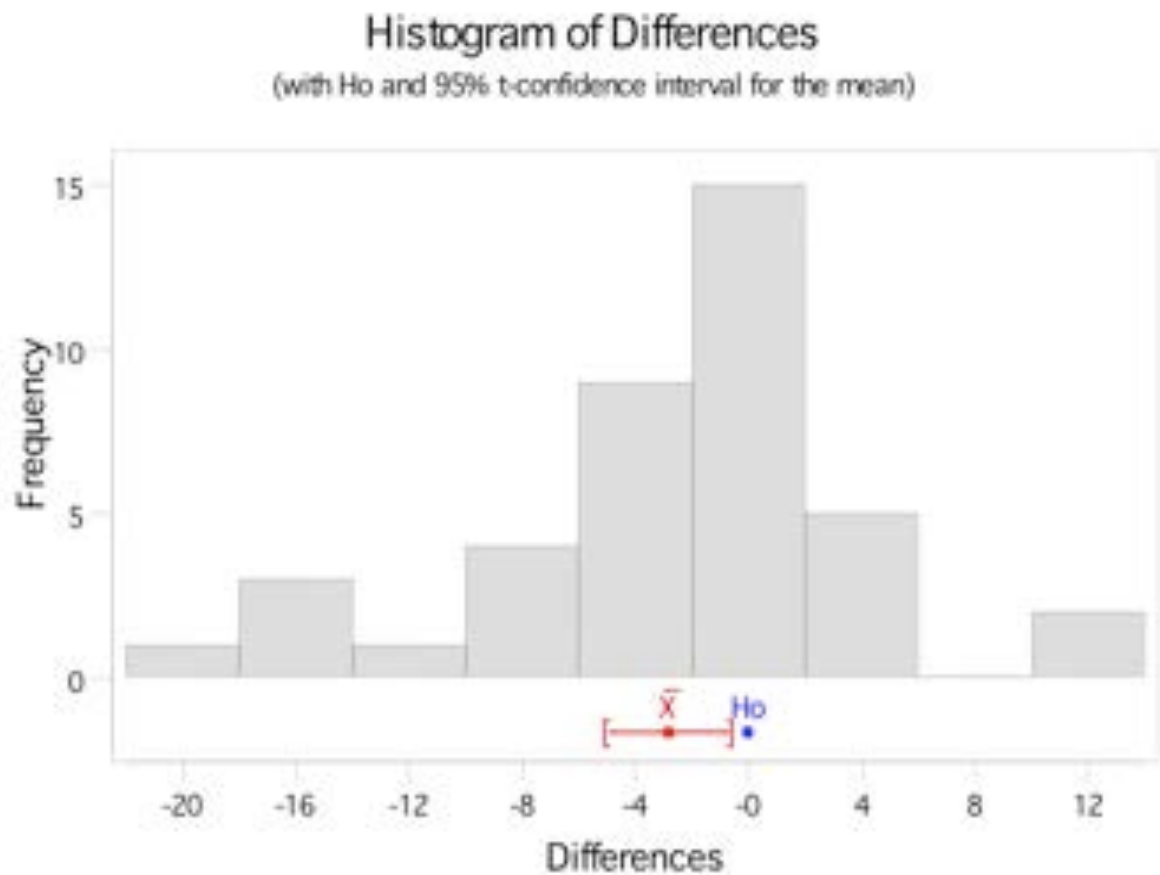
Last Two Points 10 Minute Interval Data (Paired)

Paired T-Test and CI: Placebo-TCOM Foot, Holofiber-TCOM Foot

```
Paired T for Placebo-TCOM Foot - Holofiber-TCOM Foot

                  N       Mean      St Dev    SE Mean
Placebo-TCOM      40      54.76     19.92     3.15
Holofiber-TCOM    40      59.10     21.02     3.32
Difference        40      -4.33     12.85     2.03

95% CI for mean difference: (-8.44, -0.22)
T-Test of mean difference = 0 (vs. not = 0): T-Value = -2.13  P-Value = 0.039
```


Histogram of Differences
(with Ho and 95% t-confidence interval for the mean)

Average of All
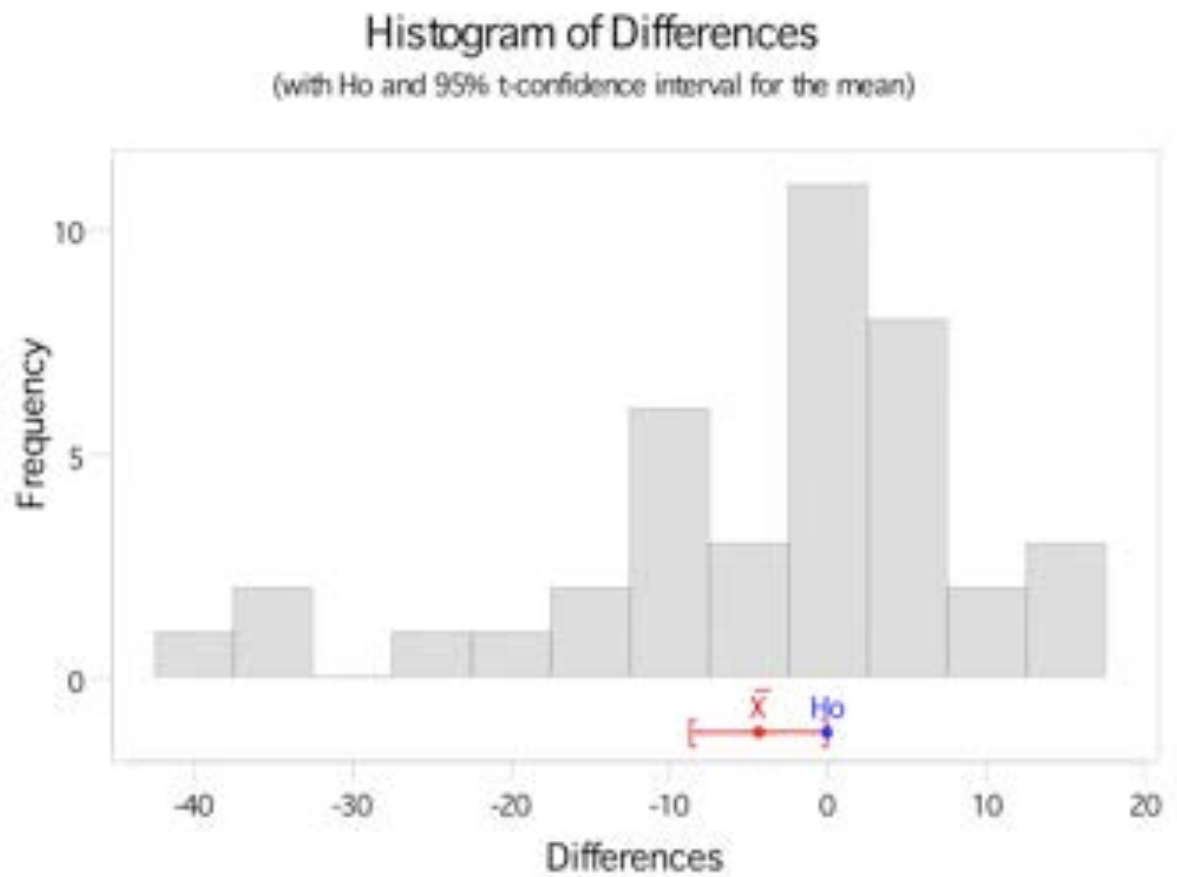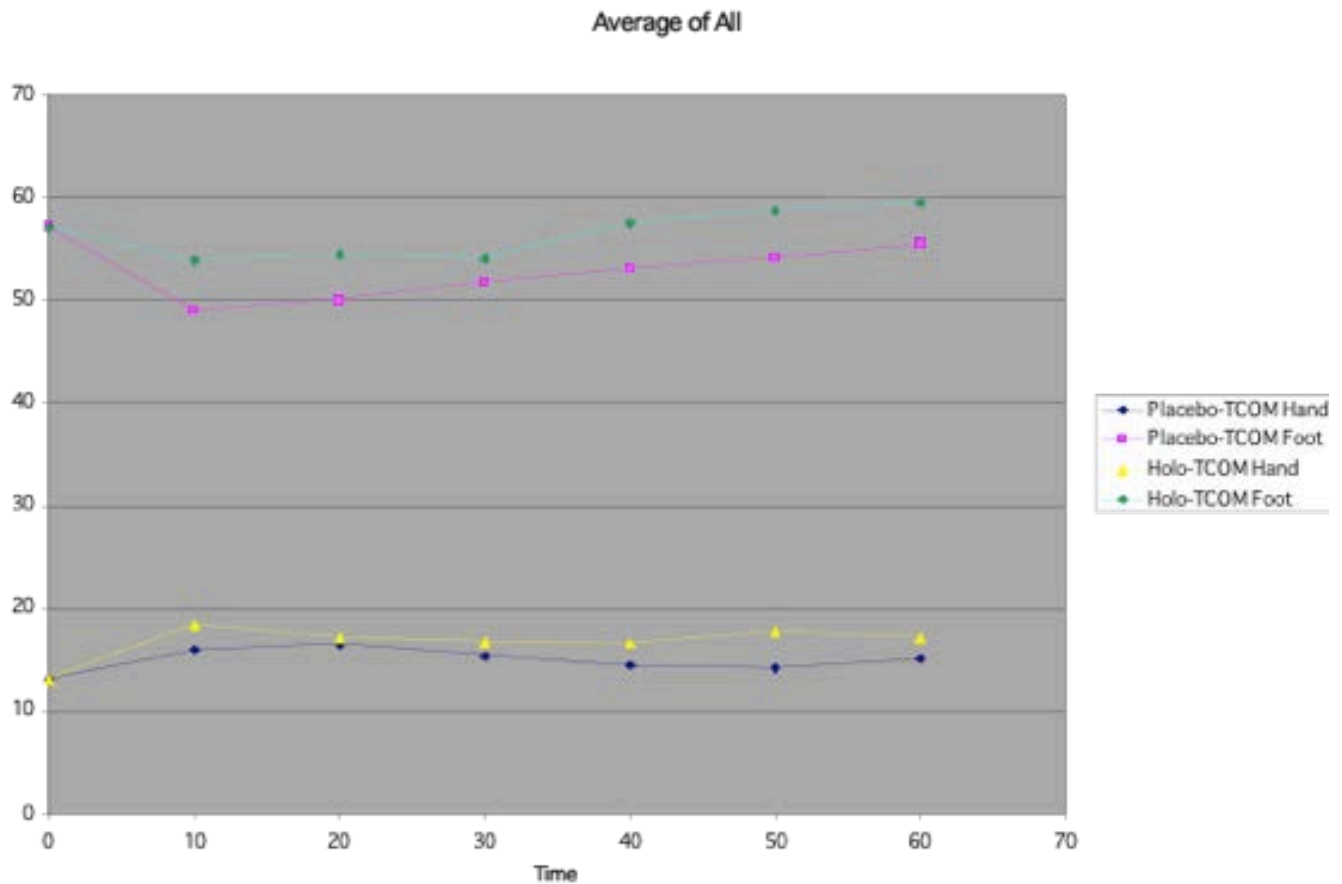
Limitations: This preliminary study provides some insight into the potential for Holofiber. This project should be considered as a pilot project to build on. Prior to beginning the project we had little scientific information about the effect that Holofiber might have on perfusion to the extremities. There is obviously a lot that we still do not understand about Holofiber and the best way to optimize its use.

Patient selection: We enrolled diabetic males with an abnormal clinical vascular examination. Our results may have been better if we included patients with more severe vascular impairment. The subjects that may benefit the most may be diabetics with very severe disease, patients with Raynaud's disease, or peripheral arterial occlusive disease.

For instance, in the future we may want to include patients with baseline transcutaneous oxygen values less than 20 or 30 mm Hg.

Duration of the evaluation: The study period for this project was one hour. This may not have been a long enough period to observe the greatest impact of the product. Several of the patients that have voiced strong subjective improvement related their symptoms did not change until they wore the garment for more than an hour.

Wash out period: It is unclear if a "wash out" period was needed for subjects that were treated with the Holofiber and subsequently were treated with the placebo garments. This would suggest that there was a lasting effect of the Holofiber material. The current analysis did not indicate there was a trend to support this theory.

Light Exposure: Since one of the theories regarding the mechanism of action of Holofiber involves infrared light, Holofiber may be more effective when the patient is exposed to natural light during the evaluation period. The current study was conducted in a room without any exposure to natural light.

Recommendations: The pilot data is compelling. I am very optimistic that we could pursue additional funding through the National Institute of Health. Probably the best bet would be to apply for a Technology Transfer Grant or through an award from the Alternative Medicine Institute of the NIH.

Future research should focus on the target markets for this product. In addition, we should identify the mechanism of action of Holofiber, if that is possible. Initially, I would build on the data from the current project and focus on vascular improvement and subjective improvement in persons with diabetes mellitus. My recommendations would be to expand the scope of the pilot study. We should expand the study population and evaluate specific "risk groups' within the diabetic population that would benefit form the product such as dialysis patients. We need to evaluate patients after they wear Holofiber over the course of hours days or weeks. We should measure vascular parameters as well

as subjective improvement in functional status, sleep habits, and perhaps even glucose control. A long term, multi-million dollar project would evaluate if Holofiber helps to prevent lower extremity complications such as ulceration, gangrene, and amputation in high-risk persons with diabetes. This type of outcome would be better than discovering penicillin.

The athletic market probably has the most potential. There are a number of sports activities and levels of competition that we could evaluate. In general, we should focus on measuring improvement in performance in athletes that use Holofiber. I would additionally evaluate subject responses from athletes after using the product, but every shoe company has a celebrity spokesman that loves the product. I know it is a cliché from the 60's, but if we can show that Holofiber helps you run faster and jump higher (like PF Flyers) you will not be able to keep it on the shelf.

Performance outcomes are easy to measure. We can measure changes in speed, jumping, weight lifting, rowing, cycling or a number of other athletic endeavors. The easiest approach would be to conduct a classic randomized clinical trial and evaluate two groups of athletes that use Holofiber or placebo garments. We could evaluate military recruits, high school, college or professional athletes. Another approach would be to use subjects as their own control and measure pre versus post Holofiber athletic performance. We could relatively easily evaluate if exposure to the product in the course of a few hours, improves a specific athletic event like weight lifting or the time to run 2 miles.

Funding for these types of projects will be harder to obtain. The NIH's focus is on disease states. We would also need pilot data that supports the hypothesis of our athletic performance research in order to obtain advanced funding.

Is there any evidence that Holofiber improves sleep patterns? This could be measured from subjective patient feedback using a pre – post evaluation of Holofiber pajamas and sheets. A more expensive approach would be to measure sleep patterns in a sleep lab. The laboratory approach will be more objective and more expensive. Objective data of

enhanced REM sleep and other sleep parameters would attract significant attention to the product.

There are a number of areas and questions that we could pursue.

1. Does Holofiber improve in persons with diabetes?

Does Holofiber improve blood flow in diabetics?

Does Holofiber improve pain-free walking in diabetic with intermittent claudication?

Does Holofiber improve wound healing in venous stasis ulcers, diabetic neuropathic ulcers, and ischemic ulcers?

id no.	Order of treatment	Transcutaneous measurement of the foot		Percentage change	Change with Holofiber
		mean values	mean values		
121	placebo - Holofiber	14.48	27.39	89.07	increase
119	placebo - Holofiber	78.74	70.92	-9.93	decrease
118	placebo - Holofiber	20.3	43.9	116.3	increase
116	placebo - Holofiber	82.35	92.58	12.42	increase
113	placebo - Holofiber	45.76	52.44	14.61	increase
112	placebo - Holofiber	57.88	60.65	4.79	increase
102	placebo - Holofiber	54.65	50.82	-7	decrease
104	placebo - Holofiber	65.5	57.96	-11.52	decrease
105	placebo - Holofiber	68.51	106.61	55.61	increase
109	placebo - Holofiber	91.73	85.74	-6.53	decrease
106	placebo - Holofiber	35.79	23.17	-35.25	decrease
107	Holofiber - placebo	53.42	37.5	29.8	increase
108	Holofiber - placebo	55.63	53.63	3.59	no change
101	Holofiber - placebo	54.34	55.82	-2.72	no change
110	Holofiber - placebo	92.91	81.88	11.86	increase
111	Holofiber - placebo	57.53	48	16.58	increase
114	Holofiber - placebo	60.69	62.37	-2.77	no change
115	Holofiber - placebo	55.1	57.75	-4.81	decrease
117	Holofiber - placebo	44.28	40.93	7.56	increase
120	Holofiber - placebo	51.06	51.92	-1.69	no change

id no.	Order of treatment	Transcutaneous measurment of the hand mean values	mean values	Percentage change	Change with Holofiber
121	placebo - Holofiber	14.82	12.63	-14.81	decrease
119	placebo - Holofiber	21.19	31.45	48.4	increase
118	placebo - Holofiber	32.5	42.77	31.61	increase
116	placebo - Holofiber	5.91	5.98	1.23	no change
113	placebo - Holofiber	13.63	14.35	5.34	decrease
112	placebo - Holofiber	14.72	15.04	2.18	no change
102	placebo - Holofiber	9.51	13.33	40.22	increase
104	placebo - Holofiber	11.19	9.95	-11.08	decrease
105	placebo - Holofiber	7.28	9.31	27.91	increase
109	placebo - Holofiber	11.64	11.95	2.69	no change
106	placebo - Holofiber	5.57	7.86	41.18	increase
107	Holofiber - placebo	5.64	4.36	22.69	increase
108	Holofiber - placebo	16.18	14.6	9.73	increase
101	Holofiber - placebo	19.91	14.46	27.36	increase
110	Holofiber - placebo	9.56	9.64	-0.89	no change
111	Holofiber - placebo	32.73	17.34	47.02	increase
114	Holofiber - placebo	22.13	28.45	-28.53	decrease
115	Holofiber - placebo	14.58	29.75	-104.02	decrease
117	Holofiber - placebo	25.59	12.93	49.47	increase
120	Holofiber - placebo	25.81	27.42	-6.27	decrease

id no.	Order of treatment	Laser doppler of the hand mean values	mean values	percentage change	Change with Holofiber
121	placebo - Holofiber	33.81	43.19	27.74	increase
119	placebo - Holofiber	84.94	69.28	-18.44	decrease
118	placebo - Holofiber	46.02	46.49	1.03	no change
116	placebo - Holofiber	51.9	30.88	-40.51	decrease
113	placebo - Holofiber	20.18	14.83	-26.5	decrease
112	placebo - Holofiber	26.66	29.35	10.08	increase
102	placebo - Holofiber	34.82	46.63	33.93	increase
104	placebo - Holofiber	27.83	29.44	5.8	increase
105	placebo - Holofiber	18.17	13.44	-26.03	decrease
109	placebo - Holofiber	15.75	15.22	-3.33	no change
106	placebo - Holofiber	6.6	5.5	-16.6	increase
107	Holofiber - placebo	12.64	19.07	-50.93	decrease
108	Holofiber - placebo	12.96	18.07	-39.48	decrease
101	Holofiber - placebo	15.52	22.87	-47.4	decrease
110	Holofiber - placebo	11.47	17.05	-48.7	decrease
111	Holofiber - placebo	24.55	22.46	8.52	increase
114	Holofiber - placebo	105.44	104.88	0.53	no change
115	Holofiber - placebo	93.59	23.89	74.47	increase
117	Holofiber - placebo	62.58	75.88	-21.25	decrease
120	Holofiber - placebo	33.81	43.19	-27.74	decrease

Id no.	Order of treatment	mean values	mean values	Percentage change	Change with Holofiber
	Laser doppler of the foot				
121	placebo - Holofiber	47.9	60.84	27.01	increase
119	placebo - Holofiber	84.28	75.54	-10.37	decrease
118	placebo - Holofiber	53.29	62.79	17.84	increase
116	placebo - Holofiber	2.71	5.57	105.29	increase
113	placebo - Holofiber	63.47	64.87	2.2	no change
112	placebo - Holofiber	63.47	64.87	2.2	no change
102	placebo - Holofiber	50.23	140.23	179.18	increase
104	placebo - Holofiber	65.84	63.16	-4.08	no change
105	placebo - Holofiber	56.78	61.78	8.79	increase
109	placebo - Holofiber	49.26	50.22	1.96	increase
106	placebo - Holofiber	61.37	57.53	-6.25	decrease
107	Holofiber - placebo	59.35	63.08	-6.27	decrease
108	Holofiber - placebo	57.21	79.87	-39.61	decrease
101	Holofiber - placebo	49.06	45.84	6.55	increase
110	Holofiber - placebo	40.44	43.57	-7.73	decrease
111	Holofiber - placebo	31.69	32.89	-3.81	no change
114	Holofiber - placebo	59.05	62.31	-5.52	decrease
115	Holofiber - placebo	58	59.67	-2.87	no change
117	Holofiber - placebo	4.31	2.3	46.72	increase
120	Holofiber - placebo	46.13	52.08	-12.89	decrease

LITERATURE CITED

1. Most RS, Sinnock P. The epidemiology of lower extremity amputations in diabetic individuals. *Diabetes Care*. 1983;6:87-91.

2. Armstrong DG, Lavery LA, Harkless LB. Validation of a diabetic wound classification system. The contribution of depth, infection, and ischemia to risk of amputation [see comments]. *Diabetes Care*. 1998;21:855-9.

3. Lavery LA, Armstrong DG, Vela SA, Quebedeaux TL, Fleischli JG. Practical Criteria for Screening Patients at High Risk for Diabetic Foot Ulceration. *Arch Intern Med*. 1998;158:158-162.

4. LaVan FB, Hunt TK. Oxygen and Wound Healing. *Clinics in Plastic Surgery*. 1990;17:463-472.

5. Hauser CJ, Klein SR, Mehringer CM, Appel P, Shoemaker WC. Assessment of perfusion in the diabetic foot by regional transcutaneous oximetry. *Diabetes*. 1984;33:527-531.

6. Pecoraro RE. Chronology and determinants of Tissue Repair in Diabetic Lower Extremity Ulcers. *Diabetes*. 1991;40:1305-1313.

7. Tooke JE. Microcirculation and diabetes. *British Medical Bulletin*. 1989;45:206-223.

8. World Health Organization. Second Report on Diabetes Mellitus. . Geneva: World Health Organization; 1980.

9. Wyss CR, Matsen FA, Simmons CW, Burgess EM. Transcutaneous oxygen tension measurements on limbs of diabetic and nondiabetic patients with peripheral vascular disease. *Surgery*. 1984;95:339-346.

10. Apelqvist J, Castenfors J, Larsson J. Prognostic value of ankle and toe blood pressure levels in outcome of diabetic foot ulcers. *Diabetes Care*. 1989;12:373-378.

11. Arnold F, He CYJ, Cherry GW. Perfusion imaging of skin island blood flow by a scanning laser Doppler device. *Brit J Plast Surg*. 1995;48:280-287.

12. Kirkwood BR. Essentials of Medical Statistics. . Oxford: Blackwell; 1988.

1. Most RS, Sinnock P. The epidemiology of lower extremity amputations in diabetic individuals. *Diabetes Care*. 1983;6:87-91.

2. Armstrong DG, Lavery LA, Harkless LB. Validation of a diabetic wound classification system. The contribution of depth, infection, and ischemia to risk of amputation [see comments]. *Diabetes Care*. 1998;21:855-9.

3. Lavery LA, Armstrong DG, Vela SA, Quebedeaux TL, Fleischli JG. Practical Criteria for Screening Patients at High Risk for Diabetic Foot Ulceration. *Arch Intern Med*. 1998;158:158-162.

4. LaVan FB, Hunt TK. Oxygen and Wound Healing. *Clinics in Plastic Surgery*. 1990;17:463-472.

5. Hauser CJ, Klein SR, Mehringer CM, Appel P, Shoemaker WC. Assessment of perfusion in the diabetic foot by regional transcutaneous oximetry. *Diabetes*. 1984;33:527-531.

6. Pecoraro RE. Chronology and determinants of Tissue Repair in Diabetic Lower Extremity Ulcers. *Diabetes*. 1991;40:1305-1313.

7. Tooke JE. Microcirculation and diabetes. *British Medical Bulletin*. 1989;45:206-223.

8. World Health Organization. Second Report on Diabetes Mellitus. . Geneva: World Health Organization; 1980.

9. Wyss CR, Matsen FA, Simmons CW, Burgess EM. Transcutaneous oxygen tension measurements on limbs of diabetic and nondiabetic patients with peripheral vascular disease. *Surgery*. 1984;95:339-346.

10. Apelqvist J, Castenfors J, Larsson J. Prognostic value of ankle and toe blood pressure levels in outcome of diabetic foot ulcers. *Diabetes Care*. 1989;12:373-378.

11. Arnold F, He CYJ, Cherry GW. Perfusion imaging of skin island blood flow by a scanning laser Doppler device. *Brit J Plast Surg*. 1995;48:280-287.

12. Kirkwood BR. Essentials of Medical Statistics. . Oxford: Blackwell; 1988.

Patient ID: 101

Holofiber - placebo

BASELINE	TCOM HAND	LASER HAND	TCOM FOOT	LASER FOOT
Mean value (Unit)	24.52	16.82	55.6	49.82
Standard Deviation (Unit)	3.57	6.9	0.48	0.29
Standard Error (Unit)	0.13	0.24	0.02	0.01
Area under curve (Unit*sec.)	1228.34	842.67	2785.16	2495.65

10 MINUTES HOLOFIBER				
Mean value (Unit)	19.89	13.29	54.6	44.08
Standard Deviation (Unit)	3.24	3.48	1.36	0.34
Standard Error (Unit)	0.11	0.12	0.05	0.01
Area under curve (Unit*sec.)	994.9	664.9	2731.59	2205.26

20M MINUTES HOLOFIBER				
Mean value (Unit)	17.93	12.42	53.86	44.25
Standard Deviation (Unit)	7.33	1.97	1.22	0.87
Standard Error (Unit)	0.26	0.07	0.04	0.03
Area under curve (Unit*sec.)	899.19	622.89	2701.65	2219.58

30 MINUTES HOLOFIBER				
Mean value (Unit)	16.01	13.11	55.61	48.34
Standard Deviation (Unit)	3.63	3.99	1.86	0.32
Standard Error (Unit)	0.13	0.14	0.07	0.01
Area under curve (Unit*sec.)	794.3	650.01	2758.62	2397.88

40 MINUTYES HOLOFIBER				
Mean value (Unit)	20.84	12.41	50.05	46.7
Standard Deviation (Unit)	4.55	1.68	1.05	0.21
Standard Error (Unit)	0.16	0.06	0.04	0.01
Area under curve (Unit*sec.)	1032.44	615.01	2479.3	2313.27

50 MINUTES HOLOFIBER				
Mean value (Unit)	23.19	15.32	51.7	49.39
Standard Deviation (Unit)	3.51	13.77	0.98	0.5
Standard Error (Unit)	0.12	0.48	0.03	0.02
Area under curve (Unit*sec.)	1157.26	764.74	2580.38	2464.88

60 MINUTES HOLOFIBER	TCOM HAND	LASER HAND	TCOM FOOT	LASER FOOT
Mean value (Unit)	18.76	12.15	54.42	46.87
Standard Deviation (Unit)	4.06	1.84	1.52	0.48
Standard Error (Unit)	0.14	0.06	0.05	0.02
Area under curve (Unit*sec.)	948.83	614.15	2752.92	2371.13

10 MINUTES PLACEBO				
Mean value (Unit)	17.96	16.39	48.23	48.87
Standard Deviation (Unit)	6	4.72	1.01	0.43
Standard Error (Unit)	0.22	0.17	0.04	0.02
Area under curve (Unit*sec.)	876.49	800.13	2353.08	2384.35

20 MINUTES PLACEBO				
Mean value (Unit)	16.23	14.01	50.2	43.88

Standard Deviation (Unit)	2.58	1.66	1.43	0.55
Standard Error (Unit)	0.09	0.06	0.05	0.02
Area under curve (Unit*sec.)	821.9	709.8	2542.56	2222.42

30 MINUTES PLACEBO

Mean value (Unit)	17.15	14.56	56.02	46.79
Standard Deviation (Unit)	2.84	2.43	2.03	0.52
Standard Error (Unit)	0.1	0.09	0.07	0.02
Area under curve (Unit*sec.)	859.03	729.36	2805.87	2343.65

40 MINUTES PLACEBO

Mean value (Unit)	16.14	13.25	52.87	45.3
Standard Deviation (Unit)	3.11	2.62	0.59	0.69
Standard Error (Unit)	0.11	0.09	0.02	0.02
Area under curve (Unit*sec.)	809.73	664.6	2651.61	2272.11

50 MINUTES PLACEBO

Mean value (Unit)	15.44	14.36	60.51	58.32
Standard Deviation (Unit)	4.63	2.19	0.95	1.29
Standard Error (Unit)	0.17	0.08	0.03	0.05
Area under curve (Unit*sec.)	775.33	721.12	3038.74	2928.89

60 MINUTES PLACEBO

Mean value (Unit)	16.08	22.06	55.53	48.87
Standard Deviation (Unit)	7.18	15.94	1.14	2.56
Standard Error (Unit)	0.26	0.57	0.04	0.09
Area under curve (Unit*sec.)	803.07	1100.69	2771.29	2439.26

Patient ID: 102   placebo-
                         Holofiber

BASELINE	TCOM HAND	LASER HAND	TCOM FOOT	LASER FOOT
Mean value (Unit)	8.66	45.65	55.22	40.67
Standard Deviation (Unit)	2.72	4.5	0.86	0.38
Standard Error (Unit)	0.1	0.16	0.03	0.01
Area under curve (Unit*sec.)	438.71	2312.2	2797.32	2059.9

10 MINUTE PLACEBO				
Mean value (Unit)	10.27	40.1	5.75	37.56
Standard Deviation (Unit)	3.28	6.94	0.96	0.44
Standard Error (Unit)	0.08	0.17	0.02	0.01

20 MINUTE PLACEBO				
Mean value (Unit)	10.15	36.71	22.45	40.96
Standard Deviation (Unit)	2.82	6.14	0.62	0.26
Standard Error (Unit)	0.1	0.22	0.02	0.01
Area under curve (Unit*sec.)	501.22	1813.7	1109.29	2023.98

30 MINUTE PLACEBO				
Mean value (Unit)	10.13	36.2	30.28	41.9
Standard Deviation (Unit)	3.92	3.14	0.83	0.75
Standard Error (Unit)	0.14	0.11	0.03	0.03
Area under curve (Unit*sec.)	514.53	1837.85	1537.66	2127.42

40 MINUTE PLACEBO				
Mean value (Unit)	11.57	34.57	33.95	47.01
Standard Deviation (Unit)	2.78	3.53	0.35	0.2
Standard Error (Unit)	0.1	0.12	0.01	0.01
Area under curve (Unit*sec.)	593.38	1772.94	1740.97	2410.22

50 MINUTE PLACEBO				
Mean value (Unit)	9.58	35.59	52.67	47.78
Standard Deviation (Unit)	1.97	3.18	0.1	0.16
Standard Error (Unit)	0.07	0.11	0	0.01
Area under curve (Unit*sec.)	484.85	1800.54	2664.69	2417.03

60 MINUTE PLACEBO				
Mean value (Unit)	8.99	33.82	55.02	50.6
Standard Deviation (Unit)	2.11	6.96	0.4	0.45
Standard Error (Unit)	0.07	0.24	0.01	0.02
Area under curve (Unit*sec.)	455.18	1712.98	2787.02	2563.31

10 MINUTE HOLOFIBER	TCOM HAND	LASER HAND	TCOM FOOT	LASER FOOT
Mean value (Unit)	8.93	43.3	37.54	59.37
Standard Deviation (Unit)	1.85	3.14	0.27	0.3
Standard Error (Unit)	0.07	0.11	0.01	0.01
Area under curve (Unit*sec.)	444.79	2155.53	1869.08	2955.84

20 MINUTE HOLOFIBER

Mean value (Unit)	9.53	41.92	38.65	57.8
Standard Deviation (Unit)	1.77	2.95	0.13	0.16
Standard Error (Unit)	0.06	0.1	0	0.01
Area under curve (Unit*sec.)	477.24	2099.87	1936.15	2895.57

30 MINUTE HOLOFIBER

Mean value (Unit)	9.67	40.85	40.17	59.47
Standard Deviation (Unit)	1.86	3.69	0.34	0.96
Standard Error (Unit)	0.07	0.13	0.01	0.03
Area under curve (Unit*sec.)	474.01	2003.64	1969.91	2915.9

40 MINUTES HOLOFIBER

Mean value (Unit)	12.06	41.65	40.43	57.87
Standard Deviation (Unit)	2.54	3.65	0.28	0.64
Standard Error (Unit)	0.09	0.13	0.01	0.02
Area under curve (Unit*sec.)	607.67	2099.4	2037.75	2916.84

50 MINUTRE HOLOFIBER

Mean value (Unit)	13.04	43.7	39.8	59.2
Standard Deviation (Unit)	2.62	3.7	0.4	0.15
Standard Error (Unit)	0.09	0.13	0.01	0.01
Area under curve (Unit*sec.)	637.89	2137.86	1946.79	2895.96

60 MINUTES HOLOFIBER

Mean value (Unit)	13.61	46.5	50.5	140.59
Standard Deviation (Unit)	3.61	5.91	1.13	2.51
Standard Error (Unit)	0.11	0.17	0.03	0.07
Area under curve (Unit*sec.)	978.71	3343.47	3630.78	10108.81

Patient ID:104   placebo - Holofiber

BASELINE	TCOM HAND	LASER HAND	TCOM FOOT	LASER FOOT
Mean value (Unit)	9.59	27.27	58.95	74.86
Standard Deviation (Unit)	4.17	5.27	0.52	0.61
Standard Error (Unit)	0.15	0.19	0.02	0.02
Area under curve (Unit*sec.)	467.46	1330.34	2876.43	3652.55

10 MIN PLACEBO				
Mean value (Unit)	22.31	43.44	65.31	68.88
Standard Deviation (Unit)	10.72	6.89	0.5	0.16
Standard Error (Unit)	0.39	0.25	0.02	0.01
Area under curve (Unit*sec.)	1057.09	2057.66	3093.45	3262.85

20 MIN PLACEBO				
Mean value (Unit)	19.91	26.3	63.01	64.9
Standard Deviation (Unit)	11.08	7.04	0.65	0.24
Standard Error (Unit)	0.28	0.18	0.02	0.01
Area under curve (Unit*sec.)	1876.28	2478.22	5938.24	6116.34

30 MIN PLACEBO				
Mean value (Unit)	13.19	28.63	67.04	65
Standard Deviation (Unit)	5.24	5.72	1.51	0.98
Standard Error (Unit)	0.14	0.15	0.04	0.03
Area under curve (Unit*sec.)	1147.35	2489.99	5831.53	5654.23

40 MIN PLACEBO				
Mean value (Unit)	11.83	29.71	64.06	63.89
Standard Deviation (Unit)	2.87	17.62	1.09	0.84
Standard Error (Unit)	0.07	0.44	0.03	0.02
Area under curve (Unit*sec.)	1200.52	3015.51	6502.62	6485.27

50 MIN PLACEBO				
Mean value (Unit)	12.13	28.64	66.07	66.32
Standard Deviation (Unit)	6.49	5.6	1.09	0.86
Standard Error (Unit)	0.16	0.14	0.03	0.02
Area under curve (Unit*sec.)	1231.21	2907.27	6706.28	6731.59

60 MIN PLACEBO				
Mean value (Unit)	11.52	27.4	63.88	63.7
Standard Deviation (Unit)	3.33	4.68	0.7	1.02
Standard Error (Unit)	0.12	0.17	0.02	0.04
Area under curve (Unit*sec.)	563.45	1339.87	3124.95	3116.03

10 MIN HOLOFIBER				
Mean value (Unit)	13.06	29.95	59.11	64.74
Standard Deviation (Unit)	6.26	5.17	0.51	2.42
Standard Error (Unit)	0.23	0.19	0.02	0.09
Area under curve (Unit*sec.)	619.53	1420.55	2803.78	3070.87

20 MIN HOLOFIBER				
Mean value (Unit)	13.21	28.82	55.27	59.2
Standard Deviation (Unit)	4.51	4.23	0.52	0.59
Standard Error (Unit)	0.16	0.15	0.02	0.02
Area under curve (Unit*sec.)	661.85	1444.08	2768.75	2965.68

30 MIN HOLOFIBER

Mean value (Unit)	13.79	26.41	55.19	61.7
Standard Deviation (Unit)	9.57	6.77	1.25	0.46
Standard Error (Unit)	0.33	0.24	0.04	0.02
Area under curve (Unit*sec.)	699.18	1338.76	2798.95	3129.3

40 MIN HOLOFIBER

Mean value (Unit)	9.03	33.09	63.95	68.85
Standard Deviation (Unit)	2.84	8.03	0.37	0.38
Standard Error (Unit)	0.1	0.28	0.01	0.01
Area under curve (Unit*sec.)	448.06	1642.01	3172.03	3414.72

50 MIN HOLOFIBER

Mean value (Unit)	14.5	31.61	61.32	67.89
Standard Deviation (Unit)	26.64	5.31	0.79	0.52
Standard Error (Unit)	0.94	0.19	0.03	0.02
Area under curve (Unit*sec.)	717.52	1563.87	3034.01	3359.13

60 MIN HOLOFIBER

Mean value (Unit)	8.52	31.54	56.9	64.22
Standard Deviation (Unit)	2.5	5.65	1.04	0.69
Standard Error (Unit)	0.09	0.2	0.04	0.02
Area under curve (Unit*sec.)	427.27	1581.51	2853.88	3221.07

Patient ID:105   placebo - Holofiber

BASELINE	TCOM HAND	LASER HAND	TCOM FOOT	LASER FOOT
Mean value (Unit)	6.83	12.06	76.89	57.94
Standard Deviation (Unit)	0.58	1.88	0.27	0.18
Standard Error (Unit)	0.02	0.07	0.01	0.01
Area under curve (Unit*sec.)	349.89	617.69	3937.57	2967.1

10 MIN PLACEBO				
Mean value (Unit)	8.72	17.24	67.06	52.94
Standard Deviation (Unit)	2.44	1.29	0.17	0.13
Standard Error (Unit)	0.08	0.04	0.01	0
Area under curve (Unit*sec.)	447.72	884.73	3442.6	2717.89

20 MIN PLACEBO				
Mean value (Unit)	7.63	12.91	69.95	53.39
Standard Deviation (Unit)	0.99	8.66	0.27	0.42
Standard Error (Unit)	0.03	0.3	0.01	0.01
Area under curve (Unit*sec.)	386.29	654.39	3543.14	2704.38
Slope (Unit/sec.)	0.01	-0.11	-0.01	0

30 MIN PLACEBO				
Mean value (Unit)	7.22	9.8	74.77	62.03
Standard Deviation (Unit)	0.61	1.66	0.18	0.43
Standard Error (Unit)	0.02	0.06	0.01	0.01
Area under curve (Unit*sec.)	369.02	500.96	3824.49	3172.94

40 MIN PLACEBO				
Mean value (Unit)	7.32	9.89	72.97	60.38
Standard Deviation (Unit)	0.78	1.41	0.43	0.4
Standard Error (Unit)	0.03	0.05	0.01	0.01
Area under curve (Unit*sec.)	374.1	505.5	3727.86	3084.74

50 MIN PLACEBO				
Mean value (Unit)	7.28	11.94	68.44	57.22
Standard Deviation (Unit)	0.39	1.7	0.35	0.62
Standard Error (Unit)	0.01	0.06	0.01	0.02
Area under curve (Unit*sec.)	372.44	610.92	3500.89	2926.78

60 MIN PLACEBO				
Mean value (Unit)	7.33	12.98	68.36	57.73
Standard Deviation (Unit)	0.4	1.86	0.21	0.34
Standard Error (Unit)	0.01	0.07	0.01	0.01
Maximum value (Unit)	8.24	18.49	68.79	58.47
Area under curve (Unit*sec.)	360.89	638.56	3364.02	2840.72

10 MIN HOLOFIBER	TCOM HAND	LASER HAND	TCOM FOOT	LASER FOOT
Mean value (Unit)	8.39	12.97	67.4	64.54
Standard Deviation (Unit)	0.96	1.22	0.33	0.25
Standard Error (Unit)	0.03	0.04	0.01	0.01
Area under curve (Unit*sec.)	427.72	660.83	3434.87	3289.18

20 MIN HOL0				
Mean value (Unit)	8.21	15.47	68.53	63.36
Standard Deviation (Unit)	0.59	2.04	0.09	0.09

Standard Error (Unit)	0.02	0.07	0	0
Area under curve (Unit*sec.)	414.41	780.64	3458.52	3197.45

30 MIN HOLOFIBER

Mean value (Unit)	8.09	13	69.57	61.65
Standard Deviation (Unit)	0.86	1.28	0.09	0.24
Standard Error (Unit)	0.03	0.04	0	0.01
Area under curve (Unit*sec.)	412.29	662.46	3545.72	3141.67

40 MIN HOLOFIBER

Mean value (Unit)	7.94	10.71	100.73	63.74
Standard Deviation (Unit)	0.53	1.04	0.11	0.29
Standard Error (Unit)	0.02	0.04	0	0.01
Minimum value (Unit)	6.68	8.36	100.53	63.05
Area under curve (Unit*sec.)	406.62	548.54	5158.38	3264.19

50 MIN HOLOFIBER

Mean value (Unit)	12.99	14.31	105.67	62.23
Standard Deviation (Unit)	10.5	3.56	0.46	0.27
Standard Error (Unit)	0.36	0.12	0.02	0.01
Area under curve (Unit*sec.)	667.91	735.84	5431.38	3198.7

60 MIN HOLOFIBER

Mean value (Unit)	8.95	10.29	107.61	60.69
Standard Deviation (Unit)	2.4	1.61	0.11	0.18
Standard Error (Unit)	0.08	0.06	0	0.01
Area under curve (Unit*sec.)	456.04	524.2	5484.28	3092.83

Patient ID: 106   placebo - Holofiber

BASELINE	TCOM HAND	LASER HAND	TCOM FOOT	LASER FOOT
Mean value (Unit)	4.97	12.13	44.65	55.53
Standard Deviation (Unit)	2.5	7.93	0.5	0.17
Standard Error (Unit)	0.09	0.28	0.02	0.01
Area under curve (Unit*sec.)	250.45	610.53	2248	2795.7

10 MIN PLACEBO				
Mean value (Unit)	6.72	11.8	33.25	55.67
Standard Deviation (Unit)	5.08	13.08	1.14	0.46
Standard Error (Unit)	0.18	0.46	0.04	0.02
Area under curve (Unit*sec.)	339.01	595.11	1675.82	2806.24

20 MIN PLACEBO				
Mean value (Unit)	6.56	18.81	33.39	56.16
Standard Deviation (Unit)	3.11	17.69	0.58	0.5
Standard Error (Unit)	0.11	0.62	0.02	0.02
Area under curve (Unit*sec.)	333.41	955.97	1695.63	2851.61

30 MIN PLACEBO				
Mean value (Unit)	6.58	15.75	31.28	55.92
Standard Deviation (Unit)	2.5	17.71	0.51	0.57
Standard Error (Unit)	0.09	0.62	0.02	0.02
Area under curve (Unit*sec.)	334.68	801	1590.1	2843.11

40 MIN PLACEBO				
Mean value (Unit)	5.61	9.79	40.6	57.55
Standard Deviation (Unit)	1.19	6.29	1.02	0.32
Standard Error (Unit)	0.04	0.22	0.04	0.01
Area under curve (Unit*sec.)	286.31	499.27	2071.89	2936.59

50 MIN PLACEBO				
Mean value (Unit)	5.56	11.51	37.27	60.23
Standard Deviation (Unit)	2.11	3.21	0.74	0.5
Standard Error (Unit)	0.07	0.11	0.03	0.02
Area under curve (Unit*sec.)	281.46	581.88	1885.38	3047.07

60 MIN PLACEBO				
Mean value (Unit)	5.74	11.77	35.16	61.53
Standard Deviation (Unit)	2.03	12.41	0.46	0.57
Standard Error (Unit)	0.07	0.41	0.02	0.02
Area under curve (Unit*sec.)	324.7	665.94	1988.04	3478.76

10 MIN HOLOFIBER				
Mean value (Unit)	6.72	16.89	22.6	59.07
Standard Deviation (Unit)	2.81	11.83	0.06	0.32
Standard Error (Unit)	0.1	0.41	0	0.01
Area under curve (Unit*sec.)	342.8	862.07	1153.21	3014.17

20 MIN HOLOFIBER				
Mean value (Unit)	8.77	16.54	24.39	60.86
Standard Deviation (Unit)	2.97	7.36	0.22	0.21
Standard Error (Unit)	0.1	0.26	0.01	0.01
Minimum value (Unit)	3.97	6.84	24.11	60.55

| Area under curve (Unit*sec.) | 444.86 | 839.7 | 1238.67 | 3090.46 |

30 MIN HOLOFIBER

Item	1 PU #1	2 PU #2	3 pO2 #3	4 pO2 #4
Mean value (Unit)	3.38	12.52	23.67	60.29
Standard Deviation (Unit)	1.68	5.84	0.06	0.42
Standard Error (Unit)	0.06	0.21	0	0.01
Area under curve (Unit*sec.)	167.23	618.67	1169.58	2979.33

40 MIN HOLOFIBER

Mean value (Unit)	5.66	20.19	24.11	61.86
Standard Deviation (Unit)	5.75	11.57	0.1	0.58
Standard Error (Unit)	0.2	0.41	0	0.02
Area under curve (Unit*sec.)	283.09	1011.32	1209.52	3102.92

50 MIN HOLOFIBER

Item	1 PU #1	2 PU #2	3 pO2 #3	4 pO2 #4
Mean value (Unit)	5.75	14.06	23.58	58.75
Standard Deviation (Unit)	3.19	9.45	0.19	0.43
Standard Error (Unit)	0.11	0.33	0.01	0.02
Area under curve (Unit*sec.)	286.12	700.39	1174.03	2925.03

60 MIN HOLOFIBER

Mean value (Unit)	5.89	7.45	23.33	57.99
Standard Deviation (Unit)	2.92	2.55	0.15	0.13
Standard Error (Unit)	0.1	0.09	0.01	0
Area under curve (Unit*sec.)	284.39	359.42	1125.44	2797.23

Patient ID:107   Holofiber - placebo

BASELINE

Item	TCOM HAND	LASER HAND	TCOM FOOT	LASER FOOT
Mean value (Unit)	3.52	6.05	80.02	63.82
Standard Deviation (Unit)	0.37	0.32	0.35	2.4
Standard Error (Unit)	0.01	0.01	0.01	0.09
Area under curve (Unit*sec.)	170.78	293.47	3879.61	3094.13

10 MIN HOLOFIBER

Item	TCOM HAND	LASER HAND	TCOM FOOT	LASER FOOT
Mean value (Unit)	4.04	6.07	60.06	52.45
Standard Deviation (Unit)	0.06	0.46	0.1	0.16
Standard Error (Unit)	0	0.02	0	0.01
Area under curve (Unit*sec.)	190.98	286.62	2837.57	2477.93

20 MIN HOLOFIBER

Item	TCOM HAND	LASER HAND	TCOM FOOT	LASER FOOT
Mean value (Unit)	4.31	6.69	61.73	57.14
Standard Deviation (Unit)	0.19	1.03	0.18	0.17
Standard Error (Unit)	0.01	0.04	0.01	0.01
Area under curve (Unit*sec.)	216.08	335.6	3096.23	2865.82

30 MIN HOLOFIBER

Item	TCOM HAND	LASER HAND	TCOM FOOT	LASER FOOT
Mean value (Unit)	4.51	5.9	57.26	55.5
Standard Deviation (Unit)	0.15	0.8	0.1	0.22
Standard Error (Unit)	0.01	0.03	0	0.01
Area under curve (Unit*sec.)	227.14	297.47	2886.1	2797.45

40 MIN HOLOFIBER

Item	TCOM HAND	LASER HAND	TCOM FOOT	LASER FOOT
Mean value (Unit)	4.54	5.84	58.9	55.27
Standard Deviation (Unit)	0.27	1.35	0.11	0.09
Standard Error (Unit)	0.01	0.05	0	0
Area under curve (Unit*sec.)	227.57	292.61	2950.67	2768.95

50 MIN HOLOFIBER

Item	TCOM HAND	LASER HAND	TCOM FOOT	LASER FOOT
Mean value (Unit)	4.41	4.82	56.98	54.73
Standard Deviation (Unit)	0.15	0.23	0.15	0.2
Standard Error (Unit)	0.01	0.01	0.01	0.01
Minimum value (Unit)	4.27	4.52	56.58	54.32
Area under curve (Unit*sec.)	221.8	242.44	2864.96	2752.06

60 MIN HOLOFIBER

Item	TCOM HAND	LASER HAND	TCOM FOOT	LASER FOOT
Mean value (Unit)	4.59	6.18	48.35	60.3
Standard Deviation (Unit)	0.37	0.87	0.36	0.31
Standard Error (Unit)	0.01	0.03	0.01	0.01
Area under curve (Unit*sec.)	228.04	306.87	2401.39	2994.84

10 MIN PLACEBO

Item	TCOM HAND	LASER HAND	TCOM FOOT	LASER FOOT
Mean value (Unit)	4.55	6.92	37.97	62.03
Standard Deviation (Unit)	0.31	4.71	0.23	2.04
Standard Error (Unit)	0.01	0.17	0.01	0.07
Area under curve (Unit*sec.)	227.99	347.09	1904.27	3111.28

20 MIN PLACEBO

Item	TCOM HAND	LASER HAND	TCOM FOOT	LASER FOOT
Mean value (Unit)	4.53	5.56	36.89	65.09

Standard Deviation (Unit)	0.52	0.2	0.45	1.24
Standard Error (Unit)	0.02	0.01	0.02	0.04
Area under curve (Unit*sec.)	226.19	277.55	1841.35	3248.56

30 MIN PLACEBO

Mean value (Unit)	5.01	4.89	38.65	64.81
Standard Deviation (Unit)	1.49	0.32	0.4	1.65
Standard Error (Unit)	0.05	0.01	0.01	0.06
Area under curve (Unit*sec.)	250.25	244.58	1931.42	3238.84

40 MIN PLACEBO

Mean value (Unit)	4.54	5.83	37.83	62.23
Standard Deviation (Unit)	0.5	0.93	0.04	0.36
Standard Error (Unit)	0.02	0.03	0	0.01
Area under curve (Unit*sec.)	228.01	292.78	1899.64	3125.22

50 MIN PLACEBO

Mean value (Unit)	4.57	7.16	37.71	62.6
Standard Deviation (Unit)	0.32	2.74	0.07	1.08
Standard Error (Unit)	0.01	0.1	0	0.04
Area under curve (Unit*sec.)	226.17	354.81	1868.13	3100.91

60 MIN PLACEBO

Mean value (Unit)	4.51	5.44	37.1	63.37
Standard Deviation (Unit)	0.34	0.28	0.15	0.77
Standard Error (Unit)	0.01	0.01	0.01	0.03
Area under curve (Unit*sec.)	226.15	272.75	1860.74	3178.5

Patient ID:108   Holofiber - placebo

BASELINE	TCOM HAND	LASER HAND	TCOM FOOT	LASER FOOT
Mean value (Unit)	10.99	12.62	64.67	65.36
Standard Deviation (Unit)	1.58	8.11	0.54	0.33
Standard Error (Unit)	0.06	0.28	0.02	0.01
Area under curve (Unit*sec.)	557.28	640.06	3279.66	3315.06
Duration (sec.)	50.78	50.78	50.78	50.78

10 min HOLOFIBER				
Mean value (Unit)	19.38	14.83	51.17	51.83
Standard Deviation (Unit)	2.02	6.5	0.93	1.97
Standard Error (Unit)	0.07	0.23	0.03	0.07
Area under curve (Unit*sec.)	976.89	747.25	2579.49	2612.72

20 MIN HOLOFIBER				
Mean value (Unit)	17.08	11.45	49.79	50.6
Standard Deviation (Unit)	1.6	1.84	0.26	0.28
Standard Error (Unit)	0.06	0.06	0.01	0.01
Area under curve (Unit*sec.)	860.7	577.1	2509.51	2550.36

30 MIN HOLOFIBER				
Mean value (Unit)	16.32	12.18	49.5	48.66
Standard Deviation (Unit)	1.83	4.92	0.18	0.29
Standard Error (Unit)	0.06	0.17	0.01	0.01
Area under curve (Unit*sec.)	829.66	618.74	2516.66	2473.87

40 MIN HOLOFIBER				
Mean value (Unit)	17.07	12.71	53.03	50.48
Standard Deviation (Unit)	1.82	7.25	0.75	0.65
Standard Error (Unit)	0.05	0.21	0.02	0.02
Area under curve (Unit*sec.)	1212.43	902.93	3767.74	3586.89

50 MIN HOLOFIBER 6				
Mean value (Unit)	16.77	19.04	52.31	51.16
Standard Deviation (Unit)	2.71	10.84	0.35	0.5
Standard Error (Unit)	0.09	0.38	0.01	0.02
Area under curve (Unit*sec.)	854.54	970.53	2665.87	2607.19

60 MIN HOLOFIBER				
Mean value (Unit)	15.99	12.58	55.56	57.65
Standard Deviation (Unit)	1.62	1.9	0.33	0.22
Standard Error (Unit)	0.06	0.07	0.01	0.01
Area under curve (Unit*sec.)	809.26	636.3	2810.94	2916.88

10 MIN PLACEBO				
Mean value (Unit)	12.9	14.1	52.2	164
Standard Deviation (Unit)	1.9	3.18	0.28	7.88
Standard Error (Unit)	0.07	0.11	0.01	0.28
Area under curve (Unit*sec.)	644.7	704.93	2608.34	8197.44

20 MIN PLACEBO				
Mean value (Unit)	13.6	16.22	51.1	43.19
Standard Deviation (Unit)	4	7.43	0.36	0.47
Standard Error (Unit)	0.14	0.26	0.01	0.02

Area under curve (Unit*sec.)	674.31	804.35	2534.63	2142.27
30 MIN PLACEBO				
Mean value (Unit)	13.69	14.34	51.85	44.83
Standard Deviation (Unit)	2.96	4.03	0.12	0.22
Standard Error (Unit)	0.1	0.14	0	0.01
Area under curve (Unit*sec.)	684.38	716.98	2591.1	2240.1
40 MIN PLACEBO				
Mean value (Unit)	12.48	15.28	51.48	44.11
Standard Deviation (Unit)	1.86	5.77	0.36	0.51
Standard Error (Unit)	0.07	0.2	0.01	0.02
Area under curve (Unit*sec.)	622.25	761.74	2565.95	2198.53
50 MIN PLACEBO				
Mean value (Unit)	13.56	16.21	52.09	41.92
Standard Deviation (Unit)	3.79	5.05	0.15	0.26
Standard Error (Unit)	0.13	0.18	0.01	0.01
Area under curve (Unit*sec.)	681.12	814.34	2615.75	2105.18
60 MIN PLACEBO				
Mean value (Unit)	13.9	15.36	54.05	107.15
Standard Deviation (Unit)	2.87	5.2	0.23	8.2
Standard Error (Unit)	0.1	0.18	0.01	0.29
Area under curve (Unit*sec.)	692.65	765.29	2692.18	5337.14

Patient ID:109   placebo -
                        Holofiber

BASELINE	TCOM HAND	LASER HAND	TCOM FOOT	LASER FOOT
Mean value (Unit)	12.37	17.97	69.93	22.66
Standard Deviation (Unit)	1.33	3.93	0.33	1.09
Standard Error (Unit)	0.05	0.14	0.01	0.04
Area under curve (Unit*sec.)	627.48	910.86	3546.44	1149.41

10 MIN PLACEBO				
Mean value (Unit)	10.94	16.36	80.45	39.43
Standard Deviation (Unit)	1.31	4.65	0.42	0.43
Standard Error (Unit)	0.05	0.16	0.02	0.02
Area under curve (Unit*sec.)	542.22	810.41	3985.22	1953.28
Slope (Unit/sec.)	0.02	0.01	-0.01	0.02

20 MIN PLACEBO 3				
Mean value (Unit)	11.01	18.53	78.56	39.61
Standard Deviation (Unit)	1.2	2.43	0.51	0.74
Standard Error (Unit)	0.04	0.09	0.02	0.03
Area under curve (Unit*sec.)	543.17	914.79	3877.33	1954.83

30 MIN PLACEBO				
Mean value (Unit)	11.41	20.12	78.08	39.34
Standard Deviation (Unit)	1.05	2.77	0.56	0.67
Standard Error (Unit)	0.04	0.1	0.02	0.02
Area under curve (Unit*sec.)	559.43	986.78	3829.11	1929.46

40 MIN PLACEBO				
Mean value (Unit)	11.25	18.91	86.07	45.31
Standard Deviation (Unit)	1.01	3.88	0.46	0.39
Standard Error (Unit)	0.03	0.1	0.01	0.01
Area under curve (Unit*sec.)	980.23	1648.17	7501.65	3949.1

50 MIN PLACEBO				
Mean value (Unit)	11.31	16.76	90.1	48.17
Standard Deviation (Unit)	1.19	2.06	1.21	0.53
Standard Error (Unit)	0.03	0.06	0.03	0.01
Area under curve (Unit*sec.)	923.86	1369.05	7361.88	3935.63

60 MIN PLACEBO				
Mean value (Unit)	12.13	20.15	90.4	48.59
Standard Deviation (Unit)	1.21	2.28	0.63	0.44
Standard Error (Unit)	0.04	0.08	0.02	0.02
Area under curve (Unit*sec.)	613.82	1019.33	4573.49	2458.45

10 MIN HOLOFIBER				
Mean value (Unit)	11.92	14.63	80.47	40.44
Standard Deviation (Unit)	1.42	1.9	2.72	1.24
Standard Error (Unit)	0.05	0.07	0.1	0.04
Area under curve (Unit*sec.)	599.46	735.61	4046.39	2033.34

20 MIN HOLOFIBER				
Mean value (Unit)	11.88	13.37	72.12	38.02
Standard Deviation (Unit)	0.95	2.01	0.58	0.57
Standard Error (Unit)	0.03	0.07	0.02	0.02

Area under curve (Unit*sec.)	602.5	677.87	3657.6	1928.26

30 MIN HOLOFIBER

Mean value (Unit)	11.77	16.7	76.19	42.17
Standard Deviation (Unit)	1.27	2.06	0.99	1.12
Standard Error (Unit)	0.04	0.07	0.03	0.04
Area under curve (Unit*sec.)	592.39	841.03	3835.59	2122.75

40 MIN HOLOFIBER

Mean value (Unit)	12.15	11.44	83.75	47.17
Standard Deviation (Unit)	1	0.92	0.68	0.64
Standard Error (Unit)	0.04	0.03	0.02	0.02
Area under curve (Unit*sec.)	609.21	573.86	4200.81	2365.71

50 MIN HOLOFIBER

Mean value (Unit)	12.43	18.18	76.08	44.63
Standard Deviation (Unit)	1.38	1.67	0.36	0.25
Standard Error (Unit)	0.05	0.06	0.01	0.01
Area under curve (Unit*sec.)	614.44	898.5	3759.35	2205.23

60 MIN HOLOFIBER

Mean value (Unit)	11.87	13.32	88.75	53.17
Standard Deviation (Unit)	1.91	1.82	1.58	0.67
Standard Error (Unit)	0.07	0.06	0.06	0.02
Area under curve (Unit*sec.)	592.94	665.79	4435.1	2657.24

Patient ID:110   Holofiber -
                                         placebo

	TCOM HAND	LASER HAND	TCOM FOOT	LASER FOOT
BASELINE				
Mean value (Unit)	6.29	12.12	64.93	52.82
Standard Deviation (Unit)	0.57	1.56	0.77	0.24
Standard Error (Unit)	0.02	0.05	0.03	0.01
Maximum value (Unit)	7.48	15.66	66.35	53.28
Minimum value (Unit)	5.13	8.06	63.78	52.55
Area under curve (Unit*sec.)	321.5	619.35	3317.14	2698.66
Slope (Unit/sec.)	0	0.03	-0.05	-0.02
10 MIN HOLOFIBER				
Mean value (Unit)	8.38	14.3	90.03	43.66
Standard Deviation (Unit)	0.7	2.06	0.25	0.12
Standard Error (Unit)	0.02	0.07	0.01	0
Area under curve (Unit*sec.)	428.97	732.38	4610.73	2235.98
20 MIN HOLOFIBER				
Mean value (Unit)	8.69	14.92	100.01	43.02
Standard Deviation (Unit)	0.98	2.13	0.31	0.12
Standard Error (Unit)	0.03	0.07	0.01	0
Area under curve (Unit*sec.)	440.17	755.67	5065.99	2178.95
30 MIN HOLOFIBER				
Mean value (Unit)	9.12	15.77	84.96	41.59
Standard Deviation (Unit)	0.59	2.17	0.6	0.13
Standard Error (Unit)	0.02	0.08	0.02	0
Area under curve (Unit*sec.)	466.04	805.7	4340.29	2124.97
40 MIN HOLOFIBER				
Mean value (Unit)	9.36	15.97	89.88	40.61
Standard Deviation (Unit)	0.71	2.96	0.81	0.12
Standard Error (Unit)	0.02	0.1	0.03	0
Area under curve (Unit*sec.)	471.94	805.31	4530.55	2047.06
50 MIN HOLOFIBER				
Mean value (Unit)	9.33	15.41	89.14	40.4
Standard Deviation (Unit)	0.72	2.58	0.83	0.17
Standard Error (Unit)	0.02	0.09	0.03	0.01
Area under curve (Unit*sec.)	475.87	786.19	4548.24	2061.61
60 MIN HOLOFIBER				
Mean value (Unit)	9.45	14.8	92.8	40.26
Standard Deviation (Unit)	0.53	2.42	0.26	0.03
Standard Error (Unit)	0.02	0.09	0.01	0
Area under curve (Unit*sec.)	455.86	713.73	4476.48	1942.11
10 MIN PLACEBO				
Mean value (Unit)	8.16	15.96	78.26	48.44
Standard Deviation (Unit)	0.72	2.4	1.72	0.74
Standard Error (Unit)	0.03	0.08	0.06	0.03
Area under curve (Unit*sec.)	414.14	810.73	3974.03	2459.69

20 MIN PLACEBO

Mean value (Unit)	8.49	17.29	83.83	47.58
Standard Deviation (Unit)	0.85	2.65	2.09	0.88
Standard Error (Unit)	0.03	0.09	0.07	0.03
Area under curve (Unit*sec.)	430.46	877.06	4251.55	2412.81

30 MIN PLACEBO

Mean value (Unit)	8.56	18.64	83.54	46.22
Standard Deviation (Unit)	0.97	3.92	0.28	0.14
Standard Error (Unit)	0.03	0.14	0.01	0.01
Area under curve (Unit*sec.)	431.51	939.79	4211.12	2329.88

40 MIN PLACEBO

Mean value (Unit)	8.96	17.94	79.84	42.63
Standard Deviation (Unit)	0.95	2.99	0.65	0.28
Standard Error (Unit)	0.03	0.1	0.02	0.01
Area under curve (Unit*sec.)	456.31	913.03	4064.21	2169.69

50 MIN PLACEBO

Mean value (Unit)	9.16	20.65	83.29	44.54
Standard Deviation (Unit)	1.04	4.5	0.5	0.08
Standard Error (Unit)	0.04	0.16	0.02	0
Area under curve (Unit*sec.)	465.88	1050.09	4234.54	2264.57

60 MIN PLACEBO

Mean value (Unit)	9.99	22.16	91.47	48.61
Standard Deviation (Unit)	1.57	6.96	1.86	1.09
Standard Error (Unit)	0.04	0.18	0.05	0.03
Area under curve (Unit*sec.)	897.12	1989.09	8211.3	4363.73

Patient ID:111   Holofiber - placebo

BASELINE	TCOM HAND	LASER HAND	TCOM FOOT	LASER FOOT
Mean value (Unit)	33.49	8.71	57.58	68.57
Standard Deviation (Unit)	6.41	2.61	1.93	3.38
Standard Error (Unit)	0.09	0.04	0.03	0.05
Maximum value (Unit)	71.81	42.51	61.22	77.76
Minimum value (Unit)	17.27	5.07	54.87	63.23
Area under curve (Unit*sec.)	10328.53	2684.65	17756.92	21146.53
Slope (Unit/sec.)	0.01	0.01	0.02	0.03

10 MIN HOLOFIBER				
Mean value (Unit)	25.68	10.68	61.46	28.98
Standard Deviation (Unit)	3.14	2.6	1.09	0.41
Standard Error (Unit)	0.06	0.05	0.02	0.01
Area under curve (Unit*sec.)	4869.38	2025.36	11652.76	5495.14

20 MIN HOLOFIBER				
Mean value (Unit)	30.11	10.61	59.18	28.57
Standard Deviation (Unit)	4.43	2.14	2.06	1.44
Standard Error (Unit)	0.09	0.04	0.04	0.03
Area under curve (Unit*sec.)	5050.32	1780.16	9925.2	4791.03

30 MIN HOLOFIBER				
Mean value (Unit)	28.25	9.94	58.3	29.19
Standard Deviation (Unit)	4.34	1.65	2.66	2.33
Standard Error (Unit)	0.08	0.03	0.05	0.04
Area under curve (Unit*sec.)	4738.63	1666.57	9777.08	4895.74

40 MIN HOLOFIBER				
Mean value (Unit)	26.16	11.55	61.93	33.59
Standard Deviation (Unit)	2.94	2.21	2.88	2.44
Standard Error (Unit)	0.06	0.04	0.06	0.05
Area under curve (Unit*sec.)	4195.76	1853.45	9934.88	5389.17

50 MIN HOLOFIBER				
Mean value (Unit)	31.71	12.47	60.23	32.63
Standard Deviation (Unit)	2.81	2.27	0.92	0.75
Standard Error (Unit)	0.06	0.05	0.02	0.02
Area under curve (Unit*sec.)	4855.39	1909.35	9221.95	4997.09

60 MIN HOLOFIBER				
Mean value (Unit)	32.53	12.07	57.38	31.65
Standard Deviation (Unit)	3.11	2.27	0.52	0.71
Standard Error (Unit)	0.07	0.05	0.01	0.02
Area under curve (Unit*sec.)	4271.81	1585.26	7534.79	4155.52

10 MIN PLACEBO				
Mean value (Unit)	13.34	22	50.03	31.34
Standard Deviation (Unit)	2.72	4.44	0.91	0.78

Standard Error (Unit)	0.05	0.08	0.02	0.01
Area under curve (Unit*sec.)	2629.01	4337.03	9861.82	6176.8
20 MIN PLACEBO				
Mean value (Unit)	15.35	18.41	50.46	31.39
Standard Deviation (Unit)	4.78	3	0.62	0.64
Standard Error (Unit)	0.09	0.06	0.01	0.01
Area under curve (Unit*sec.)	2689.27	3225.25	8840.61	5499.54
30 MIN PLACEBO				
Mean value (Unit)	14.99	15.01	51.53	32.62
Standard Deviation (Unit)	1.89	2.93	0.71	0.7
Standard Error (Unit)	0.03	0.05	0.01	0.01
Area under curve (Unit*sec.)	2954.92	2958.87	10157.22	6430.27
40 MIN PLACEBO				
Mean value (Unit)	17.76	11.82	51.37	32.11
Standard Deviation (Unit)	5.01	2.05	0.69	0.68
Standard Error (Unit)	0.09	0.04	0.01	0.01
Area under curve (Unit*sec.)	3241.05	2157.53	9375.34	5860.34
50 MIN PLACEBO				
Mean value (Unit)	16.83	16.81	51.45	33.53
Standard Deviation (Unit)	1.75	4.54	1.03	0.7
Standard Error (Unit)	0.03	0.08	0.02	0.01
Area under curve (Unit*sec.)	3808.88	3805.03	11644.76	7589.4
60 MIN PLACEBO	17.34	16.89	47.43	32.54
Standard Deviation (Unit)	1.34	2.78	0.91	0.58
Standard Error (Unit)	0.02	0.05	0.02	0.01
Area under curve (Unit*sec.)	3545.38	3452.11	9695.11	6652.54

Patient ID: 112   placebo - Holofiber

BASELINE	TCOM HAND	LASER HAND	TCOM FOOT	LASER FOOT
Mean value (Unit)	16.01	40.53	57.54	61.8
Standard Deviation (Unit)	2.99	13.56	0.35	0.51
Standard Error (Unit)	0.11	0.48	0.01	0.02
Area under curve (Unit*sec.)	795.15	2012.84	2857.73	3069
Slope (Unit/sec.)	0.08	0.76	0.02	0.03

10 MIN PLACEBO				
Mean value (Unit)	19.81	65.83	54.54	62.38
Standard Deviation (Unit)	6.77	7.89	0.6	0.68
Standard Error (Unit)	0.24	0.28	0.02	0.02
Area under curve (Unit*sec.)	992.65	3298.75	2732.23	3125.17
Slope (Unit/sec.)	0	-0.03	-0.04	-0.05

20 MIN PLACEBO				
Mean value (Unit)	14.44	49.46	55.21	63.29
Standard Deviation (Unit)	3.32	18.21	0.07	0.09
Standard Error (Unit)	0.12	0.65	0	0
Area under curve (Unit*sec.)	712.62	2441.15	2724.49	3123.51

30 MIN PLACEBO				
Mean value (Unit)	11.53	39.22	57.25	64.08
Standard Deviation (Unit)	0.75	6.95	0	0.04
Standard Error (Unit)	0.03	0.24	0	0
Area under curve (Unit*sec.)	577.31	1964.84	2868.05	3210.11

40 MIN PLACEBO				
Mean value (Unit)	14.72	36.98	56.43	62.96
Standard Deviation (Unit)	3.19	4.27	0.08	0.07
Standard Error (Unit)	0.11	0.15	0	0
Area under curve (Unit*sec.)	744.55	1871.41	2854.91	3185.09

50 MIN PLACEBO				
Mean value (Unit)	13.29	16.18	56.11	62.44
Standard Deviation (Unit)	2.71	9.12	0.15	0.2
Standard Error (Unit)	0.1	0.32	0.01	0.01
Area under curve (Unit*sec.)	670.14	815.61	2828.5	3147.15

60 MIN PLACEBO				
Mean value (Unit)	14.82	24.93	57.97	62.27
Standard Deviation (Unit)	4.36	2.89	0.61	0.14
Standard Error (Unit)	0.15	0.1	0.02	0
Area under curve (Unit*sec.)	750.88	1262.79	2936.45	3154.07

10 MIN HOLOFIBER				
Mean value (Unit)	13.27	37.71	63	67.08
Standard Deviation (Unit)	2.12	5.25	0.26	0.27
Standard Error (Unit)	0.07	0.19	0.01	0.01
Area under curve (Unit*sec.)	658.29	1870.75	3125.01	3327.29

20 MIN HOLOFIBER				
Mean value (Unit)	15.16	29.61	59.56	64.89
Standard Deviation (Unit)	3.71	7.88	0.04	0.13

Standard Error (Unit)	0.13	0.28	0	0
Area under curve (Unit*sec.)	759.79	1484.62	2983.51	3250.59

30 MIN HOLOFIBER

Mean value (Unit)	15.61	24.5	60.51	65
Standard Deviation (Unit)	2.6	4.56	0.75	0.51
Standard Error (Unit)	0.09	0.16	0.03	0.02
Area under curve (Unit*sec.)	781.98	1227.67	3031.34	3256.38

40 MIN HOLOFIBER

Mean value (Unit)	13.91	28.46	60.96	65.65
Standard Deviation (Unit)	3	5.51	0.19	0.19
Standard Error (Unit)	0.11	0.19	0.01	0.01

50 MIN HOLOFIBER

Mean value (Unit)	17.37	27.45	63.52	67.55
Standard Deviation (Unit)	6.72	4.78	1.02	0.72
Standard Error (Unit)	0.24	0.17	0.04	0.03
Area under curve (Unit*sec.)	871.64	1377.42	3186.25	3388.11

60 MIN HOLOFIBER

Mean value (Unit)	14.3	28.04	60.31	64.34
Standard Deviation (Unit)	2.5	5.69	0.08	0.11
Standard Error (Unit)	0.09	0.2	0	0
Area under curve (Unit*sec.)	718.24	1408.51	3029.02	3231.07

Patient ID: 113   placebo - Holofiber

BASELINE	TCOM HAND	LASER HAND	TCOM FOOT	LASER FOOT
Mean value (Unit)	11.73	37.11	44.18	53.16
Standard Deviation (Unit)	0.6	14.89	0.26	0.23
Standard Error (Unit)	0.02	0.6	0.01	0.01
Area under curve (Unit*sec.)	443.53	1405.21	1670.88	2010.66

10 MIN PLACEBO				
Mean value (Unit)	13.38	11.77	37.79	49.16
Standard Deviation (Unit)	0.98	3.31	0.62	0.86
Standard Error (Unit)	0.04	0.13	0.03	0.03

20M MIN PLACEBO				
Mean value (Unit)	12.79	31.57	36.21	47.2
Standard Deviation (Unit)	0.76	30.34	0.29	0.1
Standard Error (Unit)	0.03	1.25	0.01	0
Area under curve (Unit*sec.)	464.56	1147.38	1315.59	1714.9

30 MIN PLACEBO				
Mean value (Unit)	13.68	10.83	42.7	49.34
Standard Deviation (Unit)	1.25	4.02	0.09	0.16
Standard Error (Unit)	0.05	0.16	0	0.01
Area under curve (Unit*sec.)	522.46	413.97	1630.78	1884.25

40 MIN PLACEBO				
Mean value (Unit)	13.56	23.89	41.05	46.79
Standard Deviation (Unit)	0.94	32.39	0.4	0.5
Standard Error (Unit)	0.04	1.31	0.02	0.02
Area under curve (Unit*sec.)	514.29	907.18	1557.78	1775.61

50 MIN PLACEBO				
Mean value (Unit)	13.11	11.39	44.02	47.54
Standard Deviation (Unit)	0.66	8.92	0.34	0.22
Standard Error (Unit)	0.03	0.36	0.01	0.01
Area under curve (Unit*sec.)	502.26	436.37	1686.68	1821.62

60 MIN PLACEBO				
Mean value (Unit)	13.22	26.59	45.05	49.64
Standard Deviation (Unit)	1.47	17.24	0.15	0.21
Standard Error (Unit)	0.06	0.7	0.01	0.01
Area under curve (Unit*sec.)	502.46	1011.3	1712.09	1886.64

10 MIN HOLOFIBER				
Mean value (Unit)	15.03	15.44	42.68	44.94
Standard Deviation (Unit)	1.05	5.91	0.19	0.59
Standard Error (Unit)	0.04	0.24	0.01	0.02
Area under curve (Unit*sec.)	559.9	575.51	1590.17	1674.57

20 MIN HOLOFIBER

Mean value (Unit)	14.3	26.8	46.36	49.38
Standard Deviation (Unit)	3.32	44.74	0.09	0.59
Standard Error (Unit)	0.13	1.81	0	0.02
Area under curve (Unit*sec.)	539.98	1010.99	1750.52	1864.47

30 MIN HOLOFIBER

Mean value (Unit)	14.98	17.83	49.69	60.29
Standard Deviation (Unit)	1.81	7.41	1	0.66
Standard Error (Unit)	0.07	0.3	0.04	0.03
Area under curve (Unit*sec.)	565.73	673.1	1876.23	2276.41

40 MIN HOLOFIBER

Mean value (Unit)	14.24	13.77	53.91	59.06
Standard Deviation (Unit)	1.67	13.84	0.14	2.54
Standard Error (Unit)	0.07	0.56	0.01	0.1
Area under curve (Unit*sec.)	536.5	519.01	2032.21	2226.07

50 MIN HOLOFIBER

Mean value (Unit)	15.09	19.44	55.61	61.52
Standard Deviation (Unit)	2.35	14.84	0.29	0.18
Standard Error (Unit)	0.1	0.6	0.01	0.01
Area under curve (Unit*sec.)	570.79	735.48	2103.19	2326.66

60 MIN HOLOFIBER

Mean value (Unit)	14.49	12.54	52.19	52.64
Standard Deviation (Unit)	1.29	3.37	0.44	0.6
Standard Error (Unit)	0.05	0.14	0.02	0.02
Area under curve (Unit*sec.)	551.5	476.94	1986.72	2003.69

Patient ID: 114   Holofiber -
                                     placebo

BASELINE	TCOM HAND	LASER HAND	TCOM FOOT	LASER FOOT
Mean value (Unit)	16.16	29.8	53.82	26.28
Standard Deviation (Unit)	1.21	5.2	0.88	0.25
Standard Error (Unit)	0.05	0.22	0.04	0.01
Area under curve (Unit*sec.)	569.29	1049.13	1895.28	925.65

10 MIN HOLOFIBER				
Mean value (Unit)	28.72	47.2	49.62	48.58
Standard Deviation (Unit)	1.08	30.98	0.23	0.3
Standard Error (Unit)	0.04	1.26	0.01	0.01
Area under curve (Unit*sec.)	1066.78	1753.81	1842.96	1804.27

20 MIN HOLOFIBER				
Mean value (Unit)	23.56	21.1	53.96	49.08
Standard Deviation (Unit)	1.88	8.68	0.38	0.23
Standard Error (Unit)	0.08	0.35	0.02	0.01
Area under curve (Unit*sec.)	885.25	792.98	2027.29	1844.15

30 MIN HOLOFIBER				
Mean value (Unit)	24.46	23.72	53.66	51.29
Standard Deviation (Unit)	5.94	3.84	0.21	0.12
Standard Error (Unit)	0.28	0.18	0.01	0.01
Area under curve (Unit*sec.)	684.21	663.36	1500.47	1434.21

40 MIN HOLOFIBER				
Mean value (Unit)	22.82	25.35	55.94	52.34
Standard Deviation (Unit)	1.23	4.94	0.12	0.12
Standard Error (Unit)	0.06	0.22	0.01	0.01
Area under curve (Unit*sec.)	697.48	774.94	1709.74	1599.74

50 MIN HOLOFIBER				
Mean value (Unit)	23.18	22.17	58.83	55.01
Standard Deviation (Unit)	1.78	2.96	1.58	0.46
Standard Error (Unit)	0.07	0.12	0.06	0.02
Area under curve (Unit*sec.)	865.23	827.2	2195.65	2053.21

60 MIN HOLOFIBER				
Mean value (Unit)	23.22	34.93	61.01	59.54
Standard Deviation (Unit)	1.79	36.16	0.4	0.19
Standard Error (Unit)	0.07	1.47	0.02	0.01
Area under curve (Unit*sec.)	865.21	1302.78	2273.16	2218.5

10 MIN PLACEBO				
Mean value (Unit)	25.53	18.31	57.44	61.32
Standard Deviation (Unit)	2	2.59	0.56	0.69
Standard Error (Unit)	0.08	0.11	0.02	0.03
Area under curve (Unit*sec.)	925.79	664.25	2083.34	2223.99

20 MIN PLACEBO				
Mean value (Unit)	23.72	23.8	58.36	63.01
Standard Deviation (Unit)	1.47	3.55	0.06	0.13
Standard Error (Unit)	0.06	0.15	0	0.01
Area under curve (Unit*sec.)	776.45	778.68	1910.64	2062.73

Slope (Unit/sec.)	0.04	0.04	0	0.01
30M MIN PLACEBO				
Mean value (Unit)	23.61	22.49	59.07	61.56
Standard Deviation (Unit)	1.49	4.2	0.41	0.16
Standard Error (Unit)	0.06	0.18	0.02	0.01
Area under curve (Unit*sec.)	834.35	794.72	2087.6	2175.4
40 MIN PLACEBO				
Mean value (Unit)	27.04	22.16	64.38	65.88
Standard Deviation (Unit)	2.05	3.85	0.67	0.18
Standard Error (Unit)	0.08	0.16	0.03	0.01
Area under curve (Unit*sec.)	1009.22	826.95	2402.88	2459.07
50 MIN PLACEBO				
Mean value (Unit)	26.4	25.38	61.35	62.59
Standard Deviation (Unit)	1.85	6.67	0.14	0.09
Standard Error (Unit)	0.08	0.28	0.01	0
Area under curve (Unit*sec.)	959.01	922.03	2228.99	2273.99
60 MIN PLACEBO				
Mean value (Unit)	28	22.28	62.41	60.32
Standard Deviation (Unit)	1.61	2.87	0.58	0.11
Standard Error (Unit)	0.07	0.12	0.02	0
Area under curve (Unit*sec.)	973.76	775.08	2170.64	2098.21

Patient ID:115   Holofiber -
                                   placebo

BASELINE	TCOM HAND	LASER HAND	TCOM FOOT	LASER FOOT
Mean value (Unit)	8.01	74	59.65	61.72
Standard Deviation (Unit)	1.56	7.98	0.33	0.52
Standard Error (Unit)	0.07	0.34	0.01	0.02
Area under curve (Unit*sec.)	273.12	2523.81	2034.05	2104.71

10 MIN HOLOFIBER				
Mean value (Unit)	8.98	97.65	50.25	52.22
Standard Deviation (Unit)	1.26	7.4	0.17	0.13
Standard Error (Unit)	0.04	0.26	0.01	0
Area under curve (Unit*sec.)	457.48	4976.38	2560.96	2661.17

20 MIN HOLOFIBER				
Mean value (Unit)	9.42	96.64	49.54	51.55
Standard Deviation (Unit)	1.21	6.74	0.05	0.1
Standard Error (Unit)	0.05	0.26	0	0
Area under curve (Unit*sec.)	402.27	4128.6	2116.07	2202.22

30 MIN HOLOFIBER				
Mean value (Unit)	13.03	103.33	49.93	51.77
Standard Deviation (Unit)	12.79	7.62	0.19	0.16
Standard Error (Unit)	0.41	0.25	0.01	0.01
Area under curve (Unit*sec.)	774.99	6143.45	2968.93	3078.16

40 MIN HOLOFIBER				
Mean value (Unit)	12.19	104.22	52.59	54.61
Standard Deviation (Unit)	2.28	10.22	0.45	0.51
Standard Error (Unit)	0.07	0.31	0.01	0.02
Area under curve (Unit*sec.)	797.03	6816.43	3439.7	3571.91

50 MIN HOLOFIBER				
Mean value (Unit)	13.19	108.65	53.26	55.23
Standard Deviation (Unit)	2.2	10.52	0.29	0.29
Standard Error (Unit)	0.07	0.33	0.01	0.01
Area under curve (Unit*sec.)	836.74	6891.66	3378.19	3503.05

60 MIN HOLOFIBER				
Mean value (Unit)	14.97	107.18	55.44	58.77
Standard Deviation (Unit)	3.1	10.43	0.32	0.22
Standard Error (Unit)	0.09	0.32	0.01	0.01
Area under curve (Unit*sec.)	1010.21	7234.09	3742.32	3967.38

10 MIN PLACEBO				
Mean value (Unit)	21.3	100.68	58.51	62
Standard Deviation (Unit)	4.84	33.08	0.29	0.51
Standard Error (Unit)	0.15	1.05	0.01	0.02
Area under curve (Unit*sec.)	1308.59	6185.51	3595.11	3809.65

20 MIN PLACEBO				
Mean value (Unit)	21.82	110.34	57.2	59.93
Standard Deviation (Unit)	4.03	22.22	0.3	0.3
Standard Error (Unit)	0.13	0.69	0.01	0.01

Area under curve (Unit*sec.)	1383.84	6998.02	3627.8	3801.03
30 MIN PLACEBO				
Mean value (Unit)	24.02	119.21	57.44	59.5
Standard Deviation (Unit)	4.86	29.74	0.22	0.28
Standard Error (Unit)	0.16	0.96	0.01	0.01
Area under curve (Unit*sec.)	1427.97	7087.93	3415.21	3537.56
40 MIN PLACEBO				
Mean value (Unit)	26.29	102.83	57.06	59.07
Standard Deviation (Unit)	5.46	17.63	0.23	0.25
Standard Error (Unit)	0.17	0.54	0.01	0.01
Area under curve (Unit*sec.)	1719.79	6726.44	3732.44	3863.84
50 MIN PLACEBO				
Mean value (Unit)	24.5	112.79	56.39	58.63
Standard Deviation (Unit)	5.63	38.24	0.25	0.41
Standard Error (Unit)	0.18	1.21	0.01	0.01
Area under curve (Unit*sec.)	1506.26	6934.67	3466.66	3604.71
60 MIN PLACEBO				
Mean value (Unit)	25.4	94.83	58.13	60.06
Standard Deviation (Unit)	5.18	23.13	0.48	0.6
Standard Error (Unit)	0.15	0.68	0.01	0.02
Area under curve (Unit*sec.)	1816.98	6780.63	4158.57	4296.31

Patient ID:116   placebo - Holofiber

BASELINE	TCOM HAND	LASER HAND	TCOM FOOT	LASER FOOT
Mean value (Unit)	7.41	8.01	87.64	3.96
Standard Deviation (Unit)	6.55	0.79	0.44	0.19
Standard Error (Unit)	0.16	0.02	0.01	0
Area under curve (Unit*sec.)	764.23	825.69	9036.03	408.23

GENERAL CALCULATIONS : AREA 2				
Mean value (Unit)	6.4	27.82	83	7.83
Standard Deviation (Unit)	7.08	13.25	1.09	0.21
Standard Error (Unit)	0.25	0.46	0.04	0.01
Area under curve (Unit*sec.)	323.81	1406.45	4193.85	395.74

GENERAL CALCULATIONS : AREA 3				
Mean value (Unit)	10.5	35.26	80.84	8.39
Standard Deviation (Unit)	17.81	5.49	0.4	0.38
Standard Error (Unit)	0.63	0.19	0.01	0.01
Area under curve (Unit*sec.)	515.83	1731.63	3969.49	412.08

GENERAL CALCULATIONS : AREA 4				
Mean value (Unit)	5.47	28.88	78.47	6.85
Standard Deviation (Unit)	0.7	12.07	0.27	1.34
Standard Error (Unit)	0.02	0.42	0.01	0.05
Area under curve (Unit*sec.)	279.74	1476.97	4013.99	350.46

GENERAL CALCULATIONS : AREA 5				
Mean value (Unit)	6.3	21.09	85.28	3.87
Standard Deviation (Unit)	0.48	13.81	1.99	0.57
Standard Error (Unit)	0.02	0.48	0.07	0.02
Area under curve (Unit*sec.)	321.65	1077.17	4356.58	197.95

GENERAL CALCULATIONS : AREA 6				
Mean value (Unit)	6.13	29.34	77.64	6.47
Standard Deviation (Unit)	0.96	10.12	0.35	0.71
Standard Error (Unit)	0.03	0.36	0.01	0.03
Area under curve (Unit*sec.)	291.96	1397.47	3696.87	308.07

GENERAL CALCULATIONS : AREA 7				
Mean value (Unit)	6.2	40.39	85.05	2.62
Standard Deviation (Unit)	3.4	32.59	1.12	0.11
Standard Error (Unit)	0.12	1.17	0.04	0
Area under curve (Unit*sec.)	296.25	1927.41	4060.2	124.92

Mean value (Unit)	5.65	36.77	77.14	4.02
Standard Deviation (Unit)	0.47	16.61	0.93	0.12
Standard Error (Unit)	0.02	0.75	0.04	0.01
Area under curve (Unit*sec.)	172.76	1123.05	2358.01	122.96

GENERAL CALCULATIONS : AREA 9				
Mean value (Unit)	5.84	55.19	80.92	4.04

Standard Deviation (Unit)	0.85	19.91	0.55	0.73
Standard Error (Unit)	0.02	0.45	0.01	0.02
Area under curve (Unit*sec.)	695.29	6574.94	9637.78	481.01

GENERAL CALCULATIONS : AREA 10

Mean value (Unit)	6.23	65.39	90.3	4.12
Standard Deviation (Unit)	2.01	50.18	0.41	0.45
Standard Error (Unit)	0.07	1.75	0.01	0.02
Area under curve (Unit*sec.)	318.79	3345.68	4618.86	210.69

GENERAL CALCULATIONS : AREA 11

Mean value (Unit)	6.05	40.51	93.24	3.9
Standard Deviation (Unit)	0.79	17.22	0.16	0.33
Standard Error (Unit)	0.03	0.61	0.01	0.01
Area under curve (Unit*sec.)	297.11	1989.82	4578.62	191.71

GENERAL CALCULATIONS : AREA 12

Mean value (Unit)	6.1	25.81	98.14	6.4
Standard Deviation (Unit)	1.02	22.14	0.25	0.48
Standard Error (Unit)	0.04	0.77	0.01	0.02
Area under curve (Unit*sec.)	311.99	1321.22	5019.89	327.57

GENERAL CALCULATIONS : AREA 13

Mean value (Unit)	5.98	30.97	94.84	6.38
Standard Deviation (Unit)	0.95	20.91	0.48	0.24
Standard Error (Unit)	0.03	0.73	0.02	0.01
Area under curve (Unit*sec.)	305.18	1580.65	4839.29	325.37

GENERAL CALCULATIONS : AREA 14

Mean value (Unit)	6.11	33.9	92.84	4.68
Standard Deviation (Unit)	0.67	11.63	1.54	0.35
Standard Error (Unit)	0.02	0.4	0.05	0.01
Area under curve (Unit*sec.)	312.45	1733.61	4748.48	239.43

Patient ID:117   Holofiber - placebo

BASELINE	TCOM HAND	LASER HAND	TCOM FOOT	LASER FOOT
Mean value (Unit)	16.44	56.95	52.26	11.02
Standard Deviation (Unit)	2.73	5.94	0.32	0.08
Standard Error (Unit)	0.13	0.28	0.02	0
Area under curve (Unit*sec.)	449.51	1557.22	1428.92	301.3

10 MIN HOLOFIBER				
Mean value (Unit)	28.09	57.14	45.32	8.1
Standard Deviation (Unit)	2.3	5.74	0.1	0.12
Standard Error (Unit)	0.1	0.26	0	0.01
Area under curve (Unit*sec.)	879.4	1789.04	1418.89	253.64

20 MIN HOLOFIBER				
Mean value (Unit)	32.55	62.1	45.13	6.71
Standard Deviation (Unit)	2.98	10.82	0.13	0.01
Standard Error (Unit)	0.12	0.45	0.01	0
Area under curve (Unit*sec.)	1168.61	2229.22	1620.09	241.01

30 MIN HOLOFIBER				
Mean value (Unit)	31.87	63.74	44.1	7.75
Standard Deviation (Unit)	2.61	6.48	0.14	0
Standard Error (Unit)	0.12	0.29	0.01	0
Area under curve (Unit*sec.)	983.99	1968.15	1361.57	239.33

40 MIN HOLOFIBER				
Mean value (Unit)	31.84	59.1	42.44	5.46
Standard Deviation (Unit)	2.28	6.92	0.06	0.16
Standard Error (Unit)	0.1	0.3	0	0.01
Area under curve (Unit*sec.)	1026.69	1905.51	1368.12	176.01

50 MIN HOLOFIBER				
Mean value (Unit)	24.35	68.6	43.17	3.88
Standard Deviation (Unit)	1.3	4.9	0.44	0.12
Standard Error (Unit)	0.06	0.21	0.02	0.01
Area under curve (Unit*sec.)	795.71	2241.93	1410.59	126.72

60 MIN HOLOFIBER				
Mean value (Unit)	28.58	77.73	43.03	4.14
Standard Deviation (Unit)	3.11	4.23	0.32	0.14
Standard Error (Unit)	0.14	0.18	0.01	0.01
Area under curve (Unit*sec.)	934.08	2539.68	1405.82	135.37

10 MIN PLACEBO				
Mean value (Unit)	26.63	67.56	39.01	5.79
Standard Deviation (Unit)	1.2	90.84	0.39	0.12
Standard Error (Unit)	0.06	4.33	0.02	0.01
Area under curve (Unit*sec.)	726.47	1845.6	1064.31	157.92

20 MIN PLACEBO				
Mean value (Unit)	29.83	26.3	39.28	5.85
Standard Deviation (Unit)	1.74	2.51	0.12	0.19
Standard Error (Unit)	0.07	0.1	0	0.01
Area under curve (Unit*sec.)	1083.71	955.64	1427.11	212.48

30 MIN PLACEBO

Mean value (Unit)	23.12	34.13	41.55	1.77
Standard Deviation (Unit)	2.09	7.75	0.5	0.11
Standard Error (Unit)	0.09	0.33	0.02	0
Area under curve (Unit*sec.)	789.82	1165.97	1419.51	60.42

40 MIN PLACEBO

Mean value (Unit)	12.47	22.62	42.59	2.24
Standard Deviation (Unit)	2.26	2.81	0.32	0.1
Standard Error (Unit)	0.1	0.13	0.01	0
Area under curve (Unit*sec.)	368.78	668.97	1259.43	66.17

50 MIN PLACEBO

Mean value (Unit)	11.83	22.53	44.05	2.84
Standard Deviation (Unit)	5.63	2.79	0.7	0.12
Standard Error (Unit)	0.23	0.11	0.03	0
Area under curve (Unit*sec.)	440.22	838.4	1638.59	105.76

60 MIN PLACEBO

Mean value (Unit)	10.76	25.18	42.46	1.95
Standard Deviation (Unit)	1.46	1.86	0.22	0
Standard Error (Unit)	0.06	0.08	0.01	0
Area under curve (Unit*sec.)	380.94	891.19	1503.29	69.14

Patient ID:118
placebo -
Holofiber

RECORDING INFORMATION

BASELINE	TCOM HAND	LASER HAND	TCOM FOOT	LASER FOOT
Mean value (Unit)	15.59	41.17	31.08	49.12
Standard Deviation (Unit)	1.53	6.23	1.44	1.37
Standard Error (Unit)	0.03	0.14	0.03	0.03
Area under curve (Unit*sec.)	1918.73	5067.54	3825.09	6045.28

10 MIN PLACEBO				
Mean value (Unit)	17.21	52.38	14.69	45.45
Standard Deviation (Unit)	1.45	4.66	0.96	0.47
Standard Error (Unit)	0.03	0.09	0.02	0.01
Area under curve (Unit*sec.)	2596.41	7900.42	2216.16	6855.66

20 MIN PLACEBO				
Mean value (Unit)	16.38	48.01	11.81	47.41
Standard Deviation (Unit)	1.49	10.4	0.77	0.74
Standard Error (Unit)	0.03	0.19	0.01	0.01
Area under curve (Unit*sec.)	2991.91	8767.94	2155.54	8657.17

30 MIN PLACEBO				
Mean value (Unit)	24.19	49.18	13.06	48.14
Standard Deviation (Unit)	29.59	9.07	0.79	0.3
Standard Error (Unit)	0.55	0.17	0.01	0.01
Area under curve (Unit*sec.)	4418.24	8979.26	2384.3	8789.47

40 MIN PLACEBO				
Mean value (Unit)	21.59	50.58	14.66	50.69
Standard Deviation (Unit)	17.23	8.07	1.27	0.38
Standard Error (Unit)	0.32	0.15	0.02	0.01
Area under curve (Unit*sec.)	3941.82	9234.92	2677.09	9255.53

50 MIN PLACEBO				
Mean value (Unit)	22.26	48.09	14.69	51.32
Standard Deviation (Unit)	9.22	11.02	1.23	0.77
Standard Error (Unit)	0.17	0.21	0.02	0.01
Area under curve (Unit*sec.)	3887.79	8400.42	2564.92	8963.13

60 MIN PLACEBO				
Mean value (Unit)	32.42	45.58	20.07	53.5
Standard Deviation (Unit)	41.87	11.34	0.85	0.67
Standard Error (Unit)	0.73	0.2	0.01	0.01
Area under curve (Unit*sec.)	6693.43	9409.93	4142.42	11043.63

10 MIN HOLOFIBER				
Mean value (Unit)	64.13	32.45	33.81	56.45
Standard Deviation (Unit)	64.22	19.46	1.25	1.88
Standard Error (Unit)	1.18	0.36	0.02	0.03
Area under curve (Unit*sec.)	11726.08	5933.78	6182.08	10322.27

20 MIN HOLOFIBER				
Mean value (Unit)	40.82	37.76	29.93	54.97
Standard Deviation (Unit)	3.67	9.1	1.88	0.75
Standard Error (Unit)	0.07	0.17	0.03	0.01

Area under curve (Unit*sec.)	7464.39	6904.57	5473.22	10050.86

30 MIN HOLOFIBER

Mean value (Unit)	37.24	40.67	30.64	57.15
Standard Deviation (Unit)	3.53	9.68	1.01	0.45
Standard Error (Unit)	0.06	0.17	0.02	0.01
Area under curve (Unit*sec.)	7400.81	8084.58	6090.49	11358.87

40 MIN HOLOFIBER

Mean value (Unit)	38.26	40.09	31.63	55.42
Standard Deviation (Unit)	7.69	7.08	1.44	0.69
Standard Error (Unit)	0.13	0.12	0.02	0.01
Area under curve (Unit*sec.)	7908.95	8286.38	6537.93	11454.59

50 MIN HOLOFIBER

Mean value (Unit)	42.18	47.87	47.79	60.48
Standard Deviation (Unit)	4.38	4.97	3.93	2.58
Standard Error (Unit)	0.08	0.09	0.07	0.05
Area under curve (Unit*sec.)	8383.18	9514.03	9498.73	12020.27

60 MIN HOLOFIBER

Mean value (Unit)	41.98	47.64	44.73	63.55
Standard Deviation (Unit)	4.23	4.51	1.47	1.12
Standard Error (Unit)	0.09	0.09	0.03	0.02
Area under curve (Unit*sec.)	6006.76	6815.94	6400.53	9092.94

Patient ID:119   placebo - Holofiber

BASELINE	TCOM HAND	LASER HAND	TCOM FOOT	LASER FOOT
Mean value (Unit)	23.52	50.95	54.36	50.72
Standard Deviation (Unit)	2.67	21.02	1.12	0.64
Standard Error (Unit)	0.21	1.62	0.09	0.05
Area under curve (Unit*sec.)	243.36	528.2	562.72	525.14

10 MIN PLACEBO				
Mean value (Unit)	35.19	76.8	57.98	67.63
Standard Deviation (Unit)	12.13	29.13	0.29	0.29
Standard Error (Unit)	0.39	0.92	0.01	0.01
Area under curve (Unit*sec.)	2162.32	4714.42	3562.3	4155.21

20 MIN PLACEBO				
Mean value (Unit)	33.85	126.84	62.51	71.14
Standard Deviation (Unit)	15.21	114.56	1.14	1.61
Standard Error (Unit)	0.47	3.55	0.04	0.05
Area under curve (Unit*sec.)	2180.64	8174.5	4026.65	4582.78

30 MIN PLACEBO				
Mean value (Unit)	28.81	108.01	64.33	71.53
Standard Deviation (Unit)	9.77	54.75	0.52	0.81
Standard Error (Unit)	0.31	1.75	0.02	0.03
Area under curve (Unit*sec.)	1740.39	6528.88	3889.06	4323.97

40 MIN PLACEBO				
Mean value (Unit)	23.71	81.12	66.85	72.59
Standard Deviation (Unit)	6.25	22.46	0.93	0.97
Standard Error (Unit)	0.2	0.71	0.03	0.03
Area under curve (Unit*sec.)	1457.23	4984.26	4107.54	4460.26

50 MIN PLACEBO				
Mean value (Unit)	24.28	95.78	69.06	74.7
Standard Deviation (Unit)	7.34	15.73	0.26	0.24
Standard Error (Unit)	0.23	0.5	0.01	0.01
Area under curve (Unit*sec.)	1467.4	5790.62	4174.97	4515.4

60 MIN PLACEBO				
Mean value (Unit)	22.5	94.75	71.84	77
Standard Deviation (Unit)	4.97	24.66	0.72	0.72
Standard Error (Unit)	0.14	0.69	0.02	0.02
Area under curve (Unit*sec.)	1784.94	7516.97	5699.41	6108.26

10 MIN HOLOFIBER				
Mean value (Unit)	33.48	61.25	67.14	71.64
Standard Deviation (Unit)	11.29	18.59	0.64	0.5
Standard Error (Unit)	0.29	0.47	0.02	0.01
Area under curve (Unit*sec.)	3185.63	5829.21	6389.25	6817.88

20 MIN HOLOFIBER				
Mean value (Unit)	30.18	62.35	67.26	70.47
Standard Deviation (Unit)	5.45	30.2	0.91	1.13
Standard Error (Unit)	0.14	0.77	0.02	0.03
Area under curve (Unit*sec.)	2872.32	5934.04	6400.84	6706.8

30 MIN HOLOFIBER

Mean value (Unit)	29.91	57.79	68.55	69.18
Standard Deviation (Unit)	6.75	33.9	1.78	1.21
Standard Error (Unit)	0.17	0.85	0.04	0.03
Area under curve (Unit*sec.)	2965.03	5729.62	6796.24	6858.19

40 MIN HOLOFIBER

Mean value (Unit)	28.85	53.47	68.73	71.72
Standard Deviation (Unit)	5.15	18.13	0.69	0.66
Standard Error (Unit)	0.13	0.46	0.02	0.02
Area under curve (Unit*sec.)	2746.16	5088.82	6541.54	6825.3

50 MIN HOLOFIBER

Mean value (Unit)	31.32	53.98	71.36	75.16
Standard Deviation (Unit)	6.79	16.96	1.66	1.59
Standard Error (Unit)	0.15	0.37	0.04	0.04
Area under curve (Unit*sec.)	3974.71	6850.74	9056.87	9539.52

60 MIN HOLOFIBER

Mean value (Unit)	31.51	68.69	70.75	75.65
Standard Deviation (Unit)	5.98	50.86	1.25	1.4
Standard Error (Unit)	0.16	1.36	0.03	0.04
Area under curve (Unit*sec.)	2748.83	5993.38	6171.57	6599.18

Patient ID:120	Holofiber - placebo			
BASELINE	TCOM HAND	LASER HAND	TCOM FOOT	LASER FOOT
Mean value (Unit)	14.62	40.18	48.51	40.05
Standard Deviation (Unit)	7.77	7.89	0.77	1.08
Standard Error (Unit)	0.16	0.16	0.02	0.02
Area under curve (Unit*sec.)	2102.7	5779.24	6977.14	5760.26
10 MIN HOLOFIBER				
Mean value (Unit)	28.53	83.34	39.28	36.6
Standard Deviation (Unit)	9.34	68.95	2.18	0.93
Standard Error (Unit)	0.3	2.21	0.07	0.03
Area under curve (Unit*sec.)	1724.87	5038.3	2374.32	2212.52
20 MIN HOLOFIBER				
Mean value (Unit)	28.54	82.1	39.04	36.32
Standard Deviation (Unit)	9.1	67.49	2.08	1.13
Standard Error (Unit)	0.28	2.11	0.06	0.04
Area under curve (Unit*sec.)	1815.85	5224.97	2483.45	2310.99
30 MIN HOLOFIBER				
Mean value (Unit)	27.55	83.06	38.51	36.63
Standard Deviation (Unit)	9.97	19.27	0.95	0.75
Standard Error (Unit)	0.18	0.35	0.02	0.01
Area under curve (Unit*sec.)	5284.65	15934.12	7388.58	7027.39
40 MIN HOLOFIBER				
Item	1 PU #1	2 PU #2	3 pO2 #3	4 pO2 #4
Mean value (Unit)	27.13	84.15	34.32	36.2
Standard Deviation (Unit)	2.22	36.99	3.67	1.08
Standard Error (Unit)	0.07	1.13	0.11	0.03
Area under curve (Unit*sec.)	1801.68	5589.37	2278.5	2403.35
50 MIN HOLOFIBER				
Mean value (Unit)	27.7	65.54	42.87	40.44
Standard Deviation (Unit)	2	15.21	0.86	0.5
Standard Error (Unit)	0.06	0.48	0.03	0.02
Area under curve (Unit*sec.)	1729.84	4092.9	2676.46	2524.83
60 MIN HOLOFIBER				
Mean value (Unit)	24.58	60.17	47.49	41.93
Standard Deviation (Unit)	2.96	13.07	1.14	0.57
Standard Error (Unit)	0.09	0.42	0.04	0.02
Area under curve (Unit*sec.)	1510.02	3697.49	2918.27	2576.28
10 MIN PLACEBO				
Mean value (Unit)	24.48	64.62	50.15	51.08
Standard Deviation (Unit)	6.45	15.49	1.36	0.54
Standard Error (Unit)	0.13	0.32	0.03	0.01
Area under curve (Unit*sec.)	3501.99	9244.51	7174.09	7308.01
20 MIN PLACEBO				
Mean value (Unit)	37.31	70.95	47.86	48.42
Standard Deviation (Unit)	6.23	12.9	0.58	0.71
Standard Error (Unit)	0.16	0.33	0.01	0.02

Area under curve (Unit*sec.)	3557.69	6764.93	4564.05	4617.4
30 MIN PLACEBO				
Mean value (Unit)	28.94	71.24	50.17	51.49
Standard Deviation (Unit)	3.82	13.74	0.96	0.6
Standard Error (Unit)	0.12	0.44	0.03	0.02
Area under curve (Unit*sec.)	1720.64	4236.42	2983.25	3061.49
40 MIN PLACEBO				
Mean value (Unit)	21.87	90.2	48.61	50.33
Standard Deviation (Unit)	3.35	38.99	1.45	0.69
Standard Error (Unit)	0.09	0.99	0.04	0.02
Area under curve (Unit*sec.)	2085.7	8600.74	4635.14	4799.81
50 MIN PLACEBO				
Mean value (Unit)	22.24	106.75	45.99	49.16
Standard Deviation (Unit)	16.45	56.96	1.19	0.87
Standard Error (Unit)	0.39	1.34	0.03	0.02
Area under curve (Unit*sec.)	2475.36	11878.13	5116.7	5469.06
60 MIN PLACEBO				
Mean value (Unit)	27.65	79.06	52.92	53.02
Standard Deviation (Unit)	3.82	26.67	1.56	1.19
Standard Error (Unit)	0.09	0.65	0.04	0.03
Area under curve (Unit*sec.)	2850.9	8150.63	5456.89	5466.49

Patient ID:121   placebo -
                                  Holofiber

	TCOM HAND	LASER HAND	TCOM FOOT	LASER FOOT
BASELINE				
Mean value (Unit)	11.2	23.97	25.16	45.37
Standard Deviation (Unit)	0.62	6.12	0.46	0.6
Standard Error (Unit)	0.02	0.21	0.02	0.02
Area under curve (Unit*sec.)	575.41	1231.86	1293.08	2331.88
10 MIN PLACEBO				
Mean value (Unit)	14.15	43.08	8.53	43.96
Standard Deviation (Unit)	1.06	10.11	0.52	0.19
Standard Error (Unit)	0.04	0.35	0.02	0.01
Area under curve (Unit*sec.)	729.86	2222.08	439.98	2267.62
20 MIN PLACEBO				
Mean value (Unit)	15.19	43.84	10.26	43.44
Standard Deviation (Unit)	0.88	11.52	0.37	0.2
Standard Error (Unit)	0.03	0.4	0.01	0.01
Area under curve (Unit*sec.)	776.75	2242.17	524.63	2221.79
30 MIN PLACEBO				
Mean value (Unit)	16.14	43.41	8.78	44.06
Standard Deviation (Unit)	1.5	12.34	0.32	0.48
Standard Error (Unit)	0.05	0.43	0.01	0.02
Area under curve (Unit*sec.)	828.42	2228.4	450.51	2261.66
40 MIN PLACEBO				
Mean value (Unit)	15.29	30.9	12.72	46.69
Standard Deviation (Unit)	1.08	8.39	0.45	0.27
Standard Error (Unit)	0.04	0.29	0.02	0.01
Area under curve (Unit*sec.)	782.91	1582.83	651.3	2390.91
50 MIN PLACEBO				
Mean value (Unit)	14.57	36.58	13.13	45.82
Standard Deviation (Unit)	0.97	8.63	0.41	0.25
Standard Error (Unit)	0.03	0.3	0.01	0.01
Area under curve (Unit*sec.)	746.08	1873.17	672.37	2346.38
60 MIN PLACEBO				
Mean value (Unit)	14.54	35.88	14.19	47.4
Standard Deviation (Unit)	0.89	7.21	0.44	0.24
Standard Error (Unit)	0.03	0.25	0.02	0.01
Area under curve (Unit*sec.)	745.38	1840.17	727.38	2430.56
10 MIN HOLOFIBER				
Mean value (Unit)	16.17	40.79	21.14	50.58
Standard Deviation (Unit)	5.23	9.34	0.19	0.38
Standard Error (Unit)	0.18	0.33	0.01	0.01
Area under curve (Unit*sec.)	825.03	2080.56	1078.75	2581.12
20 MIN HOLOFIBER				
Mean value (Unit)	13.3	39.1	25.39	56.38
Standard Deviation (Unit)	2.09	8.46	0.25	0.25
Standard Error (Unit)	0.07	0.29	0.01	0.01

Area under curve (Unit*sec.)	680.17	2001.13	1298.74	2884
30 MIN HOLOFIBER				
Mean value (Unit)	13.04	39.02	21.29	55.7
Standard Deviation (Unit)	1.34	9.15	0.46	0.37
Standard Error (Unit)	0.05	0.32	0.02	0.01
Area under curve (Unit*sec.)	663.75	1986.12	1083.94	2835.31
40 MIN HOLOFIBER				
Mean value (Unit)	11.87	43.98	24.71	56.22
Standard Deviation (Unit)	0.99	7.03	0.29	0.43
Standard Error (Unit)	0.03	0.24	0.01	0.01
Area under curve (Unit*sec.)	604.74	2241.77	1259.2	2865.29
50 MIN HOL				
Mean value (Unit)	11.76	47.1	26.25	58.05
Standard Deviation (Unit)	0.77	6.1	0.5	0.51
Standard Error (Unit)	0.03	0.21	0.02	0.02
Area under curve (Unit*sec.)	604.95	2423.57	1350.99	2987.11
60 MIN HOLOFIBER				
Mean value (Unit)	13.53	36.17	26.13	60.84
Standard Deviation (Unit)	2.45	10.83	0.24	0.94
Standard Error (Unit)	0.09	0.39	0.01	0.03
Area under curve (Unit*sec.)	631.06	1685.51	1218.38	2836.52

Celliant Bedding Moderates Autoimmune and Inflammatory Responses

Dr. Jasmina Djuretić, Dr. Mirjana Dimitrijević, Dr. Marija Stojanović, Dr. Jelena Kotur Stevuljević, Dr. Michael R Hamblin, Dr. Ana Micov, Dr. Radica Stepanović-Petrović and Dr. Gordana Leposavić

scientific reports

OPEN

Infrared radiation from cage bedding moderates rat inflammatory and autoimmune responses in collagen-induced arthritis

Jasmina Djuretić[1,6], Mirjana Dimitrijević[2,6], Marija Stojanović[1], Jelena Kotur Stevuljević[3], Michael R. Hamblin[4], Ana Micov[5], Radica Stepanović-Petrović[5] & Gordana Leposavić[1✉]

The development of collagen type II (CII)-induced arthritis (CIA), a model of rheumatoid arthritis, in rats housed in cages with bedding composed of Celliant fibres containing ceramic particles, which absorb body heat and re-emit the energy back to the body in the form of infrared radiation (+IRF rats), and those housed in cages with standard wooden shaving bedding (−IRF control rats) was examined. The appearance of the first signs of CIA was postponed, while the disease was milder (judging by the arthritic score, paw volume, and burrowing behaviour) in +IRF compared with −IRF rats. This correlated with a lower magnitude of serum anti-CII IgG antibody levels in +IRF rats, and lower production level of IL-17, the Th17 signature cytokine, in cultures of their paws. This could be partly ascribed to impaired migration of antigen-loaded CD11b + dendritic cells and their positioning within lymph nodes in +IRF rats reflecting diminished lymph node expression of CCL19/CCL21. Additionally, as confirmed in rats with carrageenan-induced paw inflammation (CIPI), the infrared radiation from Celliant fibres, independently from immunomodulatory effects, exerted anti-inflammatory effects (judging by a shift in pro-inflammatory mediator to anti-inflammatory/immunoregulatory mediator ratio towards the latter in paw cultures) and ameliorated burrowing behaviour in CIA rats.

As a result of substantial advances in polymer chemistry, relatively recently, infrared radiation-emitting (IR) fibres (filaments) have been developed. These fibres have a porous core-sheath and groove structure allowing various optically active ceramic micron-sized particles to be incorporated into each fibre[1,2]. One type of these fibres is Celliant (Hologenix, Santa Monica, CA, USA), a polyethylene terephthalate fibre that incorporates micron-sized optically active ceramic particles exhibiting the property of temperature-dependent infrared emission. These fibres have been woven to get high-performance functional textiles[1,2]. When such functional textiles are used as garments, bandages, or bed linen, the heat energy generated by the human body can be transferred by radiation, conduction, convection to the ceramic particles[1–4]. These ceramic particles act as black-body absorbers and re-emit the absorbed energy as infrared radiation back to the body[5]. According to the classification of the International Commission on Illumination (CIE) and the classification provided in ISO 20473 standard (ISO 20473), infrared radiation has three broad categories: near infrared (0.7–1.4 μm and 0.78–3 μm according to CIE and ISO 20473, respectively), mid-infrared (0.4–3 μm and 3–50 μm according to CIE and ISO 20473, respectively) and far infrared (3–100 μm and 50–1000 μm according to CIE and ISO 20473, respectively). Considering the aforementioned data, IR fabrics are suggested to recycle the body's natural energy[5]. At physiological skin temperature, much of the body's emissive radiative power is centered between 7 and 14 μm[6,7]. Generally, infrared radiation penetrates deeply through the layers of the skin to reach the muscles and bones[8]. This radiation moderates

[1]Department of Pathobiology, Faculty of Pharmacy, University of Belgrade, Vojvode Stepe 450, Belgrade, Serbia. [2]Department of Immunology, Institute for Biological Research "Siniša Stanković"-National Institute of Republic Serbia, University of Belgrade, Bulevar despota Stefana 142, Belgrade, Serbia. [3]Department of Biochemistry, Faculty of Pharmacy, University of Belgrade, Vojvode Stepe 450, Belgrade, Serbia. [4]Laser Research Centre, Faculty of Health Science, University of Johannesburg, Doornfontein 2028, South Africa. [5]Department of Pharmacology, Faculty of Pharmacy, University of Belgrade, Vojvode Stepe 450, Belgrade, Serbia. [6]These authors contributed equally: Jasmina Djuretić and Mirjana Dimitrijević. ✉email: gordana.leposavic@pharmacy.bg.ac.rs

inflammation[9,10] and pain[4]. Additionally, it promotes tissue regeneration and wound healing by improving circulation[11,12] and/or acting directly on cells to improve mitochondrial metabolism[13], and thereby a number of cellular functions including energy generation, calcium signaling, and cell growth[14]. Given that infrared radiation is non-invasive and painless, it could be a broadly applicable therapeutic option for moderating inflammation and pain [2,8]. However, when this radiation is delivered from standard electrically-powered sources (such as IR heat lamps and IR saunas), it could cause a prolonged erythemal response due to excessive heating of the skin[2]. Additionally, when the radiation is delivered from these sources, it is difficult to delineate effects related to the increase in the core body temperature (hyperthermia) from the direct biochemical effects on living cells[2]. It is noteworthy that the infrared radiation that does not produce any detectable skin heating effects, such as the infrared radiation emitted by the ceramic particles enriched IR fabrics[2], can also produce biological effects[15,16]. Indeed, IR fabrics that mainly rely on the energy emitted from the body have been found to reduce inflammation and pain[15], so their therapeutic use may be considered. In this context, it should be added that IR fabrics, may be worn for extended periods in the form of clothing or bandages or used as bed linen to attain health benefits[2]. Rheumatoid arthritis (RA) is a chronic inflammatory autoimmune disease primarily affecting the lining of the synovial joints, and causing progressive disability, premature death, and high socioeconomic burdens[17,18]. The clinical manifestations encompass symmetrical joint involvement including arthralgia (joint pain), swelling, redness, and even a limited range of motion[17,18]. Many immune and other cell types and their cytokines play roles in the development of RA[17,18]. The synovial compartment is infiltrated with adaptive immune cells, including both T cells and B cells, and innate immune cells (monocytes and macrophages), which interact between themselves and with fibroblast-like synoviocytes to produce inflammatory mediators[17]. Effector Th17 cells acting together with arthritogenic autoantibodies are suggested to be the major driver of non-resolving joint tissue damage, and therefore prolonged inflammation in RA[17,19]. Monocytes/macrophages massively infiltrating the synovial membranes in RA[20,21], are shown to be central to the joint inflammation[22]. The imbalance between monocyte/macrophages with pro-inflammatory secretory profile and monocyte/macrophages with anti-inflammatory/immunoregulatory secretory profile is suggested to be particularly important for RA development, as a shift towards the former contributes to osteoclastogenesis (i.e. production of osteoclasts, the cells specialized for bone resorption), and thereby to bone loss that ultimately leads to the destruction of the subchondral bone and the degeneration of the overlying articular cartilage [22,23]. On the other hand, a shift towards monocyte/macrophages with anti-inflammatory/immunoregulatory secretory profile has been suggested to contribute to the regression of joint injury and inflammation in RA[24].

While there is currently no long-term cure for RA, the treatment strategy aims to alleviate arthralgia and rapidly achieve a lowering of the disease activity state[17]. The introduction of novel disease-modifying antirheumatic drugs (DMARDs) has dramatically improved the prognosis of RA patients, but a significant proportion of these patients fail to report long-term relief of arthralgia, reflecting the incomplete disease control[17]. In this context, significant efforts have been made to show that is important to put inflammation under control in the early phases of RA development[25]. Additionally, even if treatment with DMARDs does reduce arthralgia, a proportion of RA patients is still dissatisfied with its management and continue to rate the pain relief as one of their top requirements for improved health and quality of life[17]. Considering various side effects (including gastrointestinal disorders, immunosuppression, and humoral disturbances) of analgesics, which are most commonly used in RA, i.e. nonsteroidal anti-inflammatory drugs and corticosteroids, research into new options to control arthritis and arthralgia in RA is of great importance.

The most widely used RA model is rodent collagen type II (CII)-induced arthritis (CIA). This model has gained acceptance since it is reproducible, well defined, and particularly because it has proven useful for the development of new therapies for RA[26]. It has also been recommended to use rats for studying the anti-arthritic effects of various agents, as rats are less variable than mice, their joints are bigger and the inflammatory changes are more reproducible[26].

The present study was primarily undertaken to examine the effects of exposure of rats to IR fibres used as cage bedding (mimicking exposure to IR fabrics used as bed linen) on the development of autoimmune inflammation of joints in the CIA model. The study included female Dark Agouti (DA) rats as compared with male rats, they exhibit a substantially higher incidence of CIA and more severe disease[27–29]. In these rats, joint inflammation and burrowing behaviour were examined. We decided to evaluate burrowing behaviour as it was suggested to be a reliable tool to measure outcomes similar to those measured in the clinical trial evaluating effects of analgesics in chronic pain conditions (viz. spontaneous pain and overall patient healthy status), as it is RA[30]. Additionally, to elucidate the putative mechanisms standing behind the effects of infrared radiation on the development of the inflammation of paw joints in CIA rats, the indicators of ongoing humoral (the serum levels of anti-CII-specific antibodies) and cellular (the production levels of IL-17, Th17 signature cytokine, in inflamed paw cultures from CIA rats) immune responses, and inflammatory response (the production levels of the key pro-inflammatory cytokines, i.e.TNF-α, IL-1β and PGE2 and NO, and anti-inflammatory/immunoregulatory mediators IL-10 and TGF-β in RA, in inflamed paw cultures)[31–36] were examined. The main source of these mediators in RA are suggested to be activated macrophages [31–36] Of note, macrophage activation is shown to be a dynamic process; the same cells may initially take part in proinflammatory and cytotoxic reactions and later participate in the resolution of inflammation and wound healing, so in an inflammatory microenvironment, they are "blend" together critically shaping the outcome of the inflammation[37]. Given that the primary results showed that the exposure to IR fibres as cage bedding moderated development of both humoral and cellular immune responses, and that joint tissue-specific antibodies in RA/CIA may cause arthralgia in the absence of overt inflammation through direct action on sensory neurons[38], we extended our research to study the effects of exposure to IR fibres as cage bedding to the development of carrageenan-induced paw inflammation (CIPI), a model commonly used to assess the production of inflammatory mediators at sites of inflammation, the anti-inflammatory properties of agents such as nonsteroidal anti-inflammatory drugs, and the efficacy of putative analgesic compounds to

reverse cutaneous hypersensitivity[39]. Given that rats from cages with bedding from IR fibres developed paw inflammation of lower magnitude compared with those from cages with standard wood shaving bedding, the effects of rat exposure to IR fibres in a treatment paradigm were examined, as well.

Materials and methods

Animals.   In the present study four-month-old female Dark Agouti (DA) rats from a breeding colony in the Immunology Research Centre "Branislav Janković" (Belgrade, Serbia) were used. Rats were maintained in a fully controlled animal facility with a constant temperature (21–23 °C) and humidity (30–50%), a 12 h/12 h light/dark cycle, and they were provided ad libitum access to water and standard pelleted food. All experiments were performed in accordance with the Directive 2010/63/EU of the European Parliament and of the Council on the Protection of Animals used for Scientific Purposes (revised Directive 86/609/EEC), and were approved by Laboratory Animal Ethical Committee of University of Belgrade—Faculty of Pharmacy (Etička Komisija za oglede životinje, Univerzitet u Beogradu –Farmaceutski fakultet).

Induction and clinical evaluation of CIA.   Rats were immunised intradermally at the base of the tail with 300 μg of bovine CII Sigma-Aldrich Chemie GmbH, Taufkirchen, Germany) emulsified in incomplete Freund's adjuvant (IFA), as previously described[27,28]. The immunisation emulsion was prepared by mixing equal volumes of CII solution (2 mg/mL) in 0.1 M acetic acid and IFA. For immunisation 300 μL of this emulsion was injected per rat. Before the immunisation, animals were anesthetized with an intraperitoneal injection of anesthetic cocktail [50 mg/kg/body weight (BW) of ketamine/5 mg/kg BW xylazine; Ketamidor, Richter Pharma AG, Wels, Austria; Xylased, Bioveta, Ivanovice na Hané, Czech Republic]. Clinical signs of arthritis were evaluated daily from the 7th day post immunisation (d.p.i.) until the 22nd d.p.i., when the clinical severity of the disease reaches the maximum [27,28]. The severity of CIA was graded according to an arbitrary scale taking into account joint edema and erythema of the hind and front paws (one point for each inflamed metacarpophalangeal/metatarsophalangeal or interphalangeal joint, and five points for the inflamed ankle)[40] by two experienced researchers (MD and MS), independently. Thus, each paw could receive the maximum score of 15 points giving the highest arthritic score of 60. Additionally, paw volumes were measured before the immunisation (basal) and on the 22nd d.p.i. Given that pathological changes predominantly occurred in the hind paws of rats, volumes of both hind paws were measured. Of note, these measurements and all subsequent analyses were conducted by two investigators blind to the rat cage bedding.

Induction and clinical evaluation of CIPI.   Paw inflammation was induced by intraplantar injection of 1.5 mg carrageenan (λ-carrageenan, Sigma Aldrich, St.Louis, MO, USA) in 150 μL saline or 150 μL of saline (controls) into the right hind paw starting from the midline near the heel and continuing toward the base of the second or third toe as previously described[39]. The volumes of their right hind paws were measured before injection of carrageenan or saline (basal) and four times afterward at one hour intervals. The temperature of the right hind paws was measured using a digital touch-free thermometer (Microlife AG, Widnau, Switzerland) at the same time points. Of note, these measurements and all subsequent analyses were conducted by two investigators blind to the rat cage bedding.

Experimental design.   For the induction of CIA rats were randomly assigned into two groups (10 rats per group). Five days before immunisation one group of rats was housed in cages with bedding composed of IR Celliant fibres (+IRF rats), while the other group of rats was housed in cages with standard wood shaving bedding (−IRF rats). Celliant is produced using a total of 13 naturally occurring, thermoreactive minerals. These include: titanium dioxide, a photocatalyst that effectively absorbs light, silicon dioxide, which absorbs and reflects energy, and aluminium oxide, which can help increase energy reflectivity. All 13 minerals are ground up into an ultra-fine powder and then mixed with polyethylene terephthalate to create the 'Celliant master batch'. Finally, a liquid polyester resin is added to the master batch and synthesized into a stable fibre. The cage-bedding was constructed from 16 g Celliant (200 g/m²) of 42 mm fibres (thickness less than 10 μ, ceramic loading 1–1.25% by weight) and standard wood shavings (1:10 weight/weight) (Fig. S1). According to the manufacturer, the ceramics absorb the body's heat, transforming it into full-spectrum infrared energy (https://celliant.com/how-it-works) with a broad-peak cantered at a wavelength of 9.3 μm, whereas the power density depends on the proximity of the heat source (living body), but is approximately 0.25 mW/cm², so for each hour, an energy density of about 1 J/cm² is delivered. The standard wood shaving and IR Celliant beddings were changed every second day. The burrowing behaviour test was performed on the 21st d.p.i. Following the test animals were anesthetized with an intraperitoneal injection of ketamine/xylazine anesthetizing cocktail (80 mg/kg BW ketamine/8 mg/kg BW xylazine) and blood was taken by cardiac puncture. Additionally, from euthanized rats were removed lymph nodes, spleens, and hind paws for further analysis.

To examine the effects of rat exposure to IR fibres on CIPI, two sets of experiments (each consisting of two separate experiments) were performed. In the first set of experiments, rats were randomly assigned into three groups (6 rats per group). Two groups were administered with carrageenan, whereas one group (6 rats) was administered with saline (SAL rats). Five days before administration of rat hind paws with carrageenan one group of animals was transferred to cages with Celliant bedding (+IRF rats), while the other groups remained in cages with standard wooden shaving bedding (−IRF rats). In the second set of experiments, rats were randomly assigned into three groups (6 rats per group). Following the administration of right hind paws with carrageenan one group of rats was transferred to cages with Celliant bedding (+IRF rats), one group of rats was administered with 5 mg/kg Diclofenac (Diklofen, Galenika AD, Belgrade, Serbia) per os (DIC rats), whereas one group of rats

remained in cages with standard bedding (−IRF rats). The dose of Diklofen was chosen to correspond to that used in humans[41].

In one experiment from each set of experiments 240 min following the carrageenan/saline administration burrowing test (lasting for 120 min) was started. At the end of this test, rats were euthanized by an intraperitoneal injection of ketamine/xylazine anesthetizing cocktail (80 mg/kg BW ketamine/8 mg/kg BW xylazine), and their right paws were retrieved for culturing. In the second experiment from each set of experiments, right paw volume and mechanical hyperalgesia were examined at one hour intervals over 240 min from the carrageenan/saline administration.

Paw volume measurement. Paw volume was measured using a plethysmometer (Ugo Basile, Gemonio, Lombardy, Italy), as described previously[42]. The average of two consecutive volume measurements for each rat was used for further calculations. The results are expressed as the difference (dV) between post-immunisation or CIPI induction and the basal paw volume according to the following formula[42]:

$$dV = \text{volume of the inflamed paw (mL)} - \text{basal volume of the same paw (mL)}$$

Next, the effect of treatment (Celliant fibres or Diklofen) on dV was calculated according to the following formula

$$dV \text{ reduction (\%)} = \frac{\text{referent group} * \text{ average dV} - \text{dV of each rat from experimental group} **}{\text{referent group average dV}} \times 100$$

* CIA/CIPI rats from cages with standard bedding without any treatment; ** rats exposed to Celliant fibres or administered with Diklofen/saline[42].

Burrowing training and burrowing test. To assess influence of Celliant bedding on spontaneous joint pain, burrowing test, the test developed with the goal of enhancing the translational potential of preclinical findings in pain research[43] was used. This test examines burrowing behaviour, an ancient adaptive behaviour conserved across many rodent species, one in which various laboratory strains of mice and rats spontaneously engage, and, more important, one which is depressed in both mice and rats experiencing inflammatory and neuropathic pain[44,45]. It is noteworthy, that this behaviour is considered to represent a correlate of so-called "activities of daily living" in humans—tasks that are essential to satisfactory quality of life and are often impeded by pain[46]. For burrowing training and experiments, long plastic tubes (32 cm in length and 10 cm in diameter), with the open-end elevated 6 cm from the cage bottom, were filled with 2500 g of gravel (2–6 mm diameter particles). The training was performed four days before housing in cages with Celliant bedding, and both training and burrowing behaviour tests were performed during the dark phase of the daily cycle starting at 6 pm. The training was conducted in social facilitation and individual training formats. For social facilitation, the rats from one cage were placed in a cage-burrow setup for 120 min. To estimate burrowing behaviour, the weight of the burrowed gravel was calculated (weight of gravel left in the tube after completion of burrowing training or test was subtracted from the initial weight of gravel in the tube). Individual training was performed so that a single rat was placed in a cage-burrow setup for 120 min per day for three consecutive days and the average amount of burrowed gravel was determined as explained above. Rats burrowed less than 500 g (four out of 56) were classified as poor burrowers and they were excluded from further experiments as previously suggested[46]. The test was performed before immunisation/inflammation induction (to assess basal burrowing activity) and at a certain point following the immunisation/inflammation induction.

Following the test burrowing activity (BA) of each rat was calculated according to the following formula:

$$BA \text{ (\%)} = \frac{\text{BA after immunisation/inflammation induction (g)}}{\text{Basal BA}} \times 100$$

and then increase in burrowing activity was calculated according to the following formula:

$$BA \text{ increase (\%)} = \frac{\text{BA of each rat from treated group} * - \text{BA of referent group} ** \text{ (average)}}{\text{BA of referent group (average)}} \times 100$$

* rats exposed to Celliant fibres or rats administered with Diklofen; **rats from cages with standard bedding.

Electronic Von Frey test. The mechanical hyperalgesia following carrageenan injection was assessed by measuring paw withdrawal thresholds (P, expressed in g) using an electronic Von Frey anesthesiometer (IITC Life Science, Woodland Hills, CA, United States) as described previously[47,48]. The rats were placed in transparent boxes on the top of a metal grid and allowed to acclimatize for 30 min before testing. A plastic, semi-flexible filament coupled with a force transducer was used to deliver the mechanical stimulus. The tip of the filament was applied perpendicularly to the plantar surface of the right hind paw and the pressure was gradually increased until the rat withdrew its paw (that pressure was recorded automatically on a digital screen). Basal Ps were measured before inflammation induction. Basal and post-induction Ps were measured on the right hind paw. The results are expressed as the difference (dP) between basal and post-induction Ps according to the following formula[47,48]:

$$dP = P \text{ before inflammation induction (g)} - P \text{ after inflammation induction (g)}$$

Treatment reducing dP was recognized as antihyperalgesic treatment. The percentage of the antihyperalgesic activity (AHA) was calculated as previously suggested[48]:

$$\text{AHA (\%)} = \frac{\text{dP of referent group} * \text{(average)} - \text{dP of each rat in treated group} **}{\text{dP of referent group (average)}} \times 100$$

* rats from cages with standard bedding; ** rats exposed to Celliant fibres or rats administered with Diklofen.

Isolation of mononuclear cells. To obtain mononuclear single cell suspensions from lymph nodes (LNs) for the analysis of migratory capacity of innate immune cells in fluorescein isothiocyanate (FITC) painting test and spleens for in vitro analyses of adherence and phagocytic capacity of innate immune cells, LNs draining the site of FITC application (DLNs) and spleens were dissociated using a 70 μm nylon cell strainer (BD Biosciences, Erembodegem, Belgium) and obtained cells were collected in phosphate buffered saline (PBS) supplemented with 2% fetal calf serum (FCS, Gibco, Grand Island, NY, USA) and 0.01% NaN_3 (Sigma-Aldrich Chemie GmbH) (FACS buffer), respectively. The single cell splenocyte suspensions were subjected to NH_4Cl lysis to remove red blood cells and then washed in ice-cold FACS buffer. The mononuclear single cell suspensions from DLNs and spleen of each animal were enumerated using an improved Neubauer hemacytometer and trypan blue dye to exclude non-viable cells and adjusted to 1×10^7 cells/mL.

Flow cytometry analysis (FCA). Briefly, for FCA single cell suspensions from DLNs and spleen were subjected to direct or indirect immunolabeling as previously described in details[49]. After immunolabeling 50,000 cell events per sample were acquired on a FACSCalibur flow cytometer (Becton–Dickinson, Mountain View, CA, USA). Data were analysed using FlowJo software version 7.8. (TreeStar Inc, Ashland, OR, USA). Dead cells and debris were excluded from the analyses by selective gating based on forward scatter (FSC) and side scatter (SSC).

Innate immune cell functional assays. To assess the migration capacity of innate immune cells FITC painting test was used[50]. Briefly, rat left flank was shaved and painted with 300 μL of 5 mg/mL FITC dissolved in equal volumes of acetone and dibutylphthalate. After 24 h, ipsilateral (the side subjected to FITC painting) inguinal and axillary DLNs were extirpated and divided into two portions. From one portion single mononuclear cell suspensions were prepared as described above, whereas another portion was used to examine CCL19 and CCL21 expression using Reverse Transcription-Quantitative Polymerase Chain Reaction. Aliquots of 100 μL of DLN suspensions were processed for indirect immunolabeling with biotin-conjugated anti-CD11b and PerCP-conjugated streptavidin as primary and second step reagent, respectively. Following washing, cells were acquired for analysis using a FACSCalibur flow cytometer as described above. Results were expressed as % of FITC + cells within the CD11b + LN cells.

Innate immunity cells isolated from spleen were tested for cell adherence ability using a modification of previously described method[51]. Aliquots of 500 μL of splenocyte suspension (1×10^6 cells/ml) were placed in an adherence column consisting of a 1 mL syringe packed with 50 mg of nylon fibres to a height of 1.25 cm. After 10 min, the effluent containing the non-adherent cells was drained by gravity. Initial cell suspensions and effluents were processed for immunolabeling with FITC-conjugated anti-CD11b (clone ED8; Serotec, Oxford, UK) antibody. The cells were incubated with saturating concentrations of the fluorochrome-labeled antibody for 30 min, washed with FACS buffer, and subsequently subjected for FCA. Results were expressed as

$$\text{adherence index} = \frac{\% \text{ of total CD11b + cells} - \% \text{ of non-adherent CD11b + cells}}{\% \text{ of total CD11b + cells}} \times 100\%$$

To assess the phagocytic capacity of innate immune cells a previously described method was used[49]. Briefly, 100 μl aliquots of splenocyte suspensions (1×10^6 cells/ml) described, were incubated with sonicated (2 min at room temperature) 1 μm sized yellow-green fluorescent carboxylated polystyrene latex beads (Sigma-Aldrich Chemie GmbH) in complete RPMI-1640 culture medium supplemented with 5% FCS (bead:cell ratio of 50:1) for 1 h at 37 ºC. To arrest phagocytosis, the cells were placed on ice for 5–10 min. Following this step, cells were washed with ice cold PBS and incubated with biotin-conjugated anti-CD11b (BD Biosciences, Mountain View, CA, USA) antibody for 30 min at 4 ºC and then again washed with FACS buffer. In the next step, cells were incubated with PerCP-conjugated streptavidin (BD Biosciences) as the second step reagent for another 30 min, washed with FACS buffer and acquired for analysis using a FACSCalibur flow cytometer. Cells incubated with the latex beads at 4 ºC were used to set up the positive/negative cut-off for Latex + cells in FCA. Results were expressed as % of Latex + cells within the CD11b + cell population.

Reverse transcription-quantitative polymerase chain reaction. Total RNA was extracted by the ABI Prism 6100 Nucleic Acid PrepStation system (Applied Biosystems, Foster City, CA, USA) using the total RNA Chemistry Starter Kit (Applied Biosystems) and DNAse wash solution (Absolute RNA Wash Solution; Applied Biosystems). cDNA was synthesized using the High-Capacity cDNA Reverse Transcription Kit (Applied Biosystems). Triplicate 25-μL RT-qPCR reactions were performed using the TaqMan Gene Expression Master Mix (Applied Biosystems) and premade TaqMan Gene Expression Assays (Applied Biosystems) under the default Applied Biosystems 7500 Real-Time PCR System conditions. All the procedures were described in detail[52]. The following TaqMan Gene Expression Assays were used: CCL19 (Ccl19, Rn01439563_m1), CCL21 (Ccl21, Rn01764651_g1), and β-actin (Actb, Rn00667869_m1). Target mRNA expression was determined using the comparative threshold cycle (dCt) method with β-actin as a reference and SDS v1.4.0. software (Applied

Biosystems). Relative amounts of target mRNAs were shown as 2^{-dCt} values, representing the ratio of target to reference genes, where dCt = Ct target – Ct reference.

Anti-CII antibody ELISA.   Serum samples were obtained by centrifugation of blood at 2000*g* for 15 min at 4 °C. Aliquots of sera were de-complemented (56 °C, 30 min) and stored at -20 °C until analysis. The serum level of CII-specific antibodies was assayed by ELISA in 96-well plates (MaxiSorp, Nunc). The plates were coated (50 μL/well) with 5 μg/mL of CII in 50 mM carbonate buffer (pH 9.6) by overnight adsorption at + 4 °C and then incubated with 2% bovine serum albumin (BSA) in PBS (100 μL/well) for 1 h at room temperature. Serum samples were added to the plate (50 μL/well) in duplicate and incubated overnight at + 4 °C. The biotin-conjugated anti-IgG antibody was added to the plate (50 μL/well) and incubated 1 h at room temperature followed by 1 h incubation with a streptavidin–horseradish peroxidase. At each step, the plate was washed with 0.05% Tween 20/PBS (4 × 200 μL/well). Antigen–antibody interactions were visualized using the extrAvidin-peroxidase/o-phenylenediamine system (Sigma, Steinheim, Germany). Dilutions of sera (1: 100), biotin-conjugated anti-IgG antibody (1: 1000; Biolegend Inc., San Diego, CA, USA) and extrAvidin-peroxidase (1: 3000) were prepared in 2% BSA/PBS. The reaction was stopped by the addition of 1 M H_2SO_4 (50 μL/well) and absorbance was read at 492/620 nm ($A_{492/620}$). The cutoff value was defined according to the $A_{492/620}$ value obtained from "negative control" wells (2% BSA/PBS) plus 3 × Standard Deviation. Samples were considered positive when the $A_{492/620}$ value exceeded the cut off value.

Paw tissue culture.   Inflamed paws collected by incising at the fur line. Paws from CIA rats were weighed, carefully cut into small pieces and cultured in RPMI 1640 medium (Sigma-Aldrich Chemie GmbH) supplemented with 2 mM l-glutamine (Serva, Heidelberg, Germany), 1 mM Na pyruvate (Serva), 100 U/mL penicillin (ICN, Costa Mesa. CA, USA), 100 μg/mL streptomycin (ICN) and 10% fetal bovine serum, at 37 °C, in a humidified air atmosphere of 5% v/v CO2, for 4 h (for PGE_2 assay) or overnight (for analyses of NO and cytokine production levels, and redox status parameters), as previously described[28,29,53]. Following extirpation of carrageenan-inflamed paws, soft paw tissues were carefully removed, weighed, cut into small pieces and cultured as described above.

PGE2, cytokine and NO production.   Paw tissue culture supernatants were examined for inflammatory/pain mediators using the following commercial ELISA kits: IL-17A (BioLegend, San Diego, CA, USA), IL-1β (Thermo Scientific, Pierce Biotechnology, Rockford, IL, USA), PGE2, IL-10 and TGF-β (R&D Systems, Minneapolis, MN, USA), according to the manufacturer's instructions. Standard curve was calculated for each assay with limits of detection for IL-17 = 8 pg/ml, IL-1β = 6.5 pg/mL, TNF-α = 2 pg/mL, IL-10 < 10 pg/mL, TGF-β = 4.6 pg/mL and PGE2 < 39 pg/mL. Cytokines and PGE2 concentrations were normalized to paw weight.

The concentration of nitrite, as the end-product of NO production, was measured in the paw tissue culture supernatants using a method based on the Griess reaction[54]. The nitrite concentration was calculated using a $NaNO_2$ standard curve with a range from 1 to 40 μM and normalized to paw weight.

Assessment of redox status parameters.   The parameters of redox status were measured in sera and inflamed paw cultures. The levels of superoxide anion radical ($O_2^{\bullet-}$) were estimated from the rate of reduction of nitroblue tetrazolium (NBT) as described by Auclair and Voisin[55]. Results were expressed as μM of reduced NBT/min/L.

Total oxidant capacity (TOC) was determined by a modified spectrophotometric method using o-dianisidinine[56,57]. The assay was calibrated with hydrogen peroxide (aqueous solution, concentration range 10–200 mmol/L) and the results were expressed in μmol/L hydrogen peroxide per liter (mmol H_2O_2 eq./L).

Cu/Zn superoxide dismutase (SOD) activity was determined by a modified spectrophotometric method based on the ability of the SOD enzyme to inhibit the autoxidation of epinephrine in an alkaline medium or bicarbonate buffer 0.05 mmol/L pH 10.2[58]. The SOD activity was calculated as the percentage inhibition of epinephrine autooxidation.

The level of SH-groups (SHG) was determined by Ellman's method[59] using 10 mM DTNB (dinitrodithiobenzoic acid) as a reagent. DTNB reacts with aliphatic thiol compounds in the base medium (pH 9.0) and this reaction generates 1 mol of p-nitrophenol anion per mole of thiol. Calibration of the method was achieved using reduced glutathione in the concentration range from 0.1 to 1.0 mM.

Pro-oxidative-antioxidant balance (PAB) was determined by a modified PAB assay using 0.6% 3.3´, 5,5´-tetramethylbenzidine (TMB) in dimethyl sulfoxide (DMSO) as a chromogen[60]. The PAB test measures the concentration of H_2O_2 in an antioxidant environment, as TMB can react at the same time with H_2O_2 (a peroxidase-catalyzed reaction) as well as with reducing substances such as uric acid (chemical, non-catalyzed reaction). The enzymatic reaction leads to the oxidation of TMB to a blue product and its reduction to a non-colored product. The net reaction is the difference between the two opposite oxidative and reductive processes on the same substrate. The reaction is calibrated with a mixture of H_2O_2 and uric acid at different ratios, ranging from 0 to 100%.

All analyses were performed on ILAB 300 Plus analyzer (Instrumentation Laboratory, Milan, Italy) except the PAB, which was measured on the Spectro star Nano ELISA reader (BMG Labtech, Ortenberg, Germany).

Statistical analysis.   All statistical analyses were performed using GraphPad Prism Version 7 (GraphPad Software, Inc., La Jolla, CA, USA) and SigmaPlot 11 (Systat Software Inc., Richmond, CA) softwares. Data are expressed as mean ± SEM. Differences between groups were tested by Student's unpaired t-test, except differences in paw volume, temperature, and hyperalgesia in carrageenan-induced paw inflammation that were ana-
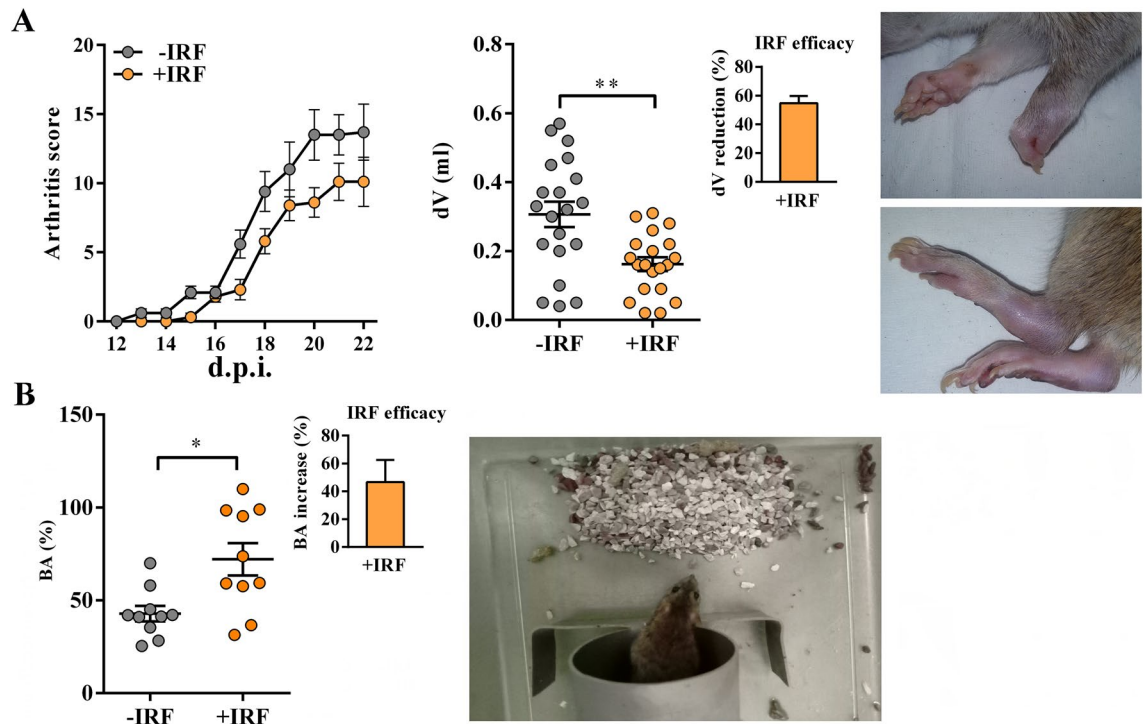
Figure 1. Influence of exposure to IR fibres on daily arthritis score, paw edema and burrowing behaviour in CIA-affected rats. **(A)** Line graph shows daily arthritis score from the 12th–22nd day post-immunisation (d.p.i.) in CIA rats housed in cages with IR-fibre bedding (+IRF rats) or in cages with standard wooden shaving bedding (−IRF rats). Of note, rats were transferred to cages with IR fibre bedding five days before immunization. Scatter plot indicates CIA-induced increase in hind paw volume (dV) in +IRF and −IRF rats. Bar graph shows the dV reduction (%) in +IRF rats relative to −IRF rats (see Material and Methods). Photographs show representative arthritic front and hind paw joints from rat with CIA. (B) Scatter plot indicates the burrowing activity (BA) of each +IRF and −IRF rat expressed as the percentage of the BA before immunisation (basal activity). Bar graph shows the increase in BA (%) in +IRF rats relative to −IRF rats (see Material and Methods). All graphs were created using GraphPad Prism version 7.00 for Windows, GraphPad Software, La Jolla, California, USA (https ://www.graphpad.com). Photograph shows a cage-burrow setup and burrowed gravel. Results are expressed as mean ± SEM. n = 10 rats/group. * p ≤ 0.05 and ** p ≤ 0.01.

lysed by two-way repeated measures ANOVA followed by Bonferroni test for post hoc comparisons. Values of p ≤ 0.05 were considered significant.

Results

Modulatory effects of IR fibres on the autoimmune response, inflammation and burrowing behaviour of CIA-affected rats.

CIA-affected rats from cages with IR fibre bedding exhibit better burrowing performance compared with their counterparts from cages with standard bedding. Generally, the kinetics of CIA development in rats housed in cages with standard bedding followed that described in our previous studies[27,28] (Fig. S2). In rats housed in cages with IR fibre bedding, the onset of the disease was slightly postponed (from the 13th to the 15th d.p.i. compared with −IRF controls (Fig. 1A). The analysis of the differences in the daily arthritic score using repeated measures two-way ANOVA showed a clear tendency to significance (p = 0.051) in the reduction of the clinical severity of the disease in rats exposed to IR fibres compared with their −IRF counterparts (Fig. 1A). Additionally, the cumulative score of the disease (the sum of daily clinical scores of each individual rat during the observation period) was lower (p ≤ 0.05) in +IRF rats (72.1 ± 9.70) when compared with −IRF ones (47.4 ± 5.56). Rats were also examined for the volumes of inflamed hind paws. In all CIA-affected rats the volumes of hind paws were increased (Fig. 1A). This increase was less (p ≤ 0.01) pronounced in +IRF rats compared with their −IRF counterparts, indicating that the exposure to infrared radiation from IR fibre bedding efficiently reduces the inflammation-induced increase in paw volume (Fig. 1A).

Furthermore, rats were examined for burrowing behaviour. Rats housed in cages with IRF bedding showed better (p ≤ 0.05) burrowing performance compared with −IRF rats (Fig. 1B, Fig. S3).

Lower serum levels of serum CII-specific IgG antibodies in CIA-affected rats from cages with IR fibre bedding and diminished IL-17 production in cultures of their hind paws. Given that (i) arthritogenic anti-CII antibodies are essential for the development of CIA[61,62] and (ii) particularly that the arthritogenic antibodies (including those specific for CII) are shown to cause pain even in the absence of overt signs of inflammation[38,63], serum levels of CII-specific IgG antibodies in CIA rats were examined. Their levels were lower (p ≤ 0.01) in sera from rats
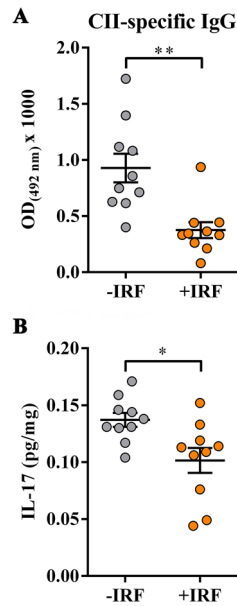
Figure 2. Influence of exposure to IR fibres on the level of CII-specific IgG antibodies in sera and the production of IL-17 in inflamed paws from CIA-affected rats. **(A)** Scatter plot indicates the level of anti-CII IgG antibodies ($OD_{492nm} \times 1000$) in sera from CIA rats housed in cages with IR fibres bedding (+IRF rats) and with standard wooden shaving bedding (−IRF rats). Of note, rats were transferred to cages with IR fibre bedding five days before immunization. **(B)** Scatter plot shows IL-17 production level in the supernatants from hind paw tissue cultures (normalized to the paw weight) from +IRF and −IRF rats. Scatter plots were created using GraphPad Prism version 7.00 for Windows, GraphPad Software, La Jolla, California,USA (https://www.graphpad.com). Results are expressed as mean ± SEM. n = 10 rats/group. * $p \leq 0.05$ and ** $p \leq 0.01$.

transferred to cages with IR fibres bedding (five days before CIPI induction) compared with their counterparts housed into cages with standard bedding (Fig. 2A).

Considering the crucial role of Th17 cells in driving joint damage and consecutive inflammation[64], the production levels of IL-17, Th17 cell signature cytokine, were examined in supernatants of inflamed paw tissue cultures. The production levels of this cytokine were lower ($p \leq 0.05$) in supernatants of inflamed paw tissue cultures from +IRF rats compared with −IRF ones (Fig. 2B).

Impaired migration, but greater phagocytic capacity of innate immune CD11b + cells from CIA-affected rats exposed to IR fibres. Considering the role of innate immune CD11b + cells in the development of joint impairment and inflammation in CIA[65], and the significance of their infiltration into inflamed joint tissue, migratory, adherence and phagocytic capacity of CD11b + cells from CIA rats housed in cages with IR fibre and standard bedding were examined.

The analysis of the frequency of FITC-labelled CD11b + cells in DLNs in the FITC painting test revealed that their frequency was lower ($p \leq 0.01$) in +IRF rats than in −IRF controls, indicating impaired migration capacity of CD11b + cells in rats from cages with IR fibre bedding (Fig. 3A). Considering that CD11b cells express CCR7 receptor so that their trafficking is substantially influenced by CCL19 and CCL21 chemokines[50,66], the expression of mRNAs for these chemokines in DLNs was examined, as well. Indeed, the exposure to IR cage bedding reduced ($p \leq 0.01$) the expression of mRNAs for both chemokines (Fig. 3A).

Next, considered that in the response to tissue inflammation CD11b + cells leave the spleen en masse to accumulate in injured tissue, and participate in the control of inflammation by phagocyting dead cells and necrotic tissue, and secreting anti-inflammatory/immunoregulatory mediators[67,68], the adherence and phagocytic capacity of CD11b + cells from spleen were examined. We failed to show any statistically significant difference between the adherence capacity of CD11b + splenocytes from +IRF rats and those from −IRF rats (Fig. 3B). The analysis of Latex bead phagocytosis showed higher ($p \leq 0.001$) phagocytic capacity of CD11b + splenocytes from rats exposed to IR fibres had compared with those from rats housed in cages with standard bedding (Fig. 4).

Exposure of CIA-affected rats to IR fibres decreases the production levels of pro-inflammatory mediators, but increases production levels of anti-inflammatory/immunoregulatory mediators in cultures of inflamed paws. To elucidate molecular mechanisms underlying less prominent paw swelling and better burrowing performance of +IRF rats, the production of the key pro-inflammatory mediators with algogenic properties (PGE_2, NO, TNF-α and IL-1β)[69,70] and anti-inflammatory/immunoregulatory mediators with analgesic properties (IL-10 and TGF-β)[71,72] was examined in cultures of their hind paws.
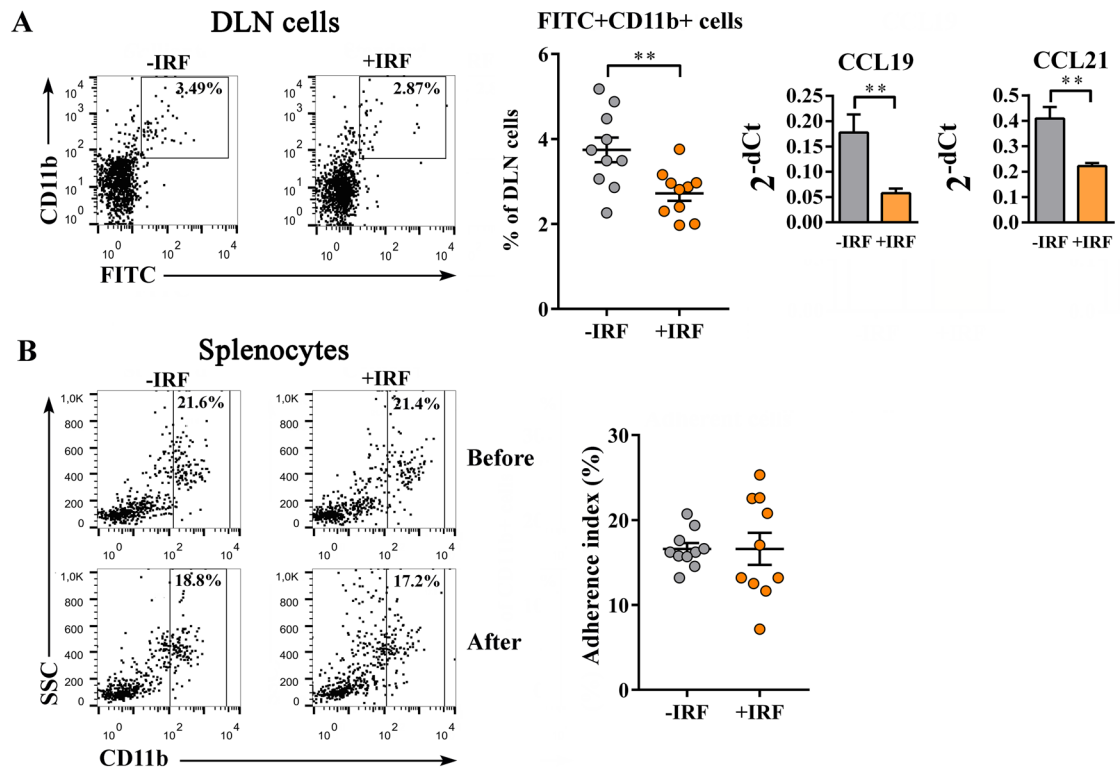
Figure 3. Influence of exposure to IR fibres on the migration and adherence capacity of innate immune CD11b + cells from CIA-affected rats. **(A)** Representative flow cytometry dot plots show the frequency of FITC-stained CD11b + cells in lymph nodes draining the site of FITC application (DLN) in FITC painting test (see Material and Methods) in CIA rats housed in cages with IR fibre bedding (+IRF rats) and with wooden shaving bedding (−IRF rats). Of note, rats were transferred to cages with IR fibre bedding five days before immunization. Bar graphs show the expression of mRNA for CCL19 and CCL21 in DLNs from +IRF and −IRF rats, as determined by RT-qPCR. Results are represented as 2^{-dCt} relative to β-actin. (B) Representative flow cytometry dot plots show CD11b expression on splenocytes from +IRF and −IRF rats before (upper dot plots) and after (lower dot plots) passage through nylon wool in the adherence assay (see Material and Methods). Scatter plot indicates the adherence index, i.e. the percentage of adherent cells of CD11b + cells from spleens of +IRF and −IRF rats (calculated as indicated in Material and Methods). (A, B) Flow cytometry profiles were generated using FlowJo Software for Windows, Version 7.8. FlowJo, LLC, Ashland, Oregon, USA (https://www.flowjo.com). Bar graphs (A) and (B) scatter plot were created using GraphPad Prism version 7.00 for Windows, GraphPad Software, La Jolla California, USA (https://www.graphpad.com). Results are expressed as mean ± SEM. n = 10 rats/group. ** p ≤ 0.01.

The production levels of PGE_2, a pro-inflammatory lipid mediator present at high levels in the synovial fluid of patients suffering from RA[73–75], were lower (p ≤ 0.01) in paw cultures from +IRF rats when compared with those from −IRF rats (Fig. 5).

Additionally, production levels of NO, the pro-inflammatory mediator with an important role in the development of joint injury and inflammation[76], were also lower (p ≤ 0.01) in inflamed paw cultures from rats exposed to IR-emitting fibres than in those from rats housed in cages with standard bedding (Fig. 5).

On the other hand, we failed to show statistically significant differences in the production levels of pro-inflammatory cytokines (TNF-α and IL-1β), which are shown to significantly contribute to the joint injury and inflammation, and consequently arthralgia in RA[77] in inflamed paw tissue cultures from +IRF rats and their −IRF counterparts (Fig. 5).

Considering that the ratio between pro-inflammatory to anti-inflammatory/immunoregulatory mediators (IL-10 and TGF-β) in inflamed tissue is more important for RA severity than their absolute levels[37] and that both IL-10 and TGF-β act as endogenous analgesics[71,72], their production levels in hind paw cultures were explored, as well. The levels of IL-10 and TGF-β were higher (p ≤ 0.05 and p ≤ 0.001, respectively) in cultures of inflamed paws from +IRF rats compared with IRF rats (Fig. 5).

CIA-affected rats from cages with IR fibres exhibit improved serum redox status compared with their counterparts from cages with standard bedding. Given that oxidative stress has been also implicated in the development of inflammation in chronic autoimmune diseases, including RA and its experimental models[78], the redox status was examined in both sera and inflamed joint tissue cultures.
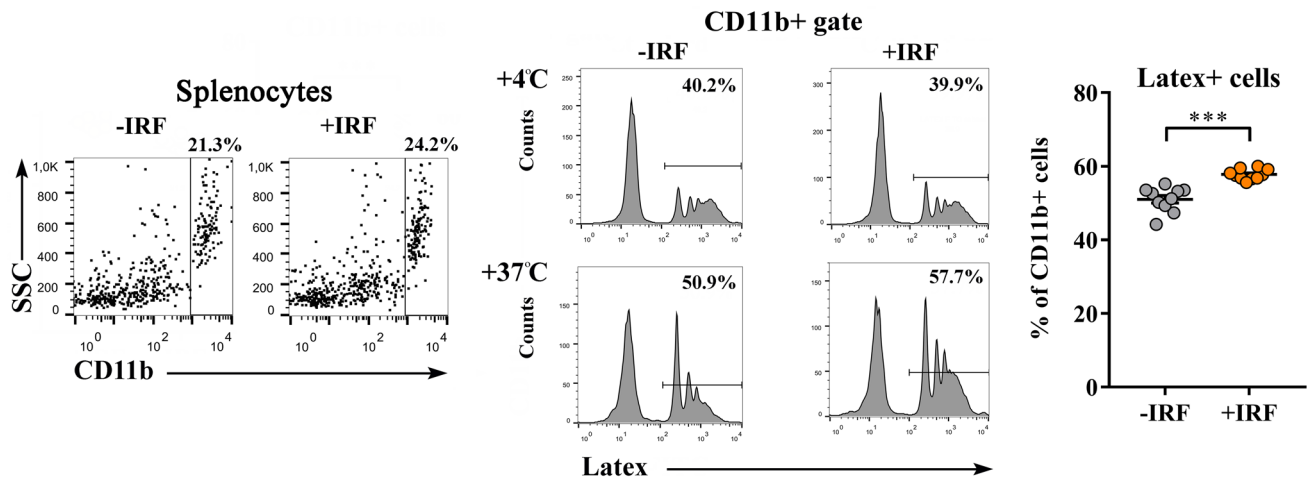
Figure 4. Influence of exposure to IR fibres on the phagocytic capacity of innate immune CD11b + cells from CIA-affected rats. Representative flow cytometry histograms show latex particle phagocytosis at + 4° C and + 37° C by CD11b + cells (gated as shown in representative flow cytometry dot plots generated using FlowJo Software for Windows, Version 7.8. FlowJo, LLC, Ashland, Oregon, USA; https://www.flowjo.com.) from CIA rats housed in cages with IR fibre bedding (+IRF rats) and with standard wooden shaving bedding (–IRF rats). Rats were transferred to cages with IR fibre bedding five days before immunization. Note that a significant difference between the groups was apparent only at 37° C. Scatter plot (created using GraphPad Prism version 7.00 for Windows, GraphPad Software, La Jolla, California, USA; https://www.graphpad.com) indicates the percentage of phagocyting (latex +) cells among CD11b + cells from the spleen of +IRF and –IRF rats (see Material and Methods). Results are expressed as mean ± SEM. n = 10 rats/group. *** $p \leq 0.001$.

The exposure of rats to IR-emitting fibres had no effects on the serum level of $O_2^{\bullet-}$ and SOD activity in CIA rats (Fig. 6). However, lower ($p \leq 0.05$) TOC levels accompanied by higher SHG ($p \leq 0.001$) levels were found in sera from +IRF rats compared with control rats (Fig. 6). Consistently, lower ($p \leq 0.05$) PAB value was detected in sera from +IRF rats compared with –IRF rats (Fig. 6).

We failed to detect any statistically significant differences in the examined redox parameters in the inflamed paw cultures (Fig. S4).

Housing of rats in cages with IF fibre bedding beginning 5 days before carrageenan administration moderates CIPI development.

Given that rats from cages with IR bedding exhibited diminished antibody and Th17 cell responses, and that anti-CII antibodies are found to induce pain behaviour acting directly on sensory neurons, viz. independently of their pro-inflammatory action as pathological antibodies[38], the study was extended to encompass CIPI model, a "classical" model of the non-autoimmune inflammatory response and inflammatory pain.

Exposure to IR fibres reduces temperature, swelling and hyperalgesia of carrageenan-inflamed rat paws and improves burrowing behaviour of CIPI-affected rats. In rats housed in the cages with IR fibre bedding the surface temperature of carrageenan-injected inflamed paw was lower than in rats housed with standard bedding at 120 min ($p \leq 0.05$), 180 min ($p \leq 0.001$) and 240 min ($p \leq 0.05$) after the injection of carrageenan (Fig. 7). The surface temperature of paws injected with saline did not change during the period of observation, and it was lower when compared with the surface temperature of carrageenan-injected paws from −IRF rats at 120 min ($p \leq 0.05$), 180 min ($p \leq 0.001$) and 240 min ($p \leq 0.001$) post-injection (Fig. 7). Besides, it was lower when compared with the surface temperature of carrageenan-injected paws from +IRF rats at 180 min ($p \leq 0.05$) post-injection (Fig. 7). Additionally, in rats housed in the cages with standard bedding, the intraplantar injection of carrageenan elicited paw swelling, as one of the cardinal signs of inflammation (Fig. 8A). In −IRF rats this increase in paw volume was at the maximum at 180 min post injection of carrageenan and remained at this level until the end of observation (Fig. 8A). In the rats transferred to cages with IR fibre bedding five days before the administration of carrageenan, the paw volume gradually increased until 240 min post the injection of carrageenan (Fig. 8A). Control SAL rats exhibited a transient increase in the affected paw volume 60 min after injection of saline, but even at this increase was lower ($p \leq 0.05$) than in carrageenan-injected −IRF rats (Fig. 8A). In rats exposed to IRF as cage bedding, the increase in the volume of the carrageenan-administered paw was lower ($p \leq 0.05$) at 60 min after the injection than in −IRF rats, and it remained lower ($p \leq 0.001$) when examined at later time points (Fig. 8A).

The analysis of burrowing performance showed that carrageenan markedly impaired ($p \leq 0.01$) burrowing activity of both −IRF and +IRF rats compared with SAL control rats (Fig. 8B, Fig. S5). However, this carrageenan-induced decrease in burrowing performance was less ($p \leq 0.05$) prominent in +IRF rats compared with their −IRF counterparts (Fig. 8B, Fig. S5), indicating that infrared radiation from IRF cage bedding ameliorates burrowing performance of CIPI rats (Fig. 8B, Fig. S5).
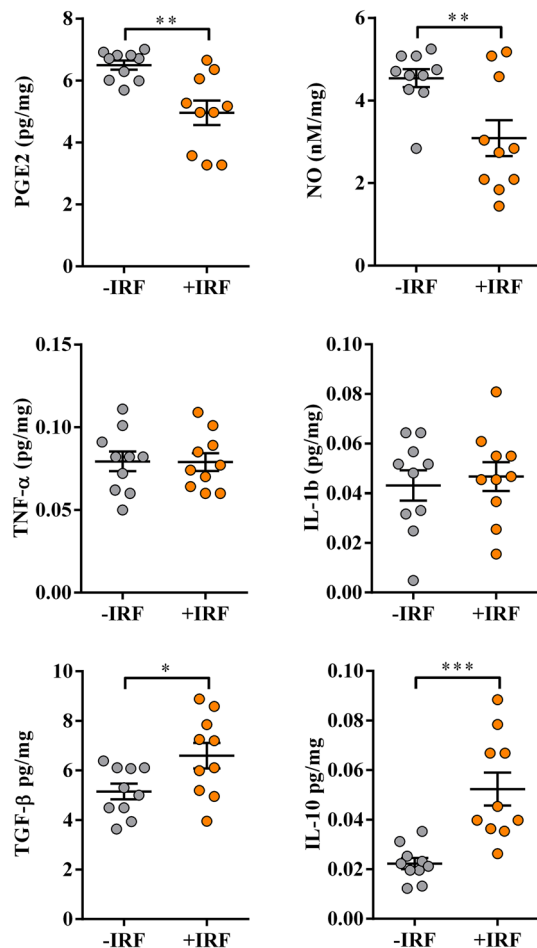
Figure 5. Influence of exposure to IR fibres on the production of PGE$_2$, NO and cytokines by inflamed paws from CIA-affected rats. Scatter plots (created using GraphPad Prism version 7.00 for Windows, GraphPad Software, La Jolla, California, USA; https://www.graphpad.com) show PGE$_2$, NO, TNF-α, IL-1β, TGF-β and IL-10 production levels in the supernatants from 4 h (PGE2) and overnight hind paw tissue cultures (normalized to the paw weight) (see "Material and methods") from CIA rats were housed in cages with IR fibre bedding (+IRF) and their counterparts housed in cages with standard wooden shaving bedding (−IRF rats). Rats were transferred to cages with IR fibre bedding five days before immunization. Hind paws were excised from CIA rats on the 22nd day post immunisation. Results are expressed as mean ± SEM. n = 10 rats/group. * p ≤ 0.05, ** p ≤ 0.01 and *** p ≤ 0.001.

Considering that differently from chronic pain conditions, in acute pain models reliability of tests evaluating spontaneous behaviours or activities of rodents in their home environments, as it is burrowing test, have not been systematically evaluated[79], pain behaviour in CIPI model was also examined using classic mechanical stimulus-evoked von Frey test (Fig. 8C). Using this test we found that, compared with the administration of saline, the administration of carrageenan produced paw hyperalgesia (p ≤ 0.001) at all examined time points (Fig. 8C). Additionally, at all examined time points following carrageenan administration rats housed in cages with IR fibre bedding developed markedly less prominent (p ≤ 0.001) paw hyperalgesia compared with rats housed in cages with standard bedding (Fig. 8C). The analysis of infrared radiation efficacy showed that its anti-hyperalgesic efficacy decreased from 180 min onwards (Fig. 8C).

Exposure to IR fibres diminishes production of proinflammatory mediators, but increases production of anti-inflammatory mediators in cultures of carrageenan-inflamed paws. The production of PGE$_2$ and NO, pro-inflammatory mediators implicated in the development of CIPI[80], was examined in the cultures of carrageenan-inflamed paws. The production levels of PGE$_2$ were reduced (p ≤ 0.05) in cultures of inflamed paw tissues from +IRF rats compared with their −IRF counterparts (Fig. 9). On the other hand, the production levels of NO were comparable in inflamed paw tissue cultures from +IRF rats and −IRF ones (Fig. 9).

Considering the significant role of TNF-α and IL-1β in development CIPI and related allodynia[81,82], their production levels in cultures of inflamed paws were also examined. The production of IL-1β by inflamed paw tissues from +IRF rats was lower (p ≤ 0.01) when compared with its production by inflamed paw tissues from −IRF
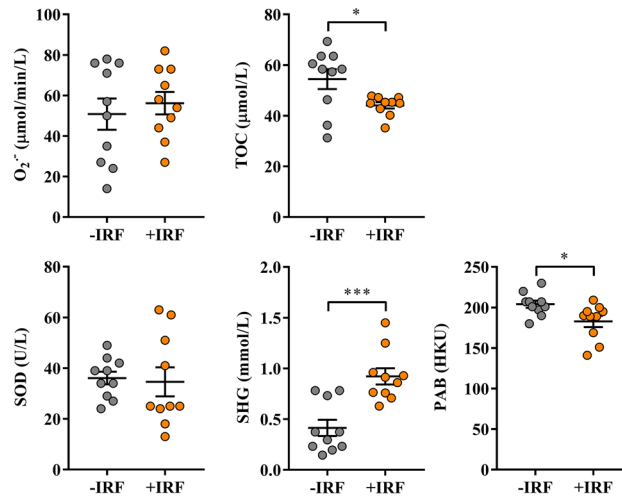
Figure 6. Influence of exposure to IR fibres on the redox status in sera from CIA-affected rats. Scatter plots show pro-oxidant parameters: superoxide anion radical ($O_2 \cdot{}^-$) level and total oxidant capacity (TOC); antioxidant parameters: superoxide dismutase (SOD) activity, and sulfhydryl groups (SHG) level; and pro-oxidant-antioxidant balance (PAB) in sera from CIA rats housed in cages with IR fibre bedding (+IRF) and their counterparts housed in cages with standard wooden shaving bedding (−IRF rats). Of note, rats were transferred to cages with IR fibre bedding five days before immunization. Sera were obtained from CIA rats on the 22nd day post immunisation. All graphs were created using GraphPad Prism version 7.00 for Windows, GraphPad Software, La Jolla, California, USA (https://www.graphpad.com). Results are expressed as mean ± SEM. $n = 10$ rats/group. * $p \leq 0.05$ and *** $p \leq 0.001$.
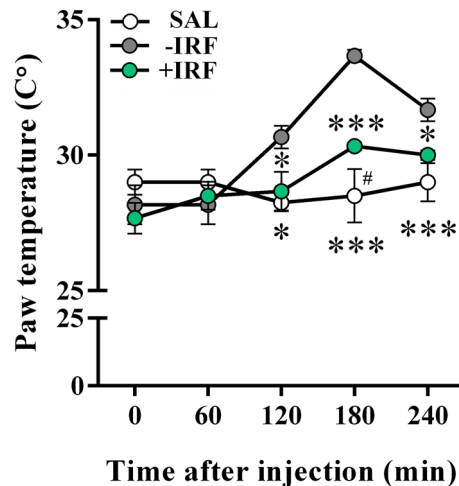
Figure 7. Influence of exposure to IR fibre bedding on the paw temperature of rats with carrageenan-inflamed paws. Rats housed in cages with IR fibre bedding (+IRF) or in cages with standard wooden shaving bedding (−IRF) were injected with carrageenan. Of note, rats were transferred to cages with IR fibre bedding five days before immunization. Rats housed in the cages with standard wooden shaving bedding were injected with saline to serve as an additional control (SAL rats). Line graph (created using GraphPad Prism version 7.00 for Windows, GraphPad Software, La Jolla California USA; https://www.graphpad.com) indicates the surface paw temperature measured before and after carrageenan or saline injection in +IRF, −IRF and SAL rats. Of note, rats were transferred to cages with IR fibre bedding five days before immunization. Results are expressed as mean ± SEM. $n = 6$ rats/group.* $p \leq 0.05$ and *** $p \leq 0.001$ vs −IRF; and $^\#$ $p \leq 0.05$ vs +IRF.

rats (Fig. 9). Differently, the production levels of TNF-α in inflamed paw tissue cultures from +IRF rats did not statistically significantly differ from those in inflamed paw cultures from −IRF rats (Fig. 9).

On the other hand, the production levels of TGF-β were higher ($p \leq 0.01$) in cultures of inflamed paw tissues from +IRF rats compared with those from −IRF ones, whereas those of IL-10 were comparable between these cultures (Fig. 9).
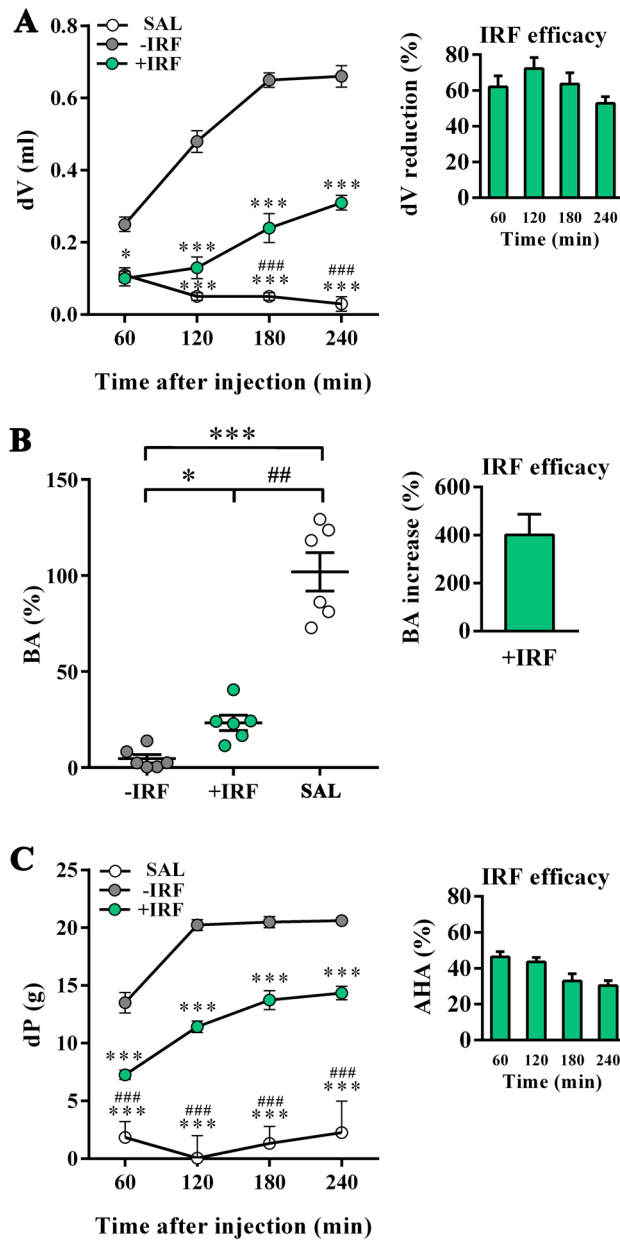
Figure 8. Influence of exposure to IR fibre bedding on paw edema, mechanical stimulus-evoked pain behaviour, and burrowing behaviours of rats with carrageenan-inflamed paws. Right hind paws of rats housed in cages with IR fibre bedding (+IRF) or in cages with standard wooden shaving bedding (−IRF) were injected with carrageenan. Of note, rats were transferred to cages with IR fibre bedding 5 days before immunization. A group of rats with right hind paws injected with saline from cages with standard wooden shaving bedding served as an additional control (SAL rats). **(A)** Line graph indicates the increase in paw volume (dV) in carrageenan or saline administered rats relative to that before the administration. Bar graph shows the dV reduction (%) in +IRF rats relative to −IRF rats (see "Material and methods"). **(B)** Scatter plot indicates the burrowing activity (BA) of each rat following carrageenan or saline administration expressed as the percentage of the BA before the administration (basal activity). Bar graph shows the increase in BA (%) in +IRF rats relative to −IRF rats (see "Material and methods"). **(C)** Line graph indicates the difference between the paw withdrawal thresholds after and before carrageenan or saline injection (dP) in +IRF, −IRF and SAL rats. Bar graph shows the antihyperalgesic activity (AHA) of exposure to IR fibre bedding (+IRF) in rats with carrageenan-induced paw inflammation (see "Material and methods"). All line graphs and scatter plots were created using GraphPad Prism version 7.00 for Windows, GraphPad Software, La Jolla, California, USA (https://www.graphpad.com). Results are expressed as mean ± SEM. n = 6 rats/group.* $p \leq 0.05$ and *** $p \leq 0.001$ vs −IRF; and ## $p \leq 0.01$ ### $p \leq 0.001$ vs +IRF.
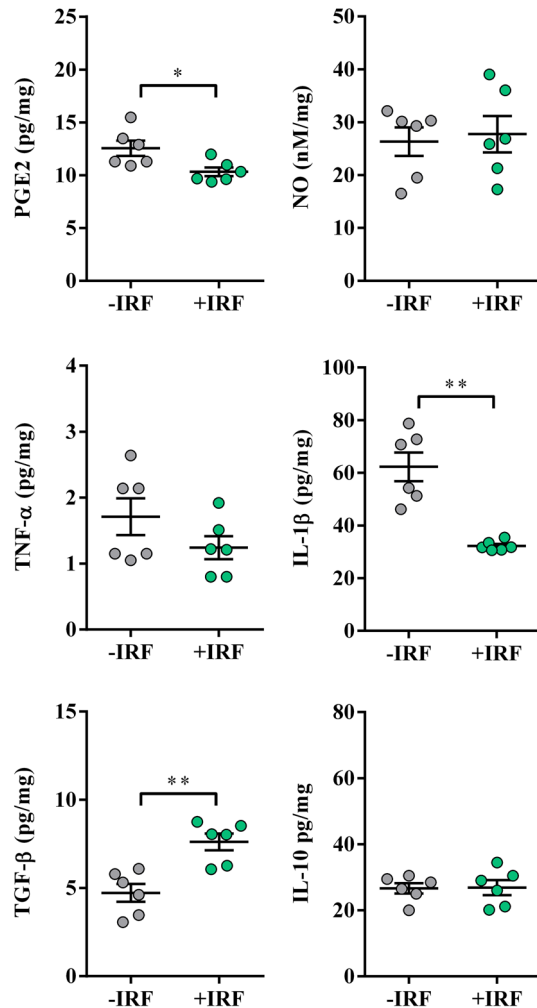
Figure 9. Influence of exposure to IR fibre bedding on the production of PGE2, NO, and cytokines by carrageenan-inflamed paws. Scatter plots (created using GraphPad Prism version 7.00 for Windows, GraphPad Software, La Jolla California USA; https://www.graphpad.com) show PGE2, NO, TNF-α, IL-1β, TGF-β and IL-10 production levels in the supernatants from 4 h (PGE2) or overnight right carrageenan-inflamed hind paw tissue cultures (normalized to the paw weight) (see Material and Methods) from rats housed in cages with IR fibre bedding (+IRF) and with standard wooden shaving bedding (−IRF rats). Results are expressed as mean ± SEM. n = 6 rats/group. * $p \leq 0.05$ and ** $p \leq 0.01$.

Effects of the exposure of rats affected with CIPI to IRF fibres as cage bedding in the treatment paradigm.

Exposure to IR fibres in the treatment paradigm reduces swelling and hyperalgesia of carrageenan-inflamed rat paws and improves burrowing behaviour of CIPI-affected rats. As described above, the carrageenan-injected paws from rats housed in the cages with standard bedding showed the increase in the volume at the examined time points, but at 180 min following the administration of carrageenan, this increase reached a plateau (Fig. 10A). At 120 min following the administration of carrageenan ($p \leq 0.01$) and at all the latter examined time points this increase was less ($p \leq 0.05$) prominent in rats transferred to cages with IR bedding following carrageenan administration compared with their counterparts housed in cages with standard bedding (Fig. 10A). Similarly, Diklofen reduced ($p \leq 0.001$) the increase in the volume of inflamed paw at all time points from 120 min onwards (Fig. 10A). Comparing the effects of IR fibres and Diklofen on the increase in the volume of inflamed paws, we found that this analgesic drug was more ($p \leq 0.001$) efficient than infrared radiation at 120 min ($p \leq 0.001$) and 240 min ($p \leq 0.001$) following carrageenan administration (Fig. 10A).

The exposure of rats to infrared radiation from cage bedding increased ($p \leq 0.001$) their burrowing performance, but to a lower extent ($p \leq 0.05$) than the administration of Diklofen (Fig. 10B, Fig. S6). Accordingly, the subsequent analysis of infrared radiation efficacy showed that this treatment was less ($p \leq 0.01$) efficient in increasing rat burrowing performance than Diklofen administration (Fig. 10B, Fig. S6).

As expected from the previous experiment, carrageenan increased paw hyperalgesia at all examined time points following carrageenan administration (Fig. 10C). The exposure to IR fibres reduced hyperalgesia ($p \leq 0.01$) at 120 min and at all examined time points onward (Fig. 10C). Differently, Diklofen decreased ($p \leq 0.001$) hyperalgesia at all examined time points (Fig. 10C). Compared with Diklofen infrared radiation from the cage bedding

14
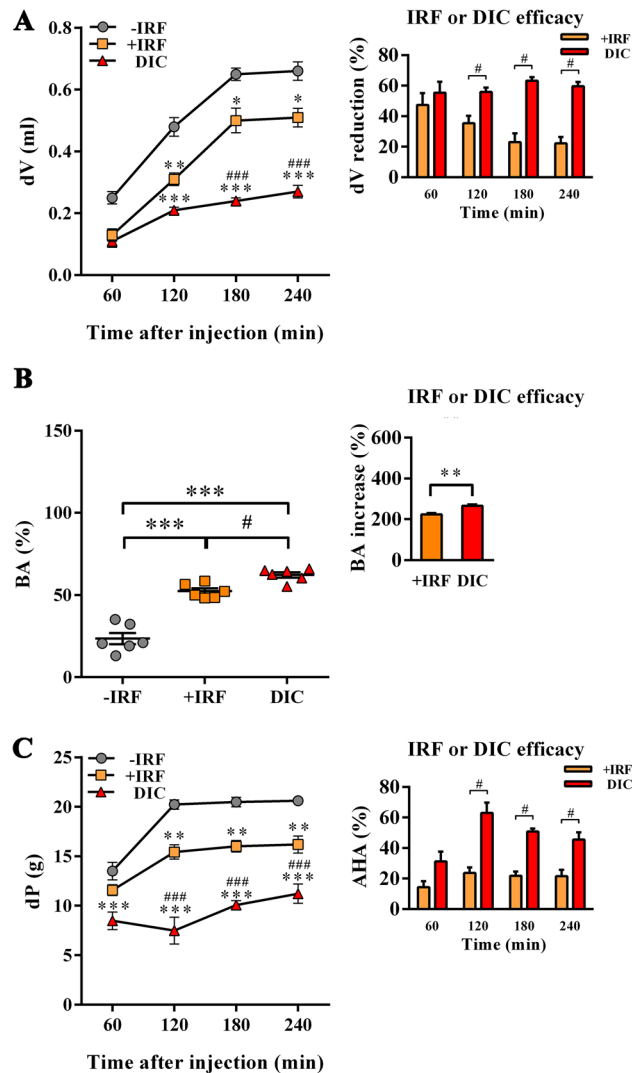
Figure 10. Influence therapeutic exposure to IR fibre on paw edema, mechanical stimulus-evoked pain behaviours and burrowing behaviour of rats with carrageenan-inflamed paws. Immediately after their right hind paws were injected with carrageenan rats were transferred in cages with IR fibre bedding (+IRF rats) or left in standard wooden shaving bedding (−IRF rats). Right paws from a randomly chosen group of −IRF rats were administered with 5 mg/kg Diklofen per os (DIC rats). (**A**) Line graph indicates the increase in paw volume after carrageenan injection (dV) in respect to that before the administration of carrageenan. Bar graph shows the dV reduction (%) in +IRF and DIC rats relative to −IRF rats (see "Material and methods"). (**B**) Scatter plot indicates the burrowing activity (BA) after carrageenan injection in +IRF, −IRF and DIC rats. Bar graph shows the increase in BA (%) in +IRF and DIC rats relative to −IRF rats (see "Material and methods"). (**C**) Line graph indicates the difference between the paw withdrawal thresholds after and before carrageenan injection (dP) in +IRF, −IRF and DIC rats. A bar graph shows the antihyperalgesic activity (AHA) of exposure to IR fibre bedding in a treatment paradigm (+IRF) and Diclofenac treatment (DIC) in rats with carrageenan-induced paw inflammation (see Material and Methods). All line graphs and bar graphs were created using GraphPad Prism version 7.00 for Windows, GraphPad Software, La Jolla, California, USA (https://www.graphpad.com). Results are expressed as mean ± SEM. n = 6 rats/group.* $p \leq 0.05$, ** $p \leq 0.01$ and *** $p \leq 0.001$ vs −IRF; and # $p \leq 0.05$, ## $p \leq 0.01$ and ### $p \leq 0.001$ vs +IRF.

was less efficient ($p \leq 0.001$) in this respect at all examined time points (Fig. 10C). The analysis of Diklofen and infrared fibres anti-hyperalgesic efficacy showed that Diklofen was more efficient at 120 min, 180 min, and 240 min that the exposure to IR fibres, whereas their efficacy was comparable at 60 min (Fig. 10C).

Exposure to IR fibres in treatment paradigm diminishes production of proinflammatory mediators, but increases production of anti-inflammatory mediators in cultures of carrageenan-inflamed paws. In accordance with the effects of IRF on paw inflammation, the production levels of PGE2 and NO were diminished ($p \leq 0.001$) in cultures of inflamed paw tissues from rats exposed to IRF as cage bedding in immediacy following e treatment
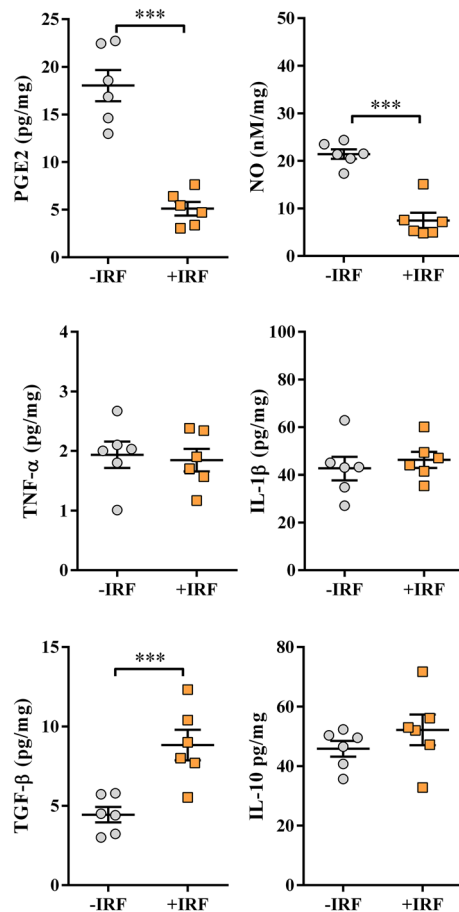
Figure 11. Influence of rat exposure to IR fibre bedding in a treatment paradigm on the production of PGE2, NO, and cytokines by carrageenan-inflamed paws. Scatter plots (created using GraphPad Prism version 7.00 for Windows, GraphPad Software, La Jolla, California, USA; https://www.graphpad.com) show PGE2, NO, TNF-α, IL-1β, TGF-β and IL-10 production levels in the supernatants from 4 h (PGE2) or overnight carrageenan-inflamed paw tissue cultures (normalized to the paw weight) (see Material and Methods) from rats transferred in cages with IR fibre bedding (+IRF rats) or in cages with standard wooden shaving bedding (−IRF rats) immediately following administration of carrageenan. Results are expressed as mean ± SEM. n = 6 rats/group. *** p ≤ 0.001.

carrageenan administration when compared with those from inflamed paw tissues from rats left in cages with standard bedding (Fig. 11).

The production of proinflammatory cytokines (IL-1β and TNF-β) was comparable in inflamed paw tissue cultures from −IRF and +IRF rats (Fig. 11).

On the other hand, the production levels of TGF-β were higher (p ≤ 0.001) in inflamed paw tissue cultures from +IRF rats compared with −IRF rats, whereas IL-10 production levels were comparable in inflamed paw tissue cultures from these two groups of rats (Fig. 11).

Discussion

The study showed clearly effects of IR cage bedding constructed from Celliant fibre on the burrowing performance (reflecting a global pain score) in CIA rat model. Generally, mechanisms underlying joint pain in CIA involve direct action of inflammatory mediators and/or CII-specific antibodies on nociceptors, specialized primary afferent sensory neurons in the pain pathway[38,83]. Our results, for the first time to the best of our knowledge, showed that infrared radiation may diminish the generation of (auto)antigen-specific potentially harmful IgG antibodies. By using modified anti-CII antibodies and transgenic or chimeric mice it was established that the interaction of these antibodies with the IgG receptor (FcγRI) on sensory neurons[84] is important for their pronociceptive properties[38]. These findings are suggested to be of translational value[38]. In favor of the inflammation-independent pronociceptive properties of CII-specific antibodies, are data indicating that: (i) joint pain precedes the appearance of visible signs of arthritis in both RA and CIA, and (ii) depending on the levels of joint tissue-specific antibodies, the perception of pain may differ between individuals with otherwise similar severity of joint inflammation[38]. In keeping with these data, our study showed that rats housed in cages with IR bedding exhibited less prominent burrowing deficit although clinical arthritis score of the disease was

only slightly, but not statistically significantly, lower compared with those housed in cages with standard bedding. However, given that CII-specific antibodies form immune complexes that bind to joint cartilage leading to attraction of inflammatory cells (a key step in the development of arthritis)[85], their contribution to burrowing deficit via promotion of tissue damage and inflammation could not be ruled out. Indeed, our results showed the increase in the average volume of the paws (inflammatory parameter which is not included in the arthritic score) was lower from +IRF rats compared with their −IRF counterparts. This suggested the beneficial effect of infrared radiation on paw swelling. Consequently, the less pronounced compression of edematous fluid on nociceptors may be expected. This finding most likely did not solely reflect the effect of infrared radiation on the degree of CII-specific antibody-mediated tissue injury, but possibly also its influence on the paw infiltration with monocytes/macrophages, as suggested by analysis of CD11b + cell migration in the painting test. To the best of our knowledge, there is no data on the influence of infrared radiation on monocyte/macrophage migration. However, there is data indicating that short exposure to near-infrared laser light may influence the migration of migratory dendritic cells[86]. Thus, it may be speculated that the rat exposure to infrared radiation from IR bedding impaired CD11 + dendritic cell migration into DLN. This could affect follicular helper T cell priming and consequently their capacity to provide help to the cognate germinal center B cells to differentiate into antibody-producing plasma cells[88]. To corroborate this assumption, our results showed that the exposure to IR fibres down-regulated the expression of CCL19 and CCL21, the key chemokines governing not only dendritic cell migration, but also their positioning within DLN, which is crucial for their interactions with T cells and productive T cell response[87,88]. Additionally, in favor of our assumption could be also added that the production of IL-17, Th17 signature cytokine, was diminished in inflamed paw cultures from +IRF rats compared with their −IRF counterparts. Furthermore, considering that the development of autoimmune response-induced damage and consequently inflammation critically depends on the magnitude of the autoimmune response in LN draining the site of immunisation[89], the delayed appearance of the first signs of inflammation in +IRF rats compared with their −IRF counterparts is also consistent with the negative influence of infrared radiation from IR cage bedding on the development of humoral and cellular autoimmune response in this rat CIA model. To corroborate different effects of the infrared radiation on dendritic cell and monocyte/macrophage migration are data indicating that their migration is influenced by many factors[90], and that all of them are not equally important for these two types of innate immunity cells[66].

To further assess mechanisms underlying the development of autoimmune inflammation and inflammatory pain in CIA, the production levels of inflammatory mediators in inflamed paw culture supernatants (mimicking their content in "inflammatory soup") were examined. The results showed that the infrared radiation-induced changes in the production of inflammatory mediators were the mediator specific. Namely, the decrease in the levels of proinflammatory mediators (PGE_2 and NO) was followed by the increase in the levels of anti-inflammatory/immunoregulatory mediators (IL-10 and TGF-β), suggesting that infrared radiation did not affect only autoimmune response, but also inflammatory response. Considering the central role of monocytes/macrophages in inflammation in RA/CIA[22], the shift in the inflammatory mediator profile in supernatants from inflamed CIA rat paws could be related to the enhanced phagocytic capacity of CD11b + cells from +IRF rats compared with their −IRF counterparts. Namely, the phagocytosis of apoptotic cells has been shown to change monocytes/macrophages secretory profile from pro-inflammatory into anti-inflammatory/immunoregulatory profile[91]. Several lines of findings taken conjointly support our results. Firstly, far infrared radiation was shown to augment phagocytosis[92]. Secondly, even short-term exposure of mice affected by chemically induced peritonitis to far infrared radiation may decrease the production of pro-inflammatory mediators by peritoneal macrophages[9]. Thirdly, endothelial cell exposure to far infrared radiation in vitro enhanced the expression of heme oxygenase-1[10], the enzyme promoting anti-inflammatory response of monocytes/macrophages[93–95]. In keeping with our findings suggesting anti-inflammatory (independent on immunomodulatory) action of infrared radiation from cage bedding are data indicating that far infrared radiation from bioceramics may produce an anti-inflammatory effect on lipopolysaccharide-induced knee joint arthritis in rabbits[96]. Moreover, it should be pointed that the reduced NO production in inflamed tissues from +IRF rats could contribute to the less prominent inflammatory response in +IRF rats through lessening NO-mediated breakdown of cartilage tissue[97,98]. To add additional weight to our finding are data indicating that the exposure to far infrared radiation may negatively affect NO synthesis in inflamed tissue[9].

To further evaluate the anti-inflammatory properties of infrared radiation, we investigated the development of CIPI in rats transferred to cages with bedding constructed from IR fibres five days before carrageenan administration. We found that paw inflammation (judging by the increase in paw volume, and paw pain) was markedly less prominent in these rats compared with their counterparts from cages with standard bedding. The analysis of inflammatory mediator production in carrageenan-inflamed paw cultures showed that the exposure to infrared radiation led to the shift in inflammatory mediator profile towards a more anti-inflammatory/immunomodulatory phenotype, as the production levels of PGE_2 and IL-1β decreased, whereas that of TGF-β increased. This finding may indicate that the effects of infrared radiation from IR ceramic particles incorporated into fibres on inflammatory mediator production depend on the type of inflammation and/or duration of the exposure period. It should be underscored that the exposure of rats to IR fibres immediately after carrageenan administration (treatment paradigm) also reduced the paw edema and exerted a beneficial effect on both mechanical-stimulus evoked pain (as shown by von Frey test) and burrowing performance. These effects of infrared radiation were less prominent than those induced by Diklofen. However, given that nonsteroidal anti-inflammatory drugs, including diclofenac, cannot entirely control severe joint pain in RA and that these drugs have (particularly at higher doses) many side-effects, it is highly likely that a combination of the exposure of inflamed joints to IR emitting material and usage of non-steroidal inflammatory drugs could (i) be more efficient in the control of this RA symptom than usage of nonsteroidal anti-inflammatory drugs alone and (ii) allow usage of these drugs at lower doses to achieve the optimal therapeutic effect. According to our literature search, the effects of

infrared radiation on inflammation/pain have not been compared in other studies. The analysis of inflammatory mediator production in carrageenan-inflamed paw cultures showed that the exposure to IR fibres in the treatment paradigm also decreased the production of proinflammatory mediators (PGE_2 and NO), but increased the production of TGF-β. Thus, it may be speculated that effects of infrared radiation from Celliant fibres on inflammatory mediator production depends on the duration of exposure to these fibres, although the influence of the temporal relationship between the treatment initiation and inflammatory stimulus application could not be completely excluded.

Furthermore, it should be pointed out that infrared radiation could influence the pain behaviour of CIA and CIPI rats, not only by reducing the intensity of inflammation and consequently the degree of tissue edema, but also by modulating the secretion of inflammatory mediators, which modulate the peripheral and central nervous sensitization and thereby nociception. The reduced level of PGE_2, a classic lipid inflammatory mediator shown to exert algogenic effects by increasing peripheral and central nervous sensitization[83], in paw cultures from +IRF rats could be associated with inhibitory effects of far infrared radiation from ceramic material on cyclooxygenase-2 expression and PGE_2 synthesis by cultured macrophages and/or chondrocyte cell lines[99]. It should be pointed out that PGE_2 may also exert pro-nociceptive effects indirectly, by promoting the differentiation of Th cells producing IL-17[100]. Thus, the reduced production of IL-17 in paw cultures from CIA rats seems to be consistent with the reduced PGE_2 production. It should be added that IL-17 does not have only an essential role in the development of joint inflammation and thereby in the inflammatory pain in CIA-affected rats[28], but also participate in the development of joint pain through sensitization of sensory neurons[101]. Additionally, in rats suffering from CIPI, the reduced production of IL-1β may contribute to the moderating effects of IR fibres on inflammatory pain. In favor of this assumption are findings indicating that exposure to infrared radiation from a pad impregnated with IR ceramic placed on the bottom of the housing unit decreases IL-1β production in skin tissue from paws administered with complete Freund's adjuvant to induce inflammation[102]. Furthermore, beneficial effects of infrared radiation from cage bedding on rat pain behaviour in both CIA and CIPI models may reflect the enhanced production of IL-10 and/or TGF-β in inflamed tissue, as they are shown to moderate peripheral and central sensory nerve sensitization, and thereby nociception[103–106]. To support this notion are data indicating that the exposure to far infrared radiation from ceramic materials diminishes IL-10 production from complete Freund's adjuvant-inflamed mice paws[102]. In favor of the contribution of diminished production of TGF-β in inflamed tissues to the moderating effect of infrared radiation from cage bedding on inflammatory pain in CIA and CIPI models are literature reports indicating that: (i) TGF-β family members act as modulators of acute and chronic pain perception through the transcriptional regulation of genes encoding endogenous opioids[106], and (ii) the anti-hyperalgesic effects of IR ceramics involve the opioid system[107].

Finally, it should be pointed that CIA is associated with adverse changes in the blood redox state reflecting not only joint cartilage destruction, but also the development of inflammatory changes in other tissues or organs[108]. Thus, the increased burrowing capacity, reflecting reduced global pain score and consequently better animal welfare[46] in +IRF rats compared with their −IRF counterparts was consistent with the improved redox status in their blood, as indicated by PAB. This finding was corroborated by previous studies indicating the beneficial effects of IR ceramics on the systemic levels of oxidative stress biomarkers[109].

In conclusion, our study (i) showed that the exposure of rats to infrared radiation from IR cage-bedding moderates the development of autoimmune joint inflammation, and consequently has beneficial effects on global spontaneous pain score and welfare and (ii) pointed to rather complex immunomodulatory and anti-inflammatory mechanisms underlying this phenomenon. While further translational studies are warranted, our findings support the use of infrared emitting bed linen, bandages, or garments as adjuvant non-pharmacological treatments for RA patients, and possibly for those suffering from other inflammatory antibody-mediated autoimmune diseases. Additionally, the study showed that the exposure to such infrared radiation may have also beneficial effect on the development of sterile inflammation and the inflammatory pain, as well as a therapeutic effect when a sterile inflammation is induced; the findings that also may have significant translatory value.

References

1. Fei, B. High-performance fibers for textiles. in *Engineering of High-Performance Textiles*, 27–58, https://doi.org/10.1016/b978-0-08-101273-4.00002-0 (2018).
2. Vatansever, F. & Hamblin, M. R. Far infrared radiation (FIR): Its biological effects and medical applications. *Photon. Lasers Med.* **4**, 255–266. https://doi.org/10.1515/plm-2012-0034 (2012).
3. Pooley, M. A., Anderson, D. M., Beckham, H. W. & Brennan, J. F. Engineered emissivity of textile fabrics by the inclusion of ceramic particles. *Opt. Express* **24**, 10556–10564. https://doi.org/10.1364/OE.24.010556 (2016).
4. York, R. M. & Gordon, I. L. Effect of optically modified polyethylene terephthalate fiber socks on chronic foot pain. *BMC Complement. Altern. Med.* **9**, 10. https://doi.org/10.1186/1472-6882-9-10 (2009).
5. Conrado, L. A. & Munin, E. Reduction in body measurements after use of a garment made with synthetic fibers embedded with ceramic nanoparticles. *J. Cosmet. Dermatol.* **10**(1), 30–35. https://doi.org/10.1111/j.1473-2165.2010.00537.x (2011).
6. Hardy, J. D. & DuBois, E. F. Regulation of heat loss from the human body. *Proc. Natl. Acad. Sci.* **23**(12), 624–631 (1937).
7. Winslow, C. E. A., Gagge, A. P. & Harrison, L. P. The influence of air movement upon heat losses from the clothed human body. *Am. J. Physiol.* **127**(3), 508–515 (1939).
8. Mero, A., Tornberg, J., Mäntykoski, M. & Puurtinen, R. Effects of far-infrared sauna bathing on recovery from strength and endurance training sessions in men. *SpringerPlus* **4**, 321. https://doi.org/10.1186/s40064-015-1093-5 (2015).
9. Chang, Y. The effect of far infrared radiation therapy on inflammation regulation in lipopolysaccharide-induced peritonitis in mice. *SAGE Open Med.* **6**, 2050312118798941. https://doi.org/10.1177/2050312118798941 (2018).

10. Lin, C. C. *et al.* Far infrared therapy inhibits vascular endothelial inflammation via the induction of heme oxygenase-1. *Arterioscler. Thromb. Vasc. Biol.* **28**, 739–745. https://doi.org/10.1161/ATVBAHA.107.160085 (2008).

11. Toyokawa, H. *et al.* Promotive effects of far-infrared ray on full-thickness skin wound healing in rats. *Exp. Biol. Med.* **228**, 724–729, https://doi.org/10.1177/153537020322800612 (2003).

12. Lin, Y. H. & Li, T. S. The application of far-infrared in the treatment of wound healing a short evidence-based analysis. *Evid. Based Complem. Altern. Med.* **22**(1), 186–188. https://doi.org/10.1177/2156587215623436 (2017).

13. de Freitas, L. F. & Hamblin, M. R. Proposed mechanisms of photobiomodulation or low-level light therapy. *IEEE J. Sel. Top Quantum Electron.* **22**, 7000417 https://doi.org/10.1109/JSTQE.2016.2561201 (2016).

14. Osellame, L. D., Blacker, T. S. & Duchen, M. R. Cellular and molecular mechanisms of mitochondrial function. *Best Pract. Res. Clin. Endocrinol. Metab.* **26**, 711–723 (2012).

15. 15Francisco José Cidral-Filho, N. D. & Martins, D. F. Neurobiological mechanisms and perspectives on far-infrared emitting ceramic materials for pain. *Relief. J. Yoga Phys. Ther.* **4**, 159, https://doi.org/10.4172/2157-7595.1000159 (2014).

16. Hsu, Y. H. *et al.* Far-infrared therapy induces the nuclear translocation of PLZF which inhibits VEGF-induced proliferation in human umbilical vein endothelial cells. *PLoS ONE* **7**, e30674. https://doi.org/10.1371/journal.pone.0030674 (2012).

17. Guo, Q. *et al.* Rheumatoid arthritis: Pathological mechanisms and modern pharmacologic therapies. *Bone Res.* **6**, 15. https://doi.org/10.1038/s41413-018-0016-9 (2018).

18. Lee, D. M. & Weinblatt, M. E. Rheumatoid arthritis. *Lancet* **358**, 903–911. https://doi.org/10.1016/S0140-6736(01)06075-5 (2001).

19. Kotake, S., Yago, T., Kobashigawa, T. & Nanke, Y. The plasticity of Th17 cells in the pathogenesis of rheumatoid arthritis. *J. Clin. Med.* **6**(7), 67. https://doi.org/10.3390/jcm6070067 (2017).

20. Burmester, G. R., Dimitriu-Bona, A., Waters, S. J. & Winchester, R. J. Identification of three major synovial lining cell populations by monoclonal antibodies directed to Ia antigens and antigens associated with monocytes/macrophages and fibroblasts. *Scand. J. Immunol.* **17**, 69–82. https://doi.org/10.1111/j.1365-3083.1983.tb00767.x (1983).

21. Kinne, R. W., Stuhlmuller, B. & Burmester, G. R. Cells of the synovium in rheumatoid arthritis. Macrophages. *Arthritis Res. Ther.* **9**, 224. https://doi.org/10.1186/ar2333 (2007).

22. Quero, L., Hanser, E., Manigold, T., Tiaden, A. N. & Kyburz, D. TLR2 stimulation impairs anti-inflammatory activity of M2-like macrophages, generating a chimeric M1/M2 phenotype. *Arthritis Res. Ther.* **19**, 245. https://doi.org/10.1186/s13075-017-1447-1 (2017).

23. Takayanagi, H. Osteoimmunology: Shared mechanisms and crosstalk between the immune and bone systems. *Nat. Rev. Immunol.* **7**, 292–304. https://doi.org/10.1038/nri2062 (2007).

24. Davignon, J. L. *et al.* Targeting monocytes/macrophages in the treatment of rheumatoid arthritis. *Rheumatology* **52**, 590–598. https://doi.org/10.1093/rheumatology/kes304 (2013).

25. Zhang, P., Han, D., Tang, T., Zhang, X. & Dai, K. Inhibition of the development of collagen-induced arthritis in Wistar rats through vagus nerve suspension: A 3-month observation. *Inflamm. Res.* **57**, 322–328. https://doi.org/10.1007/s00011-008-8070-12008 (2008).

26. Bolon, B. *et al.* Rodent preclinical models for developing novel antiarthritic molecules: Comparative biology and preferred methods for evaluating efficacy. *J. Biomed. Biotechnol.* **2011**, 569068. https://doi.org/10.1155/2011/569068 (2011).

27. Dimitrijević, M. *et al.* Collagen-induced arthritis in Dark Agouti rats as a model for study of immunological sexual dimorphisms in the human disease. *Exp. Mol. Pathol.* **105**, 10–22. https://doi.org/10.1016/j.yexmp.2018.05.007 (2018).

28. Dimitrijević, M. *et al.* Sexual dimorphism in Th17/Treg axis in lymph nodes draining inflamed joints in rats with collagen-induced arthritis. *Brain Behav. Immun.* **76**, 198–214. https://doi.org/10.1016/j.bbi.2018.11.311 (2019).

29. Dimitrijević, M. *et al.* Sex differences in Tfh cell help to B cells contribute to sexual dimorphism in severity of rat collagen-induced arthritis. *Sci Rep* **10**, 1214. https://doi.org/10.1038/s41598-020-58127-y (2020).

30. Wodarski, R. *et al.* Cross-centre replication of suppressed burrowing behaviour as an ethologically relevant pain outcome measure in the rat: A prospective multicentre study. *Pain* **157**, 2350–2365. https://doi.org/10.1097/j.pain.0000000000000657 (2016).

31. van de Loo, A. A. & van den Berg, W. B. Effects of murine recombinant interleukin 1 on synovial joints in mice: measurement of patellar cartilage metabolism and joint inflammation. *Ann. Rheum. Dis.* **49**(4), 238–45,https://doi.org/10.1136/ard.49.4.238 (1990).

32. Henderson, B. & Pettipher, E. R. Arthritogenic actions of recombinant IL-1 and tumour necrosis factor alpha in the rabbit: Evidence for synergistic interactions between cytokines in vivo. *Clin. Exp. Immunol.* **75**(2), 306–310 (1989).

33. Katsikis, P. D., Chu, C. Q., Brennan, F. M., Maini, R. N. & Feldmann, M. Immunoregulatory role of interleukin-10 in rheumatoid arthritis. *J. Exp. Med.* **179**, 1517–1527. https://doi.org/10.1084/jem.179.5.1517 (1994).

34. Cush, J. J. *et al.* Elevated interleukin-10 levels in patient with rheumatoid arthritis. *Arthritis Rheum.* **38**, 96–104. https://doi.org/10.1002/art.1780380115 (1995).

35. Cohen, S. B. A. *et al.* High level of interleukin-10 production by the activated T cell population within the rheumatoid synovial membrane. *Arthritis Rheum.* **38**, 946–952. https://doi.org/10.1002/art.1780380710 (1995).

36. Marinova-Mutafchieva, L., Gabay, C., Funa, K. & Williams, R. O. Remission of collagen-induced arthritis is associated with high levels of transforming growth factor-β expression in the joint. *Clin. Exp. Immunol.* **146**(2), 287–293. https://doi.org/10.1111/j.1365-2249.2006.03204.x (2006).

37. Laskin, D. L., Sunil, V. R., Gardner, C. R. & Laskin, J. D. Macrophages and tissue injury: Agents of defense or destruction?. *Annu. Rev. Pharmacol. Toxicol.* **51**, 267–288. https://doi.org/10.1146/annurev.pharmtox.010909.105812 (2011).

38. Bersellini Farinotti, A. *et al.* Cartilage-binding antibodies induce pain through immune complex-mediated activation of neurons. *J. Exp. Med.* **216**, 1904–1924, https://doi.org/10.1084/jem.20181657 (2019).

39. Fehrenbacher, J. C., Vasko, M. R. & Duarte, D. B. Models of inflammation: Carrageenan- or complete Freund's adjuvant-induced edema and hypersensitivity in the rat. *Curr. Protoc. Pharmacol.* **56**, 5.4.1–5.4.4., https://doi.org/10.1002/0471141755.ph0504s56 (2012).

40. Hou, W. *et al.* A systematic comparison between collagen-induced arthritis and pristane-induced arthritis in Dark Agouti rats. *Clin. Exp. Rheumatol.* **28**, 532–538 (2010).

41. Reagan-Shaw, S., Nihal, M. & Ahmad, N. Dose translation from animal to human studies revisited. *FASEB J.* **22**(3), 659–661. https://doi.org/10.1096/fj.07-9574LSF (2008).

42. Stepanović-Petrović, R. M., Micov, A. M., Tomić, M. A. & Ugrešić, N. D. The local peripheral antihyperalgesic effect of levetiracetam and its mechanism of action in an inflammatory pain model. *Anesth. Analg.* **115**(6), 1457–1466. https://doi.org/10.1213/ANE.0b013e31826c7fc2 (2012).

43. Negus, S. S., Bilsky, E. J., Do Carmo, G. P. & Stevenson, G. W. Rationale and methods for assessment of pain-depressed behavior in preclinical assays of pain and analgesia. *Methods Mol. Biol.* **617**, 79–91, https://doi.org/10.1007/978-1-60327-323-7_7 (2010).

44. Andrews, N. *et al.* Spontaneous burrowing behaviour in the rat is reduced by peripheral nerve injury or inflammation associated pain. *Eur. J Pain* **16**, 485–495. https://doi.org/10.1016/j.ejpain.2011.07.012 (2012).

45. Jirkof, P. *et al.* Burrowing behavior as an indicator of post-laparotomy pain in mice. *Front. Behav. Neurosci.* **4**, 165. https://doi.org/10.3389/fnbeh.2010.00165 (2010).

46. Deacon, R. M. Burrowing in rodents: A sensitive method for detecting behavioral dysfunction. *Nat. Protoc.* **1**, 118–121. https://doi.org/10.1038/nprot.2006.19 (2006).

47. Vivancos, G. G. *et al.* An electronic pressure-meter nociception paw test for rats. *Braz. J Med Bio Res* **37**(3), 391–399. https://doi.org/10.1590/S0100-879X2004000300017 (2004).

48. Pecikoza, U., Tomić, M., Micov, A. & Stepanović-Petrović, R. Metformin synergizes with conventional and adjuvant analgesic drugs to reduce inflammatory hyperalgesia in rats. *Anesth. Analg.* **124**(4), 1317–1329. https://doi.org/10.1213/ANE.0000000000001561 (2017).

49. Stojić-Vukanić, Z. *et al.* Strain specificities in age-related changes in mechanisms promoting and controlling rat spinal cord damage in experimental autoimmune encephalomyelitis. *Exp. Gerontol.* **101**, 37–53. https://doi.org/10.1016/j.exger.2017.11.002 (2018).

50. Gunn, M. D. *et al.* Mice lacking expression of secondary lymphoid organ chemokine have defects in lymphocyte homing and dendritic cell localization. *J. Exp. Med.* **189**, 451–460. https://doi.org/10.1084/jem.189.3.451 (1999).

51. Vida, C. *et al.* Impairment of several immune functions and redox state in blood cells of Alzheimer's disease patients. Relevant role of neutrophils in oxidative stress. *Front. Immunol.* **8**, 1974, https://doi.org/10.3389/fimmu.2017.01974 (2017).

52. Nacka-Aleksić, M. *et al.* Male rats develop more severe experimental autoimmune encephalomyelitis than female rats: Sexual dimorphism and diergism at the spinal cord level. *Brain Behav. Immun.* **49**, 101–118 (2015).

53. Sarkar, S. *et al.* Regulation of pathogenic IL-17 responses in collagen-induced arthritis: Roles of endogenous interferon-gamma and IL-4. *Arthritis Res. Ther.* **11**, R158. https://doi.org/10.1186/ar2838 (2009).

54. Green, L. C. *et al.* Analysis of nitrate, nitrite, and [15N]nitrate in biological fluids. *Anal. Biochem.* **126**, 131–138. https://doi.org/10.1016/0003-2697(82)90118-x (1982).

55. Auclair, C. & Voisin, E. in *CRC Handbook of Methods for Oxygen Radical Research.* (ed R.A. Greenwald) 123–132 (CRC Press, 1985).

56. Erel, O. A novel automated direct measurement method for total antioxidant capacity using a new generation, more stable ABTS radical cation. *Clin. Biochem.* **37**, 277–285. https://doi.org/10.1016/j.clinbiochem.2003.11.015 (2004).

57. Erel, O. A new automated colorimetric method for measuring total oxidant status. *Clin. Biochem.* **38**, 1103–1111. https://doi.org/10.1016/j.clinbiochem.2005.08.008 (2005).

58. Misra, H. P. & Fridovich, I. The role of superoxide anion in the autoxidation of epinephrine and a simple assay for superoxide dismutase. *J. Biol. Chem.* **247**, 3170–3175 (1972).

59. Ellman, G. I. Tissue sulfhydril groups. *Arch. Biochem. Biophys.* **82**, 70–77 (1959).

60. Alamdari, D. H. *et al.* A novel assay for the evaluation of the prooxidant-antioxidant balance, before and after antioxidant vitamin administration in type II diabetes patients. *Clin. Biochem.* **40**, 248–254. https://doi.org/10.1016/j.clinbiochem.2006.10.017 (2007).

61. Carnrot, C., Prokopec, K. E., Rasbo, K., Karlsson, M. C. & Kleinau, S. Marginal zone B cells are naturally reactive to collagen type II and are involved in the initiation of the immune response in collagen-induced arthritis. *Cell. Mol. Immunol.* **8**, 296–304. https://doi.org/10.1038/cmi.2011.2 (2011).

62. Stuart, J. M., Cremer, M. A., Townes, A. S. & Kang, A. H. Type II collagen-induced arthritis in rats. Passive transfer with serum and evidence that IgG anticollagen antibodies can cause arthritis. *J. Exp. Med.* **155**, 1–16, https://doi.org/10.1084/jem.155.1.1 (1982).

63. Krock, E., Jurczak, A. & Svensson, C. I. Pain pathogenesis in rheumatoid arthritis-what have we learned from animal models?. *Pain* **159**(Suppl 1), S98–S109. https://doi.org/10.1097/j.pain.0000000000001333 (2018).

64. Kotake, S., Yago, T., Kobashigawa, T. & Nanke, Y. The plasticity of Th17 cells in the pathogenesis of rheumatoid arthritis. *J. Clin. Med.* **6**(7), 67, https://doi.org/10.3390/jcm6070067 (2017).

65. Kennedy, A., Fearon, U., Veale, D. J. & Godson, C. Macrophages in synovial inflammation. *Front. Immunol.* **2**, 52. https://doi.org/10.3389/fimmu.2011.000522011 (2011).

66. Hampton, H. R. & Chtanova, T. Lymphatic migration of immune cells. *Front. Immunol.* **10**, 1168. https://doi.org/10.3389/fimmu.2019.01168 (2019).

67. Davignon, J. L. *et al.* Targeting monocytes/macrophages in the treatment of rheumatoid arthritis. *Rheumatology (Oxford, England)* **52**(4), 590–598. https://doi.org/10.1093/rheumatology/kes304 (2013).

68. Szondy, Z., Sarang, Z., Kiss, B., Garabuczi, É. & Köröskényi, K. Anti-inflammatory mechanisms triggered by apoptotic cells during their clearance. *Front. Immunol.* **8**, 909. https://doi.org/10.3389/fimmu.2017.00909 (2017).

69. Zhang, J. M. & An, J. Cytokines, inflammation, and pain. *Int. Anesthesiol. Clin.* **45**(2), 27–37. https://doi.org/10.1097/AIA.0b013e318034194e (2007).

70. Ricciotti, E. & FitzGerald, G. A. Prostaglandins and inflammation. *Arterioscler Thromb Vasc Biol* **31**, 986–1000. https://doi.org/10.1161/ATVBAHA.110.207449 (2011).

71. da Silva, M. D. *et al.* IL-10 cytokine released from M2 macrophages is crucial for analgesic and anti-inflammatory effects of acupuncture in a model of inflammatory muscle pain. *Mol. Neurobiol.* **51**(1), 19–31. https://doi.org/10.1007/s12035-014-8790-x (2015).

72. Lantero, A. *et al.* TGF-β and opioid receptor signaling crosstalk results in improvement of endogenous and exogenous opioid analgesia under pathological pain conditions. *J. Neurosci.* **34**(15), 5385–5395. https://doi.org/10.1523/JNEUROSCI.4405-13.2014 (2014).

73. Crofford, L. J. *et al.* Cyclooxygenase-1 and -2 expression in rheumatoid synovial tissues. Effects of interleukin-1 beta, phorbol ester, and corticosteroids. *J. Clin. Investig.* **93**, 1095–1101, https://doi.org/10.1172/JCI117060 (1994).

74. Fattahi, M. J. & Mirshafiey, A. Prostaglandins and rheumatoid arthritis. *Arthritis* **2012**, 239310. https://doi.org/10.1155/2012/239310 (2012).

75. Westman, M. *et al.* Expression of microsomal prostaglandin E synthase 1 in rheumatoid arthritis synovium. *Arthritis Rheum.* **50**, 1774–1780. https://doi.org/10.1002/art.20286 (2004).

76. Nagy, G. *et al.* Central role of nitric oxide in the pathogenesis of rheumatoid arthritis and systemic lupus erythematosus. *Arthritis Res. Ther.* **12**, 210. https://doi.org/10.1186/ar3045 (2010).

77. Choy, E. Understanding the dynamics: pathways involved in the pathogenesis of rheumatoid arthritis. *Rheumatology (Oxford)* **51**(Suppl 5), v3-11. https://doi.org/10.1093/rheumatology/kes113 (2012).

78. Filippin, L. I., Vercelino, R., Marroni, N. P. & Xavier, R. M. Redox signalling and the inflammatory response in rheumatoid arthritis. *Clin. Exp. Immunol.* **152**, 415–422. https://doi.org/10.1111/j.1365-2249.2008.03634.x (2008).

79. Turner, P. V., Pang, D. S. & Lofgren, J. L. A review of pain assessment methods in laboratory rodents. *Comp. Med.* **69**(6), 451–467. https://doi.org/10.30802/AALAS-CM-19-000042 (2019).

80. Salvemini, D. *et al.* Nitric oxide: A key mediator in the early and late phase of carrageenan-induced rat paw inflammation. *Br. J. Pharmacol.* **118**, 829–838. https://doi.org/10.1111/j.1476-5381.1996.tb15475.x (1996).

81. Annamalai, P. & Thangam, E. B. Local and systemic profiles of inflammatory cytokines in carrageenan-induced paw inflammation in rats. *Immunol. Invest.* **46**, 274–283. https://doi.org/10.1080/08820139.2016.1248562 (2017).

82. Rocha, A. C., Fernandes, E. S., Quintao, N. L., Campos, M. M. & Calixto, J. B. Relevance of tumour necrosis factor-alpha for the inflammatory and nociceptive responses evoked by carrageenan in the mouse paw. *Br. J. Pharmacol.* **148**, 688–695. https://doi.org/10.1038/sj.bjp.0706775 (2006).

83. Schaible, H. G., Ebersberger, A. & Von Banchet, G. S. Mechanisms of pain in arthritis. *Ann. N. Y. Acad. Sci.* **966**, 343–354. https://doi.org/10.1111/j.1749-6632.2002.tb04234.x (2002).

84. Andoh, T. & Kuraishi, Y. Direct action of immunoglobulin G on primary sensory neurons through Fc gamma receptor I. *FASEB J.* **18**, 182–184. https://doi.org/10.1096/fj.02-1169fje (2004).

85. Nandakumar, K. S. *et al.* Arthritogenic antibodies specific for a major type II collagen triple-helical epitope bind and destabilize cartilage independent of inflammation. *Arthritis Rheum.* **58**, 184–196. https://doi.org/10.1002/art.23049 (2008).

86. Morse, K. *et al.* Near-infrared 1064 nm laser modulates migratory dendritic cells to augment the immune response to intradermal influenza vaccine. *J. Immunol.* **199**, 1319–1332. https://doi.org/10.4049/jimmunol.1601873 (2017).

87. Allenspach, E. J., Lemos, M. P., Porrett, P. M., Turka, L. A, Laufer, T.M. Migratory and lymphoid-resident dendritic cells cooperate to efficiently prime naive CD4 T cells. *Immunity* **29**(5), 795–806 (2008).

88. MartIn-Fontecha, A. *et al.* Regulation of dendritic cell migration to the draining lymph node: Impact on T lymphocyte traffic and priming. *J. Exp. Med.* **198**(4), 615–621. https://doi.org/10.1084/jem.20030448 (2003).

89. Ludewig, B., Junt, T., Hengartner, H. & Zinkernagel, R. M. Dendritic cells in autoimmune diseases. *Curr. Opin. Immunol.* **13**(6), 657–662 (2001).

90. Yang, D., Chen, Q., Le, Y., Wang, J. M. & Oppenheim, J. J. Differential regulation of formyl peptide receptor-like 1 expression during the differentiation of monocytes to dendritic cells and macrophages. *J. Immunol.* **166**(6), 4092–4098. https://doi.org/10.4049/jimmunol.166.6.4092 (2001).

91. de Oliveira Fulco, T. *et al.* Effect of apoptotic cell recognition on macrophage polarization and mycobacterial persistence. *Infect. Immun.* **82**, 3968–3978, https://doi.org/10.1128/IAI.02194-14 (2014).

92. Kim, S. *et al.* Evaluation of the immunobiological effects of a regenerative far-infrared heating system in pigs. *J. Vet. Sci.* **20**(6), e61. https://doi.org/10.4142/jvs.2019.20.e61 (2019).

93. Lee, T. S. & Chau, L. Y. Heme oxygenase-1 mediates the anti-inflammatory effects of acute alcohol on IL-10 induction involving p38 MAPK activation in monocytes. *Nat. Med.* **8**(3), 240–246 (2002).

94. Ryter, S. W. & Choi, A. M. Targeting heme oxygenase-1 and carbon monoxide for therapeutic modulation of inflammation. *Transl. Res.* **167**(1), 7–34. https://doi.org/10.1016/j.trsl.2015.06.011 (2016).

95. Piantadosi, C. A. *et al.* Heme oxygenase-1 couples activation of mitochondrial biogenesis to anti-inflammatory cytokine expression. *J. Biol. Chem.* **286**(18), 16374–16385. https://doi.org/10.1074/jbc.M110.207738 (2011).

96. Leung, T. K. *et al.* Bone and joint protection ability of ceramic material with biological effects. *Chinese J. Physiol.* **55**, 47–54. https://doi.org/10.4077/CJP.2012.AMM113 (2012).

97. Abramson, S. B. Nitric oxide in inflammation and pain associated with osteoarthritis. *Arthritis Res. Ther.* **10**(Suppl 2), S2. https://doi.org/10.1186/ar2463 (2008).

98. Sharma, J. N., Al-Omran, A. & Parvathy, S. S. Role of nitric oxide in inflammatory diseases. *Inflammopharmacology* **15**, 252–259. https://doi.org/10.1007/s10787-007-0013-x (2007).

99. Leung, T. K. *et al.* In vitro cell study of possible anti-inflammatory and pain relief mechanism of far-infrared ray-emitting ceramic material. *J. Med. Biol. Eng.* **33**, 179–184. https://doi.org/10.5405/jmbe.1029 (2012).

100. Maseda, D. *et al.* mPGES1-dependent prostaglandin E2 (PGE2) controls antigen-specific Th17 and Th1 responses by regulating T autocrine and paracrine PGE2 production. *J. Immunol.* **200**, 725–736. https://doi.org/10.4049/jimmunol.1601808 (2018).

101. Kim, C. F. & Moalem-Taylor, G. Interleukin-17 contributes to neuroinflammation and neuropathic pain following peripheral nerve injury in mice. *J. Pain* **12**, 370–383. https://doi.org/10.1016/j.jpain.2010.08.003 (2011).

102. Rosas, R. F. *et al.* Far infrared-emitting ceramics decrease Freund's adjuvant-induced inflammatory hyperalgesia in mice through cytokine modulation and activation of peripheral inhibitory neuroreceptors. *J. Integr. Med.* **16**, 396–403. https://doi.org/10.1016/j.joim.2018.08.002 (2018).

103. Eijkelkamp, N. *et al.* IL4-10 fusion protein is a novel drug to treat persistent inflammatory pain. *J. Neurosci.* **36**, 7353–7363. https://doi.org/10.1523/JNEUROSCI.0092-16.2016 (2016).

104. Kwilasz, A. J., Grace, P. M., Serbedzija, P., Maier, S. F. & Watkins, L. R. The therapeutic potential of interleukin-10 in neuroimmune diseases. *Neuropharmacology* **96**, 55–69. https://doi.org/10.1016/j.neuropharm.2014.10.020 (2015).

105. Lantero, A., Tramullas, M., Diaz, A. & Hurle, M. A. Transforming growth factor-beta in normal nociceptive processing and pathological pain models. *Mol. Neurobiol.* **45**, 76–86. https://doi.org/10.1007/s12035-011-8221-1 (2012).

106. Tramullas, M. *et al.* BAMBI (bone morphogenetic protein and activin membrane-bound inhibitor) reveals the involvement of the transforming growth factor-beta family in pain modulation. *J. Neurosci.* **30**, 1502–1511. https://doi.org/10.1523/JNEUROSCI.2584-09.2010 (2010).

107. Lee, Y. C. Effect and treatment of chronic pain in inflammatory arthritis. *Curr. Rheumatol. Rep.* https://doi.org/10.1007/s11926-012-0300-4 (2012).

108. Cojocaru, M., Cojocaru, I. M., Silosi, I., Vrabie, C. D. & Tanasescu, R. Extra-articular manifestations in rheumatoid arthritis. *Maedica* **5**, 286–291 (2010).

109. da Silva, F. G. *et al.* Antioxidant effect of far infrared radiation produced by bioceramics in individuals with intermittent claudication: A randomized, controlled pilot study. *Altern. Ther. Health Med.* **25**, 34–43 (2019).

Acknowledgements

Author contributions

Conception and design of the study: G.L., M.D., R.P.S.; Acquisition and analysis of data: J.D., M.D., M.S., J.K.S., A.M.; Drafting the manuscript. J.D., M.D.; Critical revision of the manuscript: G.L., M.R.H.

Competing interests

MRH declares the following potential conflicts of interest. Scientific Advisory Boards: Transdermal Cap Inc, Cleveland, OH; BeWell Global Inc, Wan Chai, Hong Kong; Hologenix Inc. Santa Monica, CA; LumiThera Inc, Poulsbo, WA; Vielight, Toronto, Canada; Bright Photomedicine, Sao Paulo, Brazil; Quantum Dynamics LLC, Cambridge, MA; Global Photon Inc, Bee Cave, TX; Medical Coherence, Boston MA; NeuroThera, Newark DE; JOOVV Inc, Minneapolis-St. Paul MN; AIRx Medical, Pleasanton CA; FIR Industries, Inc. Ramsey, NJ; UVLRx Therapeutics, Oldsmar, FL; Ultralux UV Inc, Lansing MI; Illumiheal & Petthera, Shoreline, WA; MB Lasertherapy, Houston, TX; ARRC LED, San Clemente, CA; Varuna Biomedical Corp. Incline Village, NV; Niraxx Light Therapeutics, Inc, Boston, MA. Consulting; Lexington Int, Boca Raton, FL; USHIO Corp, Japan; Merck KGaA, Darmstadt, Germany; Philips Electronics Nederland B.V. Eindhoven, Netherlands; Johnson &

Additional information

Supplementary Information The online version contains supplementary material available at https://doi.org/10.1038/s41598-021-81999-7.

Correspondence and requests for materials should be addressed to G.L.

Reprints and permissions information is available at www.nature.com/reprints.

Publisher's note Springer Nature remains neutral with regard to jurisdictional claims in published maps and institutional affiliations.

Infrared Radiative Properties and Thermal Modeling of Ceramic Embedded Textile Fabrics

Dr. David Anderson, John Fessler, Matthew Pooley, Scott Seidel,
Dr. Michael Hamblin, Haskell Beckham and Dr. James F Brennan

Infrared radiative properties and thermal modeling of ceramic-embedded textile fabrics

DAVID M. ANDERSON,[1]* JOHN R. FESSLER,[2] MATTHEW A. POOLEY,[3] SCOTT SEIDEL,[1] MICHAEL R. HAMBLIN,[4] HASKELL W. BECKHAM,[1] AND JAMES F. BRENNAN, III[1]

[1] *Exponent, Inc., 3350 Peachtree Road NE, Suite 1125, Atlanta, GA 30326 USA*
[2] *Exponent, Inc., 15615 Alton Parkway, Suite 350, Irvine, CA 92618 USA*
[3] *Exponent, Inc., 420 Lexington Avenue, Suite 1740, New York, NY 10170 USA*
[4] *Wellman Center for Photomedicine, Harvard Medical School, 50 Blossom Street, Boston, MA 02114 USA*

*danderson@exponent.com

Abstract: The infrared optical properties of textiles are of great importance in numerous applications, including infrared therapy and body thermoregulation. Tuning the spectral response of fabrics by engineering of composite textile materials can produce fabrics targeted for use in these applications. We present spectroscopic data for engineered polyester fabric containing varying amounts of ceramic microparticles within the fiber core and report a spectrally-dependent shift in infrared reflectance, transmittance and absorptance. A thermal transport model is subsequently implemented to study the effect of these modified properties on the spectral distribution of infrared radiation incident upon the wearer of a garment constructed of this fabric.

OCIS codes: (300.6340) Spectroscopy, infrared; (110.3175) Infrared imaging; (120.6810) Thermal effects.

References and links

1. S. B. Warner, *Fiber Science* (Prentice Hall, 1995) pp. 213-229.
2. US Patent, No: 5344297 (1994).
3. M.A. Pooley, D.M. Anderson, H.W. Beckham and J.F. Brennan III , "Engineered emissivity of textile fabrics by the inclusion of ceramic particles," Opt. Express **24**(10), 10556–10564 (2016).
4. W.W. Carr, D.S. Sarma, M.R. Johnson, B.T. Do and V.A. Williamson. "Infrared absorption studies of fabrics," Textile Res. J. **67**(10) 725-738 (1997).
5. P. Hsu, A.Y. Song, P.B. Catrysse, C. Liu, Y. Peng, J. Xie, S. Fan and Y. Cui, "Radiative human body cooling by nanoporous polyethylene textile," Science **353**(6303), 1019-1023 (2016).
6. F. Vatansever and M.R. Hamblin, "Far infrared radiation (FIR): its biological effects and medical applications," Photonics Lasers Med. **1**(4), 255-266 (2012).
7. J.D. Hardy and E.F. DuBois, "Regulation of heat loss from the human body," Proc. Nat. Acad. Sci. **23**(12), 624-631 (1937).
8. C.-E. A. Winslow, A.P. Gagge and L.P. Harrison, "The influence of air movement upon heat losses from the clothed human body," Am. J. Physiol. **127**(3) 508-515 (1939).
9. ASTM E408-13, *Standard Test Methods for Total Normal Emittance of Surfaces Using Inspection-Meter Techniques,* (ASTM International, 2013).
10. F.P. Incropera and D.P. Dewitt, *Fundamentals of Heat and Mass Transfer, 5th Ed.* (John Wiley & Sons, 2002).
11. G. Nellis and S. Klein, *Heat Transfer* (Cambridge University Press, 1997).
12. E.A. Arens and H. Zhang, "The skin's role in human thermoregulation and comfort" in *Thermal and moisture transport in fibrous materials*, N. Pan and P. Gibson, Eds. (Woodhead Publishing Limited, 2006).
13. ASTM G173-03, *Spectral Solar Irradiance,* (ASTM International, 2003).
14. A.C. Guyton and J.E. Hall, *Textbook of Medical Physiology* (W.B. Saunders Company, 2000).

---

1. Introduction

The engineering of textiles to exhibit desired optical properties has long been explored, with success demonstrated in various methods including: co-spinning of different materials,

introduction of gradients in fiber cross-sectional shape, inclusion of inorganic content, or use of dyes and other additives [1,2]. Recently, increased attention has been paid to the interactions between textile products and infrared radiation, due to the potential impact in applications ranging from body cooling to industrial drying processes to infrared therapy [3–6]. Mid-infrared optical properties are of particular importance when considering interactions with the human body, as at nominal skin temperature much of the body's emissive radiative power is centered in the mid-infrared between 7 and 14 µm, and infrared heat losses account for approximately 50% of body cooling in typical indoor conditions [7,8].

In the work presented herein, we utilized Fourier transform infrared (FTIR) spectroscopy to assess the spectral optical properties – namely the near-normal reflectance, transmittance, and emittance – of textile fabrics knitted with varying percentages of ceramic-bearing polymeric fibers. The biological effects of garments manufactured from these fabrics are presently under investigation [6]. The fabrics, which we also studied in our previous work [3], were nominally identical in thickness, basis weight, knit structure, and color. All fabrics consisted of 8% elastane fibers and 92% polyethylene terephthalate (PET, i.e., polyester) based fibers; the only difference between the samples was the fraction of these fibers that contained a core of polyester blended with ceramic particles (e.g., titanium dioxide) for optical property modification.

The measured optical properties were subsequently utilized in a first-principle-based heat transfer model, accounting for emitted, reflected and transmitted radiant energy as well as thermal transport via conduction and convection, to determine the magnitude and spectral distribution of infrared energy received by a wearer of each fabric in the $0.8 – 16.7$ µm spectral region. It is demonstrated that with increasing added ceramic content, the modified textile fabrics reflect and transmit less infrared energy and thus absorb more. This is particularly evident at wavelengths shorter than 6 µm. As a result, the modified fabrics with added ceramic content can absorb incoming radiation from the sun in the near-IR region, and emit increased levels of infrared energy at longer wavelengths, as compared to the same fabric without ceramic content. Thermal modeling indicates that this effect persists over a broad range of environmental and fit factors; such a fabric could be utilized when the physical properties of a polyester blend warrant its selection over alternative fabric materials, yet modified near- and mid-infrared optical properties are desired.

2. Experimental Methods

A Nicolet iS50 FTIR spectrometer (Thermo-Fisher Scientific) was used to measure the spectral reflectance (ρ_λ) and transmittance (τ_λ) of the fabric samples with differing percentages of ceramic-bearing fibers. Because of the diffuse nature of reflection and transmission from composite surfaces [9], a mid-IR IntegratIR^{TM} integrating sphere (Pike Technologies) with a reflective gold inner coating and a deuterated triglycine sulfate detector was used to measure the reflected or transmitted infrared radiation from the fabric samples. Mid-IR measurements were conducted across a wavenumber range of $4000 – 600$ cm^{-1} (corresponding to wavelengths, λ, ranging from $2.5 – 16.7$ µm), using a potassium bromide (KBr) beam splitter. Near-IR measurements, ranging from wavenumbers of $12000 – 4000$ cm^{-1} ($0.8 < \lambda < 2.5$ µm) were conducted using a near-IR Nicolet iS50 NIR integrating sphere module (Thermo-Fisher Scientific) with an indium gallium arsenide detector.

A schematic of the FTIR setup, indicating the sample placement relative to the IR source and detector for the various reflectance and transmittance measurements is shown in Fig. 1.
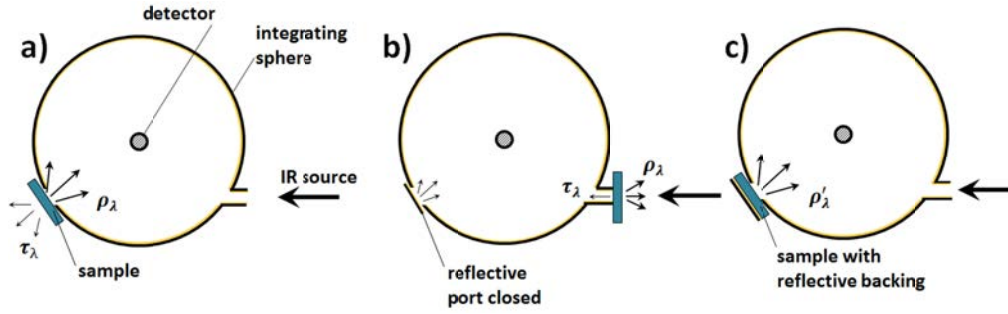
Fig. 1. Schematic illustrating an FTIR setup for measurement of a) direct reflectance, b) direct transmittance, and c) indirect transmittance via change in reflectance

Because the near-IR integrating sphere did not allow placement of the sample directly between the IR source and the sphere inlet, the transmittance was instead assessed indirectly by comparing the reflectance where transmitted IR was permitted to escape through the sample (ρ_λ) to the reflectance with a reflective backing behind the sample (ρ'_λ). The spectral transmittance can be shown to be related to the ρ_λ and ρ'_λ reflective measurements illustrated in Fig. 1(a) and Fig. 1(c), respectively, by:

$$\tau_\lambda = \left[\frac{\rho'_\lambda - \rho_\lambda}{1 + \sum_{j=1}^{\infty} \rho_\lambda^j} \right]^{1/2} \tag{1}$$

Details of this relationship are included in the Appendix. The methodology of calculating transmittance from the reflectance measurements with and without a 100% reflective backing was validated through comparison of indirect to direct transmittance measurements with the mid-IR integrating sphere setup where such direct measurement was possible.

To minimize the effect of absorption by water vapor and other trace gas compounds, the integrating sphere was surrounded with desiccant and the interior was swept with 5 scfh (standard cubic feet per hour) of inert nitrogen gas during all measurements.

Four different fabric samples were examined, each containing 0, 0.82, 0.91 or 1.18 weight percent inorganic content from modified ceramic-bearing fibers. For each fabric sample, absorption and transmission spectra were calculated by averaging the respective spectra measured for 5 unique specimens. For each specimen, the absorption and transmission spectra were obtained from 256 scans at a resolution of 16 cm^{-1}.

3. Experimental Results

The results of the FTIR measurements are reported in this section. Although reflectance and transmittance are often used interchangeably with reflectivity and transmissivity, respectively, the terminology ending in '-ance' is used in this paper to note that textiles are a mixture of fibers and air, and not pure substances. Because radiation properties such as reflectance and transmittance of non-conducting materials such as textiles do not vary for incidence angles less than 70° from normal [10], the values measured according to the schematic shown in Fig. 1 are reported as near-normal properties.

While not directly measured, the spectral absorptance (α_λ) of each fabric can be determined because the reflectance, transmittance and absorptance must sum to unity ($\rho_\lambda + \tau_\lambda + \alpha_\lambda = 1$). Also, according to Kirchoff's law, the spectral near-normal emittance (ε_λ) must equal the near-normal absorptance [10].

3.1 Mid-IR reflectance, transmittance and emittance

The spectral mid-IR properties of the textile samples are shown in Fig. 2. The most significant difference between the various fabrics appears in wavenumbers greater than approximately 1700 cm^{-1} (wavelengths below 6 μm). Each of the fabric samples exhibit similar overall spectral patterns, with a series of narrow absorption peaks between 3000 – 2000 cm^{-1} wavenumbers. Increasing amounts of ceramic content, however, generally decreases the reflectance and transmittance, and increases absorptance, in the 4000 – 2000 cm^{-1} region. Similar behavior occurs at smaller wavenumbers; however, the effect is less pronounced because the overall absorptance is already high at these longer wavelengths.
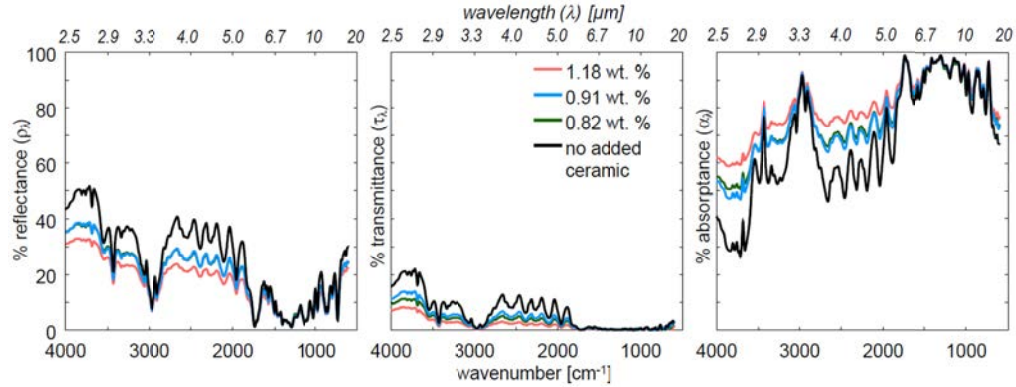
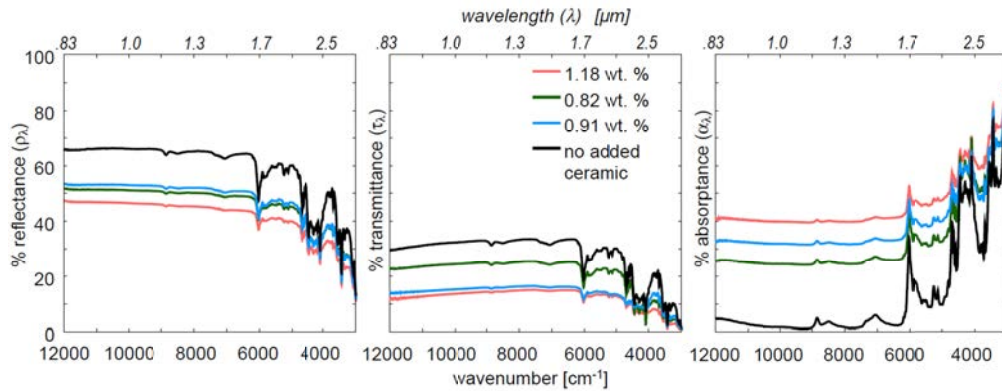Fig. 2. Spectral reflectance (ρ_λ), transmittance (τ_λ), and absorptance (α_λ) in the mid-IR region for knit textile fabrics consisting of varying wt. % of ceramic contained in the fiber cores. All plots have a common y-scale ranging from 0-100%.

To better illustrate how the optical properties align with infrared radiation emitted by the human body, Fig. 3 plots these properties as a function of wavelength, as opposed to wavenumber, for the fabric with the maximum amount of added ceramic (1.18 wt. %) and with no added ceramic. The figure also illustrates the spectral distribution of intensity of radiation emitted by a blackbody at a nominal skin temperature of 35°C. This emission is described by Planck's distribution:

$$E_b(\lambda, T) = \frac{C_1}{\lambda^5 \left[e^{C_2/\lambda T} - 1 \right]} \tag{2}$$

where the first and second radiation constants are C$_1$ = 3.742 × 10^8 W·μm^4/m^2 and C$_2$ = 1.439 × 10^4 μm^4·K, respectively [10].

As can readily be seen in Fig. 3, the spectral region where the impact of added ceramic is greatest ($\lambda < 6$ μm) corresponds to an area with less significant magnitude of radiation at nominal body temperature; less than 5% of the total radiation of a blackbody at 35°C is contained in this region [10]. To provide a representative value for an optical property, it must be spectrally weighted by its source of radiation. For example, the average reflectance over a wavelength range of λ_1-λ_2 is:

$$\overline{\rho}_{\lambda_1 - \lambda_2} = \frac{\int \rho_\lambda \cdot E_b(\lambda, T) \cdot d\lambda}{\int E_b(\lambda, T) \cdot d\lambda} \tag{3}$$
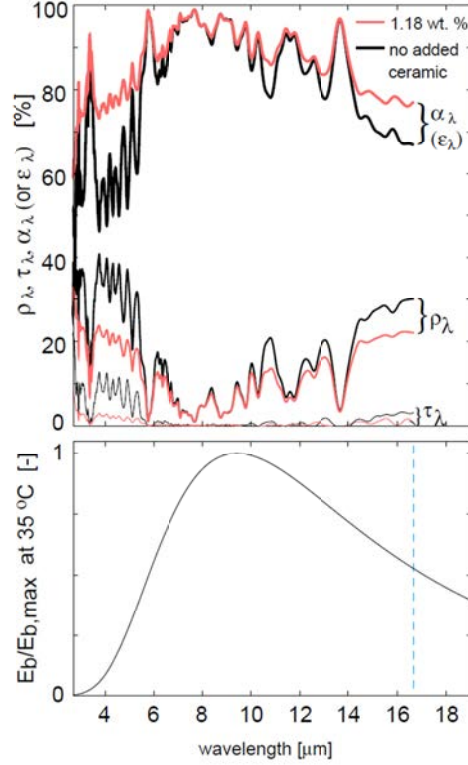
Fig. 3. (Top) Spectral optical properties of the fabric samples containing the maximum (1.18 wt. %) and minimum (0 wt. %) added ceramic content. (Bottom) Normalized Planck's distribution for a blackbody at 35°C.

Similarly, the average spectral transmittance and absorptance/emittance are given by:

$$\overline{\tau}_{\lambda_1 - \lambda_2} = \frac{\int \tau_\lambda \cdot E_b(\lambda, T) \cdot d\lambda}{\int E_b(\lambda, T) \cdot d\lambda} \tag{4}$$

$$\overline{\varepsilon}_{\lambda_1 - \lambda_2} = \overline{\alpha}_{\lambda_1 - \lambda_2} = \frac{\int \alpha_\lambda \cdot E_b(\lambda, T) \cdot d\lambda}{\int E_b(\lambda, T) \cdot d\lambda} \tag{5}$$

In our prior study we used an IR camera, with spectral sensitivity between 7.5 – 14 μm, to investigate the same four fabrics considered herein, and found a statistically significant trend of increasing emittance with increasing added ceramic content [3]. The FTIR emittance and absorptance results in Fig. 2 and Fig. 3 can be weighted by the source power distribution for a wider wavelength range. The emittance values measured via FTIR in the present work agree well with the prior IR camera measurements (i.e., Pooley, et al.) for the 7.5 – 14 μm spectral range used in that study; the slope of the ceramic content vs. emittance linear best fit curve in Fig. 4 matches between measurement techniques. Moreover, while the absolute values of emittance are slightly lower when assessed by the FTIR, the differences are within the experimental error bars.
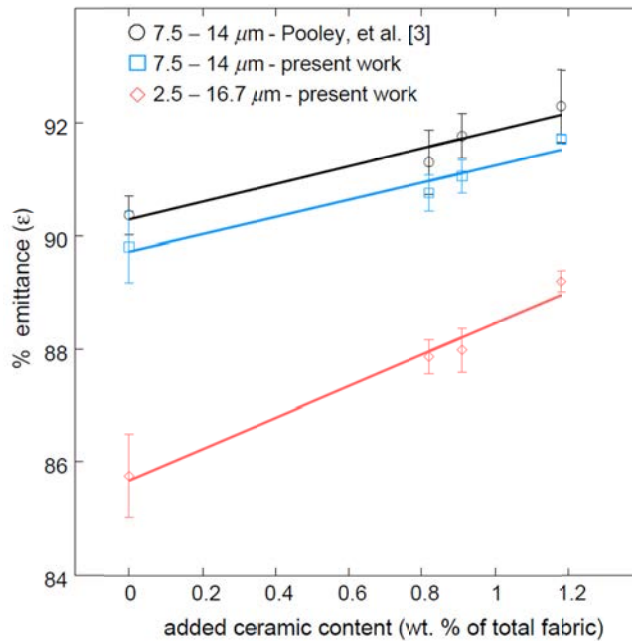
Fig. 4. Emittance of the fabric samples as a function of added ceramic material. Data points for the present work represent the mean of spectrally averaged emittance values from five independent samples. Two separate spectral ranges – 7.5-14 µm to match the detection range of the IR camera and the entire 2.5-16.7 µm measurement range – are utilized to calculate average emittance values.

When the broader 2.5 – 16.7 µm mid-IR spectral range is considered, the impact of added ceramic content on emittance is even greater, as evidenced by the steeper gradient for this wavelength range in Fig. 4, due to the more significant difference in properties where $\lambda < 6$ µm. Table 1 summarizes the spectral average mid-IR properties of the four fabric samples with varying wt. % added ceramic content. It should be noted that the wt. % values reported in our prior study [3] did not account for the inorganic additive present in standard polyester; hence the values reported in Table 1 vary slightly from what was previously reported for the same samples. However, these slight variations do not affect the conclusions from that study, which remain unchanged.

Table 1.   Spectral average mid-IR optical properties at 35°C (2.5 – 16.7 µm)

Sample No.	Wt. % ceramic from modified fibers[a]	Transmittance [%]	Reflectance [%]	Emittance [%]
1	1.18	0.34 +/- 0.19	10.5 +/- 0.2	89.2 +/- 0.2
2	0.91	0.68 +/- 0.21	11.3 +/- 0.3	88.0 +/- 0.4
3	0.82	0.53 +/- 0.10	11.6 +/- 0.3	87.9 +/- 0.3
4	0	0.92 +/- 0.15	13.3 +/- 0.8	85.8 +/- 0.7

[a] Calculated from the ratio of the ceramic mass contained in the modified fibers to the overall mass of the fabric, using ash-content data collected using ASTM D5630. The ceramic content in standard polyester was determined from the fabric sample that did not contain added ceramics (Sample 4).

3.2 Near-IR reflectance, transmittance and emittance

At its relatively modest temperature, the human body does not emit significant radiation at near-IR wavelengths; however, optical properties in this region are of interest due to

interactions with radiation from hotter sources (most notably, the sun). The reflectance and transmittance of the fabric samples in the near-IR region are shown in Fig. 5.

Fig. 5. Near-IR spectral reflectance (ρ_λ), transmittance (τ_λ), and absorptance (α_λ) of the knit textile fabrics. Spectral data down to 3000 cm^{-1} are included; the data for wavenumbers from 3000 – 4000 cm^{-1} were collected using the mid-IR integrating sphere, illustrating that the data are continuous and consistent between setups and regardless of whether the direct or indirect approach was utilized to measure transmittance.

The fabric with no added ceramic exhibits significantly higher reflectance and transmittance, and therefore lower absorptance, than fabrics that do contain fibers impregnated with ceramic particles. The magnitude of the impact on ceramic content in the near-IR region is even more significant than the impact in the mid-IR region shown in Fig. 2; this will have significant impact on the solar radiation absorbed by and transmitted through the fabric, as approximately 50% of the solar spectrum falls in the near-IR region [11].

4. Impact of optical properties on infrared irradiation received by body

4.1 Heat transfer model

To understand the impact of the change in radiative optical properties on the wearer of a fabric, an energy-conservation-based heat transfer model was developed. This model accounts for all possible modes of radiative interaction – reflection, absorption, and transmission – between the body, fabric and environment, as well as non-radiative heat transfer via conduction and convection. The fabric is modeled as being in instantaneous thermal equilibrium with its surroundings. The ambient surroundings are approximated as being sufficiently large relative to the fabric surface such that radiation is exchanged with the fabric as if the surroundings behave like a blackbody at T_{amb}. The fabric is assumed to be sufficiently thin such that its temperature is uniform and cross-fabric thermal gradients can be neglected. Evaporative cooling is neglected in the model, as the goal of the model is to compare the relative radiative heat transfer rates for fabrics with different ceramic contents, and evaporative cooling is expected to be relatively independent of this effect [12]. Under these assumptions, the skin-fabric-environment system and pertinent mechanisms of heat exchange are shown in Fig. 6.
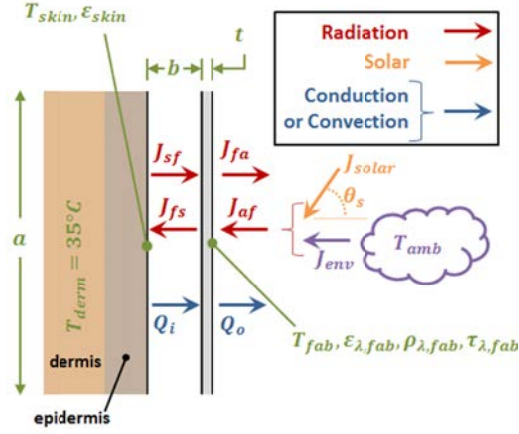
Fig. 6. Fabric geometry and relevant modes of heat transfer

Each radiative heat flux component, shown in red, includes reflected and transmitted radiation in addition to emitted radiation (i.e., it represents a radiosity [10]). Radiative energy is transferred from the skin to the fabric (J_{sf}), the fabric to the skin (J_{fs}), the fabric to the ambient surroundings (J_{fa}), and from the ambient surroundings to the fabric (J_{af}). The radiative heat flux from the surroundings can include both solar irradiation (J_{solar}) and irradiation from the surroundings (J_{env}) at ambient temperature (T_{amb}). The non-radiative heat fluxes due to convection and/or conduction (Q_i and Q_o) are shown in blue. The fabric of thickness t is located between the wearer (at temperature T_{skin}) and the surroundings (at T_{amb}) and is separated from the wearer's skin by a gap of b thickness.

At steady state, the energy conservation on the fabric can be represented, on a per unit area basis [W/m^2] by:

$$(J_{sf} + Q_i + J_{af}) - (J_{fs} + J_{fa} + Q_o) = 0 \tag{6}$$

The general form of the non-radiative heat fluxes is $Q = h_{eff} \cdot (T_{surface} - T_{surroundings})$ where h_{eff} is the average convective heat transfer coefficient and is a function of the geometry and flow characteristics. Conduction across the air gap for Q_i is a special case of $h_{eff} = k_{air}/b$, where k_{air} is the thermal conductivity of air, that occurs when the gap b is sufficiently small such that viscous forces damp out buoyancy effects [10,11]. It is important to note that in the case of $T_{amb} > T_{fab}$, the direction of heat transfer will change; however, this is accounted for appropriately in the model (i.e., Q_o and Q_i will be negative, indicating heat flow in the opposite direction of the arrow shown in Fig. 6). The total radiative fluxes (represented by uppercase J's in Fig. 6) are determined by integrating the spectral flux, or the radiative heat flux leaving surface x in the direction of surface y is $J_{xy} = \int j_{xy}(\lambda) \cdot d\lambda$. Similarly, the solar irradiation is determined by integrating the spectral solar intensity normal to the fabric surface, or $J_{solar} = \int j_{solar}(\lambda) \cdot \cos(\theta_s) \cdot d\lambda$. The spectral solar intensity, accounting for atmospheric transmission losses, is taken from ASTM G-173 [13].

The spectral radiative heat flux leaving each surface has a component of emission, reflection, and transmission and can be written as:

$$j_{af}(\lambda) = E_b(\lambda, T_{amb}) + j_{solar}(\lambda) \cdot \cos(\theta_s) \tag{7}$$

$$j_{fa}(\lambda) = \varepsilon_{\lambda, fab} \cdot E_b(\lambda, T_{amb}) + \rho_{\lambda, fab} \cdot j_{af}(\lambda) + \tau_{\lambda, fab} \cdot j_{sf}(\lambda) \tag{8}$$

$$j_{sf}(\lambda) = \varepsilon_{skin} \cdot E_b(\lambda, T_{skin}) + \rho_{skin} \cdot j_{fs}(\lambda) \tag{9}$$

$$j_{fs}(\lambda) = \varepsilon_{\lambda, fab} \cdot E_b(\lambda, T_{fab}) + \rho_{\lambda, fab} \cdot j_{sf}(\lambda) + \tau_{\lambda, fab} \cdot j_{af}(\lambda) \tag{10}$$

Equations (8) - (10) are circularly defined with dependence upon one another. They are made independent by substituting Eq. (10) into Eq. (9) and solving explicitly for $j_{sf}(\lambda)$:

$$j_{sf}(\lambda) = \frac{\varepsilon_{skin} \cdot E_b(\lambda, T_{skin}) + \rho_{skin} \cdot \left[\varepsilon_{\lambda, fab} \cdot E_b(\lambda, T_{fab}) + \tau_{\lambda, fab} \cdot j_{af}(\lambda) \right]}{1 - \rho_{skin} \cdot \rho_{\lambda, fab}} \quad (11)$$

An iterative solution procedure can be used to solve for the required fabric temperature to satisfy the energy balance given in Eq. (6). The specific heat transfer correlations used to determine the effective heat transfer coefficients in determining the non-radiative heat transfer components Q_i and Q_o, as well as the procedure for adjusting the epidermis skin temperature based on the external heat transfer rate, can be found in the Appendix.

4.2 Spectral shift in incident infrared radiation to the body

Of interest for therapeutic applications is the magnitude and spectral distribution of radiation received by the body as a result of wearing a fabric, namely $j_{fs}(\lambda)$ given by Eq. (10). A common set of baseline input parameters, provided in Table 2, are used in the thermal model. The fabric gap, ambient temperature, air velocity and solar incidence angle can all be adjusted in the model to evaluate sensitivity to these environmental and fit factors.

Table 2. Thermal model simulation parameters

Property	Value	Notes
dermis temp (T_{derm})	35°C	regulated by vasoconstriction/vasodilation [12]
skin emittance (ε_{skin})	0.98	greybody, opaque ($\rho_{skin} = 1 - \varepsilon_{skin}$) [10]
height (a)	0.3 m	estimate of torso dimensions [12]
width (w)	0.3 m	estimate of torso dimensions [12]
fabric gap (b)	5 mm	adjustable parameter
ambient temp (T_{amb})	23°C	adjustable parameter
air velocity (v)	1 m/s	adjustable parameter
solar angle (θ_s)	45°	adjustable parameter

Under the baseline conditions of Table 2, Fig. 7 shows the resulting spectral distribution of infrared radiation incident on the skin $j_{fs}(\lambda)$ for the fabrics with the maximum (1.18 wt. %) and minimum (0 wt. %) added ceramic content.
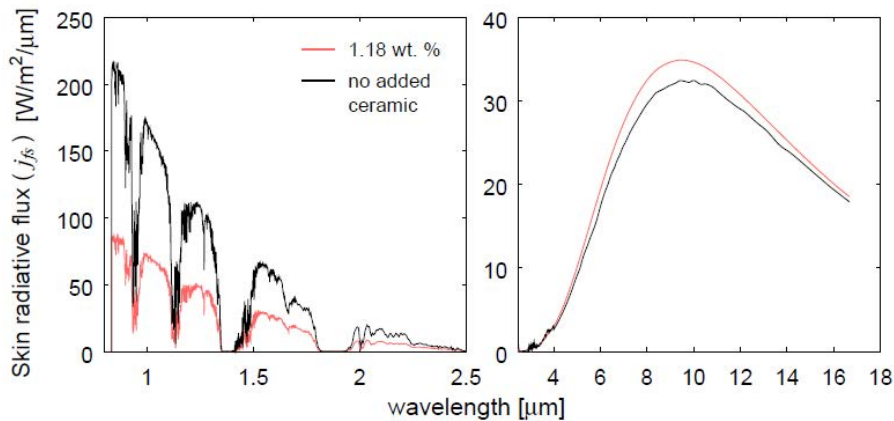
Fig. 7. Comparison of spectral distribution of infrared radiation received by the skin in the near-IR (left) and mid-IR (right) regions for the maximum (1.18 wt. %) and minimum (0 wt. %) added ceramic content fabric.

In the near-IR spectrum, the body will receive more infrared when wearing a garment composed of fabric with no added ceramic, due to the higher transmittance in this spectral region relative to the fabric with added ceramic. In contrast, the fabric with 1.18 wt. % added ceramic is able to absorb more of this solar near-IR radiation which is then re-emitted by the fabric at longer wavelengths. This shift in spectral incident radiation can be seen in the mid-IR portion of Fig. 7, where there is an increase in j_{fs} for wavelengths greater than 4 μm.

To determine if the increase in incident mid-IR radiation persists over a variety of environmental and fit factors, the model was run at different skin-fabric gap distances, ambient temperatures, wind speeds, and incident solar angles. The results of these simulations, used to calculate the total incident radiation in the mid-IR spectrum from 2.5 – 16.7 μm by integrating over this wavelength region for both the 0 wt. % and 1.18 wt. % added ceramic fabrics, are reported in Table 3. For the baseline case, all model input parameters match those listed in Table 2. For the other cases, only the parameter noted is changed from the baseline; the other parameters are held at the baseline state.

Table 3.   Infrared radiation (2.5 – 16.7 μm) received by skin under various environmental and fit conditions

		Mid-IR Power [mW/cm^2]		
Parameter	Value	0 wt. %	1.18 wt. %	Δ
——— baseline ———		30.7	32.6	1.9
fabric gap (b)	10 mm	30.3	32.5	2.2
	1.0 mm	31.8	32.8	1.0
ambient temp (T_{amb})	30 °C	32.4	34.4	2.1
	10 °C	27.7	29.4	1.8
air velocity (v)	3.0 m/s	30.1	31.6	1.5
	0.1 m/s	31.3	33.6	2.4
solar angle (θ_s)	70°	30.4	31.3	0.9
	20°	30.8	33.4	2.6

Table 3 illustrates that the spectral shift in incident radiation to the wearer of a ceramic-embedded garment to the mid-IR region is present under a variety of scenarios. The incidence angle of solar irradiation appears to have the most significant effect on the magnitude of the shift; a similar effect to a less-normal incidence angle would be expected for cloudy days where the intensity of solar irradiation is reduced.

Increased solar absorption and subsequent re-emission of energy at longer wavelengths may be beneficial in numerous textile applications. The impacts of infrared radiation consisting of wavelengths ranging from 3 – 12 μm on tissue oxygenation and cell stimulation are under investigation [6]. Additionally, performance thermal outerwear designed for cold-weather applications could benefit from additional absorption from the solar spectrum to warm the outer surface of the garment and provide this heat to the wearer of the garment. Experimental studies of such ceramic-modified garments incorporating the use of thermal manikins or similar techniques should be conducted to assess these potential applications.

In summary, this study employed spectrophotometric measurements of textile fabrics modified with ceramic particles, finding favorable agreement with prior measurements using a scientific grade infrared camera on such fabrics. The increase in absorptance and emittance was mainly found to be focused in wavelengths below 6 μm, below the typical wavelength of human body radiation. However, in applications where the fabric receives radiation in this near-IR spectral region (e.g., via sunlight), thermal modeling indicates that the wearer will receive increased infrared radiation at wavelengths in the mid-IR (2.5 – 16.7 μm) portion of the electromagnetic spectrum, encompassing the wavelengths of human body radiation.

Acknowledgments

Appendix

A.1 Mathematical relationship to determine reflectance through the indirect method

Equation (1) shows the mathematical relationship between the spectral reflectivity with (ρ'_λ) and without (ρ_λ) a reflective backing (cf. Fig. 1). This relationship can be derived by considering the additional radiation reflected by the sample when a highly reflective backing is present, as shown in Fig. A-1.
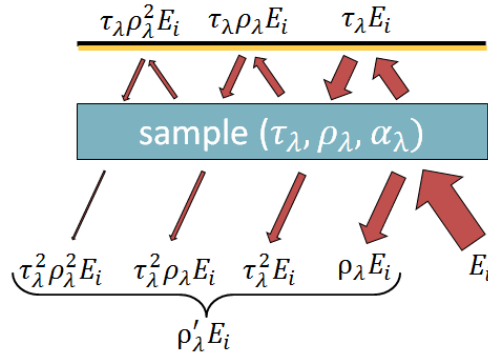
Fig. A-1. Reflection from a semi-transparent sample with reflective backing.

From Fig. A-1, it can readily be seen that:

$$\rho'_\lambda = \rho_\lambda + \tau_\lambda^2 \left[1 + \rho_\lambda + \rho_\lambda^2 + ... \right] \tag{A.1}$$

Because the reflectivity must be less than 1, each term inside the brackets moving rightward becomes increasingly smaller, and Eq. (A.1) can be rewritten as:

$$\rho'_\lambda = \rho_\lambda + \tau_\lambda^2 \left[1 + \sum_{j=1}^{\infty} \rho_\lambda^j \right] \tag{A.2}$$

A.2 Heat transfer correlations for non-radiative thermal transport coefficients

The general form of the convection heat flux (units, W/m^2) from a surface to its surrounding medium is given by Newton's law of cooling:

$$Q = \overline{h} \cdot \left(T_{surface} - T_{surroundings} \right) \tag{A.3}$$

where $\overline{h}$ is the average convective heat transfer coefficient, which is a function of the geometry and external flow characteristics [10]. Dimensionless variables describing the flow and geometry, such as the Reynolds number (Re_L) and/or Grashof number (Gr_L) are first calculated to understand the characteristics of the heat and momentum transfer, and along with the fluid's Prandtl number (Pr) these values are used to calculate an average dimensionless heat transfer coefficient ($Nu = f(Re_L, Gr_L, Pr)$). The dimensional average heat

transfer coefficient $\bar{h}$ is then the Nusselt number multiplied by the characteristic length (L_c) divided by the fluid thermal conductivity $\left(\bar{h} = Nu \cdot L_c \big/ k_{fluid} \right)$ [10,11].

In certain geometries, such as the gap between two parallel plates at different temperatures (i.e., between the skin and fabric), Eq. (A.3) can be employed regardless of whether conduction or convection is the dominant mode of heat transfer. If dimensionless analysis indicates that viscous dissipation forces outweigh the buoyancy forces generated by local differences in fluid density, conduction will prevail over convection and the Nusselt number will become unity (when $Nu = 1 = \bar{h} \cdot L_c / k_{fluid}$, it follows that $\bar{h} = k_{fluid} / L_c$, where the characteristic length L_c is the width of the gap between the plates). It can readily be seen that in this scenario, Eq. (A.3) becomes $Q = \bar{h} \cdot \Delta T = k_{fluid} \cdot \Delta T / L_c$ which is simply Fourier's law for steady-state one-dimensional conduction through a solid of uniform thermal conductivity.

A.2.1 Outer convection heat transfer coefficient

Convective heat transfer from the fabric to the ambient surroundings can occur by forced convection (resulting from external flow, such as wind, with a "free stream" velocity u_∞), free convection (driven by local buoyancy differences induced by a temperature gradient), or a combination of both. To determine which of these (or both) is significant; the Reynolds and Grashof numbers must be calculated [10,11].

$$\mathrm{Re}_L = \frac{\rho u_\infty L_c}{\mu} \tag{A.4}$$

$$Gr_L = \frac{g L_c^3 \beta \left| T_{amb} - T_{fab} \right|}{v^2} \tag{A.5}$$

where ρ is the fluid density, L_c is the characteristic length (in this case, the width of the plate w in Table 2), μ is the dynamic viscosity of the fluid, g is acceleration due to gravity, β is the coefficient of thermal expansion (reciprocal of absolute temperature for an ideal gas), and v is the kinematic viscosity (v=μ/ρ). All fluid properties are evaluated at the "film temperature," or the average of the fabric and ambient temperature. Three scenarios are possible and must be considered in estimating the average convective heat transfer coefficient:

1. The wind velocity u_∞ is sufficiently high for forced convection to dominate natural (free) convection. This is the case when $Gr_L/Re_L^2 \ll 1$. If $Gr_L/Re_L^2 < 0.1$, the average Nusselt number should be calculated based on forced convection correlations. If the Reynolds number is less than the critical Reynolds number of $Re_{crit} = 5.5 \times 10^5$, the flow is laminar and Eq. (A.6) applies. If not, the flow is turbulent and Eq. (A.7) is used [11].

$$Nu_{fc} = \frac{0.6674 Pr^{1/3} Re_L^{1/2}}{\left[1 + \left(0.0468 / Pr \right)^{2/3} \right]^{1/4}} \tag{A.6}$$

$$Nu_{fc} = \frac{0.6674 Pr^{1/3} Re_{crit}^{1/2}}{\left[1 + \left(0.0468 / Pr \right)^{2/3} \right]^{1/4}} + 0.037 Pr^{1/3} \left(Re_L^{0.8} - Re_{crit}^{0.8} \right) \tag{A.7}$$

2. In cases where the wind velocity is low, natural convection may dominate forced convection ($Gr_L/Re_L^2 \gg 1$). If $Gr_L/Re_L^2 > 10$, the dimensionless Rayleigh number ($Ra_L = Gr_L \cdot Pr$) must be calculated and used to determine the average Nusselt

number from natural convection correlations. The Rayleigh number is first used to calculate both the laminar and turbulent Nusselt numbers [11].

$$Nu_{nc,lam} = \frac{2.0}{\ln\left[1 + 2.0/\left(C_{lam} \cdot Ra_L^{1/4}\right)\right]} \tag{A.8}$$

$$Nu_{nc,turb} = \frac{C_{turb,V} \cdot Ra_L^{1/3}}{1 + \left(1.4 \times 10^9\right) \cdot Pr / Ra_L} \tag{A.9}$$

where C_{lam} and $C_{turb,V}$ are dimensionless parameters given by:

$$C_{lam} = \frac{0.671}{\left[1 + \left(0.492 / Pr\right)^{9/16}\right]^{4/9}} \tag{A.10}$$

$$C_{turb,V} = \frac{0.13 \cdot Pr^{0.22}}{\left[1 + 0.61 \cdot Pr^{0.81}\right]^{0.42}} \tag{A.11}$$

The average Nusselt number can then be determined by asymptotically averaging the laminar and turbulent Nusselt numbers through the following empirical formula:

$$Nu_{nc} = \left[\left(Nu_{nc,lam}\right)^6 + \left(Nu_{nc,turb}\right)^6\right]^{1/6} \tag{A.12}$$

3. If the Grashof number is of the same order of magnitude as the square of the Reynolds number ($0.1 < Gr_L/Re_L^2 < 10$), the average Nusselt number can be determined by asymptotically averaging the natural and forced convection Nusselt numbers from Eqs. (A.6) – (A.12) through the following empirical formula [11]:

$$Nu = \left[\left(Nu_{nc}\right)^3 + \left(Nu_{fc}\right)^3\right]^{1/3} \tag{A.13}$$

Once the average Nusselt number is determined, the outer convection heat transfer coefficient can be determined [10,11].

$$\bar{h}_o = Nu \cdot k_{fluid} / w \tag{A.14}$$

A.2.2 Convection heat transfer coefficient between skin and fabric

Similar dimensional analysis can be used to determine the inner convection heat transfer coefficient. It is assumed that the fabric is impermeable and, as such, no bulk flow exists in the space between the fabric and the skin. For the case of two vertically-oriented parallel plates, the convection coefficient will again depend on the Rayleigh number. In this case, the characteristic length is the gap between the parallel plates (b), as opposed to the plate width [10,11]:

$$Ra_b = Gr_b \cdot Pr = \frac{gb^3 \beta \left|T_{skin} - T_{fab}\right|}{v^2} \cdot Pr \tag{A.15}$$

The average Nusselt number and heat transfer coefficient will depend on the magnitude of the Ra_b compared to a critical Rayleigh number (Ra_{crit} = 1708). If $Ra_b \leq Ra_{crit}$, the viscous dissipation forces of the fluid in the gap will outweigh buoyancy-driven forces. As a result, convection cannot be established and conduction is the dominant heat transfer mode across the gap (Nu=1). For $Ra_b > Ra_{crit}$, the Nusselt number will be greater than unity due to the presence of convective flows, but the appropriate correlation depends on the magnitude of Ra_b. The overall relations for various levels of Ra_b can be summarized as [11]:

$$Nu = 1 \qquad\qquad\qquad\qquad\qquad Ra_b \leq 1708 \qquad\qquad (A.16)$$

$$Nu = 0.42 Ra_b^{1/4} Pr^{0.012} \left(a/b\right)^{-0.3} \qquad 1708 < Ra_b \leq 10^6 \qquad\qquad (A.17)$$

$$Nu = 0.046 Ra_b^{1/3} \qquad\qquad\qquad 10^6 < Ra_b \leq 10^9 \qquad\qquad (A.18)$$

Once the average Nusselt number is determined from Eqs. (A.16) – (A.18), the average inner convection coefficient between the skin and the fabric can be determined [10,11]:

$$\overline{h_i} = Nu \cdot k_{fluid} / b \qquad\qquad\qquad\qquad (A.19)$$

A.2.3 Determination of skin temperature

The human skin consists of the inner dermis and the outer epidermis, which are roughly 2 mm and 0.15 mm thick, respectively. The epidermis thermal conductivity ($k_{epidermis}$) is 0.21 W/m·K [14]. It is assumed that the dermis is maintained at the consistent temperature of 35°C due to vasoconstriction and vasodilation. However, it is necessary to account for the temperature drop across the epidermis where there is no blood vessel or capillary thermoregulation.
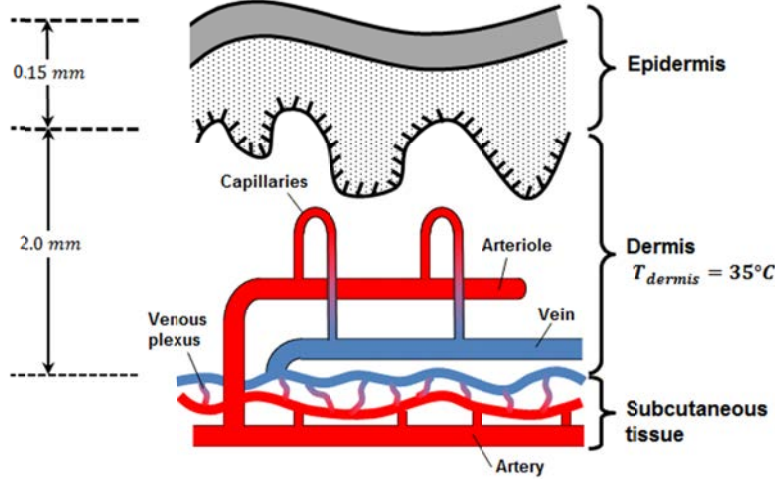
Fig. A-2.   Skin vascular system (adapted from Guyton and Hall, 2000) [14].

The epidermis is modeled as a solid material experiencing one-dimensional, steady-state conduction. As such, the heat flow from the dermis must match the net heat leaving the skin towards the fabric ($Q_{loss,net} = Q_i + J_{sf} - J_{fs}$). Fourier's law of conduction then can be used to determine the temperature drop across the epidermis:

$$T_{skin} = T_{dermis} - \left[Q_i + J_{sf} - J_{fs} \right] \cdot t_{epidermis} / k_{epidermis} \qquad\qquad (A.20)$$

Engineered Emissivity of Textile Fabrics by the Inclusion of Ceramic Particles

Dr. David Anderson, Matthew Pooley, Haskell Beckham and Dr. James F Brennan

Engineered emissivity of textile fabrics by the inclusion of ceramic particles

Matthew A. Pooley,[1,*] David M. Anderson,[2] Haskell W. Beckham,[3] and James F. Brennan III[4]

[1]*Electrical Engineering and Computer Science, Exponent, Inc., 420 Lexington Avenue, Suite 1740, New York, New York 10170, USA*
[2]*Thermal Sciences, Exponent, Inc., 3350 Peachtree Road NE, Suite 1125, Atlanta, Georgia 30326, USA*
[3]*Polymer Science and Materials Chemistry, Exponent, Inc., 3350 Peachtree Road NE, Suite 1125, Atlanta, Georgia 30326, USA*
[4]*Electrical Engineering and Computer Science, Exponent, Inc., 3350 Peachtree Road NE, Suite 1125, Atlanta, Georgia 30326, USA*
[*]*mpooley@exponent.com*

Abstract: Composite textile materials, created from a blend of different fibers, have long been used to engineer the properties and performance of fabrics to combine comfort with functionality, such as to create materials with differing optical properties. Some changes to the optical properties of materials in the infrared are subtle and difficult to measure. We present a measurement technique, experimental apparatus, and associated data analysis procedure for detecting small changes in the emissivity of fabrics in the mid-infrared wavelength range (7.5–14 µm). Using this technique, we demonstrate that the emissivity of polyester fabric can be engineered controllably via the inclusion of ceramic microparticles within the fabric fibers.

References and links

1. S. B. Warner, *Fiber Science* (Prentice Hall, 1995), pp. 213–229.
2. W. H. Hills, "Apparatus for making profiled multi-component yarns," US Patent, No: 5344297 (1994).
3. X. Hu, M. Tian, L. Qu, S. Zhu, and G. Han, "Multifunctional cotton fabrics with graphene/polyurethane coatings with far-infrared emission, electrical conductivity, and ultraviolet-blocking properties," Carbon **95**, 625–633 (2015).
4. ISO 20473:2007(E), *Optics and Photonics – Spectral Bands*, (International Organization for Standardization, 2007).
5. F. P. Incropera and D. P. Dewitt, *Fundamentals of Heat and Mass Transfer*, 5th ed (John Wiley & Sons, 2002), pp. 713–717.
6. D. D. Horinek and M. E. Foumberg, "Lightweight x-ray and gamma radiation shielding fibers and compositions," US Patent Application Publication, No: 2013/0045382 A1 (2013).
7. ASTM D1777–96 (2015), *Standard Test Method for Thickness of Textile Materials*, (ASTM International, 2015).
8. ASTM D3776 / D3776M–09 (2013), *Standard Test Methods for Mass Per Unit Area (Weight) of Fabric*, (ASTM International, 2013).
9. S. Schleimann-Jensen and K. Forsberg, *New Test Method for Determination of Emissivity and Reflection Properties of Protective Materials Exposed to Radiant Heat* (ASTM International, 1986).

1. Introduction

Optical properties of textile fibers can be modified by incorporating a large variety of dyes and other additives, varying the fiber cross-sectional shape, or co-spinning of multi-materials [1,2]. The optical properties of the fabrics constructed from fibers are related to the fiber optical properties. While this has been extensively studied for optical properties in the visible region, less has been published on the optical properties of fabrics and other engineered fibrous structures in the infrared regime. Optical properties of fabrics in the infrared regime

are of current commercial interest. Manipulation of the infrared absorption and emission characteristics of fabrics may find applications across a range of different fields, for example in radiative heat management systems that require flexible surfaces or in thermal camouflage coverings.

In the work presented in this article, the infrared optical effects resulting from incorporation of ceramic particles within polyester fibers utilized in textile fabrics were studied. In particular, changes in the mid-infrared (MIR) emissivity of fabrics that are knitted with differing amounts of ceramic-bearing fibers were investigated. Specifically, we developed a method to measure the emission of textile fabrics between 7.5 and 14 μm. While this region is sometimes referred to as the far-infrared (FIR), especially in the textile field [3], we are using the ISO definition of the divisions of the infrared spectrum [4], and therefore will refer to this region as the MIR in this report. The method we present incorporates spatially resolved radiance imaging and data analysis techniques to enable increased sensitivity when measuring small differences in emissivity between samples.

The amount of radiation emitted from an object at a given temperature, T, is proportional to the emissivity, ϵ, of the surface. Ideal emitters, known as black bodies, have an emissivity of 1 and emit a power spectrum as a function of wavelength, λ, described by Planck's law [5]

$$P(\lambda, T) = \frac{2hc^2}{\lambda^2 \left(\exp\left(hc \middle/ k_B T \right) - 1 \right)},\tag{1}$$

where h, c, and k_B are the Planck constant, the speed of light in a vacuum, and Boltzmann's constant, respectively. The radiance of a black body, W_b, is given by the integral of the power spectrum, $W_b = \int P(\lambda, T) \, d\lambda$.

Non-ideal emitters, such as the fabric samples in this study, have an emissivity of $0 < \epsilon < 1$, which may vary with temperature and wavelength. If the ranges of wavelengths and temperatures under investigation are narrow compared to the spectral variability of the object, a useful approximation is to assume that the object is a grey body and exhibits a temperature-dependent radiance given by

$$W_g(T) = \epsilon W_b(T).\tag{2}$$

The radiance of an object is thus determined by both the object temperature and its emissivity. Consequently, manipulation of an object's emissivity enables the total radiated power of an object at a given temperature to be varied.

In the present study, we approximate textile fabrics as grey body emitters and test this assumption over temperature ranges of interest. We measure fabrics that were engineered to have varying degrees of emissivity in the MIR and show that, by including ceramic particles in the core of the fibers used in the fabric, the MIR emissivity can increase over 2%. We observed a statistically significant positive correlation between the amount of ceramic-bearing fibers added to the fabric and the increase in emissivity.

2. Sample information

Fabric samples, made from fibers produced by Hologenix, LLC (Santa Monica, CA), contained varying amounts of ceramic-bearing polymeric fibers. These specialty fibers are similar in construction to multimode optical fibers, except the core of the fiber is a blend of polyethylene terephthalate (PET, i.e., polyester) and ceramic particles (e.g., titanium dioxide), and the cladding of the fiber, which dictates visual appearance and shields the fiber core [6], is PET. Fabrics were knitted using differing amounts of the ceramic-containing fibers to produce fabrics with three different compositions, along with a control fabric that contained no added specialty fibers. All the fabrics were reported to contain 8% elastane fibers, with the

remaining 92% made from polyester or a blend of polyester and ceramic-containing polyester fibers. The fabrics were nominally identical except for the percentage of ceramic-containing polyester fibers.

The ceramic content of the fabrics was measured using an ash analysis technique. Approximately 2 g of each fabric was heated in air at 850°C for 2.5 hours to burn off the polyester and elastane fibers. The mass remaining was composed of the inorganic material contained by the samples. The increased percentage mass remaining of the three ceramic-bearing samples, compared with that of the control sample, gives the percentage mass of these fabrics due to the additional ceramic particles. Table 1 shows the ceramic content, along with the thickness, measured in general accordance with the American Society for Testing and Materials (ASTM) standard ASTM D 1777 [7] under a mass delivering 0.045 g/mm^2 of pressure, and the basis weight, measured in general accordance with ASTM D 3776 [8] for each of the four sample fabrics.

Table 1. Physical Properties of Sample Fabrics [a]

Sample No.	Thickness (mm)[b]	Basis weight (g/m^2)[c]	Ceramic content (% mass)
1	0.58	152	1.22 ± 0.04
2	0.58	152	1.03 ± 0.06
3	0.59	156	0.53 ± 0.03
4	0.58	150	0

[a]Sample 4 is the control and contains no ceramic material; samples 3 to 1 contain increasing amounts of ceramic material as indicated. Errors bars are derived from the standard deviation of multiple measurements.
[b]Thickness was measured under a compression of 0.045 g/mm^2; standard deviations are $\leq$ 0.01 mm.
[c]Standard deviations are $\leq$ 3 g/m^2.

Optical microscopy was used to confirm that all the fabric samples exhibited the same color, knit structure, and texture, as shown in Fig. 1.
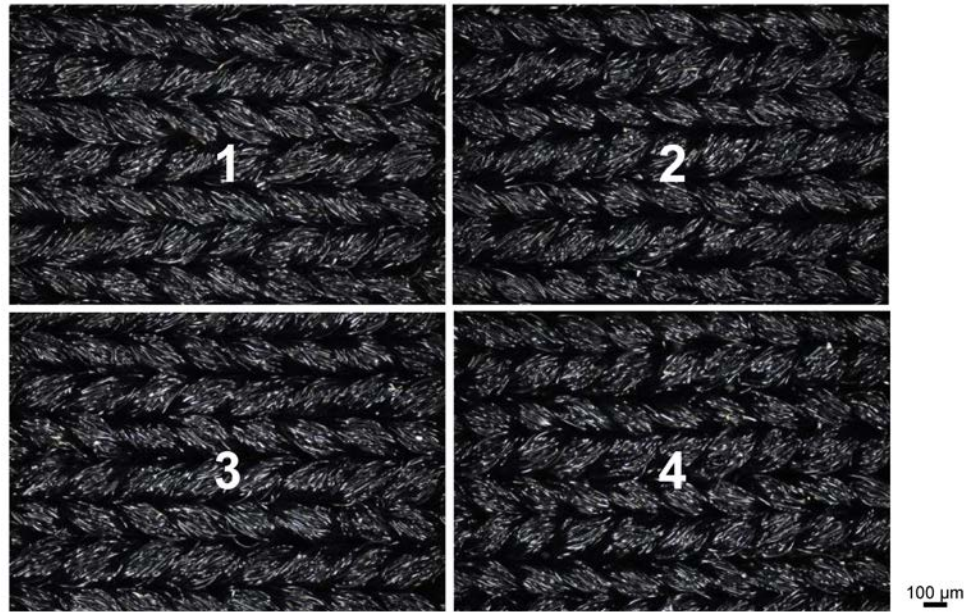
Fig. 1. Color optical microscope images of the fabric samples confirm that all samples have the same color and knit structure. Sample identifier numbers are overlaid in white.

3. Experimental details

Briefly, we used an MIR-sensitive camera to measure the infrared emission from a set of fabric samples as they were all held at the same temperature, as shown in Fig. 2. To obtain statistically significant results, we used temporal averaging over 50 images to reduce the effects of pixel noise and spatial averaging to reduce effects due to variations across fabric surfaces. Finally, the spatially and temporally averaged infrared emission values were used, in conjunction with measured values for blackbody and background ambient reflected radiation, to calculate the emissivity of each fabric sample.

3.1. Experimental apparatus

As shown in Fig. 2(a), four fabric samples, nominally 32-mm-square swatches, were placed on a 152.4-mm-diameter copper disk, with all samples being placed at the same radial distance from the disk center and each sample positioned within its own 72° segment. A plate of polished brass (emissivity of 0.03 [9]) was placed in the remaining segment to act as a surface with approximately 100% reflectivity. To provide good thermal contact between the copper disk and the samples, the fabric and brass were adhered to the copper disk using thermal paste with a conductivity of 0.92 W/m•K. A uniform and consistent thickness of the thermal paste was ensured by first placing a thin template with a square cutout matching the dimensions of the fabric sample on the copper disk, then using a blade extended across the template to pull the paste down the application area. Upon removal of the template, a square section of paste with a thickness matching that of the template was left behind. To ensure that each fabric sample was placed on the thermal paste with uniform contact pressure, a 19-mm-thick copper square with dimensions matching that of the fabric sample was briefly placed on top of each fabric sample once it was situated on top of the thermal paste. To aid with the automatic image analysis described below, the brass plate was framed with high emissivity tape.

    A circular resistive heating pad (Omega P/N SRMU0206D-P) with a diameter equal to that of the copper disk was placed under the copper disk and connected to a variable voltage supply (Payne Controls, McMaster-Carr P/N 3641K43). The cylindrical symmetry of the apparatus helped ensure that each sample position was exposed to nominally identical thermal conditions during the experiment. To confirm a uniform, and minimum in magnitude, radial temperature gradient, six high-aspect-ratio holes (3.18-mm diameter by 19-mm deep) were drilled into the 25.4-mm-thick copper disk: one in the disk center and five near the edge of the disk in the angular centers of each of the 72° segments. These holes acted as blackbody resonant cavities, with an effective emissivity of 1, and enabled accurate measurement of the local temperature and maximum possible (i.e., blackbody) emissive power of the heated copper disk. Using the measured cavity temperature of each hole, the maximum deviation in temperature from center to edge of the disk was measured to be less than 0.2°C for a nominal disk temperature of 35°C. The deviation in temperature between the outer holes in different segments was measured to be less than 0.1°C, confirming uniform thermal conditions for all sample positions.
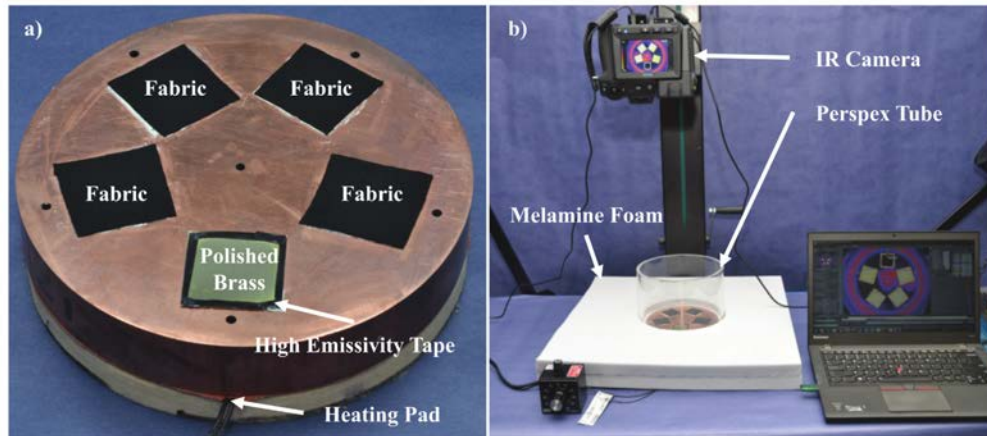
Fig. 2. Experimental apparatus: a) samples mounted to copper disk, four fabric samples containing different amounts of ceramic additive and one highly reflective brass plate are positioned around the disk at a constant radial distance; b) the copper disk within the measurement rig, an infrared camera is positioned above the disk, melamine foam reduces the radial temperature gradient of the copper and a clear acrylic tube limits convection.

Figure 2(b) shows the experimental apparatus configuration used for measurements. The copper disk was surrounded in melamine foam to reduce the radial temperature gradient, and a clear poly(methyl methacrylate) (PMMA) cylindrical tube was mounted around the copper disk to limit the effects of convective heat transfer in the vicinity of the samples. A scientific grade thermal imaging camera (FLIR Systems, Inc., Model T650sc, Wilsonville, OR) was mounted directly over the samples to acquire images at an angle normal to the surface of the copper disk. The camera was set to detect the radiance in the MIR wavelength range between 7.5 – 14.0 μm using a 640 x 480 array of microbolometer sensors with a pitch of 25 μm, and the vertical distance between the camera and the samples was 430 mm.

3.2. Measurement methodology and image processing

With the samples mounted, the copper disk was heated to a nominal temperature of 35°C by adjusting the voltage controller. For these thin fabrics with a ~0.6-mm measured thickness, it was assumed that the temperature gradient across the thickness of the fabric could be neglected. At thermal equilibrium, the temperature of the fabric surface was taken to be equal to that of the copper disk, and differences in radiance measured were due solely to emissivity differences of the materials.

Once the copper disk and fabric samples reached a temperature of 35°C and stabilized for a minimum of 1 minute, a series of 50 images were acquired by the camera at a frequency of 7.5 Hz. The images were processed to create a single composite image in which each pixel is the mean radiance of the corresponding pixels in every image within the series. This process was used to temporally average the images, thereby smoothing out random noise fluctuations in the camera sensors to increase the signal-to-noise ratio.
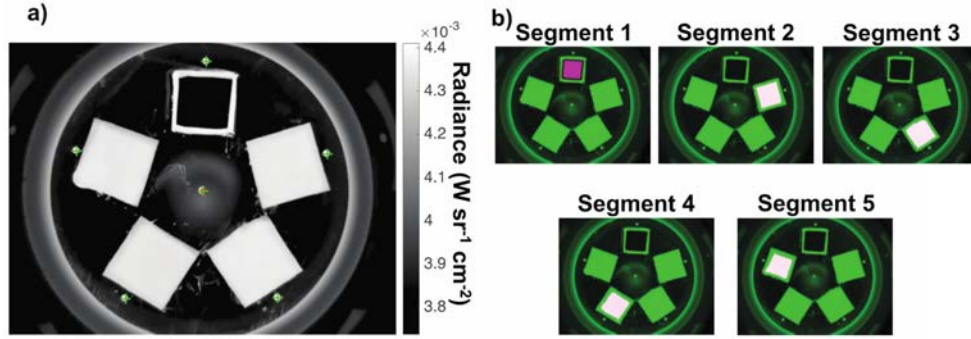
Fig. 3. Example composite radiance image and regions extracted for analysis: a) The fabric samples, cavity holes, and the tape framing the brass plate show up as regions of high radiance. The position of the cavity holes and the center of the copper disk, as detected by the automatic image analysis are indicated with green crosses and a red circle, respectively; b) The regions from which radiance data were extracted from each segment are indicated with fabric surface regions shown in white and the brass region shown in pink.

The spatial average of the radiance over the surface of each sample was extracted from the composite image via an image processing analysis technique. An example composite image is shown in Fig. 3(a), the location of the cavity holes and the disk center are indicated with green crosses and a filled red circle, respectively. Using the disk center, the copper disk was divided into equal-sized 72° segments that each contained one sample position. Thresholding and image masking techniques were used to extract and average the values of the pixels from each of the fabric samples and the brass plate. To avoid capturing any emission from the thermal paste, which can extrude slightly beyond the edge of samples, values near the edge of the sample regions were not included in the spatial averaging. Figure 3(b) shows the image from Fig. 3(a) with the regions from which radiance values were extracted for each of the fabric samples and the brass plate indicated. The spatial averaging, which reduces the measurement variation over the surface of the samples due to fabric sample properties, allowed an average value of detected radiance to be extracted from each fabric sample and the brass plate. In addition, the radiance values from the six cavity holes were calculated.

The emissivity of the fabric samples was calculated from the average detected radiance values. Other laboratory measurements have confirmed that the fabrics are opaque to this region of infrared radiation, so it is a valid assumption that no radiation from the copper disk penetrates the fabric. The detected radiance from a given fabric sample, W_d, was taken to be comprised of two components: radiation directly emitted by the fabric sample and ambient radiation that is reflected from the fabric sample. The radiance due to emission from the fabric is the product of the radiance of a black body at the sample temperature, taken as the average radiance from the cavity holes in the copper block, and the emissivity of each sample surface. The radiance due to the reflected ambient radiation, W_a, was calculated as the average detected radiance from the polished brass plate with a reflectivity of ~1. Thus, the emissivity of each fabric sample was obtained as

$$W_d = \epsilon W_b + (1-\epsilon) W_a$$
$$\Rightarrow \epsilon = \frac{W_d - W_a}{W_b - W_a}, \tag{3}$$

where ϵW_b is the component directly emitted by the fabric and $(1-\epsilon) W_a$ is the component reflected from the fabric sample due to ambient radiation from the surrounding environment. Note that as the sample temperature approaches the ambient room temperature, W_a

approaches W_d and W_b, leading to a reduction in the signal-to-noise ratio for the measured emissivity. Thus, Eq. (3) dictates that measurements using this experimental method must be made at sample temperatures that are above or below the ambient room temperature.

The above experiment was repeated several times with different fabric samples in each position of the copper block. Since the magnitude of the measured changes in emissivity were small, the cumulative measured emissivity results were monitored, using the standard deviation for each fabric type, to estimate the reliability of the measured emissivity values as data were accumulated. After 12 experimental runs, it was determined that further repeated measurements were yielding little change to the average calculated emissivity of each sample and would therefore not increase the measurement reliability. For each experimental run, the location of the different samples was varied to ensure that any measured changes in infrared emissive power were not due to non-ideal cylindrical symmetry of the sample thermal environment.

4. Results and discussion

Figure 4 shows the emissivity of the fabric samples as a function of the percentage mass of ceramic material in the fabric, x_c. The data points are the mean value of the 12 independent measurements and the error bars have a length of one standard deviation above and below the mean. A linear fit to the data yields a trend line described by $\epsilon = 0.0148x_c + 0.9039$, and the resulting line of best fit to these mean values, shown in black on the figure, has an R^2 value of 0.976.
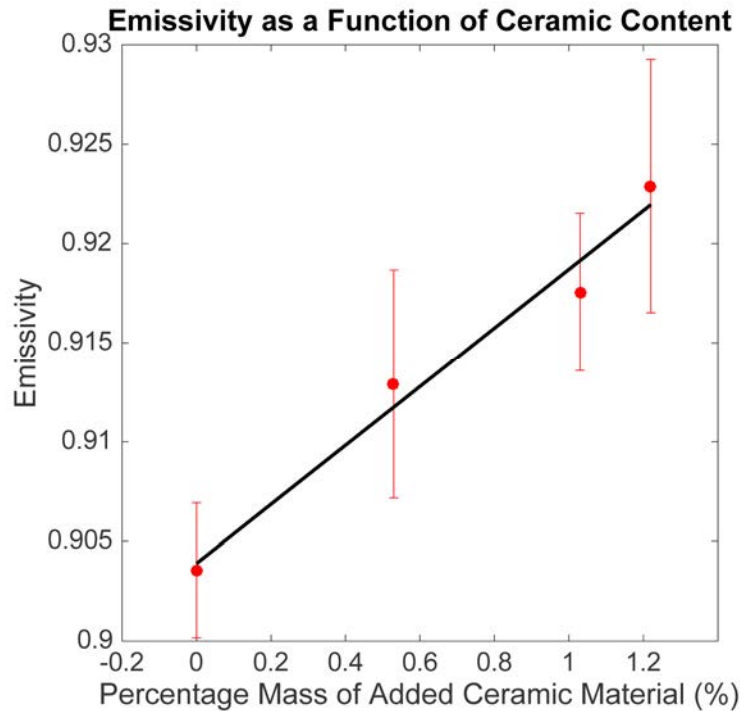
Fig. 4. Emissivity of the fabric samples as a function of the percentage mass of added ceramic material. Data points are the mean of 12 independent measurements and the error bars a range of one standard deviation above and below the data point values. The black line shows a linear fit to the data with an R^2 value of 0.976.

The emissivity of the fabric is 0.904 ± 0.003 when the fabric contains no added ceramic particles, 0.913 ± 0.006 when the fabric contains 0.53 ± 0.03 wt% added ceramic particles,

0.918 ± 0.004 when the fabric contains 1.03 ± 0.06 wt% added ceramic particles, and 0.923 ± 0.006 when the fabric contains 1.22 ± 0.04 wt% added ceramic particles. When ceramic material is added to be 1.22% of the fabric mass, the emissivity is increased by 2.1% over the case where no additional ceramic is added to the polyester/elastane blend.

The experimental methods described above were used to investigate the effects of temperature on the fabric sample that contained 1.22% added ceramic material by mass, achieved by mounting four samples of the 1.22% fabric on the copper disk, along with the high reflectivity brass plate. Figure 5 shows that the resulting emissivity is independent of temperature over the wavelength range of 7.5 – 14 μm; there is no statistically significant correlation between the emissivity and temperature with a p-value for linear correlation of 0.216.
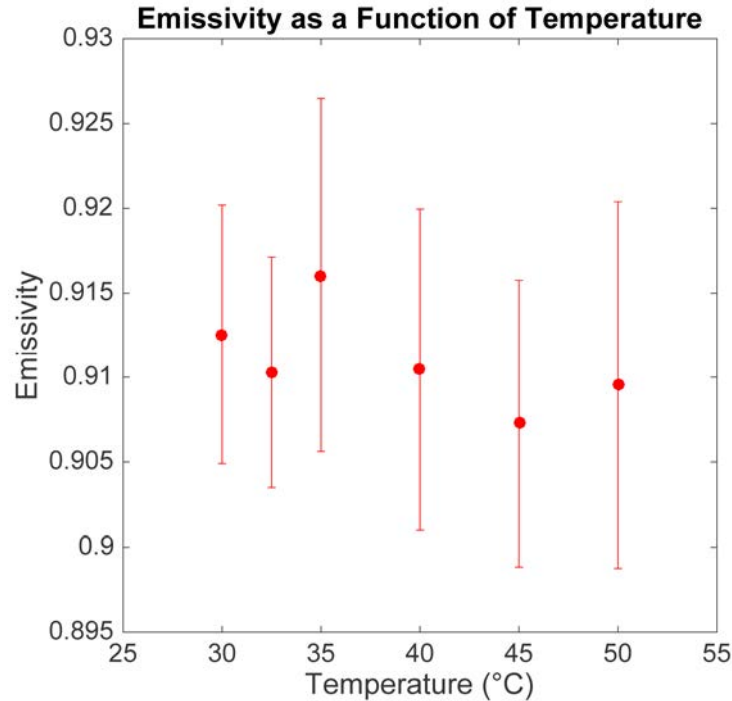
Fig. 5. Emissivity of the fabric containing 1.22% mass of added ceramic particles as a function of temperature over the wavelength range of 7.5 – 14 μm.

These experiments center on the range of temperatures that may be encountered by fabrics in garments during typical wearing activities in temperate climates. The increase in emissivity as more ceramic is incorporated into the fabric, combined with the temperature-independent nature of the emissivity, offer encouragement that these results may be extrapolated to a broader range of scenarios involving more extreme temperature ranges and larger ceramic contents.

This methodology for measuring small variations in the emissivity of fabric surfaces, and possibly other surfaces, may find applications across a variety of fields ranging from textile technology to research into the properties and deposition of thin-film materials. An immediate application of this work is to use the techniques detailed above to investigate the emissive properties of other fabrics, such as cotton or man-made fibers. This could enable, for example, effects on the thermal performance of garments due to modifications of fabric structure, surface texture or coating, and fiber or additive content, to be assessed. In addition, such investigations could be used to optimize fabric structure or composition for use in specific thermal conditions.

Far Infrared Radiation (FIR): Its Biological Effects and Medical Applications

Dr. Michael R Hamblin and Dr. Fatma Vatansever

PHOTONICS & LASERS IN MEDICINE

FREE ONLINE ACCESS
TO **VOLUME 1** AVAILABLE AT
WWW.DEGRUYTER.COM/PLM
TOKEN: FLAVOR

TOPIC ISSUE
LOW-LEVEL LASER THERAPY

ISSUE EDITORS
Michael R. Hamblin
Arkady Mandel

EDITORS-IN-CHIEF
Frank Frank
Lothar Lilge
Carsten M. Philipp
Ronald Sroka

DEUTSCHE GESELLSCHAFT
FÜR LASERMEDIZIN e.V.

schweizerische arbeitsgemeinschaft für laserchirurgie

Fatma Vatansever and Michael R. Hamblin*

Far infrared radiation (FIR): Its biological effects and medical applications

Ferne Infrarotstrahlung: Biologische Effekte und medizinische Anwendungen

Abstract

Far infrared (FIR) radiation (λ=3–100 μm) is a subdivision of the electromagnetic spectrum that has been investigated for biological effects. The goal of this review is to cover the use of a further sub-division (3–12 μm) of this waveband, that has been observed in both *in vitro* and *in vivo* studies, to stimulate cells and tissue, and is considered a promising treatment modality for certain medical conditions. Technological advances have provided new techniques for delivering FIR radiation to the human body. Specialty lamps and saunas, delivering pure FIR radiation (eliminating completely the near and mid infrared bands), have became safe, effective, and widely used sources to generate therapeutic effects. Fibers impregnated with FIR emitting ceramic nanoparticles and woven into fabrics, are being used as garments and wraps to generate FIR radiation, and attain health benefits from its effects.

Keywords: far infrared radiation; radiant heat; black body radiation; biogenetic rays; FIR emitting ceramics and fibers; infrared sauna.

Zusammenfassung

Ferne Infrarotstrahlung (far infrared, FIR) (λ=3–100 μm) ist ein Unterbereich des elektromagnetischen Spektrums, der hinsichtlich seiner biologischen Effekte von wissenschaftlichem Interesse ist. Das vorliegende Review konzentriert sich auf den Spektralbereich von 3–12 μm, der sowohl in *In-vitro-* als auch in *In-vivo*-Studien mit Blick auf die Stimulation von Zellen und Gewebe untersucht wurde und der eine vielversprechende Behandlungsmodalität für verschiedene medizinische Konditionen darstellt.

Dank des technischen Fortschrittes konnten verschiedene neue Techniken zur Applikation von FIR-Strahlung am menschlichen Körper entwickelt werden. Spezielle Lampen und Saunas, die reine FIR-Strahlung (ohne Anteile von Nahinfrarot- und Mittelinfrarotstrahlung) liefern, sind immer sicherer und effektiver geworden und werden verbreitet für therapeutische Zwecke genutzt. Fasern, die mit FIR-emittierenden Keramik-Nanopartikeln imprägniert und zu Stoffen weiterverarbeitet werden, finden Verwendung als Kleidung oder Verbandsstoffe, die aufgrund der generierten FIR-Strahlung gesundheitliche Vorteile bewirken können.

Schlüsselwörter: Ferne Infrarotstrahlung (FIR); Strahlungswärme; Schwarzkörperstrahlung; biogenetische Strahlen; FIR-emittierende Keramiken und Fasern; Infrarotsauna.

*Corresponding author: Michael R. Hamblin, Wellman Center for Photomedicine, Massachusetts General Hospital, Boston, MA, USA, e-mail: hamblin@helix.mgh.harvard.edu
Michael R. Hamblin: Department of Dermatology, Harvard Medical School, Boston, MA, USA; and Harvard-MIT Division of Health Sciences and Technology, Cambridge, MA, USA
Fatma Vatansever: Wellman Center for Photomedicine, Massachusetts General Hospital, Boston, MA, USA; and Department of Dermatology, Harvard Medical School, Boston, MA, USA

1 Introduction

All living organisms are subjected to the natural electromagnetic radiation reaching the earth from the sun. Living organisms experience the beneficial as well as adverse effects of it at all levels, starting from sub-cellular organelles and ending with the whole body. Thermal radiation (or infrared) is a band of energy in the complete electromagnetic spectrum and it has been used effectively for millennia to treat/ease certain maladies and discomforts. Heated saunas are only one of the avenues (and perhaps the oldest)

to deliver the radiation in a controlled environment and within a convenient treatment time. With the development of better technology to deliver pure far infrared radiation (FIR), the benefits from its effects have widened. Nowadays, specialty FIR emitting heat lamps and garments made up of filaments (fibers) impregnated with FIR emitting nanoparticles are becoming used to deliver these thermal radiation effects. In this paper we explore the use of FIR as a promising treatment modality for certain medical conditions. We cover both traditional applications and novel applications, and survey the latest technological advancements and most recent scientific studies in the field.

1.1 What is FIR radiation?

With respect to the complete electromagnetic radiation spectrum, the infrared radiation (IR) band covers the wavelength range of 750 nm–100 μm, frequency range of 400 THz–3 THz, and photon energy range of 12.4 meV–1.7 eV. It lies between the long wavelength red edge of the visible and the short edge of the terahertz (starting at 3 THz) spectral bands (Figure 1).

The classification of the International Commission on Illumination (CIE) has three sub-divisions for the IR radiation as given in Table 1. An alternative classification provided in ISO 20473 standard for the sub-division of the IR ranges is given in Table 2.

In the IR radiation bands, only FIR transfers energy purely in the form of heat which can be perceived by the thermoreceptors in human skin as radiant heat [1]. Not only is FIR absorbed by the human body but it is also emitted by the body in the form of black body radiation (3–50 μm with an output peak at 9.4 μm).
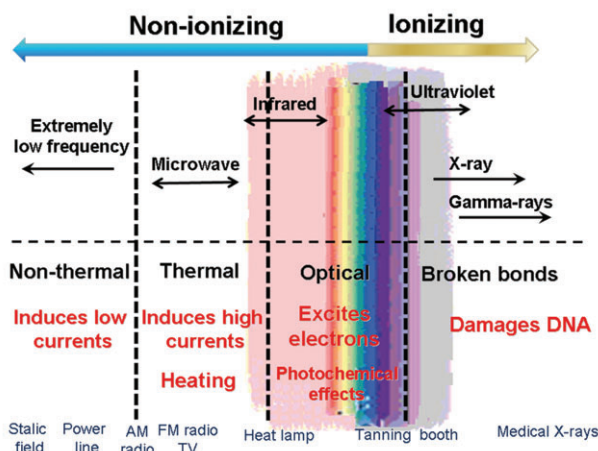
Figure 1 The spectrum of electromagnetic radiation and some biological changes it may induce.

Name/abbreviation	Wavelength	Photon energy (THz)
Near infrared/IR-A	0.7–1.4 μm (700–1400 nm)	215–430
Mid infrared/IR-B	1.4–3.0 μm (1400–3000 nm)	100–215
Far infrared/IR-C	3.0–100 μm (3000 nm–0.1 mm)	3–100

**Table 1** CIE classification of IR radiation.

The term "black body" was first used by Gustav Kirchoff in 1860. In essence, all matter absorbs electromagnetic radiation to some degree and an object that absorbs all radiation falling on it (at all wavelengths and frequencies) is called a black body, i.e., a perfect absorber. When a black body is at a uniform temperature state, it emits back this absorbed energy, and it is termed as "black body radiation". This is a type of radiation and has continuous frequency/intensity which depends only on the black body's temperature, and the type of spectrum it generates is called the Planck spectrum. In this type of spectrum, spectral peaks at characteristic frequencies are shifted to higher values (shorter wavelengths) with increasing temperature values. For instance, at room temperature most of the emission of the black body is in the infrared region of the electromagnetic spectrum. At a typical environmental background temperature, which is around 300 K, the peak emission is at about 9.7 μm (and the curve covers the FIR region as well); at around 1800 K (temperature of molten steel), the peak is shifted to 1.6 μm; at around 6000 K (surface temperature of the sun), the peak is shifting even further, 0.48 μm, which now is in the visible (blue) region of the spectrum. Peak shifts of some representative black body temperatures and the range of electromagnetic radiation they fall into are given in Figure 2A, B. This type of shift in the emission peaks of the black bodies (to shorter wavelengths at higher temperatures) is governed by Wien's displacement law.

1.2 Biological effects of FIR

FIR application in medicine requires understanding and knowledge of the interactions of electromagnetic

Name/abbreviation	Wavelength (μm)
Near IR, NIR	0.78–3
Mid IR, MIR	3.0–50
Far IR, FIR	50–1000

Table 2 ISO 20473 standard for sub-division of the IR.
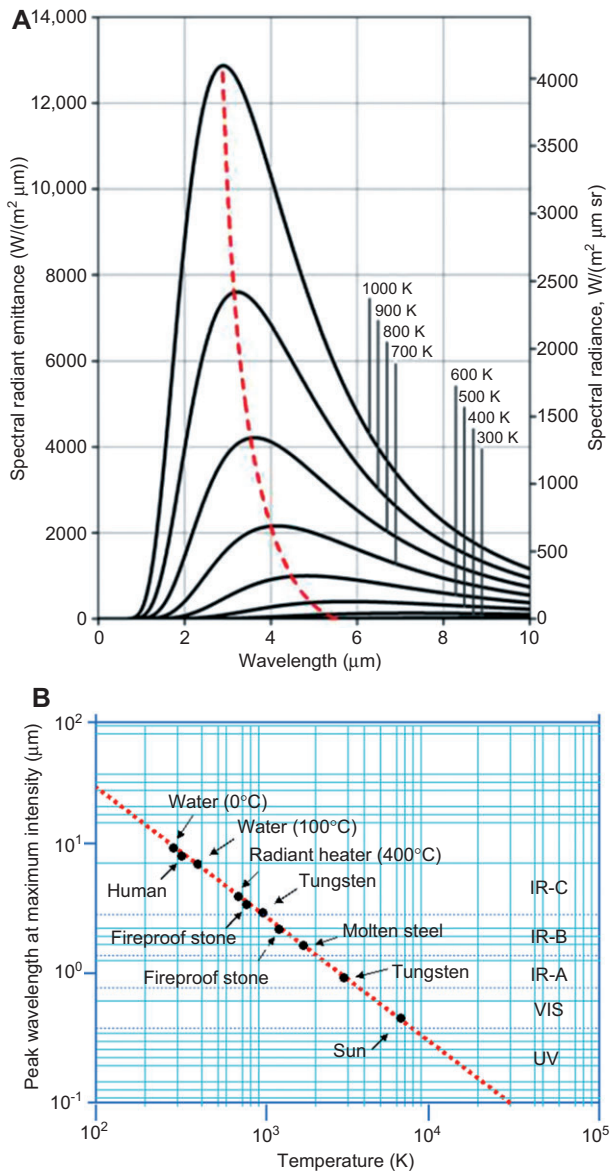
Figure 2 (A) Planck's law. Dependence of spectral radiant emittance (ωλ) for perfect black bodies as a function of wavelength (λ). (B) Wien's displacement law. The wavelength of maximal radiant exitance (λ$_{max}$) as a function of the absolute temperature (T) for a perfect black body (dashed line) and different bodies.

radiation at FIR range with biological structures (including cells, cell membranes, cell fluids – especially water, DNA/proteins) and functioning of the living systems in general. At the cellular level, the underlying biophysical mechanisms of the interaction of electromagnetic radiation with living cells can be framed in terms of altered cell membrane potentials and altered mitochondrial metabolism [2]. FIR energy (photons with quantum energy levels of 12.4 meV–1.7 eV) is absorbed by vibrational levels of bonds in molecules. There are six vibrational modes

covering symmetric and antisymmetric stretching, scissoring, rocking, wagging and twisting. Considering the high concentration of water in biological systems, association of water molecules with ions (solvation effect), the dielectric properties of the water and the large dipole moment that this effect generates, this will be a dominant factor in biological solutions. It is known that at lower frequencies water molecules are able to rotate freely in an oscillating electric field with little or almost no energy loss. However, if the frequency of the electric field reaches 10^8 Hz levels, the rotational mode becomes hindered (due to "dielectric friction" effect) and the absorbed energy starts dissipating by collision or nearest neighbor interactions in the media [2]. The dielectric relaxation of water at 310 K is around 25 GHz where the rotational response of the dipoles to the electromagnetic field is spread over a broad frequency range.

In living systems, in addition to the water molecules association with the electromagnetic field and effects of that, one has to consider the "meso-structure" effect where proteins and charged groups (located at specific sites on the proteins) are crucial for the overall biological activity. These specifically located charged groups associate with the water molecules and by doing this influence the dielectric behavior of the whole molecular-assembly, which in turn effects its biologic functioning. Thus, the dielectric properties of tissues (even at cellular level) depend on and vary with the water content. In addition, the relaxation of these molecular "meso-structures" can show variations with frequency. For these reasons, water content is a critical factor in the interaction between FIR and living organisms.

In this regard, the dynamics of water-clusters has attracted considerable interest since there is a noticeable difference with respect to the dynamics of bulk-liquid-water, and this may have significant implications in biological environments. Local changes in the molecular environment (caused by solvation or confinement) are shown to affect substantially the translational and vibrational modes in FIR frequency range. It is found that water cluster size and temperature affect the FIR absorption spectrum significantly [3].

2 Medical applications of FIR

For FIR used as a therapeutic modality the alternative terms "biogenetic radiation" and "biogenetic rays" have been coined and widely used in the popular literature. FIR wavelength is too long to be perceived by

the eyes, however, the body experiences its energy as a gentle radiant heat which can penetrate up to 1.5 inches (almost 4 cm) beneath the skin. FIR energy is sufficient to exert rotational and vibrational modes of motion in bonds forming the molecules (including the water molecules) as well as resonate with cellular frequencies. Resulting epidermal temperature is higher when the skin is irradiated with FIR than if similar thermal loads from shorter wavelengths are used. The prolonged erythermal response due to FIR exposure has been proposed to be due to increased epidermal temperatures associated with it, but levels of FIR that do not produce any detectable skin heating can also have biological effects.

2.1 Biomedical laboratory studies using FIR sources

2.1.1 FIR heat lamps

There have been many attempts to use FIR as a therapeutic intervention where devices known as "infrared heat lamps" that emit more or less FIR are been used. Unfortunately, "pure" FIR emitting lamps are expensive, and thus, in some instances lamps that have "mixed" emission, i.e., emit in shorter (mid infrared, MIR; near infrared, NIR and even visible light) wavelength ranges are been used. A common type of specialized infrared heat lamp emits 2–25 μm radiation. IR saunas are often used and the most effective types have ceramic FIR emitting panels that remain cool to the touch. However, most IR saunas on the market do not use the expensive FIR panels, which can be touched since they remain always cold.

There have been a few laboratory studies that have reported the biological effects of FIR. A recent important paper describes the *in vitro* use of an FIR generator (WS TY-301R®; M/s WS Far Infrared Medical Technology Co., Ltd., Taipei, Taiwan; see Figure 3) as a radiation source to irradiate human umbilical vein endothelial cells (HUVECs) [4]. In the study, FIR exposure (a low non-thermal irradiance) of 0.13 mW/cm² for 30 min inhibited proliferation and the vascular endothelial growth factor (VEGF)-induced phosphorylation of extracellular signal-regulated kinases in HUVECs. Furthermore, FIR exposure induced the phosphorylation of endothelial nitric oxide synthase (eNOS) and nitric oxide (NO) generation in VEGF-treated HUVECs. Both VEGF-induced NO and reactive oxygen species (ROS) generation was involved in the inhibitory effect of FIR. Nitrotyrosine formation increased significantly in HUVECs treated with

Figure 3 Medical FIR sources. (A) WS TY-301R® and (B, C) WS TY-101N® FIR lamps (both by WS Far Infrared Medical Technology Co., Ltd., Taipei, Taiwan).

VEGF and FIR together. Inhibition of phosphoinositide 3-kinase (PI3K) by wortmannin abolished both the FIR-induced phosphorylation of eNOS and serine/threonine-specific protein kinase in HUVECs. In addition to that, FIR exposure upregulated the expression of PI3K p85 at the transcriptional level. It was observed that FIR exposure induced the nuclear translocation of promyelocytic leukemia zinc finger protein in the cells. These data provide information on how FIR exposure could affect microcirculation, independent from thermal effects. The same group had previously shown that non-thermal FIR therapy increased skin blood flow in rats [5]. Toyokawa et al. [6] used home-made ceramic FIR emitters to stimulate full thickness excisional skin wound healing in rats. After constant exposure to FIR, wound healing was significantly quickened and transforming growth factor (TGF)-beta1 expressing myofibroblasts and collagen content were increased.

Along the same lines, Akasaki et al. [7] studied *in vivo* the effects of repeated FIR irradiation on angiogenesis in a mouse model of hindlimb ischemia. Following reports that FIR therapy upregulated the expression of arterial eNOS in hamsters (and it is known that NO constitutively produced by eNOS plays an important role in angiogenesis) they took a step further to investigate whether the FIR therapy increases angiogenesis in mice with the hindlimb ischemia. In their study, unilateral hindlimb ischemia was induced in apolipoprotein E-deficient mice and the group to receive the FIR irradiation was placed in a FIR dry sauna at 41°C for 15 min and then

at 34°C for 20 min once daily, with total duration of the experiment of 5 weeks. Laser-Doppler perfusion imaging demonstrated that at the ischemic limb, blood perfusion ratio in the irradiated group increased significantly in comparison with the control group (0.79 ± 0.04 vs. 0.54 ± 0.08, $p < 0.001$). Also, in the treated group, significantly greater capillary density was observed (757 ± 123 per mm^2 vs. 416 ± 20 per mm^2, $p < 0.01$). Western blotting showed that thermal therapy has increased markedly the hindlimb eNOS expression. Furthermore, to study possible involvement of eNOS in thermally induced angiogenesis, the same FIR therapy was given to mice with hindlimb ischemia with or without N(G)-nitro-L-arginine methyl ester (L-NAME) administration for the duration of 5 weeks. It was observed that L-NAME treatment eliminated angiogenesis induced using the FIR thermal therapy and that the therapy did not increase angiogenesis in eNOS-deficient mice. The study led to the conclusion that angiogenesis can be induced via eNOS using FIR thermal therapy in mice with hindlimb ischemia.

Ishibashi et al. [8] did an *in vitro* study with five human cancer cell lines (A431, vulva; HSC3, tongue; Sa3, gingival; A549, lung; and MCF7, breast) to assess the effects of FIR irradiation. For that purpose, they used a tissue culture incubator with an imbedded FIR lamp that could continuously irradiate cells with FIR (lamp operating wavelength range being 4–20 µm with an emission peak height at 7–12 µm). The overall observation was that the FIR effect varied in these five cancer cell line types, as can be expected. The study results showed that basal expression level of heat shock protein (HSP) 70A mRNA was higher in A431 and MCF7 cell lines in comparison with the FIR-sensitive HSC3, Sa3, and A549 cell lines. The study showed that the over expression of HSP70 inhibited FIR-induced growth arrest in HSC3 cells, and that HSP70 siRNA inhibited the proliferation of A431 cells after FIR treatment. A summary of the results of this study indicated that the proliferation-suppressing effect of FIR, in some cancer cell lines, is controlled by the basal expression level of the HSP70A. These findings suggest that FIR irradiation may be used as an effective medical treatment avenue for some cancer cells which have low levels of HSP70.

2.1.2 FIR emitting ceramics and fabrics

FIR emitting ceramics have been known for some time [9, 10]. All ceramics have the property of emitting IR radiation depending on their temperature. In the age of gas lighting, ceramic mantles were heated by gas flames to emit both IR and visible radiation depending on the temperature attained. The exact chemical composition of the ceramic material governs the relationship between the temperature and the amount of IR radiation. The radiated energy follows the Stefan-Boltzmann law which says that the total energy radiated per unit of surface area per unit of time is directly proportional to the fourth power of the black body's absolute temperature. The wavelength range also depends strictly on the temperature according to Wien's displacement law [11].

The boron-silicate mineral, tourmaline (known as a gemstone in its crystalline form) when milled into fine powders also emits FIR [12] and the characteristics of the FIR emission depend on the particle size. Preparations containing tourmaline powder have been applied to the skin with the aim of affecting the blood flow [13]. In a similar manner discs of FIR emitting ceramics have been attached to the skin with the intent of producing a beneficial effect (see later).

Small particles (nanoparticles and microparticles) of FIR-emitting ceramic material have been incorporated into fibers that are then woven into fabrics. These fabrics can be manufactured into various garments that can be worn on different parts of the body.

When FIR emitting ceramics or fabrics are employed as therapeutic devices, it is pertinent to analyze the thermodynamics of the process. The first law of thermodynamics states that energy can neither be created nor destroyed. Heat (molecular vibrational energy) is transferred from one body to another in three forms: radiation, convection and conduction. Thus, it is clear that the principle source of energy needed to power the FIR emission from the garments comes from the human body, since it is at a significantly higher temperature than the surrounding air. So energy from the human body is transferred to these ceramic particles, which are acting as "perfect absorbers", maintain their temperature at sufficiently high levels and then emit FIR back to the body. It is plausible that FIR emitted from the skin is absorbed by the ceramic particles, which then re-emit the same FIR back to the skin. Although this may appear to be an energy neutral process and to cancel itself out, this is not in fact the case because the FIR emitting material will prevent the loss of FIR that would otherwise have escaped through normal clothing. However the same effect could have been achieved with a FIR reflective foil suit or suchlike. Other sources of heat that can transfer energy from the body to the ceramic particles with a net gain of FIR are either convection, conduction, or both. The balance between conduction and convection will depend on how close the contact is between

the garment and the skin. If the garment is skin tight, then conduction may be important, while if it is loose fitting then convection (heating up a layer of air between the skin and the garment) may be important.

Ting-Kai Leung and colleagues have studied the effect of FIR-emitting ceramic powders in a range of biological studies [14–19]. In one set of studies, they cultured murine myoblast cells (C2C12) with bags of ceramic powder under the culture plates and found that FIR irradiation improved cell viability and prevented lactate dehydrogenase release under hydrogen peroxide (H_2O_2)-mediated oxidative stress, and also elevated the intracellular levels of NO and calmodulin [14]. In the study, they used electro-stimulation of amphibian skeletal muscle and found that FIR emitting ceramics delayed the onset of fatigue, induced by muscle contractions [14]. In another set of studies, they showed that ceramic-emitted FIR (cFIR) could increase the generation of intracellular NO in breast cancer cells [15] and inhibit growth of murine melanoma cells [16]. Similarly, they found that cFIR increased calmodulin and NO production in RAW 264.7 macrophages [17]. cFIR also has been shown to increase the viability of murine macrophages with different concentrations of H_2O_2 [15]. In this study [15] it was shown that cFIR significantly inhibited intracellular peroxide levels and lipopolysaccharide (LPS)-induced peroxide production by macrophages. In the same study, it was also demonstrated that cFIR blocked ROS-mediated cytotoxicity (shown by measurements of cytochrome c and the ratio of NADP+/NADPH) [15].

The same research group went on to study a rabbit model of rheumatoid arthritis in which rabbits received intra-articular injections of LPS to induce inflammation that mimics the rheumatoid arthritis [18]. Fluorodeoxyglucose(^{18}F) coupled with positron emission tomography (FDG-PET) scans were used to monitor the inflammation in 16 h and 7 days after the LPS injection. Rabbits to be treated with cFIR were placed in a cage surrounded by paper sheets impregnated with a thin layer of the ceramic powder, while the control group was surrounded by the same sheet without the material. Comparison of the final and initial uptakes of FDG isotopes in the LPS-injected left knee-joints of the rabbits indicated larger decreases in the cFIR exposed group than in the control group indicating that FIR reduced inflammation.

In their most recent study the Leung group studied the repair effect of cFIR in human breast epithelial cells (MCF-10A) after H_2O_2 and after ionizing radiation from an X-ray source [19]. Their results show that in both, H_2O_2 toxicity and radiation exposure models, the cFIR treated cells demonstrated significantly higher cell survival rates than

the control groups. In view of the experimental results and taking into account the relationship between indirect ionizing radiation and the oxidative stress-induced cell damage, and accumulation of free radicals, they proposed that the ionizing radiation protective ability of cFIR occurs predominantly through an antioxidant mechanism. They are suggesting that cFIR provides cells with a defensive mechanism during the irradiation process and promotes cell repair during post exposure period through hydrogen peroxide scavenging and COX-2 inhibiting activities.

2.2 Means that are used to deliver the FIR radiation

We analyzed the peer-reviewed applications of therapeutic FIR delivery systems and realized that there are three main techniques for FIR radiation delivery: i) FIR saunas, ii) FIR ray devices and iii) FIR emitting ceramics and fabrics.

2.2.1 FIR saunas

In these cabins, the heating elements are typically heated to about 300–400°C and the emission is in the FIR range, that is, the heat exchange between the body and the environment is almost purely radiative (radiant heating) with cabin air temperature being at around 40°C or less (Figure 4). Heating of the skin with FIR warming cabins is faster (in comparison with the conventional saunas) but higher irradiance of the skin must be applied in order to produce noticeable sweating. These cabins are frequently used in Japan where the practice is called "Waon therapy" [20, 21]. Waon therapy has been used extensively in Japan [22] and Korea [23] for cardiovascular conditions and diseases, particularly chronic heart failure [24, 25] and peripheral arterial disease [26, 27]. FIR sauna therapy has been used to improve cardiac and vascular function and reduce oxidative stress in patients with chronic heart failure [28]. Beever [29] asked whether FIR saunas could have a beneficial effect on quality of life in those patients with type II diabetes. The study consisted of 20 min, three times weekly infrared sauna sessions, over a period of 3 months. Physical health, general health, social functioning indices, and visual analogue scales (VAS) measurements for stress and fatigue all improved in the treatment group. A study of patients with rheumatoid arthritis and ankylosing spondylitis showed a reduction in pain, stiffness, and fatigue during infrared sauna therapy [30].
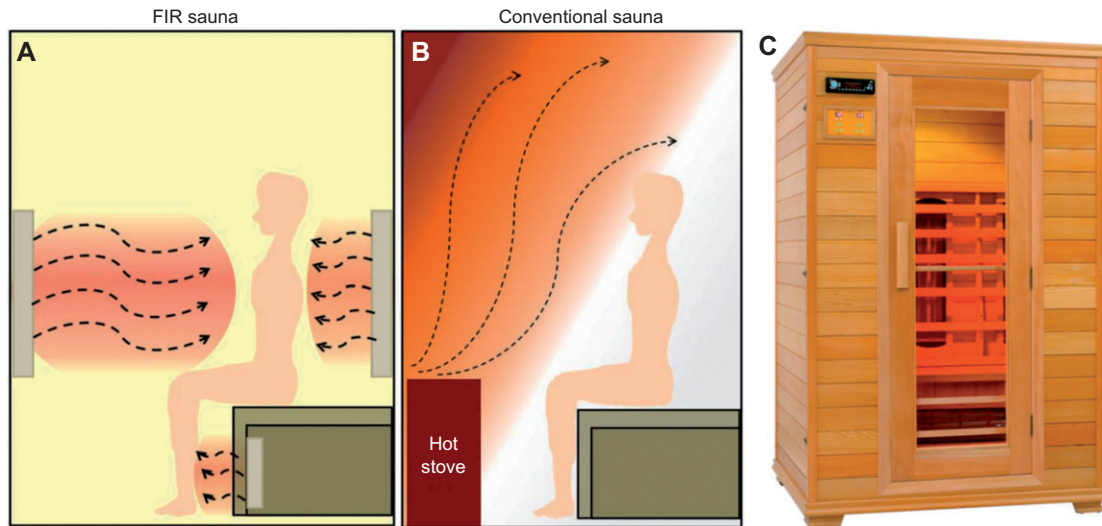
Figure 4 FIR sauna. (A, B) Comparison of FIR sauna with conventional heated sauna. (C) Cabin incorporating FIR emitting "cold" unit(s) (Anhui Hi-Tech Electronic Commerce Co., Ltd., Hefei, China).

2.2.2 FIR ray devices

Common devices are WS TY-101N® and WS TY-301R® (made by WS Far Infrared Medical Technology Co., Ltd., Taipei, Taiwan; see Figure 3). A report from Hu and Li [31] describes the treatment of allergic rhinitis. A WS TY-101N® FIR emitter was placed 30 cm from the patient's nasal region. The treatment was performed for 40 min every morning for 7 days. Every day, patients recorded their symptoms in a diary before and during treatment. Each symptom of rhinitis was rated on a 4-point scale (0–3) according to severity. During the period of FIR therapy, the symptoms of eye itching, nasal itching, nasal stuffiness, rhinorrhea, and sneezing were all significantly improved. Smell impairment was improved after the last treatment. Lin et al. [32] used a WS TY-101N® FIR emitter to treat vascular access malfunction with an inadequate access flow (Qa) in hemodialysis (HD) patients. This randomized trial demonstrated that FIR therapy could improve access flow and potency of the native arteriovenous fistula (AVF) in a total of 145 HD patients (73 in the control group and 72 in the FIR-treated group). FIR was used for 40 min, and hemodynamic parameters were measured by the HD02 monitor (M/s Transonic System Inc.), during the hemodialysis. In comparison with control subjects, patients who received FIR therapy for 1 year had a lower incidence (12.5 vs. 30.1%; p<0.01) and relative incidence (one episode per 67.7 vs. one episode per 26.7 patient-months; p=0.03) of AVF malfunction. Hausswirth et al. [33] showed that FIR

therapy reduced symptoms of exercise-induced muscle damage in athletes after a simulated trail running race.
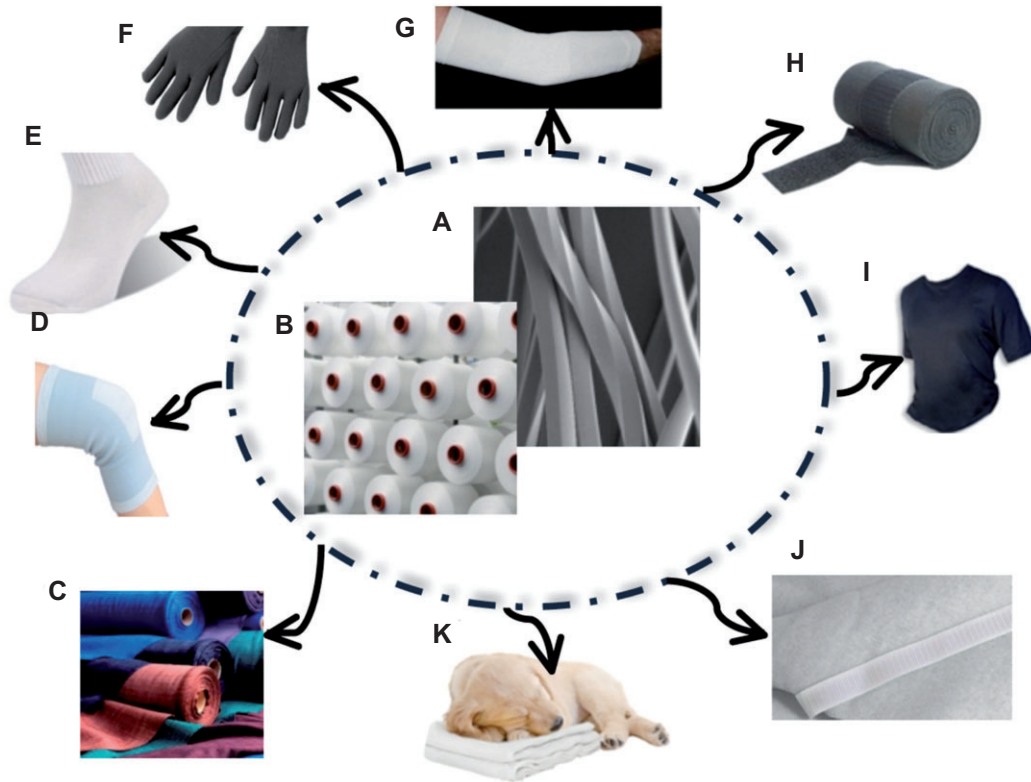
2.2.3 FIR emitting ceramics and fabrics

Discs and garments manufactured of FIR emitting ceramic material have been applied to the human body (Figure 5). For instance, a blanket containing discs has been reported to improve quality of sleep [34] and single discs were applied to the breasts of women who encountered difficulty in producing sufficient breast milk during lactation [35]. Gloves have been made out of FIR emitting fabrics and there have been reports that these gloves can be used to treat arthritis of the hands and Raynaud's syndrome [36].

Belts made out of these fabrics have been used for weight reduction. In one study, Conrado and Munin [37] investigated whether the use of a garment made with synthetic fibers embedded with powdered ceramic led to a reduction in body measurements. The study population comprised 42 women divided into two groups: active and placebo. The volunteers used clothing either impregnated or not impregnated with ceramic powder for at least 8 h/day for 30 days. The experimental data showed a reduction in body measurements, which may be a consequence of an increment in microcirculation and peripheral blood flow, and these changes might promote improved general health.

A belt containing FIR-emitting sericite mineral (a fine grained mica) was used to study the relief of menstrual

Figure 5 FIR emitting garments and fabrics manufactured from fibers impregnated with ceramic nanoparticles (Celliant®, Hologenix, Santa Monica, CA, USA). (A) fibers, (B) yarns, (C) fabrics, (D) knee bandage brace, (E) socks, (F) gloves, (G) elbow bandage brace, (H) multi-purpose bandage, (I) performance apparel, (J) mattress, and (K) puppy blanket.

pain [38]. In this study, 104 patients with primary dysmenorrhea were randomized to wear a sericite or placebo belt during sleep for three menstrual cycles, and then followed up for two additional menstrual cycles with no belt. Hot packs were used to heat the ceramics and ensure slight pain relief in both groups. Although the severity of dysmenorrhea decreased during the treatment period in both groups, it was found that during the follow-up period, the decreased VAS (pain) score was maintained in the experimental group, whereas the VAS score gradually returned to baseline in the control group, which resulted in significant difference between the groups ($p=0.0017$).

In their recent clinical study, Liau et al. [39] looked into the benefits of using an FIR emitting belt for managing the discomfort of primary dysmenorrhea in female patients. Taking into account several parameters, such as body temperature, abdominal blood flow, pain assessment, and heart rate variability, they showed that FIR belts used increased the local surface body temperature as well as the abdominal blood flow; in addition to reducing the pain and the discomfort from it. In this particular study, a THERMEDIC FIR belt (LinkWin Technology Co.,

Ltd., Taiwan) with the capability to generate 11.34 mW/cm^2 at 50°C was used.

Rao et al. [40] used garments made out of bioceramic-coated neoprene in conjunction with a "topical cream" to treat cellulite of the legs. Each subject was randomized to receive occlusion by the garment on either the right or left leg, with the contralateral side serving as a control with no occlusion. Of the 17 subjects who completed the study, 76% noticed an overall improvement in their cellulite, with 54% reporting greater improvement in the thigh that received garment occlusion. Further, the evaluators found the occluded thighs to show greater improvement than the non-occluded thighs in 65% of subjects. Bioceramic-coated neoprene garment occlusion potentiated the effect of the topical agent in cellulite reduction. A follow up two-center, double-blinded, randomized trial found similar results [41].

Celliant® (Hologenix, Santa Monica, CA, USA) is a polyethylene terephthalate (PET) fiber that incorporates FIR emitting ceramic nanoparticles. York and Gordon [42] studied socks manufactured from Celliant® fiber material in patients with chronic foot pain resulting from diabetic neuropathy or other disorders. A double-blind,

randomized trial with 55 subjects (38 men, 17 women, average age 59.7±11.9 years) enrolled 26 patients with diabetic neuropathy and 29 with other pain etiologies. Subjects twice completed the VAS, brief pain inventory (BPI), McGill pain questionnaire (MPQ), and a multipurpose, short form health survey with 36 questions (SF-36) a week apart [W(1+2)] before receiving either control or Celliant® socks. The same questionnaires were answered again 1 and 2 weeks later [W(3+4)]. The questionnaires provided nine scores for analyzing pain reduction: one VAS score, two BPI scores, five MPQ scores, and the bodily pain score on the SF-36. Mean W(1+2) and W(3+4) scores were compared to measure pain reduction. More pain reduction was reported by Celliant® subjects for eight of the nine pain questions employed, with a significant (p=0.043) difference between controls and Celliant® for McGill question III. In neuropathic subjects, Celliant® caused greater pain reduction in six of the nine questions, but not significantly. In non-neuropathic subjects eight of nine questions showed better pain reduction with the Celliant® socks.

3 Hypothesis for molecular and cellular mechanisms of FIR effects

Despite all these different uses of FIR in medical applications, the exact mechanisms of the hyperthermic effects and biological activities of FIR irradiation are still poorly understood. It is clear that two kinds of FIR therapy may exist. The first type (FIR saunas and some FIR generators powered by electricity) uses irradiances or power densities (tens of mW/cm²) that are sufficient to heat up the tissue, while others such as ceramic discs, powders, and fabrics (that use no external power but rely on energy from the body) have such low irradiances that they do not heat the tissue (0.1–5 mW/cm²). The question arises to what extent are the fundamental mechanisms of these two forms of FIR therapy the same, and to what extent are they different? Furthermore, the question may be posed as to what degree of similarity that FIR therapy has with the reasonably well-established therapy called low level laser (light) therapy (LLLT) also known as photobiomodulation (PBM). Pertinent to this question is the fact that many devices used to deliver therapeutic visible or NIR light were approved by the US Food and Drug Administration as being equivalent to an "infrared heat lamp". The cellular and molecular mechanisms of LLLT/PBM

are to some extent understood and involve absorption of red or NIR light by mitochondrial chromophores such as cytochrome c oxidase (CCO, unit IV of the mitochondrial respiratory chain) [43]. This photon absorption activates the enzyme possibly by photo-dissociating the inhibitory molecule, NO, from the copper B (CuB) site [44]. This loss of NO allows electron transport, oxygen consumption, and adenosine triphosphate (ATP) to rapidly increase and results in a marked rise in mitochondrial membrane potential (MMP) that gives rise to a brief burst of ROS [45]. Signaling pathways are activated by ATP, NO, and ROS and these lead to activation of transcription factors (such as NF-κB) [46] that lead to the long-term effects on tissue (healing, anti-inflammatory and pain relief [47]) seen after relatively transient periods of illumination.

Since the principle chromophore at FIR wavelengths is not CCO but rather water, we must ask ourselves how can the biological effects of red and NIR absorption be so similar to those seen with FIR? Perhaps some clue can be obtained by considering the difference between the two types of FIR therapy (heating and non-heating). While heating FIR therapy is reported to increase blood flow, this result may be the simple response of increased thermoregulation that is known to occur when tissue is warmed. However, it is possible that the increase in blood flow, seen in non-heating FIR therapy, may be similar in nature to that seen in LLLT, in other words, a vasodilation due to NO release from stores in CCO [48] as well as from NO bound to hemoglobin and myoglobin [49]. How are we to explain cellular responses from low fluences of FIR that are insufficient to produce bulk heating of water in the tissue? Perhaps the answer lies in the concept of nanostructured water layers [50]. These are thin (nanometers) layers of water that build up on hydrophobic surfaces such as cellular membranes, and they can be considered as "concentrated water" [51]. If this description is correct, it is reasonable to assume that relatively small amounts of vibrational energy delivered by non-heating FIR could perturb the structure of the membrane underlying the nanoscopic water layer without bulk heating. Small perturbations in membrane structure could have big effects at the cell level if the membrane contains an ion channel. Ion channels (many kinds for both cations and anions [52]) are present in all cell membranes, but are particularly common in mitochondrial membranes (both inner and outer [53]). If mitochondrial ion channels (particularly calcium channels [54]) could be opened by non-heating FIR, thus increasing mitochondrial respiration, it would explain how the overall therapeutic outcomes of LLLT and non-heating FIR therapy are so similar.

It cannot be excluded that FIR could itself have effects on CCO activity. A recent study has elucidated the existence of weakly H-bonded water molecules in bovine CCO that might change during catalysis [55]. Fitting with Gaussian components indicated the involvement of up to eight waters in the photolysis transition. The fact that Fourier transform infrared (FTIR) spectroscopy is extensively employed to study the structure, function, and dynamics of CCO [56, 57] suggests that it is possible that the same wavelengths (FIR uses comparable wavelengths to FTIR) could produce changes in conformation affecting enzyme activity or binding of NO to the CuB site.

It must be emphasized that the above remains a hypothetical explanation at present, but is clearly a testable hypothesis. One could ask whether exposure of cells to non-heating FIR can affect mitochondria by for instance increasing ATP, increasing oxygen consumption, producing NO and ROS, affecting MMP and calcium levels. One could also ask whether cells that are rich in mitochondria respond well to non-heating FIR, in the same way as they do to LLLT.

4 Conclusion

If it can be proved that non-heating FIR has real and significant biological effects, then the possible future applications are wide ranging. Not only could bandages and dressings made out of NIR emitting fabrics be applied for many medical conditions and injuries that require healing, but there is a large potential market in lifestyle enhancing applications. Garments may be manufactured for performance enhancing apparel in both leisure activities and competitive sports areas. Cold weather apparel would perform better by incorporating FIR emitting capability and sleeping environments could be improved by mattresses and bedding emitting FIR.

References

[1] Plaghki L, Decruynaere C, Van Dooren P, Le Bars D. The fine tuning of pain thresholds: a sophisticated double alarm system. PLoS One 2010;5(4):e10269.

[2] Sheppard AR, Swicord ML, Balzano Q. Quantitative evaluations of mechanisms of radiofrequency interactions with biological molecules and processes. Health Phys 2008;95(4): 365–96.

[3] Lee MS, Baletto F, Kanhere DG, Scandolo S. Far-infrared absorption of water clusters by first-principles molecular dynamics. J Chem Phys 2008;128(21):214506.

[4] Hsu YH, Chen YC, Chen TH, Sue YM, Cheng TH, Chen JR, Chen CH. Far-infrared therapy induces the nuclear translocation of PLZF which inhibits VEGF-induced proliferation in human umbilical vein endothelial cells. PLoS One 2012;7(1):e30674.

[5] Yu SY, Chiu JH, Yang SD, Hsu YC, Lui WY, Wu CW. Biological effect of far-infrared therapy on increasing skin microcirculation in rats. Photodermatol Photoimmunol Photomed 2006;22(2): 78–86.

[6] Toyokawa H, Matsui Y, Uhara J, Tsuchiya H, Teshima S, Nakanishi H, Kwon AH, Azuma Y, Nagaoka T, Ogawa T, Kamiyama Y. Promotive effects of far-infrared ray on full-thickness skin wound healing in rats. Exp Biol Med (Maywood) 2003;228(6):724–9.

[7] Akasaki Y, Miyata M, Eto H, Shirasawa T, Hamada N, Ikeda Y, Biro S, Otsuji Y, Tei C. Repeated thermal therapy up-regulates endothelial nitric oxide synthase and augments angiogenesis in a mouse model of hindlimb ischemia. Circ J 2006;70(4): 463–70.

[8] Ishibashi J, Yamashita K, Ishikawa T, Hosokawa H, Sumida K, Nagayama M, Kitamura S. The effects inhibiting the proliferation of cancer cells by far-infrared radiation (FIR) are

controlled by the basal expression level of heat shock protein (HSP) 70A. Med Oncol 2008;25(2):229–37.

[9] Wang F, Liang J, Tang Q, Li L, Han L. Preparation and far infrared emission properties of natural sepiolite nanofibers. J Nanosci Nanotechnol 2010;10(3):2017–22.

[10] Liang J, Zhu D, Meng J, Wang L, Li F, Liu Z, Ding Y, Liu L, Liang G. Performance and application of far infrared rays emitted from rare earth mineral composite materials. J Nanosci Nanotechnol 2008;8(3):1203–10.

[11] Heald MA. Where is the "Wien peak"? Am J Phys 2003;71(12): 1322–3.

[12] Meng J, Jin W, Liang J, Ding Y, Gan K, Yuan Y. Effects of particle size on far infrared emission properties of tourmaline superfine powders. J Nanosci Nanotechnol 2010;10(3):2083–7.

[13] Yoo BH, Park CM, Oh TJ, Han SH, Kang HH, Chang IS. Investigation of jewelry powders radiating far-infrared rays and the biological effects on human skin. J Cosmet Sci 2002;53(3):175–84.

[14] Leung TK, Lee CM, Tsai SY, Chen YC, Chao JS. A pilot study of ceramic powder far-infrared ray irradiation (cFIR) on physiology: observation of cell cultures and amphibian skeletal muscle. Chin J Physiol 2011;54(4):247–54.

[15] Leung TK, Lin YS, Lee CM, Chen YC, Shang HF, Hsiao SY, Chang HT, Chao JS. Direct and indirect effects of ceramic far infrared radiation on the hydrogen peroxide-scavenging capacity and on murine macrophages under oxidative stress. J Med Biol Eng 2011;31(5):345–51.

[16] Leung TK, Chan CF, Lai PS, Yang CH, Hsu CY, Lin YS. Inhibitory effects of far-infrared irradiation generated by ceramic material on murine melanoma cell growth. Int J Photoener 2012; doi:10.1155/2012/646845.

[17] Leung TK, Shang HF, Chen DC, Chen JY, Chang TM, Hsiao SY, Ho CK, Lin YS. Effects of far infrared rays on hydrogen peroxide-scavenging capacity. Biomed Eng Appl Basis Commun 2011;23(2):99–105.

[18] Leung TK, Chen CH, Lai CH, Lee CM, Chen CC, Yang JC, Chen KC, Chao JS. Bone and joint protection ability of ceramic material with biological effects. Chin J Physiol 2012;55(1):47–54.

[19] Leung TK, Lee CM, Wu CH, Chiou JF, Huang PJ, Shen LK, Hung CS, Ho YS, Wang HJ, Kung CH, Lin YH, Yeh HM, Hsiao WT. Protective effect of non-ionized radiation from far infrared ray emitting ceramic material (cFIR) against oxidative stress on human breast epithelial cells. J Med Biol Eng 2012. doi: 10.5405/jmbe.1133.

[20] Taylor J. Recent pioneering cardiology developments in Japan: Japanese cardiologists have discovered Waon therapy for severe or refractory heart failure and extracorporeal cardiac shock wave therapy for severe angina pectoris. Eur Heart J 2011;32(14):1690–1.

[21] Miyata M, Tei C. Waon therapy for cardiovascular disease: innovative therapy for the 21st century. Circ J 2010;74(4): 617–21.

[22] Cho GY, Ha JW. Waon therapy, can it be new therapeutic modality in heart failure patients? J Cardiovasc Ultrasound 2010;18(2):43–4.

[23] Sohn IS, Cho JM, Kim WS, Kim CJ, Kim KS, Bae JH, Tei C. Preliminary clinical experience with Waon therapy in Korea: safety and effect. J Cardiovasc Ultrasound 2010;18(2): 37–42.

[24] Kihara T, Miyata M, Fukudome T, Ikeda Y, Shinsato T, Kubozono T, Fujita S, Kuwahata S, Hamasaki S, Torii H, Lee S, Toda H, Tei C. Waon therapy improves the prognosis of patients with chronic heart failure. J Cardiol 2009;53(2):214–8.

[25] Miyata M, Kihara T, Kubozono T, Ikeda Y, Shinsato T, Izumi T, Matsuzaki M, Yamaguchi T, Kasanuki H, Daida H, Nagayama M, Nishigami K, Hirata K, Kihara K, Tei C. Beneficial effects of Waon therapy on patients with chronic heart failure: results of a prospective multicenter study. J Cardiol 2008;52(2):79–85.

[26] Shinsato T, Miyata M, Kubozono T, Ikeda Y, Fujita S, Kuwahata S, Akasaki Y, Hamasaki S, Fujiwara H, Tei C. Waon therapy mobilizes CD34+ cells and improves peripheral arterial disease. J Cardiol 2010;56(3):361–6.

[27] Tei C, Shinsato T, Miyata M, Kihara T, Hamasaki S. Waon therapy improves peripheral arterial disease. J Am Coll Cardiol 2007;50(22):2169–71.

[28] Fujita S, Ikeda Y, Miyata M, Shinsato T, Kubozono T, Kuwahata S, Hamada N, Miyauchi T, Yamaguchi T, Torii H, Hamasaki S, Tei C. Effect of Waon therapy on oxidative stress in chronic heart failure. Circ J 2011;75(2):348–56.

[29] Beever R. The effects of repeated thermal therapy on quality of life in patients with type II diabetes mellitus. J Altern Complement Med 2010;16(6):677–81.

[30] Oosterveld FG, Rasker JJ, Floors M, Landkroon R, van Rennes B, Zwijnenberg J, van de Laar MA, Koel GJ. Infrared sauna in patients with rheumatoid arthritis and ankylosing spondylitis. A pilot study showing good tolerance, short-term improvement of pain and stiffness, and a trend towards long-term beneficial effects. Clin Rheumatol 2009;28(1):29–34.

[31] Hu KH, Li WT. Clinical effects of far-infrared therapy in patients with allergic rhinitis. Conf Proc IEEE Eng Med Biol Soc 2007;2007:1479–82.

[32] Lin CC, Chang CF, Lai MY, Chen TW, Lee PC, Yang WC. Far-infrared therapy: a novel treatment to improve access blood flow and unassisted patency of arteriovenous fistula in hemodialysis patients. J Am Soc Nephrol 2007;18(3):985–92.

[33] Hausswirth C, Louis J, Bieuzen F, Pournot H, Fournier J, Filliard JR, Brisswalter J. Effects of whole-body cryotherapy vs. far-infrared vs. passive modalities on recovery from exercise-induced muscle damage in highly-trained runners. PLoS One 2011;6(12):e27749.

[34] Inoué S, Kabaya M. Biological activities caused by far-infrared radiation. Int J Biometeorol 1989;33(3):145–50.

[35] Ogita S, Imanaka M, Matsuo S, Takebayashi T, Nakai Y, Fukumasu H, Matsumoto M, Iwanaga K. Effects of far-infrared radiation on lactation. Ann Physiol Anthropol 1990;9(2): 83–91.

[36] Ko GD, Berbrayer D. Effect of ceramic-impregnated "thermoflow" gloves on patients with Raynaud's syndrome: randomized, placebo-controlled study. Altern Med Rev 2002;7(4):328–35.

[37] Conrado LA, Munin E. Reduction in body measurements after use of a garment made with synthetic fibers embedded with ceramic nanoparticles. J Cosmet Dermatol 2011;10(1):30–5.

[38] Lee CH, Roh JW, Lim CY, Hong JH, Lee JK, Min EG. A multicenter, randomized, double-blind, placebo-controlled trial evaluating the efficacy and safety of a far infrared-emitting sericite belt in patients with primary dysmenorrhea. Complement Ther Med 2011;19(4):187–93.

[39] Liau BY, Leung TK, Ou MC, Ho CK, Yang A, Lin YS. Inhibitory effects of far-infrared ray-emitting belts on primary dysmenorrhea. Int J Photoener 2012. doi:10.1155/2012/238468.

[40] Rao J, Paabo KE, Goldman MP. A double-blinded randomized trial testing the tolerability and efficacy of a novel topical agent with and without occlusion for the treatment of cellulite: a study and review of the literature. J Drugs Dermatol 2004;3(4):417–25.

[41] Rao J, Gold MH, Goldman MP. A two-center, double-blinded, randomized trial testing the tolerability and efficacy of a novel therapeutic agent for cellulite reduction. J Cosmet Dermatol 2005;4(2):93–102.

[42] York RM, Gordon IL. Effect of optically modified polyethylene terephthalate fiber socks on chronic foot pain. BMC Complement Altern Med 2009;9:10.

[43] Chung H, Dai T, Sharma SK, Huang YY, Carroll JD, Hamblin MR. The nuts and bolts of low-level laser (light) therapy. Ann Biomed Eng 2012;40(2):516–33.

[44] Lane N. Cell biology: power games. Nature 2006;443(7114):901–3.

[45] Chen AC-H, Huang YY, Arany PR, Hamblin MR. Role of reactive oxygen species in low level light therapy. Proc SPIE 2009. doi:10.1117/12.814890.

[46] Chen AC, Arany PR, Huang YY, Tomkinson EM, Sharma SK, Kharkwal GB, Saleem T, Mooney D, Yull FE, Blackwell TS, Hamblin MR. Low-level laser therapy activates NF-κB via generation of reactive oxygen species in mouse embryonic fibroblasts. PLoS One 2011;6(7):e22453.

[47] Huang YY, Chen AC, Carroll JD, Hamblin MR. Biphasic dose response in low level light therapy. Dose Response 2009;7(4):358–83.

[48] Hamblin MR. The role of nitric oxide in low level light therapy. Proc SPIE 2008. doi:10.1117/12.764918.

[49] Zhang R, Mio Y, Pratt PF, Lohr N, Warltier DC, Whelan HT, Zhu D, Jacobs ER, Medhora M, Bienengraeber M. Near infrared light protects cardiomyocytes from hypoxia and reoxygenation injury by a nitric oxide dependent mechanism. J Mol Cell Cardiol 2009;46(1):4–14.

[50] Sommer AP, Zhu D, Mester AR, Försterling HD. Pulsed laser light forces cancer cells to absorb anticancer drugs – the role of water in nanomedicine. Artif Cells Blood Substit Immobil Biotechnol 2011;39(3):169–73.

[51] Sommer AP, Caron A, Fecht HJ. Tuning nanoscopic water layers on hydrophobic and hydrophilic surfaces with laser light. Langmuir 2008;24(3):635–6.

[52] Ravna AW, Sylte I. Homology modeling of transporter proteins (carriers and ion channels). Methods Mol Biol 2012;857:281–99.

[53] Perez-Pinzon MA, Stetler RA, Fiskum G. Novel mitochondrial targets for neuroprotection. J Cereb Blood Flow Metab 2012;32(7):1362–76.

[54] Calì T, Ottolini D, Brini M. Mitochondrial Ca(2+) as a key regulator of mitochondrial activities. Adv Exp Med Biol 2012;942:53–73.

[55] Maréchal A, Rich PR. Water molecule reorganization in cytochrome c oxidase revealed by FTIR spectroscopy. Proc Natl Acad Sci USA 2011;108(21):8634–8.

[56] Rich PR, Breton J. Attenuated total reflection Fourier transform infrared studies of redox changes in bovine cytochrome c oxidase: resolution of the redox Fourier transform infrared difference spectrum of heme a(3). Biochemistry 2002;41(3):967–73.

[57] Heitbrink D, Sigurdson H, Bolwien C, Brzezinski P, Heberle J. Transient binding of CO to Cu(B) in cytochrome c oxidase is dynamically linked to structural changes around a carboxyl group: a time-resolved step-scan Fourier transform infrared investigation. Biophys J 2002;82(1 Pt 1):1–10.